68-24.2

21 Oct '71

Final Report

HEAT PIPE TECHNOLOGY FOR ADVANCED ROCKET THRUST CHAMBERS

Report 697-F

15 September 1971

AEROJET LIQUID ROCKET COMPANY

A DIVISION OF AEROJET-GENERAL

SACRAMENTO, CALIFORNIA

FOREWORD

This is the final report for Contract NAS 7-697, Heat Pipe Technology for Advanced Rocket Thrust Chambers. The work reported was performed during the Period 1 July 1970 to 31 July 1971. The program was conducted for NASA/JPL by the Engine Components Department of Aerojet Liquid Rocket Company, Sacramento, California. Major portions of the heat pipe design, fabrication, and testing work were done on a subcontract by the Special Power Devices Engineering Department, RCA Corporation, Lancaster, Pennsylvania. The JPL technical manager was R. W. Riebling and the NASA project manager was F. E. Compitello. At Aerojet, the program manager was N. E. Van Huff and the project engineer was D. C. Rousar and the technical consultant was R. J. LaBotz. The RCA subcontract management consisted of R. W. Longsderff, project engineering leader, and R. A. Freggens, project engineer. Significant contributions to this program were also made by G. Y. Eastman and W. E. Harbaugh at RCA and by the following ALRC personnel.

R. L. Boyce
D. G. Chandler
J. W. Daily
J. I. Ito
D. M. Jassowski
H. V. Kiser
J. S. Sullivan
E. M. Vanderwall

HEAT PIPE TECHNOLOGY
FOR
ADVANCED ROCKET THRUST CHAMBERS

Final Report on Contract NAS 7-697

by

D. C. Rousar

Report 697-F

15 September 1971

Prepared for

NATIONAL AERONAUTICS AND SPACE ADMINISTRATION
4800 Oak Grove Drive
Pasadena, California 91103

AEROJET LIQUID ROCKET COMPANY

TABLE OF CONTENTS

APPENDIXES

LIST OF TABLES

FIGURE LIST

Figure List (cont.)

Figure No.

CONVERSION FACTORS

Quantity	British System	SI System
Density	lbm/ft^3	$16.02\ kg/m^3$
Film coefficient	$Btu/in.^2\text{-}sec\text{-}°R$	$2.94 \times 10^2\ watt/cm^2\text{-}°K$
Heat flux	$Btu/in.^2\text{-}sec$	$163.42\ watt/cm^2$
Length	inch	2.54 cm
Mass flow rate	lbm/sec	0.454 kg/sec
Pressure	$lbf/in.^2$	$6.895\ kN/m^2$
Temperature	°R	(1/1.8) °K
Thermal conductivity	Btu/in.-sec-°R	7.47×10^2 watt/cm-°K
Thrust	lbf	4.448 N
Velocity	ft/sec	0.3048 m/sec

I. INTRODUCTION AND SUMMARY

This report documents the work performed during the follow-on portion of Contract NAS 7-697. The initial program work was previously reported in Reference 1. The objective of the program was to evaluate adaptation of the heat pipe principle to the cooling of rocket engine thrust chambers. Concept evaluation studies for a 4448 N thrust, 689.5 kN/m^2 chamber pressure, OF_2/B_2H_6 thrust chamber were conducted previously and a regeneratively cooled concept (sketched in Figure 1) was chosen.

In the regeneratively cooled system, the heat pipe performs a heat flux transformer and heat flux averaging function so that propellants that are considered poor coolants may be used to regeneratively cool thrust chambers with high heat fluxes. The heat pipe evaporator, which is located at the thrust chamber wall, consists of a structural layer backed by a wick containing liquid working fluid. Heat from the combustion gases evaporates the working fluid and the vapor flows outward to the propellant-cooled condenser where the heat flux transmitted to the coolant is much lower than the peak thrust chamber heat flux and is relatively uniform. The condenser is comparatively easy to cool as a result of this low, uniform heat flux and the cooling limits due to critical heat flux and pressure drop are much less severe. The heat pipe also acts as a "heat distributor", in that local regions which tend to become hot will receive less heat, and this mechanism prevents coolant passage burnout.

The specific thrust chamber concept considered during this follow-on program consists of an annular-shaped heat pipe that operates with sodium working fluid. The condenser wall is cylindrical and is regeneratively cooled with diborane, which enters the cooling jacket as a subcooled liquid and exits as a superheated gas.

Although the initial propellant system considered was OF_2/B_2H_6, the heat pipe principle is by no means limited to this combination and future work could include application studies for other propellant combinations (FLOX/MMH and F_2/N_2H_4, for example).

I, Introduction and Summary (cont.)

The major problem areas to be contended with in applying the heat flux principle to thrust chamber cooling are evaporator heat flux limits, fabrication capabilities, and startup. Work on this program has emphasized the investigation of heat flux limits and the demonstration of fabrication capabilities.

The specific work performed on this follow-on program consisted of advanced design analysis (Task 4), evaporator wick development (Task 5), preliminary thrust chamber design (Task 6), injector design and fabrication (Task 7), and documentation (Task 8). The initial goal of the follow-on program was to design and fabricate a heat-pipe-cooled thrust chamber capable of operating with space storable propellants. However, the thrust chamber design work was de-emphasized so that efforts could be concentrated on the development of heat pipe wicking systems capable of operating at high heat fluxes.

The wick development work consisted of design, fabrication, and testing of cylindrical sodium heat pipes similar to those shown in Figures 2 and 3. Eight heat pipes were tested at heat fluxes up to 650 watts/cm^2 (4 Btu/$in.^2$-sec). In seven of the eight heat pipes, the evaporator consisted of a layer of sintered nickel powder, and one of the evaporators was a composite screen structure. During the testing, wick degradation problems were encountered in the form of black deposits and wick erosion. The occurrence of this wick degradation was related to oxygen contamination and the problem was solved by distillation loading of the sodium heat pipes and by incorporating zirconium oxygen-getters into the internal heat pipe design. Careful cleaning procedures were an additional requirement to avoid contamination. The wick development work is discussed in detail in Section III of this report.

An injector for testing the first heat-pipe-cooled thrust chamber was designed, fabricated, cold-flow tested, and delivered to JPL for checkout testing with the copper thrust chamber delivered to JPL previously on Contract

I, Introduction and Summary (cont.)

NAS 7-713. For reasons of testing economy, this injector simulates the OF_2/B_2H_6 wall heat transfer by utilizing FLOX (70 wt% F_2, 30 wt% O_2) and gaseous hydrogen propellants. The injector work is described in Section IV.

In the preliminary thrust chamber design work, detailed design concepts for a thrust chamber heat pipe and the condenser cooling jacket were established and analyzed. In addition, potential problem areas were identified and evaluated. The preliminary design work is discussed in Section V.

The advanced design analysis work under Task IV applied specifically to the wick development, preliminary design, and injector work and has been included in the appropriate sections. Several conclusions and recommendations were established as a result of the work on this program and they are listed in Section II. Two appendices, also included in this report, document a computer program for cooling jacket thermal design (Appendix A) and a thermocouple error analysis (Appendix B).

II. CONCLUSIONS AND RECOMMENDATIONS

1. The evaporator wick degradation which occurred during the testing of sodium/nickel heat pipes (black deposits and wick erosion) was related to the presence of oxygen contamination within the heat pipe.

2. The wick degradation problem was eliminated by: (1) distillation loading of the heat pipe, (2) placing zirconium "getters" inside the heat pipe, and (3) following the fabrication procedures outlined for Heat Pipe 14 in Section III,C,7.

3. Heat pipes which are free from contamination can be operated normally up to substantial heat flux levels. During testing on this contract, normal operation was observed at heat fluxes up to 797 watt/cm^2 (4.9 Btu/$in.^2$-sec) with Heat Pipe 7 and 433 watt/cm^2 (2.66 Btu/$in.^2$-sec) with Heat Pipe 14.

4. Of the heat pipe designs tested which are applicable to a thrust chamber heat pipe, Heat Pipe 14 yielded the best performance. The major design features of Heat Pipe 14 were: (a) sintered nickel powder evaporator wick, (b) platelet liquid return feeders, (c) screen condenser wick, (d) carefully made screen joints connecting the feeders to the condenser and evaporator wicks.

5. Degradation of sintered nickel powder wicks will occur in sodium heat pipes if the wick is allowed to dry out locally and overheat.

6. Future heat pipe testing should emphasize the use of an annular geometry so that the mechanical problems inherent to flat evaporator walls are avoided, and the test results will be more directly applicable to the thrust chamber configuration.

7. The following heat pipe design features are recommended for future high heat flux work with annular heat pipes: sintered powder and screen evaporator wicks, platelet-type feeders, screen condenser wicks, argon gas loading.

II, Conclusions and Recommendations (cont.)

8. A study of the applicability of the heat-pipe-cooled thrust chamber concept to engines utilizing propellants other than OF_2/B_2H_6 is recommended. The F_2/N_2H_4 and FLOX/MMH systems, for example, present potential applications. An advantage of the F_2/N_2H_4 heat-pipe-cooled thrust chamber is that a short N_2H_4 monopropellant burn could be utilized to thaw the heat pipe and heat it to its operating temperature.

9. The heat pipe testing and preliminary design work indicate that the heat-pipe-cooled concept is feasible and the heat pipe performance is limited by the heat flux capability of the wick system. Hydrogen permeation represents another potential problem that should be considered in future work.

III. EVAPORATOR WICK DEVELOPMENT

A. OBJECTIVE AND SCOPE OF WORK

The objective of the wick development task was to further investigate the heat flux capabilities of the wick concepts which appeared the most promising for thrust chamber applications as indicated by the results of the previous work. Tests were conducted on eight cylindrical heat pipes similar in design to the seven heat pipes tested previously. The working fluid was sodium and the heat pipe components were fabricated from 200 series nickel. Some of the heat pipes were inert-gas-loaded with argon. The heat pipes tested are described in Reference 1 (Heat Pipes 1, 2, 3, 4, 5, 6 and 7) and in Table 1 (Heat Pipes 8, 9, 10, 11, 12, 13, 14 and 15). The general configuration of the heat pipes is depicted in Figures 2 and 3. The heat flux goal was 1000 watt/cm^2 (6.12 Btu/$in.^2$-sec) which corresponds to the maximum heat flux expected for a $FLOX/H_2$ or OF_2/B_2H_6 thrust chamber operating at 4448 N thrust and 689.5 kN/m^2 chamber pressure without film or barrier cooling.

During the previous testing, the highest heat fluxes were achieved using sintered nickel powder evaporator wicks. The best performance was obtained with Heat Pipe 7 which contained a 0.178-cm - thick sintered nickel powder wick. The Heat Pipe 7 design is diagramed in Figure 2 and the evaporator wall temperature and heat flux data are shown in Figure 4. These data indicate normal operation up to 797 watt/cm^2 (4.9 Btu/$in.^2$-sec) heat flux as the evaporator midpoint temperature is about equal to the predictions from one-dimensional axial conduction theory. (The low temperature measured 1.9 cm from the evaporator midpoint was probably caused by two-dimensional conduction and sodium subcooling effects.) The beginning of a temperature excursion is evidenced by the data at 805 watt/cm^2 heat flux and further heat flux increases produced burnout of the evaporator wall.

As a result of this previous successful testing, the sintered powder design was the basis for most of the evaporator wick designs tested on the follow-on program. Sintered nickel powder evaporator wicks were utilized

III, A, Objective and Scope of Work (cont.)

in seven of the eight heat pipes tested (Heat Pipe 8, 9, 10, 11, 12, 13 and 14). The best performance was obtained with Heat Pipe 14 which was operated to a heat flux of 652 watt/cm^2 (4 Btu/$in.^2$-sec); however, abnormal operation was observed with Pipe 14 at heat fluxes greater than 433 watt/cm^2 (2.66 Btu/$in.^2$-sec).

High performance levels have not been achieved with screen wicks; however, screens may be advantageous from the standpoint of thrust chamber fabrication and may also be less susceptible to contamination effects. For these reasons, a composite screen wick was tested in Heat Pipe 15.

The evaporator wick development work was performed by both the RCA Corporation, which functioned as a heat pipe subcontractor and performed all the heat pipe testing, and the Aerojet Liquid Rocket Company. The work breakdown is as follows: Heat Pipes 8, 10 and 11 were designed and fabricated by RCA; Heat Pipes 9, 12 and 13 designs were established jointly by ALRC and RCA and the units were fabricated by RCA; Heat Pipe 14 was also a joint design effort and was fabricated by ALRC with certain components supplied by RCA; Heat Pipe 15 was designed and fabricated by ALRC.

The philosophy of the test plan followed was to develop the high heat flux wick system in an evolutionary manner because the scope of the program was not sufficient to allow separate evaluations of the fundamental design variables, operating parameters and fabrication techniques. For this reason, the specific heat pipe design and test results are presented and discussed in chronological order in Section III,C of this report. The design features of each heat pipe and the maximum heat flux data are summarized in Table 1, and more detailed tabulations of the test data are given in Table 2. Additional discussions of the results are presented in Section III,D. The test apparatus and procedures are described in the following section.

III, Evaporator Wick Development (cont.)

B. TEST APPARATUS AND PROCEDURES

1. Heat Pipe Design and Operating Conditions

The test heat pipes were cylindrical in geometry and were constructed from a length of 3.8-cm-OD tubing about 15 cm long. The evaporator wicks were located on one of the flat ends of the cylinder while the condenser wicks were fabricated from 60 or 120 mesh nickel screen and positioned on the cylindrical surface. The general configuration of the heat pipes tested is shown in Figure 3, which is a sketch of Heat Pipe 12. The design of the other heat pipes differed from this somewhat in that different evaporator designs and condenser cooling systems were utilized. In addition, some heat pipes were controlled by inert gas pressurization while others were not, and some were "processed" prior to final closure and testing. The specific design details of each heat pipe are given in Section III,C and the major design features of each are summarized in Table 1.

Initial tests were conducted using water as the condenser coolant. However, the demand for greater thermal load variation prompted the use of argon, helium, and nitrogen gas for low power level testing, and the use of a nitrogen gas/water mixture at higher power levels. In most of the heat pipes, chromel-alumel thermocouples were installed inside the evaporator wall and along the length of the heat pipe. The thermocouple measurements were used to evaluate the heat pipe performance and operating conditions.

All the heat pipe designs tested were nearly prototype in that the liquid return wicks (through which liquid sodium replenished the evaporator wick) were positioned within the heated zone of the evaporator. Note that this was not the case in the work reported previously. The majority of testing was done with screen return wicks; however, a return structure fabricated from photoetched plates was utilized in the Heat Pipe 14 and 15 designs. All testing

III, B, Test Apparatus and Procedures (cont.)

was done with the heat pipe in a horizontal position (evaporator wick vertical) with the evaporator end elevated a few degrees above horizontal so that any excess sodium would accumulate in the condenser end of the heat pipe.

The desired range of heat pipe temperature (the vapor temperature just above the evaporator) was established as 870 to 920°K (about 1100 to 1200°F) based on the following considerations:

(1) Previous testing indicated that high heat flux levels could be achieved in this temperature range (Heat Pipe 7).

(2) Lower temperatures are not advisable because heat flux limits due to sonic flow and evaporation kinetics approach 1000 watt/cm^2 (the program goal) at temperatures below 870°K. The sonic flow limit published by LASL (Ref 2) and the evaporation limit estimated by RCA are shown in Figure 5.

(3) Higher temperatures are not desirable because excessive wall temperatures become difficult to avoid. For example, if the total thickness of the wick and wall is about 0.1 in., a wall temperature of 1250 to 1300°K (about 1800 to 1900°F) would be expected at 1000 watt/cm^2 heat flux and 870 to 920°K heat pipe temperature.

The vapor temperature range of 870 to 920°K corresponds to a sodium vapor pressure of approximately 2.7 to 6.6 kN/m^2 (20 to 50 mm Hg).

2. Electron Bombardment Heater

The evaporator end of the heat pipe was heated in a vacuum atmosphere by electron bombardment from a thoriated tungsten heater. The evaporator wall was electrically connected so that it was positive with respect to the heater, thus forming the equivalent of a vacuum diode. Heat input to the evaporator was controlled by adjustment of the voltage between the heater and heat pipe. The heater filament design used previously was modified to

III, B, Test Apparatus and Procedures (cont.)

permit operation at heat fluxes up to 1230 watt/cm^2. This increase in heat flux capability necessitated the addition of heater wire turns to accommodate the increased current density demands. The resulting decrease in wire spacing probably improved heat input uniformity on the evaporator. The modified heater element design is shown in Figure 6. A drawing of the heater assembly installed on Heat Pipe 12 is given in Figure 7. The heater filament was positioned parallel to the evaporator wall and about 0.25 cm from it.

An electrostatic field plot of the heater electrode configuration was employed to determine the evaporator area that would be actively heated by the heater. The consequent flux lines which intersect the equipotential lines at right angles are plotted in Figure 8. Since electrons tend to follow flux lines, the area heated will be encompassed by the outermost flux lines. The heated area was determined to be 6.11 square centimeters from this plot. In a second method of evaluation, a 0.071-cm-thick molybdenum disk was subjected to steady-state electron bombardment from the heater and the temperature profile across the face of the disk was measured using optical instruments. A sketch of the disk and the temperature measurements are shown in Figure 9. The temperature gradient across the face was reasonably uniform and is in approximate agreement with the previous heater test data (Ref 1) from which the heat flux uniformity was estimated as $\pm$10%. A heated area of 6.49 sq cm was determined from observations of the disk and this area was used to calculate all heat flux values given in this report. Heat input to the evaporator was calculated from electrical measurements assuming that all of the electron bombardment energy and 40% of the filament heating power were absorbed by the evaporator. Calorimetric measurements with Heat Pipe 8 showed this input heat value was within 6% of the calorimetric value and therefore sufficiently accurate.

III, B, Test Apparatus and Procedures (cont.)

3. Test System

The test system used for the heat pipe testing was basically the same as that employed previously (Ref 1) and a schematic diagram of it is shown in Figure 10. The basic elements of the test system are a vacuum system, a bell jar, the heater power supply, the condenser coolant system, and a recorder for measuring thermocouple outputs. The entire heat pipe and heater assembly was enclosed inside a 46 cm dia x 76 cm high pyrex vacuum bell jar and evacuated to approximately 1.3×10^{-7} kN/m^2 during testing. The test facility was also equipped with an auxiliary vacuum and gas dispensing system to permit gas loading (Research Grade Argon) of the heat pipe. This auxiliary system included metering and control valves for pressure control of the system.

Auxiliary heaters (nichrome wire insulated with ceramic beads) were used for heating the condenser end during start-up and under special test conditions.

4. Test Procedures

The following general procedure was followed after "processing" or "wetting in" operations were completed:

(1) Preheat test device using radiation from filament until vapor temperature is 470°K. (Open gas port and adjust gas pressure to desired value prior to heating if device is gas-loaded.)

(2) Increase electron bombardment power to yield 100 watt/cm^2 heat flux. Add gas/water cooling to condenser load as needed.

III, B, Test Apparatus and Procedures (cont.)

(3) Adjust power density until stable condition is achieved. (The heat pipe temperature was controlled by the gas-pressure setting on the gas-loaded heat pipes and by the condenser thermal resistance in non-gas-loaded heat pipes.)

(4) Increase the heat flux incrementally until an evaporator wall temperature excursion is observed or some other testing limit is reached. Adjust gas/water coolant as needed for control of heat pipe temperature or the position of the vapor/gas interface.

III, Evaporator Wick Development (cont.)

C. SPECIFIC HEAT PIPE DESIGNS AND TEST RESULTS

1. Heat Pipe 8

a. Design and Fabrication

The Heat Pipe 8 design is shown in Figure 11. The evaporator wick design was the same as Heat Pipe 7 except that an additional liquid return wick was added near the center of the evaporator wick. As in Heat Pipe 7, the evaporator wick consisted of a 0.178-cm-thick layer of sintered nickel powder. The "center-feed" return wick bottomed out on the evaporator wall and was positioned so that the calculated wicking limit of the center and the outer annulus area of the evaporator were about the same (1300 watt/cm^2). The condenser and return wick structure were fabricated from 120 mesh nickel screen.

Other new features incorporated into this design were:

(1) A flexible condenser thermal resistance arrangement consisting of three separate cooling circuits.

(2) A 0.089-cm-thick evaporator wall which yields a more prototype evaporator thermal resistance than the 0.232-cm-thick wall utilized on most of the other heat pipes.

Evaporator wall instrumentation consisted of three 0.0254 cm diameter sheathed chromel-alumel thermocouples inserted into holes which were drilled so that junctions were located on the center line of the two evaporator regions and under the center feeder as shown in Figure 12. The thermocouple junction center lines were located about 0.0444 cm from the wick/wall interface.

III, C, Specific Heat Pipe Designs and Test Results (cont.)

Significant fabrication problems were encountered with Heat Pipe 8. These were related to: (1) the thin evaporator wall, (2) the small thermocouple diameter, (3) maintenance of uniform wick thickness, and (4) attempts to braze the evaporator wall thermocouples in place. Time consuming hand operations (polishing, lapping) were required to obtain a uniform evaporator wall thickness. In addition, the thin wall design was conducive to welding difficulties due to the small clearance between the thermocouple hole and the edge of the evaporator wall where a weld seam was required. A small thermocouple diameter was necessary because of the thin wall thickness and the required diameter thermocouple holes were difficult to drill because of the long lengths required.

It appears that the difficulty encountered in obtaining uniform wick thickness was related to furnace vibration and to the limited area available for pouring the powder onto the evaporator wall after the return wick/condenser wick assembly had been installed. The area through which the powder was poured is shown in Figure 13. Some improvement in thickness uniformity was obtained by changing furnaces; however, post-test inspection revealed that the problem had persisted and was difficult to detect when the heat pipe was assembled.

It was desired initially to braze the evaporator wall thermocouples in place so as to minimize installation errors. This was done in the first evaporator fabrication attempt. The thermocouples were brazed into the holes using a 40-nickel/60-palladium alloy (braze temperature - 1511°K or 2360°F) and the electron bombardment heater as a heat source. It appears that the braze alloy adversely affected the mechanical properties of the thermocouples as the thermocouples broke off during subsequent fabrication operations.

III, C, Specific Heat Pipe Designs and Test Results (cont.)

Heat Pipe 8 fabrication was completed using the following procedure:

(1) Electron Beam weld evaporator disk to the heat pipe cylinder.

(2) Assemble mesh screen liquid return subassembly into heat pipe cylinder.

(3) Cast nickel powder for evaporator wick into device.

(4) Braze condenser water loads into condenser area of heat pipe cylinder.

(5) Load heat pipe with solid sodium in a "dry box" (under argon atmosphere)

(6) TIG weld aft end cap (opposite the evaporator) in place.

(7) Install three evaporator thermocouples and five condenser thermocouples (no brazing).

The Heat Pipe 8 components are shown in Figure 14 prior to final assembly and Figure 15 shows the completed assembly.

b. Testing

Testing of Heat Pipe 8 commenced by "RCA processing" of the unit. During these processing operations, the heat pipe was slowly heated until the vapor temperature was about 1070°K and operated for about 1/2 hour with the small closure tube located on the aft end cap open so that a small amount of sodium could escape. The tube was then sealed. During initial processing of Heat Pipe 8, a sodium leak developed at the center evaporator thermocouple hole after the heat pipe temperature had been increased to about 1070°K. The unit was removed from the test mount and the leak was repaired by

III, C, Specific Heat Pipe Designs and Test Results (cont.)

welding. The assembly was then remounted vertically and processing was completed. The heat pipe was then remounted in a horizontal position and at this time it was observed that the evaporator had bowed outward approximately 0.05 cm. The evaporator was mechanically flattened and the device remounted for testing. During subsequent testing, the evaporator showed signs of poor performance since thermocouples No. 2 and 3 were substantially higher than expected as shown in the following sketch. A burnout of the evaporator wall occurred when the heat flux was 229 watt/cm^2 (1.4 Btu in.^{2}-sec) at the location noted. A photograph of the burnout is given in Figure 16.

HEAT PIPE 8

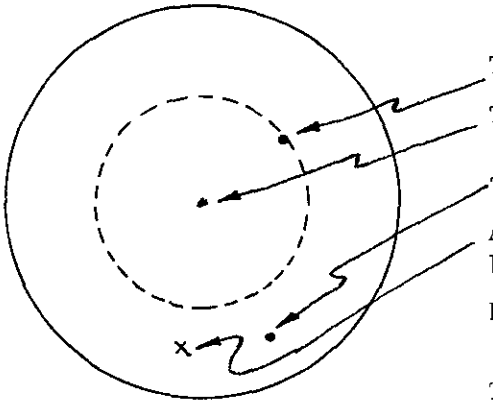

In post test operations, the sodium was removed and the evaporator was cut away from the heat pipe body. It is shown in post test condition in Figure 17. Examination of the wick showed that the nickel powder was very porous in the area of the center liquid return feeder. This porosity was almost symmetrical around the feeder and extended outward to the point of burnout. It appears that the porosity may have resulted from an intermetallic alloying reaction. Some reaction was also observed in the outer fluid return wick structure. This reaction probably occurred due to contamination of the heat pipe via the thermocouple hole in the evaporator

III, C, Specific Heat Pipe Designs and Test Results (cont.)

wall where the sodium leak was noted during initial processing. Another undesirable feature observed on the evaporator wick was that the thickness was not uniform and varied by about ± 0.04 cm from the nominal value. As a result of these irregularities, it is believed that a valid evaluation of the Heat Pipe 8 wick system was not obtained.

2. Heat Pipe 9 and 9A

a. Design and Fabrication

Preliminary thrust chamber design studies were conducted in parallel with the Heat Pipe 8 work. As a result of these studies and the difficulties encountered with Heat Pipe 8, it was decided that Heat Pipe 9 would be designed to incorporate features more applicable to the working model thrust chamber and less likely to produce testing problems. In the initial design considered for Heat Pipe 9, the liquid returned to the evaporator through feeder wicks which consisted of two rectangular-shaped screen structures formed by spot welding nine layers of 120 mesh screen together. As shown in Figure 18, the feeders were joined to the cylindrical condenser wick on one end and to plate-type wick holders on the other. These plate structures were positioned across the top of the 0.178-cm-thick sintered nickel powder evaporator wick in the manner shown in Figure 19 and were spot-welded to 0.025-cm-diameter wires cast into the evaporator wick. The condenser wick was constructed from four layers of 60 mesh screen.

The exterior configuration of Figure 20 was chosen for Heat Pipe 9 so that existing hardware could be utilized. The evaporator wall thickness was increased to 0.152 cm so as to avoid the thin wall fabrication problems and provide more structural rigidity. The evaporator wick was

III, C, Specific Heat Pipe Designs and Test Results (cont.)

sintered onto the evaporator wall before the wall was welded in place. The sintering of the wick was done inside a stainless steel mold so that good thickness uniformity was obtained.

The initial design was fabricated, and during the processing of it, severe sodium leaks occurred around the thermocouple to be used for the measurement of sodium vapor temperature. As a result of this difficulty, it became necessary to replace the entire wick assembly since interior contamination of the heat pipe was considered very likely to have occurred. Following a review of this problem and the initial design it was decided that the replacement heat pipe design, designated Heat Pipe 9A, would be modified in the following manner:

(1) The evaporator wall and vapor temperature thermocouples were deleted so as to eliminate the thermocouple fabrication problems and expedite the fabrication. Exterior thermocouples were added on the adiabatic wall above the evaporator for measuring heat pipe vapor temperature.

(2) Grooves into which the return wicks are placed were incorporated into the evaporator wick design so that some bowing of the wall could occur without disastrous results. The grooves were 0.076 cm deep and included shoulders near the edges of the evaporator wick so that a clearance of 0.005 to 0.018 cm was maintained between the bottom of the feeder and the bottom of the groove. This revised evaporator/feeder design is shown in Figure 19.

(3) The liquid return path provided by screen layers installed between the condenser and evaporator wicks along the cylindrical surface was interrupted so that liquid could return to the evaporator only through the screen-plate feeder.

III, C, Specific Heat Pipe Designs and Test Results (cont.)

The fabrication of Heat Pipe 9A was accomplished and the unit was loaded with 28 grams of sodium and "processed" at an average heat flux of 150 watts/cm^2. Loading and processing were done using essentially the same procedures outlined for Heat Pipe 8.

b. Testing

Heat Pipe 9A was tested in a horizontal position (evaporator vertical) with the two parallel liquid return feeders at about a 45° angle. Burnout of the evaporator wall occurred near the center of the evaporator at 234 watt/cm^2 (1.43 Btu/$in.^2$-sec) heat flux. Adiabatic wall temperatures of 858°K (1085°F) and 756°K (1085°F) were measured 0.3 cm and 2.2 cm above the evaporator surface at the maximum heat flux. Post-test examination revealed the raised area or "blister" in the evaporator wick shown in Figures 21 and 22.

It is believed that the burnout occurred because the liquid feeders did not operate properly and that the raised wick area was formed either by flashing of superheated vapor or by thermal stresses produced by local overheating of the wick. Furthermore, it is believed that the wick was wetted only in the immediate area of the feeders and that heat transfer within the evaporator consisted of conduction to the vicinity of the feeders and then sodium evaporation in the usual heat pipe manner (the adiabatic wall temperature data indicate heat pipe action did occur).

This postulated behavior is indicated by one-dimensional conduction calculations performed assuming that part of the wick is dry. For this condition, the temperature drop from the heated surface at evaporator midpoint to the feeders may be estimated from Equation 1 (nomenclature defined at the end of this report).

III, C, Specific Heat Pipe Designs and Test Results (cont.)

$$\Delta T = (\Delta T)\,\text{lateral} + (\Delta T)\,\text{axial} \qquad \text{Eqn (1)}$$

The (ΔT) axial value is the temperature drop that would occur if the evaporator operated normally and is given by:

$$(\Delta T)\,\text{axial} = \phi \left[\left(\frac{t}{k}\right)_{\text{wall}} + \left(\frac{t}{k}\right)_{\text{wick}}\right] \qquad \text{Eqn (2)}$$

The (ΔT) lateral value represents the temperature drop which occurs in the dry region of the evaporator in the direction perpendicular to the feeders and can be derived from an evaporator wall energy balance (neglecting axial conduction effects) as shown on Figure 23. The resulting expression is:

$$(\Delta T)\,\text{lateral} = \frac{\phi\, x^2}{2\, k\, t_{\text{eff}}} \qquad \text{Eqn (3)}$$

For Heat Pipe 9, the appropriate ΔT value was taken to be the difference between the melting point of nickel and the measured adiabatic wall temperature. Solving equation (1) for 2x (the total dry zone width) yields a value of 1.8 cm which corresponds to the 1.75 cm spacing between feeders. Therefore the conduction calculations indicate that the evaporator wick was dry. However, it is believed that heat pipe action occurred in a limited area in the vicinity of the feeder.

The inadequate feeder performance probably occurred because the pressure difference between the sodium vapor above the evaporator and the sodium liquid at the feeder outlet was too great for a meniscus in the groove to support. Consequently only a small area of the groove was available for feeding the wick and a correspondingly large pressure drop occurred in the liquid circuit at this point.

III, C, Specific Heat Pipe Designs and Test Results (cont.)

3. Heat Pipe 10

a. Design and Fabrication

The Heat Pipe 10 design incorporated the sintered evaporator wick and screen feeders utilized in Heat Pipe 9A; however, these two components were joined together utilizing a different fabrication technique. The design of the evaporator and the feeder/evaporator joint is illustrated in Figure 24. The evaporator wick structure was modified to include two ribs which protruded 0.1 cm above the wick surface. Four layers of 120 mesh screen were spot-welded together and cast into each rib to about the level of the evaporative surface. The liquid return feeders, consisting of twelve 120 mesh layers spot-welded together, were then spot-welded onto the four cast-in-place layers in a "tongue-in-groove" fashion. This design provides a continuous flow path for the returned condensate and removes the feeder/evaporator joint from the superheated region of the wick. In addition, it more closely approximates the liquid return design features of Heat Pipe 7. It was also necessary to utilize the 0.236-cm-thick evaporator wall used previously (Ref 1) so that 0.051-cm-diameter chromel-alumel thermocouples could be utilized for measuring evaporator wall temperature. These larger thermocouples were chosen because they are reliable, can be installed almost routinely, and provide adequate temperature data even though the installation error can become significant for high heat flux operation. Thermocouples were positioned at the evaporator midpoint and under one of the feeders at a distance of 0.122 cm from the wick/wall interface. The thermocouple positions are shown in Figure 25.

The condenser wick consisted of one wrap of 120 x 120 mesh screen covering the entire inside diameter of the heat pipe to within 0.63 cm of the evaporator surface and five wraps of 60 x 60 mesh screen in

III, C, Specific Heat Pipe Designs and Test Results (cont.)

the condenser area only. The feeder wick screen was connected directly to the condenser wick as shown in Figure 26. Other photographs of Heat Pipe 10 components taken prior to assembly are shown in Figure 27. During fabrication, the unit was loaded with 28 gm of solid sodium under an argon atmosphere.

b. Testing

Heat Pipe 10 testing was initiated by "processing" which consisted of the following series of events:

(1) The heat pipe was heated to 1090°K vapor temperature over a period of 2-1/2 hours. The closure orifice was open during this time and the heat pipe was vertical. The maximum heat flux was 164 watt/cm^2.

(2) The vapor temperature was reduced to 620°K and the closure orifice was sealed.

(3) The heat pipe was reheated to about 1070°K to verify sealing of the closure orifice (heating period approximately 2 hours).

The evaporator wall temperature at the maximum processing heat flux was uniform and somewhat higher than predicted as shown in the following sketch.

HEAT PIPE 10
(Processing)

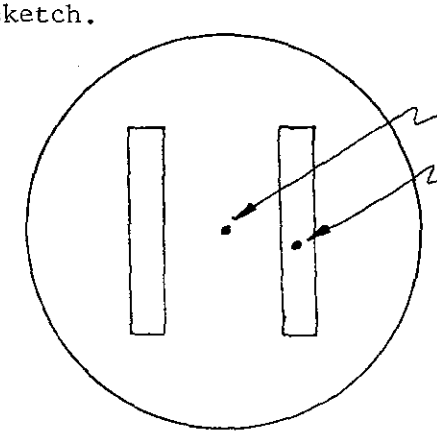

III, C, Specific Heat Pipe Designs and Test Results (cont.)

Following processing the unit was mounted horizontally (evaporator a few degrees above horizontal) and tested to a heat flux of 486 watt/cm^2 (2.97 Btu/in.^{2}-sec). Testing was terminated at this point due to an excessive wall temperature, 1475°K (2195°F) measured midway between the two liquid return feeders. The evaporator wall temperature distribution at this heat flux is shown in the following sketch.

HEAT PIPE 10

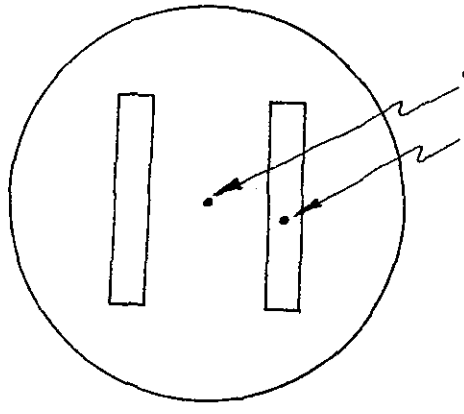

T1 = 1475°K (2195°F)
T2 = 1147°K (1605°F)
T_{vapor} (T4) = 909°K (1177°F)
Heat flux = 486 watt/cm^2
(2.97 Btu/in.^{2}-sec)
T_{1D} = 1149°K (1612°F)

The high evaporator midpoint temperature between feeders did not develop suddenly as a result of a temperature excursion but was consistently higher than expected as the heat flux was increased. This is shown by the test data graph of Figure 28 which shows measured and predicted ΔT_{wall} values as a function of heat flux. The wall temperature beneath the feeder appears normal throughout the test.

The high wall temperature at the evaporator midpoint is indicative of abnormal operation. If Heat Pipe 10 had been operating normally, all wall temperatures would have been about equal to the temperature calculated assuming one-dimensional conduction in the axial direction. The low temperature measured directly beneath one of the feeders indicates that the heat pipe was operating satisfactorily in the vicinity of the feeders and that the returned liquid may have been slightly subcooled. The one-dimensional model described by Equation (3) was applied to the Heat Pipe 10 results by assuming that the difference between T1 and T2 measurements is

III, C, Specific Heat Pipe Designs and Test Results (cont.)

representative of $(\Delta T)_{lateral}$. A "dry zone" width of 1.02 cm was calculated, indicating that the evaporator was not operating properly over about 65% of the open area between feeder ribs.

These indications of a dry zone are consistent with visual post test observations. Post test examination of Heat Pipe 10 revealed that it contained significant amounts of a black deposit consisting of very fine particles. Most of the deposits were found on the evaporator wick and were concentrated near the center of the evaporator region. The wick was deposit-free near the feeders. Small amounts of deposits were also found in the liquid return and condenser wicks. A cross-section of the evaporator revealed that some erosion had occurred within the sintered evaporator wick which significantly increased the pore size locally. The erosion was generally most severe where the black deposits were most dense.

Similar black deposits had been observed previously in Heat Pipe 5 and 6 but they were not as extensive as those found in Heat Pipe 10. Spectrographic analyses of these deposits were obtained and the results, shown in Table 3, indicated that the major constituent was nickel. Traces of other elements were also found and these are consistent with the impurities also found in the nickel materials. These results indicated that the black deposits were the result of nickel being dissolved by liquid sodium and left as a residue when the sodium vaporizes at the evaporator surface.

4. Heat Pipe 11

a. Design and Fabrication

After evaluation of the Heat Pipe 10 results, it was concluded that additional testing was needed to evaluate the black deposits

III, C, Specific Heat Pipe Designs and Test Results (cont.)

problem since it was not known whether these deposits were due to some accident of fabrication or whether a consistent and repeatable phenomenon was being encountered. In addition, at this point in the program a near term requirement for a heat-pipe-cooled thrust chamber existed and the high evaporator wall temperature characteristic obtained with Heat Pipe 10 was considered undesirable for a thrust chamber design. Reference to Equation (3) indicated that, even if the black deposit persisted in future work, the maximum wall temperature might be reduced to more acceptable levels by closer spacing of the feeders; consequently, a design similar to Heat Pipe 10 but with more closely spaced feeders was chosen for Heat Pipe 11. The Heat Pipe 10 design was modified by incorporating an additional feeder at the evaporator centerline so that the evaporator wick was fed by three feeders positioned on 0.876-cm centers. Drawings of the evaporator and the evaporator/feeder joint designs are shown in Figure 29 and a photograph of the evaporator wick after sintering and before final assembly of the feeders is shown in Figure 30. The evaporator wall was instrumented with 0.051-cm-diameter thermocouples as shown in Figure 31.

b. Testing

Heat Pipe 11 was processed in a manner similar to Heat Pipe 10. The heat pipe orientation was vertical and the temperature was increased to 1107°K over a 2-1/2 hour period before sealing the closure orifice. After sealing of the orifice, the pipe was reheated for 1 hr and 20 min to 1083°K vapor temperature. The maximum heat flux during processing was 180 watt/cm^2 and the evaporator wall temperatures' profile appeared normal at this condition as shown in the following sketch.

III, C, Specific Heat Pipe Designs and Test Results (cont.)

HEAT PIPE 11
(Processing)

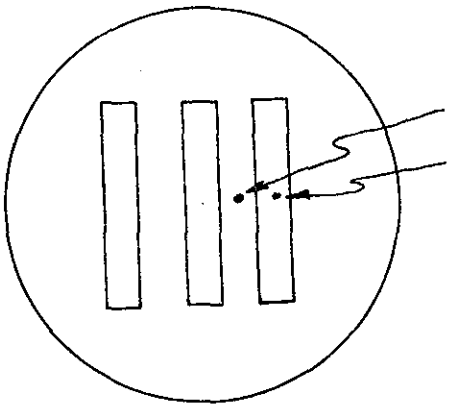

T1 = 1213°K (1728°F)
T2 = 1188°K (1680°F)
T_{vapor} = 1108°K (1535°F)
Heat flux = 180 watt/cm^2
T_{ID} = 1213°K (1828°F)

The unit was then oriented to a horizontal position and operated to 478 watt/cm^2 (2.93 Btu/in.^{2}-sec) heat flux. The test was terminated at this point because the evaporator wall temperature was becoming excessive and sufficient data had been obtained to evaluate the heat pipe performance. The test data at the maximum heat flux condition are summarized in the following sketch, and the evaporator wall temperatures are shown as a function of heat flux in Figure 32.

HEAT PIPE 11

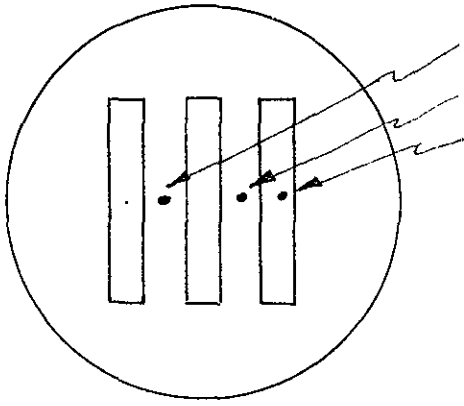

T3 = 1388°K (2041°F)
T1 = 1383°K (2032°F)
T2 = 1205°K (1712°F)
T_{vapor} = 925°K (1205°F)
Heat flux = 478 watt/cm^2
T_{ID} = 1186°K (1676°F)

The wall temperature data show that at the maximum heat flux the evaporator wall was much hotter at the midpoints between feeders than directly under the feeders. One of the midpoint temperatures, T1, showed nearly normal behavior up to 350 watt/cm^2 heat flux but the other, T3, was consistently high. The wall temperature under the feeder appears normal. Therefore, these

temperature data indicate that Heat Pipe 11 was similar to Heat Pipe 10 in that the evaporator functioned adequately in the vicinity of the feeders but not in the region between feeders. However, as expected, the No. 11 wall temperatures tend to be lower due to the decreased feeder spacing.

Here again, the evaporator midpoint temperature was sufficiently high to suggest that a significant amount of the input heat was conducted laterally within the evaporator wall toward the feeders. A dry zone width of 0.63 cm was calculated for Heat Pipe 11 from the one-dimensional lateral conduction model (Equation 3) and this represents 70 - 90% of the available evaporator surface area between feeders.

Posttest examination of Heat Pipe 11 revealed that it also contained substantial amounts of black deposits. Most of the deposits were concentrated near the center of the evaporator region; however, they were also found in the liquid return and condenser wicks. In one area a mound of deposits was found about 0.30 cm deep and 0.5 cm in diameter; however this was unusual as the deposit layer was generally rather thin (0.025 to 0.050 cm). Post test photographs of the Heat Pipe 11 evaporator are shown in Figure 33, Spectrographic analysis results obtained for the Heat Pipe 11 deposits were similar to the previous results (Table 3); i.e., the major constituent was found to be nickel. X-ray diffraction tests were also conducted on the black deposits but an exact determination of the constituents was not obtained. The results reported by RCA indicated an unidentified oxide was present. Tests conducted at ALRC indicated that NiO, Ni_2O_3, and $NaNiO_2$ were possible constituents and that the deposit could also be an alloy of the sodium-nickel-oxygen systems. Therefore, although an exact analysis of the black deposits was not obtained, the indications were that the deposits were related to the presence of oxygen contamination within the heat pipe.

III, C, Specific Heat Pipe Designs and Test Results (cont.)

Another factor which confused interpretation of the No. 11 data somewhat was that the electron bombardment heater characteristics were apparently changed when a water leak developed at the condenser cooling coils early in the test. Some significant differences in temperature readings were obtained by rotating the heater and retesting. However, the wall temperature data plot in Figure 34 shows that the temperature variations due to heater orientation were not sufficient to explain the consistently higher temperatures measured between feeders.

5. Heat Pipe 12

a. Design and Fabrication

Results from the Heat Pipe 10 and Heat Pipe 11 tests clearly demonstrated that the black deposits and erosion, or wick degradation, represented a serious heat pipe performance problem. After the Heat Pipe 11 testing and prior to the establishment of the Heat Pipe 12 design, all test results obtained on this contract were reviewed by JPL, ALRC, and RCA personnel. It was subsequently decided that additional heat pipe testing would be conducted and that the primary objective would be to eliminate the black deposits. (Final design and fabrication of a heat-pipe-cooled thrust chamber were deleted from the program plan at this point in the program.) The previous results most pertinent to the Heat Pipe 12 design (other than the Heat Pipe 10 and 11 results) were those obtained with Heat Pipe 7 (maximum heat flux = 4.9 Btu/in.^{2}-sec, normal evaporator wall temperatures). Heat Pipe 7 was fabricated using essentially the same procedures followed for Heat Pipes 10 and 11; but there were two notable design differences:

(1) Heat Pipe 7 had been the only heat pipe tested previously with argon gas loading.

(2) The Heat Pipe 7 evaporator wick was fed from the bottom of the condenser wick in an unheated zone. As a result of this feature, less screen was contained inside Heat Pipe 7 than inside Heat Pipes 10 and 11.

III, C, Specific Heat Pipe Designs and Test Results (cont.)

Argon gas loading was used as a device for controlling the vapor temperature in Heat Pipe 7, however it is possible that oxygen contaminants diffused into the argon during testing and were removed during subsequent decreases in the argon pressure. The amount of screen present was also judged to be important since screens are inherently difficult to clean due to the large number of overlapping wire joints. After the previous results were reviewed, it was agreed by the JPL/ALRC/RCA personnel that Heat Pipe 12 would be an inert-gas loaded version of Heat Pipe 10 so that the effect of gas loading could be evaluated. At this time the logic chart shown as Figure 35 was devised so that the results of Heat Pipe 12 testing would determine the direction of future testing.

The Heat Pipe 12 design and wall thermocouple locations are shown in Figures 36 and 37. The unit was inert gas loaded with argon and the evaporator wick and liquid return feeder design were identical to those of Heat Pipe 10. The outer shell and condenser hardware were those utilized with Heat Pipe 7. Heat Pipe 12 was also loaded with sodium using the dry box method.

b. Testing

Heat Pipe 12 processing was done in the same manner as Heat Pipe 10 and 11 except that testing difficulties prolonged the processing period so that the heat pipe was operated for over 12 hours before the closure orifice was sealed. The heat pipe was operated to 1116°K vapor temperature. Maximum heat flux during processing was 179 watt/cm^2 (1.1 Btu/$in.^2$-sec). The wall temperature data obtained at the highest processing heat fluxes are given in the following sketch.

III, C, Specific Heat Pipe Designs and Test Results (cont.)

HEAT PIPE 12
(Processing)

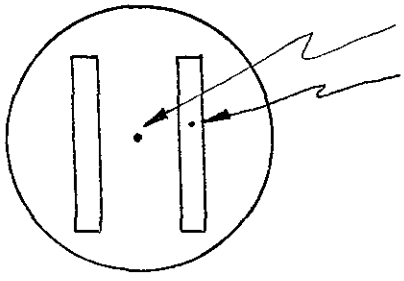

T1 = 1183°K (1670°F)
T2 = 1165°K (1645°F)
T_{vapor} = 1108°K (1535°F)
Heat flux = 179 watt/cm^2
T_{1D} = 1186°K

These wall temperatures appear normal as they compare well with predictions and the evaporator temperature distribution is relatively uniform. However, it appears that simple gravity flooding of the evaporator with excess sodium produced this uniform distribution and those noted previously for Heat Pipe 10 and 11 during processing (vertical position). In each of these heat pipes, an unusually high evaporator midpoint temperature was observed when the heat pipe was tested in a horizontal position.

After processing, Heat Pipe 12 was repositioned into a horizontal position and pressurized to 8 kN/m^2 pressure with pure research grade argon gas. A testing sequence which approximated that used for Heat Pipe 7 was employed. In addition, a procedure was followed in which the sodium was melted in the presence of argon, frozen, and then the argon was evacuated. This was done three times prior to testing.

Initial testing was done with water cooling of the condenser. However, with water cooling the argon/sodium interface tended to be too low on the condenser so that the area available for liquid flow away from the condenser was small and this tended to produce premature evaporator dryout. The problem was corrected by cooling the condenser with a less effective coolant. Some testing was done with argon and helium cooling but the maximum power level was limited due to high gas outlet temperatures. A system was

III, C, Specific Heat Pipe Designs and Test Results (cont.)

then devised in which nitrogen gas and water vapor were mixed and used as the coolant. With this system the argon/sodium interface could be effectively controlled and no power input limitations were experienced due to the coolant. The majority of the test data were obtained using the N_2/water mixture as coolant.

Testing was done at heat fluxes up to 607 watt/cm^2 and was eventually terminated due to an excessive wall temperature at the evaporator midpoint. The test data at the maximum heat flux are summarized in the following sketch.

HEAT PIPE 12

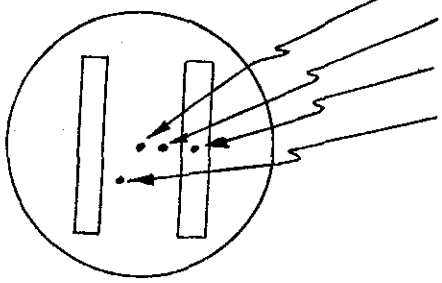

T1 = 1438°K (2130°F)
T3 = 1322°K (1920°F)
T2 = 1246°K (1780°F)
T5 = 1321°K (1920°F)
T_{vapor} = 850°K (1215°F)
T_{ID} = 1196°K (1550°F) (corrected for ΔT_{evap} = 80°K)

The wall temperature and heat flux data are given in Figure 38 and they indicate that the general performance characteristics of Heat Pipe 12 were similar to those of Heat Pipes 10 and 11. Relatively high wall temperatures were measured at the evaporator midpoint and normal values were measured in the vicinity of the liquid feeder. In comparing the data to predictions in Figure 38 it was necessary to account for the temperature drop at the evaporating surface, ΔT_{evap}, because calculations indicate this temperature drop is significant at the Heat Pipe 12 test conditions (T_{vapor} less than 873°K). The values estimated for ΔT_{evap} are shown in Figures 39 (Ref 3).

III, C, Specific Heat Pipe Designs and Test Results (cont.)

As was done previously, a "dry zone" width was calculated from Equation 3 using the measured evaporator midpoint-to-feeder temperature difference. The calculated value was 0.685 cm and comparison of this value to the 1.02 cm "dry zone" width previously calculated for Heat Pipe 10 (identical evaporator) indicates that the performance of Heat Pipe 12 was improved over that of Heat Pipe 10. This slight improvement is, of course, also indicated by the wall temperature data as shown in Figure 40. For example, at a heat flux of 500 watt/cm^2 (about 3 Btu/in.^{2}-sec), the No. 10 evaporator midpoint temperature is 593°K (576°F) higher than predicted while for Heat Pipe No. 12 the excess in temperature is 483°K (378°F).

The performance of Heat Pipe 12 was judged to be "fair" since it performed somewhat better than Heat Pipe 10 but not as well as Heat Pipe 7. It had been planned to retest the unit without gas loading (in accordance with the test plan logic shown in Figure 35); however, this was not possible because a sodium leak developed at the weld between the evaporator end cap and cylindrical shell. Consequently, it was assumed that no improvement in performance would have been obtained by testing without gas loading. The pipe was then opened for inspection and the foregoing assumption was justified because the pipe contained significant amounts of black deposits. The deposit was relatively light except in the center area of the evaporator where it was approximately 0.32 cm thick (this is where thermocouple T1 was located). Photographs of the interior components are shown in Figure 41. A thin black coating or stain was evident throughout the heat pipe. The stain on the condenser end cap and the thin layer of deposit on the liquid return feeders near the evaporator/return wick joint can be seen in Figure 41.

The sodium was removed from Heat Pipe 12 by evaporation. Thus, it was not necessary to introduce alcohol and water for reaction of the sodium (as was done for all the other heat pipes) and all deposits in the heat pipe remained as they existed during actual heat pipe operation. When Heat

III, C, Specific Heat Pipe Designs and Test Results (cont.)

Pipe 12 was removed from the test position, it was found that the evaporator had "bowed" inward by about 0.10 cm. It is not known when this deflection occurred.

Post test metallurgical examination of the Heat Pipe 12 evaporator showed an erosion pattern similar to that noted on Heat Pipes 10 and 11; however, the degree of erosion was much less. It was concluded from the Heat Pipe 12 test results that the contamination or wick degradation problem could not be solved merely by inert-gas loading the heat pipe. The performance did, however, appear somewhat improved, indicating some benefit had been obtained.

6. Heat Pipe 13

a. Design and Fabrication

Since the wick degradation problem persisted with Heat Pipe 12, it was decided that future work would consist of evaluating design concepts and fabrication techniques which would reduce heat pipe contamination. It was agreed by JPL, ALRC, and RCA personnel that the following design and fabrication features were desirable:

(1) Loading of the sodium into the heat pipe by distillation.

(2) Incorporation of a sacrificial evaporator to be used during processing only.

(3) Placement of oxygen "getters" inside the heat pipe.

(4) A reduction in the amount of screen used to fabricate the wick structures.

(5) The use of other structural materials for the heat pipe such as Nickel 270 (a higher purity nickel) or molybdenum.

III, C, Specific Heat Pipe Designs and Test Results (cont.)

The first three of these features were incorporated into the Heat Pipe 13 design which is depicted in Figure 42. The evaporator wick, wall, and instrumentation were identical to Heat Pipe 12. A sacrificial evaporator fabricated from a felt-type metal (the same material used previously in the evaporator of Heat Pipe 2) was positioned on the cylindrical wall between the condenser and evaporator wicks. The sacrificial evaporator was hydraulically joined to the normal evaporator wick but not to the condenser wick. It was planned that during the processing only the sacrificial evaporator would be heated so that sodium would flow through the normal evaporator to the sacrificial evaporator. The sacrificial evaporator was held in place by a zirconium retainer spring which acted as a getter material for oxygen inside the heat pipe. The sacrificial evaporator components consisted of a 0.107 cm thick layer of FM-1205, Feltmetal, approximately 1 meter of 0.05 cm diameter zirconium wire, and one layer of 120 x 120 mesh nickel screen. The inert gas loading feature was also incorporated into the No. 13 design, mainly because of the testing flexibility which this feature provides.

The sodium was loaded by vacuum distillation through the closure orifice previously used only for outgassing during processing. Solid sodium was first loaded into an evaporation pot in an argon atmosphere. The evaporation pot was then attached to the heat pipe as shown in Figure 43. With valve V1 (Figure 43) in a closed position and valve V2 in an open position, the evaporation pot was heated to approximately 1070°K for four (4) hours. Following transfer of the sodium the valve positions were reversed and the heater on the evaporation pot replaced with water cooling coils to trap any sodium vapor which might escape during processing.

b. Testing

During the initial processing operation, the sacrificial evaporator was heated by an electron bombardment heater specially constructed

III, C, Specific Heat Pipe Designs and Test Results (cont.)

for Heat Pipe 13 testing. After about one hour operation, when the average input heat flux had been increased to 70 watt/cm^2 (0.43 Btu/$in.^2$-sec) and the heat pipe temperature was about 920°K, sodium leakage was observed at a small burnout hole on the sacrificial evaporator wall. This local wall melting was the result of a heat flux concentration probably caused by nonuniform spacing of the heater wire or by wire temperature nonuniformities. Thermal radiation heating was then used to drive all the sodium from the heat pipe and in subsequent operations: (1) the hole was repaired by welding in an argon filled glove box, (2) the heat pipe was re-loaded by distillation, and (3) processing was completed, using radiation heating from the sacrificial evaporator heater (approximately 30 watt/cm^2 heat flux). It is possible that the wick structure was contaminated during this re-loading despite careful attempts to avoid it. The maximum heat pipe temperature during processing was reduced so that nickel solubility effects would be minimized. The maximum vapor temperature was 670°C and the total heating period was about 2 and 1/2 hours.

Upon completion of the processing the unit was tested in the same manner as in previous tests. Testing was terminated at 306 watt/cm^2 (1.87 Btu/$in.^2$-sec) heat flux when a thermal runaway was observed and melting of the evaporator wall occurred in the area directly beneath one of the feeders, in the vicinity of the T1 and T3 thermocouples. Consistently high temperatures were observed in this area during the testing.

After testing, Heat Pipe 13 was disassembled and examined. The parts are shown in post test condition in Figure 44. The post test inspection revealed 2 significant facts: (1) An insufficient amount of sodium had been transferred into the heat pipe due to accidental blockage of the distillation system by zirconium "getter" material placed inside the distillation pot. This sodium shortage probably caused the inadequate feeder performance. Twenty-four grams of sodium were found left in the

III, C, Specific Heat Pipe Designs and Test Results (cont.)

distillation pot whereas 40 grams had been loaded initially. Consequently, only 16 grams were transferred into the heat pipe and the minimum amount required for proper operation was about 30 grams. Because of this inadequate sodium quantity, the Heat Pipe 13 performance data are considered inconclusive. (2) Inspection of the heat pipe interior revealed the presence of black deposits on the zirconium retainer spring, within the condenser wick/feeder assembly, and on the evaporator wall. No black deposits were found on the sacrificial evaporator and it was noted that the deposit layer on the evaporator wall was much thinner than in previous heat pipes.

These observations indicated that the severity of the black deposits problem had been significantly reduced although the test results were clouded because of the low sodium quantity and because of the possibility of contamination during reloading after the sacrificial evaporator had burned out. The zirconium wire appeared to have performed its intended getter function (i.e., chemically tie up oxygen) because it was very black. The relatively clean appearance of the sacrificial evaporator indicates that either this material is not as susceptible to the degradation problem as sintered nickel powder, the proximity of the zirconium spring somehow prevented degradation, or that relatively high heat fluxes are required before the degradation occurs.

7. Heat Pipe 14

a. Design and Fabrication

Due to the inconclusive performance results obtained with Heat Pipe 13, it was felt that additional testing of this design was warranted. Consequently, the Heat Pipe 13 evaporator design was retained in Heat Pipe 14. The salvaged outer shell from Heat Pipe 13 was also utilized to fabricate Heat Pipe 14. One major design modification was made in that the

screen feeder wicks were replaced with platelet feeders. These structures were made by diffusion bonding together eight platelets onto which sodium flow channels had been photoetched. A typical platelet feeder and etched plates are shown in Figure 45. The platelet thickness was 0.02 cm and the channel depth was 0.0076 cm. The platelet feeder wicks are advantageous because they are more easily cleaned than screens. An additional design advantage of the platelet feeder is that the frictional pressure loss in the feeder wick is reduced from 50% to 2% of the total system pressure loss.

The screen condenser wick was formed by spot welding 4 layers of 120 mesh screen in a cylindrical shape. Fluid connection joints between feeders and the evaporator and condenser wicks were made by carefully spot welding 120 mesh screen layers in place as shown in Figures 46 and 47. Zirconium strips 0.6 cm wide x 10 cm long x 0.007 cm thick were installed on the interior side of the platelet feeders prior to loading of the sodium.

The completed Heat Pipe 14 is shown mounted on the RCA test system in Figure 47 (vacuum bell jar not shown for clarity). A view of the heat pipe assembly before welding of the end caps and sodium loading is shown in Figure 48. The two 0.63 cm tubes on the aft end of the heat pipe were used to connect the heat pipe to the sodium pot and vacuum system during loading. The tube between the heat pipe and pot was eventually crimped and welded off. An all metal valve (NUPRO Valve Model SS-4H), was installed on the other tube prior to loading and this valve remained part of the heat pipe assembly during loading and testing of the pipe.

The cleaning and final assembly procedures for Heat Pipe 14 fabrication were similar to those followed on previous heat pipes. The specific procedures for Heat Pipe 14 were as follows:

III, C, Specific Heat Pipe Designs and Test Results (cont.)

(1) Screen materials were subjected to a hydrogen furnace treatment at 1270°K for 1/2 hour at a pressure slightly above atmospheric before being used for wick fabrication. Prior to this, the screens were degreased, and rinsed with water and methanol.

(2) A shallow machine cut was taken on the ID of the Heat Pipe 13 body so as to remove all the material previously exposed to sodium.

(3) The completed wick assembly was heated in a hydrogen furnace at 1270°K for 1/2 hour.

(4) The wick assembly was welded onto the heat pipe body and the 0.63 cm fill and argon tubes were welded to the condenser end cap.

(5) The entire heat pipe was heated in a hydrogen furnace at 1170°K for 1/2 hour.

(6) Zirconium strips were spot welded onto each platelet feeder and the entire heat pipe was heated in a vacuum furnace at 1170°K for 1/2 hour.

(7) The condenser end cap was welded in place while flowing argon through the heat pipe via the 0.63 cm tubing. When this was completed the tubes were capped off and the unit was ready for sodium loading.

The sodium procedure was thoroughly reviewed and modified somewhat before loading of Heat Pipe 14. The significant modification consisted of utilizing a large ID fitting on the distillation pot so that the sodium could be loaded in larger solid pieces with relatively small surface areas. A smaller fitting was used on the No. 13 distillation pot and the sodium was rolled into a cylinder of the appropriate diameter before insertion into the pot. This rolling was done on a metallic surface which, although thoroughly cleaned, may have introduced oxides onto the metallic sodium.

III, C, Specific Heat Pipe Designs and Test Results (cont.)

Thirty-three grams of sodium were distillation loaded into Heat Pipe 14 with the system sketched in Figure 49. The loading procedure is outlined in the following paragraphs.

(1) Solid sodium was inserted into the sodium container or "pot". This was done inside a glove box under an argon atmosphere. The argon was filtered through drying agents (anhydrone, $Mg\,ClO_4$) before being introduced into the glove box. The sodium pieces loaded were cut from a cylinder of sodium with a lever-type knife. Any oxidized sodium was trimmed until the metal was bright and shiny. The metal was then cut into pieces of the appropriate size, weighed, and inserted into the pot. Strips of zirconium metal were previously placed inside the pot to scavenge any oxygen in the system. Handling of the sodium, exposure of it to the glove box atmosphere, and contact between the sodium and other metallic surfaces were minimized as much as possible. The pot was capped before removal from the glove box.

(2) The sodium pot and heat pipe were connected by a length of 0.63 cm stainless steel tubing and installed into the loading system. Atmospheric contamination of the sodium was avoided by purging argon through the heat pipe and into the pot as the cap was removed and the connection made.

(3) The heat pipe and sodium pot were evacuated to a pressure of 4×10^{-6} kN/m^2.

(4) Sodium transfer into the heat pipe was induced by heating the sodium pot to about 920°K. The temperature of the pot, transfer tube, and heat pipe were continuously monitored and the beginning of sodium transfer was evidenced by a sudden rise in the transfer tube temperature and a more gradual rise in the heat pipe temperature. About 45 minutes were required to transfer 33 grams. When the sodium transfer was completed, the tube temperature dropped dramatically and the pot temperature increased. Auxiliary heaters were used to maintain

III, C, Specific Heat Pipe Designs and Test Results (cont.)

the heat pipe temperature at about 500°K during transfer so that the condensed sodium would remain liquid and fill the entire wick assembly.

(5) When the transfer was complete, the sodium was frozen inside the heat pipe by flowing nitrogen gas through the condenser cooling tube.

(6) The heat pipe and pot were disconnected while argon flowed through the heat pipe and the pipe was capped and pressurized to about 35 kN/m^2 with ultrapure argon. The pot was then examined visually. No significant amounts of sodium were found and the zirconium strips were found to be discolored. The heat pipe was weighed and comparison to the weight measurement obtained prior to loading confirmed the amount of sodium transferred.

(7) The transfer tube was crimped, cut and welded off. The heat pipe was evacuated to 4×10^{-6} kN/m^2 to ensure that it was leak proof, and then pressurized to 35 kN/m^2 with ultrapure argon for shipping.

b. Testing

The initial testing of Heat Pipe 14 consisted of a "wetting in" treatment which was started by heating the evaporator with thermal radiation from the heater and cooling the condenser by radiation to the surroundings. The initial argon pressure applied was 6.7 kN/m^2. Electron bombardment heating and convective cooling of the condenser with a N_2/H_2O mixture were eventually added as the heat flux was increased to 123 $watt/cm^2$ (0.75 $Btu/in.^2$-sec) and the heat pipe temperature raised to 873°K over a 2 hour period. This heat flux level and a heat pipe vapor temperature of 873-973°K was then maintained for 1/2 hour.

During this wetting in treatment it was found that the Heat Pipe 14 design was very susceptible to plugging of the argon fill line

III, C, Specific Heat Pipe Designs and Test Results (cont.)

with sodium. Plugging could be detected by comparing the vapor temperature and argon pressure to the sodium vapor pressure curve and by evaluating the transient response of the heat pipe wall temperatures. In addition, condensation in the aft end could be detected by thermocouples attached to the end cap and the argon fill tube. Plugging of the argon line occurred before convective cooling was applied to the condenser. The line was cleared by heating the aft end and argon tube with an auxiliary heater and then suddenly pressurizing the argon tube to about 1 atm.

During subsequent testing, performance data for Heat Pipe 14 in the horizontal position was obtained during three separate test series. These data are summarized in Figure 50. During the first test series (data points 1a - 4a) the general operating characteristics were evaluated up to 280 watt/cm^2 (1.7 Btu/$in.^2$-sec) heat flux. The wall temperature data obtained indicate normal heat pipe operation. During this first test series it was noticed that sodium vapor to the aft end of the heat pipe was influenced by the condenser heat flux. When N_2 gas cooling only was used, significant sodium flow to the end cap occurred and when nearly 100% water cooling was utilized the end cap temperature was maintained at a low level. Evidently the argon/sodium vapor interface was more clearly defined at the higher condenser heat flux. The disadvantage of water cooling this particular design was that the argon/vapor interface existed near the evaporator end of the condenser due to the relatively high condenser wall conductance. As a result, the flow area available for liquid sodium returning from the condenser was limited.

The second test series was conducted utilizing water cooling and reasonably satisfactory results were obtained. The wall temperature data indicate normal heat pipe operation up to a heat flux of 433 watt/cm^2 (2.7 Btu/$in.^2$-sec) (data point 6). As the heat flux was increased from this

III, C, Specific Heat Pipe Designs and Test Results (cont.)

point (data points 7 to 19), an excess in evaporator midpoint temperature developed. The heat flux was eventually increased to 650 watt/cm^2 (4 Btu/$in.^2$-sec) where a 1200°C evaporator midpoint temperature was measured. It is believed that the high evaporator midpoint temperature was due to a localized dryout. The wicking limit had been estimated to be about 2000 watt/cm^2 (12.2 Btu/$in.^2$-sec) by assuming that the argon/vapor interface was positioned at the condenser midpoint or 4.45 cm from the evaporator end of the condenser. The data indicate that the interface was irregular and about even with the evaporator end of the condenser and consequently the frictional pressure drop in the condenser wick/feeder joint was much higher than anticipated.

Prior to the third test series it was decided that the plugging problem would be tolerated and that N_2 gas would be used to cool the condenser so that a more reasonable flow area would be available for sodium flow into the feeder. This was done and although the argon tube eventually plugged, data were obtained at heat fluxes ranging up to 440 watt/cm^2 (data points 21 - 24). The wall temperature data show that dryout occurred at a lower heat flux than during the previous test series, thereby indicating that the evaporator wick had degraded when the high temperatures were experienced during the first dryout. Testing with Heat Pipe 14 was terminated at data point 24 because it was clear that the dryout could not be "cured".

When the No. 14 testing was completed, the sodium was chemically removed. The wick assembly was then removed and it was found that the heat pipe was extremely clean and free from black deposits except for the zirconium strips which were discolored (grey to black). A very small amount of deposits were found on the evaporator wick surface above the region where dryout occurred, indicating some wick degradation, or erosion had indeed occurred in this area. It is believed that this small amount of

III, C, Specific Heat Pipe Designs and Test Results (cont.)

deposits developed after the initial dryout occurred and were formed when residual sodium in the dryout area dissolved portions of the sintered nickel wick when it became overheated (the wick temperature in the dryout area probably approached 1400 to 1500°K at the 650 watt/cm^2 heat flux conditions). The dissolved nickel was left behind as a residue when the residual sodium evaporated. The deposition was much less severe than in previous heat pipes, and might have gone unnoticed if the wick had not been examined closely. About 95% of the evaporator wick and all of the other heat pipe components were completely free of deposits and appeared to be in pre-test condition. Post test photograph of the No. 14 wick system are shown in Figure 51. A dry zone width of 0.38 cm was calculated from Equation (3) for the data point 24 conditions and this is in reasonable agreement with the diameter of the deposition zone and the hot wall zone evidenced on the heated surface of the evaporator wall.

Testing with Heat Pipe 14 produced 3 significant results:

(1) The <u>almost complete absence of black deposits</u> is the most significant test result since the wick contamination and degradation problem severely hindered progress toward the development of high heat flux wick systems during this program. The No. 14 heat pipe was operated above 870°K vapor temperature for 3.8 hours and therefore the contamination problem appears to have been solved by employing the loading and cleaning procedures described previously and by incorporating zirconium "getters" with significant surface areas inside the heat pipe.

(2) The <u>normal heat pipe operation</u> obtained up to 433 watt/cm^2 represents a significant achievement because a completely normal wall temperature characteristic such as this had not been observed since Heat Pipe 7 was tested.

(3) The <u>maximum test heat flux of 650 watt/cm^2</u> is the highest heat flux achieved during this testing program.

III, C, Specific Heat Pipe Designs and Test Results (cont.)

8. Heat Pipe 15

a. Design and Fabrication

Designs for Heat Pipe 14 and Heat Pipe 15 were chosen at about the same time and the fabrication of these 2 heat pipes was done in parallel. The Heat Pipe 15 design was similar to No. 14 except that the evaporator wick was constructed from alternate layers of 120 mesh and 200 mesh screen which were spot welded to each other and to the evaporator wall. The evaporator wick design is shown in Figure 52 . A screen evaporator design was chosen because:

(1) The screen wicks appear to be more easily fabricated into the shape required for a thrust chamber than sintered powder wicks.

(2) It is possible that sintered powder wicks may be more susceptible to the degradation problem (erosion, black deposits) than screen wicks because of the fine particle size and small pore size of the powder wicks.

(3) Scheduling and financial considerations precluded the fabrication of another sintered powder evaporator wick.

Platelet feeder wicks were also utilized for Heat Pipe 15. The feeders were fabricated from six platelets instead of the eight utilized for No. 14 because this simplified the evaporator/feeder joint design and the difference in sodium pressure drop was small. The evaporator/feeder joint design is shown in Figure 46 . The condenser wick was identical to Heat Pipe 14.

Two additional modifications were incorporated into the No. 15 design as a result of the testing problems encountered with No. 14:

III, C, Specific Heat Pipe Designs and Test Results (cont.)

(1) Two screen baffles were positioned in the adiatatic section above the condenser, so as to prevent flow of sodium vapor to the end cap. A 0.76 cm gap spacing was maintained on either side of the baffles which were fabricated from 1 layer of 120 mesh screen. A 90° pie section was cut from each baffle and these openings were oriented 180° apart so that sodium vapor could not flow straight to the end cap. The baffle nearest the end cap was positioned so that the opening lined up with the sodium fill tube. The baffles were hydraulically connected to the condenser wick by 2 layers of 120 mesh spotwelded onto the cylinder wall.

(2) The lower one inch of the condenser cooling jacket was thermally disconnected from the cooling circuit by shortening the coolant tube and by machining a circumferential groove through the nickel bars. This was done so that more area would be available for sodium flow from the condenser wick into the feeders regardless of where the argon/vapor interface was located.

Heat Pipe 15 was fabricated and loaded using essentially the same procedure followed for Heat Pipe 14. The furnace firing was altered somewhat in that the 1270°K H_2 furnace treatment of the completed wick assembly was deleted and the 1170°K vacuum furnace cycle was performed after the end cap was welded in place.

b. Testing

Heat Pipe 15 did not perform well due to mechanical failure of the bond between the evaporator wick and wall. The maximum heat flux achieved was about 80 watt/cm^2; however the evaporator was not functioning properly at this point since the wall-to-vapor temperature difference was 285°K and the predicted value is only 45°K. It appears that the evaporator wick failed at a heat flux less than 50 watt/cm^2. Post-test inspection revealed that the screen evaporator wick had separated from the wall and that a small gap existed between the wick and wall over the entire evaporator area.

III, C, Specific Heat Pipe Designs and Test Results (cont.)

During the initial testing, it was postulated that the poor performance was possibly caused by sodium plugging of the entire heat pipe in the region where the baffles were installed. Post-test inspection revealed this was not true; however as a result of the initial postulation, the aft end of the heat pipe was heated overnight so that any large sodium pieces would be melted and absorbed into the wick system. Consequently, the entire heat pipe was maintained at 670 to 870°K at low heat flux for a period of over 16 hours. This long heating period has significance because the sodium and the wick assembly were found to be extremely clean afterwards and this is an additional indication that the black deposit problem was solved.

III, D, Additional Discussion of Results (cont.)

evaporator wall temperatures were measured and it appears these were caused by dry zones in the evaporator wick which were not operating properly. The degradation failure mechanism is discussed in more detail in the next section of this report.

A logical extension of the dry zone hypothesis is that the evaporative heat flux is higher than the input heat flux as a result of the decreased surface area. For example, the evaporative heat flux estimated for Heat Pipe 12 was estimated to be 980 watt/cm^2 and evaporative heat fluxes in the range of 1630 watt/cm^2 were estimated for some of the other heat pipes as shown in Table 1 . These estimates are subject to error but they are indications that operation at the high input heat fluxes that exist in a rocket thrust chamber can be achieved with sodium heat pipes.

It is possible that sintered powder wicks may be more susceptible to the degradation problem than other wicks because of their small pore sizes (easily plugged) and nickel particle size (more easily dissolved than larger structures); however, further testing is needed to evaluate this possibility. Such a susceptibility would probably be influenced by sintering conditions and particle size. Experience on this program has shown that with other wick structures, a problem even more serious than degradation is encountered in that there is a tendency toward poor wick-to-wall bonding characteristics (Heat Pipe 15 for example) and poor thermal contact is the result. This mechanical bonding problem is probably most severe on flat wall evaporators such as those tested on this program. Screen wicks are still considered a potential candidate for thrust chamber applications since this bonding problem would be minimized for an annular heat pipe where a continuous screen wick is positioned on the OD of a cylindrical evaporator. It is believed that screen wicks merit further investigation for the annular geometry. For flat wall evaporators, sintered powder wicks and possibly screens sintered in place should be considered in future work.

III, Evaporator Wick Development (cont.)

D. ADDITIONAL DISCUSSION OF RESULTS

The following paragraphs present additional discussions of the heat pipe test results with respect to the failure mechanisms observed during testing on this contract and a photographic study of the sintered powder wicks. Detailed test data tabulations for the heat pipes tested on this contract are given in Table 2 and in the interim report (Ref. 1). A summary of the maximum heat flux conditions are given in Table 1 and a discussion of the specific test results is given in chronological order in Section II, C.

1. Heat Pipe Failure Modes

A review of all the heat pipe test results obtained on this contract indicated that each heat pipe tested could be categorized in terms of the failure mode which appear to have limited its operation. A total of six limiting modes were identified: (1) wick degradation (black deposits and erosion); (2) mechanical failure; (3) inadequate feeder joint operation; (4) wicking limit; (5) limits related to heat pipe temperature; and (6) insufficient sodium quantity. The apparent failure modes for each heat pipe tested on this contract are listed in Table 4.

It is apparent from this tabulation that early in the program (Heat Pipes 1, 2, 3 and 4) operation was limited either by mechanical failure or by limits related to heat pipe temperature (the onset of boiling within the evaporator wick is a possibility because these units were all tested at a quite high heat pipe temperature where the allowable superheat values are low (1)). The performance was improved substantially in subsequent heat pipes which incorporated sintered nickel powder wicks and relatively high heat fluxes were achieved with Heat Pipes 5, 7, and 14. The failure mode most consistently observed with sintered powdered wicks was wick degradation in the form of black deposits and wick erosion. Whenever wick degradation occurred, unusually high

III, D, Additional Discussion of Results (cont.)

2. The Wick Degradation Problem

Wick degradation is probably a potential problem for all high heat flux sodium/nickel heat pipes. The work on this program indicates it is caused by oxygen contamination since the problem was solved by adding features which tend to decrease the amount of oxygen present within the heat pipe. It is clear that this problem can be avoided in future work by following the fabrication procedures outlined for Heat Pipe 14 in Section II,C,7 and these are recommended for future high heat flux work.

Photographic studies of the degraded wicks were made so that the problem could be more fully evaluated. A series of micro-photographs of cross-sectioned evaporators from Heat Pipes 7, 10, 11 and 12 were combined to form a composite photograph approximately 38 times the normal evaporator dimensions. The center portions of these photographs are shown in Figure 53. The photograph of Heat Pipe 7 shows the burnout hole in the evaporator and the localized melting of the wick structure along the wick/wall interface. There is also evidence of erosion at this interface in areas away from the burnout hole. This erosion probably developed after the evaporator wall temperature excursion occurred as Heat Pipe 7 was operated for several minutes at a high wall temperature before burnout occurred (data shown in Figure 3). The photograph of device No. 10 shows a "layering" pattern in the wick which indicates that erosion and redeposition took place, moving from the interface toward the feeder or innersection of the heat pipe. The molecular structure of the wick has been altered in these areas where erosion has taken place. Large void areas are evident throughout the wick structure.

The photograph of device No. 11 shows evidence of severe erosion near the interface and in the area near the feeder returns. An enlarged microphotograph of a section of this area is shown in Figure 54.

III,D, Additional Discussion of Results (cont.)

The original interface between wick and wall is evident; however, it can also be seen that the nickel evaporator wall was eroded, and nickel solute redeposited on the eroded surface. Examination of the photograph of No. 12 shows a much lower rate of erosion, with erosion occurring only at the wick/wall interface. This device was operated to a heat flux of 605 watt/cm^2, total test time was also longer than most other devices tested, and it operated with lower wall temperatures than Heat Pipe 10 (identical evaporator). Thus, it appears that evaporator performance and the degree of contamination are directly related.

The wick degradation mechanism postulated is that the presence of oxygen or oxides within the heat pipe promotes the solubility of nickel in sodium and possibly the formation of nickel oxides and sodium nickelate. When the sodium evaporates, very small particles of nickel and the other materials are left behind as a residue on the evaporator surface. The effect of this process is possibly three-fold: (1) as the nickel is dissolved the capillary pumping pore is enlarged and the capillary action is reduced, (2) as the residue collects on the surface the surface pores can become plugged, (3) the presence of the residue may inhibit good wetting of the wick.

It is not clear which of these three effects predominates, but in either case a dry zone, or localized dryout in the evaporator can result. When such a dryout occurs, incoming heat must be conducted laterally to a point where sodium evaporation is taking place. As a result, high wall temperatures develop near the center of dry regions as predicted by Equation (3). The data summarized in Table 1 show that abnormally high wall temperatures and wick degradation occurred on Heat Pipes 5, 8, 10, 11, 12 and 13. The calculated dry zone widths shown for each heat pipe corresponds roughly to the areas in which black deposits were found after testing. The relatively thick evaporator wall utilized on this program (0.236 cm) was conducive to lateral conduction and consequently the heat pipes could be operated to a reasonably high heat flux

III,D, Additional Discussion of Results (cont.)

even though a dry zone existed. Heat Pipe 7 was fabricated and loaded in the same manner as those heat pipes which suffered wick degradation and it therefore seems curious that the problem did not develop in the No. 7 evaporator wick. It is possible that Heat Pipe 7 was not contaminated due to fortuitous loading circumstances.

The most severe deposition and erosion were consistently found near the midpoint between liquid feeders. This seems reasonable because, due to subcooling effects, most of the sodium evaporation normally takes place near the center region of the evaporator and therefore it is logical that most of the residue would be found there. Subcooling and two dimensional effects would tend to produce lower temperatures near the feeders, consequently the maximum wick temperature occurs at the evaporator midpoint. Nickel solubility in sodium increases with temperature, therefore it is logical that the most severe erosion would occur at the evaporator midpoint.

A review of background information that exists on the compatibility of nickel with alkali metals, indicated that two aspects of the corrosive behavior of nickel in sodium relate to the wick degradation problem (4). The first concerns the effect of temperature on the rate of corrosion. Up to 820°K, nickel is extremely resistant to attack by sodium, showing only negligible weight changes in long-time ($\sim$ 5000 hr) exposures in non-isothermal flowing systems. At about 870°K, however, nickel alloys begin to show much greater rates of mass transport and the condition is exaggerated with increasing temperature. Thus, dissolution of nickel by sodium is to be expected in systems operating at temperatures on the order of 1270°K. This explains the slight amount of deposits found in Heat Pipe 14. It appears that wick degradation will produce dryout and, conversely, the occurrence of dryout will promote wick degradation.

III,D, Additional Discussion of Results (cont.)

The second important feature regarding the behavior of nickel in sodium is that studies have indicated that unlike other metals, the solubility in sodium of nickel changes little as a function of the oxygen contamination of sodium up to relatively high levels of contamination ($\sim$500 PPM O_2). This tends to conflict with the postulated wick degradation mechanism; however, it is possible that the oxygen effects are more severe when the impurities existing in commercial grade nickel are present.

IV. INJECTOR DESIGN, FABRICATION, AND COLD FLOW TESTING

A. INJECTOR DESIGN

Injector design work consisted of conducting a preliminary design study for an OF_2/B_2H_6 injector, and establishing a completely finalized design for a FLOX/H_2 injector. These efforts are documented in the following sections.

1. OF_2/B_2H_6 Injector Design

a. Review of Previous Work

Initial efforts were devoted to reviewing previous design and test experience with OF_2 (or FLOX)/B_2H_6 injectors up to June 1970. A comprehensive summary of this experience was found in Reference 5. Pertinent details were also obtained from contractor reports (Refs 6, 7, and 8). and by personal communication with R. W. Riebling, the program technical manager. This review indicated that the pertinent OF_2/B_2H_6 injector design problems were: (1) solid deposits on the injector face and combustion chamber walls, (2) injector face heat transfer, and (3) inter-propellant heat transfer within the injector.

The solid deposits problem was considered the most critical and was therefore emphasized in selecting a design concept. The face heat transfer and inter-propellant heat transfer problems were also considered significant; however, it was felt that these problems could be effectively attacked once an acceptable concept from the point of view of solid deposition had been chosen. Some general aspects of the deposition problem noted during the review of previous work are listed below:

IV, A, Injector Design (cont.)

(1) Solids deposition appears to be time dependent.

(2) The solids are oxides of boron and elemental boron (probably the result of pyrolysis).

(3) When a fuel rich environment exists locally near the injector face, the occurrence of deposition appears related to the presence of recirculating oxidizer rich combustion gases and a relatively cool injector face.

(4) Stagnant areas such as the corner where the injector and chamber meet are subject to severe deposit buildup.

(5) Some evidence indicates that large contraction ratios produced heavier deposition; however, deposits have been observed at contraction ratios as low as 1.5/1.

(6) In one case, swirl injection of fuel film cooling resulted in a deposit free chamber wall.

(7) Deposits were eliminated in short duration tests when the fuel was injected as a gas, and when F_2 was utilized instead of OF_2.

(8) Small B_2H_6 flow passages are susceptible to internal plugging.

b. Concept Selection

As noted in Item 7, certain of the test data indicated gas/liquid or gas/gas injectors may be relatively deposit free. These types of injectors are applicable to the heat pipe thrust chamber since one or both of the propellants will be vaporized while cooling the condenser. However, the available JPL test facilities did not include equipment for producing gaseous propellants and the fabrication of a suitable heat exchanger was beyond the scope of this program. Therefore, checkout testing of a gas/liquid

IV, A, Injector Design (cont.)

or gas/gas injector could not be conducted prior to its use with a heat-pipe-cooled thrust chamber. Use of an untested injector for initial testing on a heat-pipe-cooled thrust chamber was considered undesirable, consequently a liquid/liquid OF_2/B_2H_6 concept was chosen.

Design concepts for liquid/liquid injectors were established which, in view of the previous test experience, appeared potentially applicable to the OF_2 (or FLOX)/B_2H_6 propellant system. The major design ground rules followed are listed below.

(1) Strive for an injection pattern in which the propellants do not mix near the cool injector face. The philosophy here is that the formation of boron oxides and elemental boron cannot occur at the face if there is no chemical reaction.

(2) Use swirl injection fuel film cooling for boundary cooling. This technique had been demonstrated to minimize wall deposits. Since it was desirable to conduct initial tests with a low heat flux, the criteria was established that the design must be able to function with up to 40% of the fuel used as film coolant.

(3) Incorporate void regions which will thermally isolate the two propellants within the injector. Thermal isolation was needed to reduce the possibility of freezing the B_2H_6 and vaporizing the oxidizer.

(4) Do not consider the self impinging doublet type injector because deposition problems have persisted with this design despite significant development work.

(5) Injector Operating Conditions:

4448 N thrust
689.5 kN/m^2 chamber pressure
3.0 overall mixture ratio

Five concepts were established; sketches of them are shown in Figures 55, 56, and 57, and they are discussed in the following

IV, A, Injector Design (cont.)

paragraphs. (These sketches are conceptual and do not indicate the most desirable fabrication technique or injection pattern).

(1) Impinging Sheet Concept

In the impinging sheet concept, the entire injector face is flooded with propellant. One propellant is injected radially outward along the face from a central spud, while the other is injected radially inward from the injector periphery. Both propellants flood the face locally and are deflected in an axial direction by a circular shaped ridge. Combustion occurs in an annular pattern where the sheets impinge. Injector face flooding is designed to prevent combustion products from reaching the face and provide thermal protection (film cooling) for the face. The preferred system is one which fuel is injected on the periphery so that a single manifold can be utilized for active and film coolant orifices. Detailed examination of this concept showed that the active fuel flow was not sufficient to provide adequate face coverage unless the active fuel was injected from the central spud. This configuration requires complex manifolding and produces an undesirable oxidizer rich environment adjacent to the film coolant. Therefore, this concept was discarded due to anticipated poor wall compatibility and manifolding complexity.

(2) Unlike Doublet Slot Concept

This concept was patterned after the impinging sheet injector which appeared promising in short duration tests at JPL. Unlike the JPL design, this concept provides for regenerative cooling passages within the face. Propellants are injected through slots, in unlike impinging pairs. The concept was discarded because: (1) the relatively large areas between slots appeared susceptible to the same deposition problem encountered

IV, A, Injector Design (cont.)

with like-on-like doublet patterns, and (2) experience at Aerojet indicates that unlike impinging FLOX/B_2H_6 injectors are difficult to face cool adequately by regenerative techniques.

(3) Vortex Concept

The vortex concept was considered because in short duration tests with OF_2/B_2H_6 it was relatively deposit free. In the standard vortex concept, oxidizer is injected radially from a center spud and all of the fuel is injected in a tangential direction near the radius midpoint or adjacent to the chamber wall. Excessive overheating of the center spud bottom was encountered with the previous OF_2/B_2H_6 vortex injectors. This area could possibly be regeneratively cooled by utilizing relatively thin walls and a contoured configuration at the bottom of the spud. The vortex concept was discarded for the current OF_2/B_2H_6 application because of the unknown character of the spud heat transfer environment and because of its inability to allow fuel film coolant variation.

(4) Modified Vortex Concept

In the modified vortex concept, the center spud would be replaced by self impinging doublet orifices. This design approach may eliminate the spud heat transfer problem but it is a relatively unknown system and this concept was discarded because of the lack of experience with it.

(5) Showerhead Tube Concept

In this design the face is flooded with oxidizer and fuel is injected through small tubes which extend from the injector face. The objective of this type of injection is to maintain combustion at a

IV, A, Injector Design (cont.)

substantial distance from the face so that recirculation patterns will not bring fuel in contact with the face. The oxidizer flooding of the face is intended to block the fuel rich gases from the face and provide face cooling.

This design concept was chosen for experimental OF_2/B_2H_6 injector work because it appeared capable of overcoming all 3 major OF_2/B_2H_6 injector problems: solid deposits, excessive face heating, and inter-propellant heat transfer. A similar concept was successfully employed with N_2O_4/Alumizine propellants at Aerojet (except fuel showerhead orifices were used instead of tubes) and a reasonably similar concept has been used with FLOX/Methane injectors (Ref 9). Burnoff of the fuel tubes is a potential problem in this design. The tubes must be thin walled and the diborane velocity within them sufficiently high that adequate cooling is obtained. An additional design problem is that an oxidizer rich environment exists adjacent to the film coolant and a sleeve arrangement for protection of the film coolant in the region between the injector face and the tube tip is required.

c. Detailed Design

A more detailed design which incorporated the showerhead tube concept was subsequently established and it is sketched in Figure 58 . A self impinging oxidizer doublet pattern was chosen as the method for achieving the flooded injector face condition and it was planned that two designs which incorporated different fuel tube configurations would be fabricated and tested at JPL. The final design was to have been established based on the results of these tests. However, the injector design work was redirected by the JPL technical manager toward the use of FLOX/H_2 propellants before the fully detailed designs were completed. The performance and heat transfer aspects of the showerhead tube design concept were evaluated and these are discussed in the following paragraphs.

IV, A, Injector Design (cont.)

(1) Performance Evaluation

The performance characteristics of the showerhead-tube injector shown in Figure 58 were evaluated analytically and the results are summarized in the following table.

Fuel Tube Diameter, cm	Oxidizer	T_{ox}, °K	T_{fuel}, °K	Estimated Energy Release Efficiency, ERE
0.094 (Figure 66) (0.037 in.)	OF_2	78	117	87.6
	OF_2	78	211	91.8
	OF_2	144	211	95.5
	FLOX (70-30)	78	117	91.0
	FLOX (70-30)	78	211	95.5
0.0478 (0.0188 in.)	OF_2	78	117	90.4
	OF_2	78	211	94.0
	OF_2	144	211	97.8
	FLOX (70-30)	78	117	93.6
	FLOX (70-30)	78	211	97.8

These results indicate that the major performance parameters are fuel tube diameter and propellant temperature. (The range of temperatures shown were those specified in the original program work statement). A significant performance improvement is predicted when the oxidizer is FLOX rather than OF_2 because of the higher volatility of FLOX. The 0.094 cm diameter tube was chosen because smaller diameters would yield a design with excessive fabrication costs. The desired energy release efficiency was 98% and the calculations indicate that this value would be approached with the 0.094 cm tube configuration when relatively warm B_2H_6 is utilized. It is possible that the performance increase produced by small orifices could also be obtained by modifying the tube ends to produce smaller liquid droplets.

IV, A, Injector Design (cont.)

(2) Injector Tube Heat Transfer

A heat transfer analysis of the diborane tubes indicated that two potential problems existed: (1) melting or burn-off of the tube tip, and (2) freezing of the diborane on the tube walls where the tubes protrude through the oxidizer manifold. The tip burn-off problem appeared to be the most critical. Heat transfer calculations indicated that if the tube were exposed to combustion gases at mixture ratio 3.0 the heat flux into the tube would exceed the diborane burnout heat flux and film boiling would occur. This is undesirable since estimates of the B_2H_6 film boiling characteristics indicated that if film boiling occurs the tube will melt. Due to the potential severity of this problem, the fuel tubes were shortened to 0.25 cm (0.10 in.).

Calculations for the inter-propellant heat transfer zone of the fuel tube indicated that at steady state the tube wall temperature would be above the diborane freezing point (108°K) and that the decrease in diborane bulk temperature would be negligible. A potential problem does exist at startup, however, if the injector is preconditioned to a temperature below 108°K. It is believed that this problem can be alleviated by avoiding very small orifices and by maintaining relativel high ($\sim$ 30 m/sec) B_2H_6 velocities. Furthermore, it is understood that the JPL test stand can supply FLOX higher than 108°K, therefore the possibility of freezing during startup can be eliminated for the initial testing by utilizing warm FLOX as the oxidizer.

2. <u>FLOX/H_2 Injector Design</u>

In order to economize testing costs, it was decided that the injector for the first heat-pipe-cooled thrust chamber would simulate OF_2/B_2H_6

IV, A, Injector Design (cont.)

combustion by utilizing liquid FLOX and gaseous hydrogen propellants. Consequently the injector work on this program was redirected to the extent that the injector would be designed and fabricated for use with liquid FLOX and gaseous hydrogen propellants. The gaseous hydrogen was intended to simulate the gaseous diborane which would be generated in the heat pipe condenser cooling jacket.

Checkout tests of the FLOX/H_2 injector were to be conducted by JPL prior to testing on the heat-pipe-cooled thrust chamber using the instrumented copper thrust chamber delivered by Aerojet to JPL under contract NAS 7-713 (Ref.10)(Aerojet P/N 1155930). The interior contour of the heat pipe thrust chamber was subsequently chosen to be identical to that of this copper chamber so that the experimental heat flux results would be directly applicable to the heat-pipe-cooled thrust chamber.

As a result of this redirection, the program was changed in the following manner: (1) work on OF_2/B_2H_6 injectors was stopped, (2) the experimental injector design work was deleted, and (3) a FLOX/H_2 injector was designed, fabricated, and delivered to JPL. The design which was established is shown in Figures 59 and described in the following paragraphs. Two adapter rings were also designed and they are shown in Figures 60 and 61. These adapter rings provide for installation of the injector onto the copper thrust chamber and for mounting the injector onto the JPL test facility at Edwards AFB. An assembly drawing for the injector, adapters, and thrust chamber is shown as Figure 62.

The design philosophy for the FLOX/H_2 injector is defined by the following list of basic design elements and the design ground rules chosen for each element.

IV, A, Injector Design (cont.)

	Design Element	Design Ground Rules
1.	Injector Operating Conditions	1. (a) Simulate OF_2/B_2H_6 Thrust Chamber Heat Fluxs
		(b) Allow Operation at Low Thrust Chamber Wall Heat Flux
2.	Injector Elements and Pattern	2. (a) Provide good wall compatibility
		(b) Use a proven concept
		(c) Performance level should be adequate (Design Goal is 92% c* efficiency)
		(d) Provide for separate film cooling circuit and adjustable GH_2 film coolant flow rate.
3.	Manifolding	3. (a) Provide uniform distribution of propellants.
		(b) Thermally isolate injector from the heat pipe and liquid FLOX from gas H_2.

These design elements and other pertinent aspects of the design are discussed further in the following paragraphs.

a. Injector Operating Conditions

(1) Nominal Mixture Ratio

The throat heat flux for a heat-pipe-cooled thrust chamber operating with FLOX/H_2 propellants at 689.5 kN/m^2 chamber pressure was estimated using the procedure described in the Interim Report (1). The results are shown in Figure 63 where throat heat flux is plotted as a function

IV, A, Injector Design (cont.)

of FLOX/H_2 mixture ratio for an engine operating at 4448 N thrust and 689.5 kN/m^2 chamber pressure and without any boundary cooling. Combustion temperature and generalized heat transfer coefficient are also shown. These results indicate that the FLOX/H_2 propellant combination will yield a good simulation of the OF_2/B_2H_6 thermal environment. The maximum heat flux is 930 watt/cm^2 (1260°K wall temperature) and occurs at a mixture ratio of about 5.0. This is nearly the same as the throat heat flux previously estimated for the OF_2/B_2H_6 engine without any boundary cooling (1000 watt/cm^2). Consequently, the 5.0 value was chosen as the nominal mixture ratio for the FLOX/H_2 injector.

(2) Film Cooling Requirements

Hydrogen film cooling requirements for low thrust chamber wall heat flux operation were also evaluated. Several analytical models of the film cooling process were considered during the course of the film cooling analysis because the heat pipe thrust chamber design is dependent on adequate predictions of both the maximum heat flux and the total heat transfer rate and therefore it is desirable to utilize the best model available. Predictions from the models considered are shown in Figure 64 for the case of 20% fuel film cooling. Much previous work at Aerojet had been based on the Entrainment and Seban models which are described in Reference 6. Initial work at Aerojet on Contract NAS 3-14343 led to the development of an improved film cooling model which can be approximated with a modified version of the Seban Model. This modified Seban Model was chosen as the best available model and was used in all subsequent calculations. Free stream turbulence effects indicated by the data of Reference 11 were included in the model and the final form used is shown in Figure 65.[1]

[1] Further improvements have been made in the film cooling model which will be described in the Interim Report for Contract NAS 3-14343 (scheduled for publication during November 1971).

IV, A, Injector Design (cont.)

.Heat flux predictions for the throat of the heat pipe cooled thrust chamber are shown as a function of film coolant flow rate and slot height in Figure 66. The slot height effect is mainly due to changes in the film-coolant-to-core-gas velocity ratio. A slot height of 0.076 cm was chosen for the FLOX/H_2 injector because this value can be obtained with conventional machining techniques and because it yields velocity ratios within the range of the data from which the analytical model was correlated (velocity ratio = 0.2 to 0.5 in the 10% to 25% film cooling range).

Adiabatic wall temperature distributions calculated for a 0.076 cm slot height and a range of film coolant rates were used in the calculation of the axial heat flux distributions shown in Figure 67. The heat flux values were calculated assuming that the heat pipe thrust chamber is designed for an 1260°K maximum evaporator wall temperature, 980 watt/cm^2 heat flux, and 895°K heat pipe temperature. The thermal network utilized is shown below.

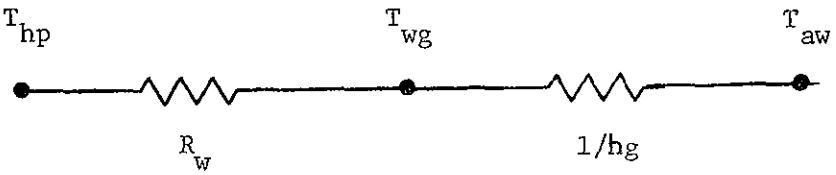

The maximum heat flux with 15% film cooling is 650 watt/cm^2. This is considered the maximum design heat flux for a heat-pipe-cooled thrust chamber at this time since the maximum heat flux capability demonstrated to date is 800 watt/cm^2 and a safety margin of at least 25% is desirable. For this reason, 15% film cooling was chosen as the nominal injector design condition. The Figure 67 heat flux distributions are discussed further in Section III, Preliminary Thrust Chamber Design.

IV, A, Injector Design (cont.)

b. Injector Element and Pattern

The 70% FLOX/H_2 propellant combination proceeds according to the following stoichiometry:

$$2\ F_2 + O_2 + 4\ H_2 \longrightarrow 4\ HF + 2\ H_2O$$

Its 13.4 stoichimetric mixture ratio implies that at the chosen design point (O/F = 5.0) 63% of the fuel acts as a diluent. Therefore, a primary injector design criterion is to select an injector element concept which most advantageously utilizes the excess fuel coolant to assure injector face and chamber wall compatibility as well as adequate performance. Four types of injector elements were considered: (1) coaxial, (2) fuel-oxidizer-fuel (F-O-F) triplet, (3) showerhead oxidizer and fuel, and (4) showerhead oxidizer with self-impinging fuel doublets. A sketch of these elements which is pertinent to the following discussions is shown in Figure 68.

The coaxial injection element design which has successfully been demonstrated in the past with the liquid oxygen/gaseous hydrogen propellant combination (RL-10, J-2, and M-1 engines)appeared to offer the highest potential for success with minimum development, and was therefore chosen for the FLOX/H_2 injector. This concept has a low velocity liquid oxidizer stream in the center which is sheared, atomized, mixed, and combusted by the high velocity GH_2 fuel in the annulus. The high velocity excess fuel surrounds the combustion zone on the element axis, thereby enhancing injector face and chamber wall compatibility.

The F-O-F triplet design concept, like the coaxial, uses the fuel to mechanically augment oxidizer stream breakup and mixing. The excess fuel forms parallel sheets on each side of the oxidizer spray fan.

IV, A, Injector Design (cont.)

While providing fair chamber compatibility, it may be less compatible than the coaxial near the injector face. It is possible to have some oxidizer splashback from the two edges of the oxidizer spray fan perpendicular to the fuel streams, causing face erosion, and chamber streaking may also occur where the oxidizer-rich lobe intersects with the chamber wall.

Both the all-showerhead and the showerhead oxidizer/self impinging fuel injection concepts were eliminated from consideration because of possible face erosion problems and lower performance than the coaxial or triplet for a given number of oxidizer elements. The showerhead oxidizer orifice is completely surrounded by a raw oxidizer-rich atmosphere. Due to the axial oxidizer stream injection velocity, a recirculation zone is created around each oxidizer jet which has resulted in face erosion with LO_2/GH_2 injectors in the past. Similarly, these showerhead oxidizer concepts are considered high risk designs from a face compatibility standpoint with $FLOX/GH_2$. Furthermore, to achieve 92% c* efficiency with 15% fuel film cooling would require a 0.0043 cm mass median droplet radius which would necessitate 185 showerhead oxidizer elements to achieve the required atomization efficiency.

Compared to the showerhead-tube OF_2 (or FLOX)/B_2H_6 injector performance analysis summarized previously, the $FLOX/H_2$ injector performance will be significantly higher. This is because FLOX has a much higher volatility than OF_2 at the same temperature. Furthermore, the need to atomize and vaporize the liquid B_2H_6 is completely eliminated by substitution of gaseous hydrogen as fuel.

It is desirable from a compatibility standpoint to have most of the FLOX vaporization and chemical reaction completed in the forward half of the 15.2 cm long convergent chamber section. This requires a mass median oxidizer droplet radius of 0.0015 cm based upon the Aerojet Liquid Rocket

IV, A, Injector Design (cont.)

Company's modified Priem propellant vaporization analysis. The necessary oxidizer atomization efficiency can be achieved with 15 to 30 coaxial or F-O-F triplet elements, provided a 240 to 420 m/sec fuel to oxidizer velocity differential mechanically augments the oxidizer spray breakup. A 25 coaxial element injector pattern was chosen which is analytically predicted to satisfy all of these requirements.

The above injector/chamber/propellant combination is predicted to achieve 99% energy release efficiency. At 5.0 overall mixture ratio, the nominal 15% fuel film coolant performance loss is predicted to be 2.4% for an overall c* efficiency of 96.6%. It is predicted that up to 38% fuel film cooling can be utilized and still satisfy the 92% efficiency requirement. The following table summarizes the performance analyses conducted for the FLOX/H_2 injector.

% FFC	0	15	25	38
$(O/F)_{core}$	5.00	5.88	6.67	8.00
η_{c*}	99.0	96.6	94.8	92.2
η_{I_s}	92.7	91.4	90.2	88.2
$\dot{w}_T$, kg/sec	1.01	1.025	1.035	1.06

One additional aspect of the FLOX/H_2 performance analysis is that based upon the use of gaseous hydrogen fuel and the calculated 70% FLOX vaporization profile, the FLOX/H_2 injector is predicted to have a 10% Rayleigh loss in the 1.56 contraction ratio, 15.2 cm conical chamber. Thus, approximately 768 kN/m^2 face pressure will be required to achieve 689.5 kN/m^2 nozzle throat stagnation pressure.

IV, A, Injector Design (cont.)

c. Manifolding and Mechanical Design

The mechanical design of the FLOX/H_2 injector design was heavily influenced by three design factors:

(1) Thrust chamber wall compatibility
(2) Heat transfer to the FLOX
(3) Peak thrust chamber heat flux

The injector design features which relate to each of these factors are discussed in the following paragraphs. Other notable design features not relating to the above three factors are:

Seal: The injector/chamber seal consists of a 347 stainless steel O-ring which is installed in a "V" groove.

Injection Tubes: The oxidizer injector tubes are fabricated in a one piece assembly, termed the element cluster, which is subsequently brazed into the injector body (see Figure 59, -3 detail).

Valve Interface: A valve seat which matches the geometry of the OF_2/B_2H_6 valve being developed at ALRC on Contract NAS 7-733 is incorporated on top of the injector at the oxidizer inlet.

(1) *Thrust Chamber Wall Compatibility*

Good thrust chamber wall compatibility is desired since the function of this injector is to provide a known heat flux source to the heat-pipe-cooled thrust chamber. In order to achieve good compatibility, the injector manifolding system was designed to yield as uniform a distribu- as possible. In order to assure uniform distribution, "tuning" orifices were

IV, A, Injector Design (cont.)

designed into each circuit so that they could be "tuned" during cold flow tests to yield satisfactory distribution before final assembly of the injector. In the fuel circuit, the circumferential distribution could be "tuned" by modifying the diameter of the feed holes through which hydrogen flows from the outer manifold to the inner manifold. The radial fuel flow distribution could be adjusted by enlarging the holes in the perforated plate. The flow in each oxidizer tube could be adjusted by enlarging the orifice diameter at the tube inlet.

Combustion analyses indicate that sufficient mixing of the oxidizer and fuel streams will occur before the outer element streams impinge on the wall and therefore significant streaking under the coaxial elements is not anticipated. However, the element spacing was chosen so that the elements can be positioned directly in line with the thermocouples installed in the walls of the copper thrust chamber so that streaking effects can be detected during the injector checkout tests.

An additional design feature influencing wall heat transfer is that the injector face protrudes 1.27 cm into the thrust chamber so that the wall in this region is exposed only to the film coolant. This provides an unheated zone for locating the thrust chamber flange and injector mounting studs.

(2) Heat Transfer to the FLOX

It is desirable to minimize heat transfer to the FLOX so that the operational problems associated with two phase oxidizer flow can be avoided. Three design features were incorporated to minimize heat input to the FLOX: (1) the hydrogen manifolding was arranged so that no direct conduction path exists between the FLOX and the heat pipe; (2), a void cavity was incorporated between the FLOX and H_2 circuits which provides thermal insulation between the FLOX and ambient temperature H_2 gas. This void cavity can also be used as an LN_2 flow passage for pre-fire chilldown of the injector; (3) silica phenolic insulation sleeves were selected for surrounding the injector bolts and reducing heat transfer into the injector body.

IV, A, Injector Design (cont.)

Heat transfer to the FLOX in the injector tubes from the hydrogen is expected to be relatively small. The pressure drop at the inlet orifices of the oxidizer tubes provide some protection against two phase flow oscillations since liquid FLOX will exist at the tube inlet even if 2 phase flow occurs in the downstream portions of the tube.

(3) Peak Thrust Chamber Heat Flux

An adjustable and predictable thrust chamber heat flux is desired so that the heat-pipe-cooled thrust chamber can be tested under specified heat flux conditions. The adjustable heat flux feature was incorporated into the FLOX/H_2 injector design by incorporating separate core fuel and fuel film cooling circuits. The injector is designed to operate at an overall mixture ratio of 5.0 with the fuel film cooling flow rate ranging from 5% to 25% of the total fuel flow. This yields a peak heat flux range of 326 to 895 watt/cm^2 (2 to 5.5 Btu/$in.^2$-sec).

d. Injector Hydraulics

The FLOX/H_2 injector consists of three separate hydraulic circuits which are provided for the oxidizer, main fuel injector, and fuel film coolant. The injector pattern consists of 25 co-axial injection elements.

(1) Oxidizer Circuit

The oxidizer inlet is situated at the injector axis, for symmetry. The oxidizer decelerates from an inlet velocity of 7.5 m/sec into the oxidizer plenum on top of the injector. A 0.140 cm diameter metering orifice is provided at the inlet of each oxidizer element. This metering orifice provides non-cavitating liquid flow control as well as

IV, A, Injector Design (cont.)

a method for calibrating each injection element during cold flow tests. The oxidizer element is step drilled for ease of fabrication and has a 0.140 cm injection tip diameter. The nominal injection velocity is 19.5 m/sec and the total oxidizer pressure drop is approximately 241 kN/m^2.

(2) Main Fuel Circuit

To minimize the fuel manifold volume and yet obtain relatively uniform fuel manifold distributions, two inlets are provided 180° apart and aligned with the fuel film coolant pie sections. Nominal fuel inlet velocity is 225 m/sec. The fuel is decelerated in the constant area circumferential manifold and then accelerated to 480 m/sec through the 20 cross feed orifices which feed the main fuel plenum from the circumferential manifold. Since the circumferential fuel manifold is above the plane of the radial fuel pie manifolds, the cross feed orifices can be directed at a 50° angle with the pie manifold plane. In this way a splash diffuser effect is obtained in that the high fuel cross feed velocity is dissipated.

The radial inflow velocity into the fuel plenum is approximately 195 m/sec. In order to minimize the plenum inlet cross velocity effect upon the fuel injection distribution, a perforated sheet metal plate, the diffuser plate, was provided at about the fuel plenum midpoint above the fuel injection elements. The nominal fuel velocity through the screen is 255 m/sec. This mild axial flow acceleration will tend to straighten out the radial fuel injection distribution and restrict the fuel recirculation zones to the upper half of the fuel plenum away from the fuel elements. Once through the perforated screen the fuel diffuses in the lower plenum providing all fuel injection elements with a relatively uniform feed condition. The fuel element design pressure drop is 217 kN/m^2 at 810 m/sec injection velocity.

IV, A, Injector Design (cont.)

(3) Fuel Film Cooling Circuit

The film coolant injection slot configuration produces a film coolant injection velocity of 510 m/sec at an 82 kN/m^2 injection pressure drop for the nominal 15% fuel flow rate. Since the film coolant circuit is much softer than the main fuel circuit, low film coolant manifold velocities must be utilized in order to minimize coolant maldistributions.

The two film coolant inlets are also situated 180° apart and aligned with the main fuel pie sections. The 240 m/sec inlet velocity is deadheaded against the main pie manifold and decelerated to approximately 120 m/sec in the circumferential manifold. The coolant velocity is progressively accelerated to 150 m/sec and 180 m/sec in the pie manifold and downfeed slots, respectively. The maximum velocity in the circumferential distribution manifold immediately above the coolant injection slots is 180 m/sec. Some circumferential nonuniformities are expected for the film coolant circuit; however, the variation is predicted to be within $\pm$ 8% of the nominal design flowrate.

e. Injector Heat Transfer

(1) Heat-Pipe-to-Injector Heat Transfer

The total heat transfer rate to the injector from the heat pipe thrust chamber was estimated to be 38.6 kW (heat pipe vapor temperature of 925°K assumed). The film coolant hydrogen absorbs 8.3 kW and the core flow hydrogen absorbs 30.4 kW. This yields maximum hydrogen temperatures of about 325°K for the film cooling circuit and 310°K for the core fuel flow.

IV, A, Injector Design (cont.)

(2) Interpropellant Heat Transfer

Heat can flow from the H_2 gas to the FLOX through the oxidizer injector tubes; however, the estimated heat transfer rate is small and the total FLOX temperature increase between the injector inlet and injector orifice is expected to be no more than 5°K. The FLOX saturation temperature at 689 kN/m^2 is 108°K; therefore if the inlet temperature is near 78°K the subcooling will be more than sufficient to prevent FLOX bulk boiling.

The heat flux estimated through the wall of the FLOX injector tubes is 260 $watt/cm^2$ based on the tube inside area. This is about equal to the FLOX peak nucleate boiling heat flux and therefore some subcooled film boiling may occur within the tubes. This is not expected to be a problem since the calculated void fraction is small ($\sim$0.5%) and the pressure drop characteristics of subcooled film boiling flows are not known to be such that peculiar flow behavior will result. Subcooled film boiling is beneficial from the standpoint that heat transfer from the hydrogen is minimized due to the low heat transfer coefficients associated with film boiling.

(3) Hot Gas to Injector Heat Transfer

Heating of the injector by combustion gases is not expected to influence the propellant temperatures within the injector but does control the injector face temperature. The maximum injector face temperature was evaluated with a 2-dimensional conduction analysis using the SINDA-3G computer program (12). Convective cooling by the H_2 gas in the injection orifices and on the backside of the injector were accounted for and a constant input heat flux on the face of 326 $watt/cm^2$ was assumed (about 1/2 the chamber wall heat flux with no film cooling). The maximum injector face temperature was determined to be an allowable 980°K.

IV, Injector Design, Fabrication, and Cold Flow Testing (cont.)

B. INJECTOR FABRICATION AND COLD FLOW

1. Fabrication

The FLOX/H_2 injector was fabricated in the following manner:

a. The injector element cluster was machined using EDM techniques prior to installation in the injector body and prior to final machining of the main fuel injection annulus surrounding each oxidizer tube. The completed element cluster is shown in Figure 69.

b. The injector body was machined using conventional procedures, the fuel manifolds were welded in place, and the injector element cluster was brazed in place.

c. Cold flow testing of the fuel circumferential feed holes, the film coolant distribution manifold, and the fuel injector orifices was done.

d. The injector face and oxidizer inlet orifices discs were brazed in place.

e. Cold flow testing of the oxidizer circuit was done.

f. The top and bottom covers were brazed in place, the ribbed film coolant slot and annular fuel orifices were EDM machined, and the backside fittings were welded on. Fabrication of the required adapters was also accomplished and the completed injector and adapter are shown in Figures 70 and 71.

A system for aligning the injector with respect to the thrust chamber wall thermocouples was devised which consists of aligning scribe marks on the injector adapter, chamber flange, and chamber wall. The alignment procedure is as follows: (1) position the injector-chamber adapter (Figure 79) with respect to the injector so that the chamber pressure fitting is in alignment with the scribe labeled "P_c" on the adapter (this alignment

IV, B, Injector Fabrication and Cold Flow (cont.)

remains fixed); (2) align the "P_c" scribe on the adapter with the "A", "B", or "C" scribe on the thrust chamber flange; (3) rotate the thrust chamber flange with respect to the thrust chamber so that the "A" scribe is in alignment with the "1" or "2" scribe on the thrust chamber wall. The combinations of thermocouple-orifice alignments which are obtained are indicated in Table 5.

2. Cold Flow Testing

Cold flow testing of the FLOX/H_2 injector was done to ensure adequately uniform propellant injection and the design was modified to some extent as a result of the cold flow tests. Flow testing of the main fuel and film coolant circuits was done with N_2 gas and the oxidizer circuit was flow tested with water. The cold flow work is described in the following paragraphs.

a. Circumferential Distribution in Fuel Circuits

The N_2 gas flow was measured in each of the feed holes which connect the outer fuel distribution manifold to the portion of the fuel plenum located directly behind the perforated diffuser plate. Initial data showed an irregular distribution in that the flow in the feed holes nearest the two fuel inlets was about 30% below nominal. This problem was corrected by enlarging the fuel inlet port diameter to 2.18 cm. After this was done, the measured flow in each feed hole was within 13% of nominal. The cold flow data and test conditions are given in Table 6 and the quadrant and feed hole nomenclature is diagramed in Figure 72.

The flow distribution in the four ports which connect the outer and inner film cooling manifolds was also determined by flowing N_2 gas. The flow in each port was found to be within 6% of the nominal and this was considered satisfactory.

IV, B, Injector Fabrication and Cold Flow (cont.)

b. Injector Face Propellant Distribution

The active fuel and oxidizer flow distributions were measured at the injector face using gaseous N_2 and water as simulants for the gas hydrogen and liquid FLOX propellants. The cold flow test setups are shown in Figure 73. For the final injector configuration, the propellant flow at each element was found to be within 6% of the average. The propellant distribution is listed in Table 3 (orifice nomenclature in Figure 74).

During initial flow tests of the oxidizer circuit, the flow through the outer row of orifices was irregular and non-uniform (orifices A1 through A12 in Figure 74). It was found that this was due to a peculiar manifold flow effect. A satisfactory flow pattern was obtained by increasing the oxidizer manifold thickness by 1/4 in. A 0.63 cm spacer ring was subsequently machined and incorporated into the oxidizer manifold design.

V. PRELIMINARY THRUST CHAMBER DESIGN

Preliminary thrust chamber design studies are documented in this section. This work consisted of further and more detailed evaluations of the heat-pipe-cooled thrust chamber design concept chosen previously [1]. The design studies are incomplete in some areas because the thrust chamber design work was de-emphasized so that efforts could be concentrated on the heat pipe testing described in Section III.

The chosen heat-pipe-cooled thrust chamber concept, illustrated in Figure 1 , consists of an annular sodium heat pipe fabricated from nickel. The interior surface forms the thrust chamber contour and is the heat pipe evaporator. The heat pipe condenser wall is located on the cylindrical OD of the heat pipe. The condenser is regeneratively cooled by diborane flowing in an appropriately designed cooling jacket positioned on the exterior of the heat pipe. The preliminary design work was broken down into 2 parts: (1) thrust chamber heat pipe design and (2) condenser cooling jacket design.

A. THRUST CHAMBER HEAT PIPE DESIGN

The initial configuration chosen for the thrust chamber heat pipe design is illustrated in Figure 75 . This configuration was established by combining the matchup requirements for the injector and the diffuser at the JPL test facility, and by choosing the internal contour of the copper thrust chamber planned for use in the injector checkout tests. The Figure 75 geometry allows for firing into a low back pressure and consequently includes a 5.6/1 nozzle expansion area ratio.

The heat flux distributions of Figure 67 define the thermal design requirements for the evaporator of the Figure 75 thrust chamber configuration. a significant feature of these heat flux distributions is that negative heat fluxes are shown near the injector for the film cooled cases. This indicates heat transfer out of the wall and into the film coolant. The "negative" heat

V, Preliminary Thrust Chamber Design (cont.)

flux estimated for the point adjacent to the injector is quite large and subject to considerable error since the hydrogen-to-wall film coefficient in this region is difficult to predict. The significance of this "internal-regenerative" effect is that sodium condensation will occur on the evaporator wall in this region and the heat pipe must be designed to facilitate this condensation. Further discussion of these calculated heat flux distributions is given in the injector design section of this report (Section III,A,2,a).

The heat transfer rates expected to be transmitted from the heat pipe wall to the film coolant (Q_{FC}) and from the heat pipe condenser to the regenerative cooling jacket (Q_{CJ}) are tabulated on Figure 67 . The cooling jacket heat transfer rates and the corresponding diborane outlet temperatures are listed in the following tabulation. (Assumptions: 133°K inlet temperature, 0.292 kg/sec flow rate, and 1380 kN/m^2 average pressure):

% Film Cooling	Q_{CJ}, kW	T_{out}, °K	
0	530	618	
5	479	580	
10	390	489	
15	306	378	
20	211	122	(saturated vapor)
25	151	122	(2 phase)

It was found that the design and fabrication of the working model design could be simplified a great deal without compromising the technical objectives of the program by designing the thrust chamber to operate at sea level. The configuration was subsequently modified and the pertinent design parameters for the modified configuration are listed below:

V. Preliminary Thrust Chamber Design (cont.)

1. Nozzle Expansion Ratio = 1.875
2. Nozzle Exit Diameter = (1.78 in.) 4.52 cm
3. Axial Distance Between Throat and Exit Plane = (2.0 in.) 5.08 cm
4. Static Pressure at Nozzle Exit = (13.5 psia) 93 kN/m^2
5. Cooling Jacket Flow Rate = (0.35 lb/sec)(Diborane) 0.158 kg/sec
6. Diborane Cooling Jacket Temperatures:
   Inlet = (240°R) 133°K
   Outlet = (660°R)(with 15% film cooling) 367°K
7. Design Operating Conditions as follows:

% Film Cooling	Maximum Heat Flux, $watt/cm^2$	Cooling Jacket Heat Transfer Rate, kW
15	650	156
25	326	54

The preliminary thrust chamber heat pipe design established by RCA is presented in Figure 76 . This design concept is based on a cast nickel powder evaporator wick with axial rectangular feeders. The feeders could be either the screen layer type design or the platelet type design which are described in Section II. The condenser wick is a screen mesh wick and is attached to the condenser wall. The condenser wall shown actually represents the inside diameter wall of the cooling jacket. Axial thermal expansion mismatch between the evaporator wick and the feeder sections is relieved by slotting the evaporator/feeder interface joint. Radial thermal expansion mismatch between the evaporator and condenser walls is relieved by forming full radius convolutions in the condenser end of the feeder sections. There are 30 feeders equally spaced radially about the evaporator giving a center-to-center feeder spacing at the thrust chamber throat of 0.76 cm. A condenser diameter of 30.5 cm was chosen for this preliminary configuration.

V, Preliminary Thrust Chamber Design (cont.)

Fabrication of the evaporator wick for the thrust chamber from sintered nickel powder will be substantially more involved than the wick fabrication performed for the cylindrical heat pipes discussed in Section II of this report. In order to evaluate this fabrication problem, the fabrication experiment wick design shown in Figure 77 was devised. The fabrication experiment wick consists of sintered nickel powder cast onto a cylindrical surface in three 120° sections (each section cast separately). Wick casting techniques would be developed and evaluated during the fabrication of this device.

An RCA radial heat pipe computer program was used to conduct the required design analyses. Initial efforts using this program provided design parameters not directly correlatable to the application since the program used a uniform heat addition/removal and constant diameter geometry. The actual device possesses varying cross-sectional input area and a varying heat flux rate along the thrust chamber axial length. Thus, a geometric shape and total thermal capacity of the heat pipe could not be established.

The RCA computer program for radial heat pipes was subsequently modified to enable the conditions of varying input area and heat flux to be accounted for. The program was modified by dividing the heat pipe into eight individual cells along the axial length of the heat pipe as shown in Figure 78. Thus, each cell was treated according to its respective input area and thermal flux. Using this approach, average vapor temperatures were calculated for normal and $\pm$ 30% heat input levels at the 15% and 25% barrier cooling conditions and for fluid temperatures of 870°K (1112°F) and 920°K (1200°F). The results are summarized in Table 8. Other design parameters were calculated for the 15% and 25% barrier cooling conditions at a fluid temperature of 920°K (1200°F) and they are summarized in Table 9.

V, Preliminary Thrust Chamber Design (cont.)

Gas-side wall temperature distributions for a film cooled heat pipe thrust chamber were determined to evaluate the possibility of freezing the sodium in the vicinity of the thrust chamber where the relatively cold (ambient temperature) H_2 film coolant is introduced. Gas-side wall temperatures calculated for representative values of wall thermal resistance and film coolant flow rate are shown in Figure 79. The gas-side wall temperature was found to be 220°K or more above the sodium melting point (370°K) in the region where heat flows into the film coolant (axial distance less than 7.6 cm for 25% fuel film cooling). Since the sodium temperature is always between the gas-side wall temperature and the heat pipe temperature, it is clear that freezing of the sodium cannot occur.

The use of OF_2/B_2H_6 or $FLOX/H_2$ as propellants presents a hydrogen rich atmosphere in the thrust chamber combustion area, particularly when boundary cooling is utilized. Hydrogen is capable of permeating through nickel at the range of wall temperatures anticipated. Sodium in the presence of hydrogen forms a hydride, NaH which reduces at approximately 1070°K (1472°F). However, there is no analytical evidence available to predict the effects of this reaction on critical parameters such as wetting angle. Limited test results obtained at RCA on cylindrical sodium heat pipes tested in a flame heat source indicated the heat pipes became "gas loaded" with H_2 when subjected to the flame for 1/2 hr to 2 hr periods. Operation of these heat pipes in a vacuum environment, using a different heat source, would remove the hydrogen. However, performance always appeared to be somewhat degraded following such operations. Therefore, a preliminary investigation was made to determine the approximate degree of hydrogen penetration into the heat pipe chamber at an operating temperature of 1070°K (1562°F). The calculations indicate that in a 1000 second test it is possible to accumulate up to 3.9 atmospheres of hydrogen in the heat pipe chamber. This estimate is extreme and was obtained assuming 100% hydrogen is available over the entire surface area of the thrust chamber and that none of the permeating hydrogen will escape from the heat pipe chamber during the 1000 second test. While neither of the assumed conditions is likely to prevail, the condition appears severe enough to warrant attention.

V, Preliminary Thrust Chamber Design (cont.)

The hydrogen gas which does permeate into the heat pipe will most likely escape at the low pressure end of the thrust chamber. With this in mind, it then becomes a question of what reactions take place during the time the hydrogen gas is present with the sodium and what heat pipe vapor temperature will prevail during the desired 15 minute operation. A study of the reactions between sodium and hydrogen from Reference 13 showed the following:

1. Sodium hydride forms with sodium in solid form.
2. Sodium hydride is not soluble in liquid sodium below 420°K (302°F).
3. Maximum temperature of formation is 470 - 620°K (392-662°F).
4. It forms as a white crystalline solid.
5. There is no melting point recroded but rather NaH appears to dissociate to N_a and H_2 fully before melting.
6. Thin layers of solid NaH form to impede further reaction, however, the layer dissolves in liquid Na above 420°K (302°F).

The dissociation pressure for NaH is given by the following equation which is plotted in Figure 80.

$$\text{Log } P \text{ (mm)} = A/T + B$$

where: $A = -6100$, $B = 11.66$, T = Temperature, °K

The thrust chamber heat pipe operating pressure will be on the order of one atmosphere and the temperature will be in the range of 870 to 1020°K(1100 to 1400°F). Therefore, according to Figure 13, it is doubtful that any solid NaH will exist for appreciable time intervals since decomposition of the NaH should occur as soon as it is formed. However, if solid NaH were to form it would form in the evaporator wick where it could impede the flow of sodium and for this reason, the hydrogen permeation has been a matter of concern.

V, Preliminary Thrust Chamber Design (cont.)

RCA has indicated that the H_2 permeation will probably have no effect on the operation of the thrust chamber heat pipe for relatively short firing durations (less than 2 minutes). However, they feel it is possible for operation to be impaired over relatively long time periods (10 to 20 minutes). The potential for hydrogen permeation can be eliminated by utilizing different thrust chamber wall materials (molybdenum for example) or by applying permeation barrier coatings such as aluminum oxide to the thrust chamber wall. Because of this potential problem, it is believed that future thrust chamber heat pipe designs should include adequate temperature and pressure instrumentation so that the heat pipe performance can be monitored during relatively long tests.

B. COOLING JACKET DESIGN

Preliminary cooling jacket design was initiated by the preparation of a computer program for the thermal design of the condenser cooling channels. Heat transfer within the cooling channel is relatively complex because the diborane will enter as a subcooled liquid and exit as a superheated gas and consequently some substantial variations in heat transfer coefficient can occur within the channel. The computer program was written assuming diborane as a coolant but it can be easily modified so that other coolants can be considered. The best available diborane physical properties were incorporated and interpolations and extrapolations of the properties data were made when necessary. The computer program was utilized to obtain the design analysis results presented in this section. A listing of the program and a brief summary of the formulation is given in Appendix A.

The initial thermal design calculations for the cooling jacket were performed assuming the 5/1 nozzle geometry shown in Figure 75. The initial results are shown in Figure 81 which show the relationship between condenser length and diameter (cylindrical shape assumed) for the 15% film cooling case.

V, Preliminary Thrust Chamber Design (cont.)

The parameters shown are coolant pressure drop and the ratio of condenser wall thermal resistance to the total cooling jacket thermal resistance.

The curves in Figure 81 were established by analyzing a series of cooling channel designs. The assumed configuration, shown in Figure 82, consists of a single constant width rectangular channel with a spiral flow path and linearly increasing flow area. A copper wall incorporating lands which act as conduction fins between channels was also assumed. (Additional wall thermal resistance can be provided by a grooved nickel cylinder brazed to the cooling jacket ID as shown in Figure 53 of the Interim report). In these initial calculations, the wall thermal resistance and inlet velocities values were established assuming an average coolant side heat transfer coefficient equal to the value at the channel inlet. The channel area ratio for which this assumption was true and the corresponding pressure drop were then calculated. The calculations showed that it is desirable for the flow area to increase along the channel length so that excessive gas velocities do not occur.

This initial design study indicated that the primary design variables are condenser diameter and wall thermal resistance. Spacecraft packaging constraints and propellant tank pressure limits dictate that the diameter should not exceed 25 to 30 cm and that the pressure drop should not exceed about 172 kN/m^2. It is desirable for a relatively large portion of the condenser thermal resistance to be contained within the wall due to the uncertainties involved in estimating the local heat transfer coefficient with two phase flow; however, the calculations show that large wall resistance values require large diameters or high pressure drop.

In subsequent work, the thermal analysis was revised to include the shorter chamber geometry and lower diborane coolant flow rate chosen for the sea level thrust chamber design. The initial calculations were also performed for the single channel, spiral flow, copper wall concept. This design has certain drawbacks, but was considered a good starting point for thermal design

V, Preliminary Thrust Chamber Design (cont.)

analyses. Fixed values of wall thermal resistance and a channel with constant passage width and land width were assumed since this represents the simplest spiral configuration to fabricate.

The results of the copper wall thermal analyses are summarized in Table 10 in which channel designs are listed for assumed values of condenser diameter and wall thermal resistance. The major design variables are inlet velocity and channel area ratio and the designs were established by finding combinations of these parameters which yielded the desired total heat transfer rate of 158 kW. These results show that smallest coolant pressure drops are obtained with relatively large condenser diameters and small values of wall thermal resistance. A condenser diameter of about 25 cm appears to provide a reasonable configuration.

For a given wall thermal resistance, the effect of increased diborane inlet velocity is to decrease the coolant pressure drop. This is because higher heat fluxes are obtained in the liquid diborane region and consequently lower velocities are required in the gas region where the pressure drop is high. The higher inlet velocities also yield a more uniform heat flux distribution along the cooling channel and this is advantageous in that it minimizes sodium cross flow in the heat pipe condenser wick. For example, for a 25 cm diameter condenser with 0.63 cm nickel wall, a 3 m/sec inlet velocity channel design would produce a $\pm$ 40% heat flux variation while the variation would be $\pm$ 20% in a 6 m/sec design. The drawback of high inlet velocities is that fairly large channel flow area ratios are required and this tends to produce excessive cooling jacket weight.

A critical review of the foregoing cooling jacket design concept indicated that braze joints between the heat pipe condenser wick and the cooling channels were undesirable since an unknown thermal resistance could easily be introduced if a 100% braze joint were not obtained. Consequently, a design concept incorporating an integral cooling jacket/condenser wall fabricated from

V, Preliminary Thrust Chamber Design (cont.)

nickel was chosen.

Thermal design results for the spiral flow, nickel wall concept were obtained and they are summarized in Table 11. The general trends are the same as noted for copper wall designs. Comparison of the Tables 10 and 11 results show that the nickel wall designs tend to have higher pressure drop due to the reduced fin effect produced by the land area between channels with nickel walls. The coolant pressure drop for a design with 3 spiral channels flowing in parallel is much lower than in a single channel design due to the lower L/D values obtained and this indicates that parallel circuits are advantageous. Cooling jacket weights were also calculated for the nickel designs. The weight values are strongly influenced by the assumed condenser wall thickness and therefore weight values shown merely indicate trends. A thicker wall tends to require higher coolant velocities and consequently smaller channels, lower weight and higher pressure drop. The trade off between weight and pressure drop produced by choice of wall thickness must be further evaluated before a final design is chosen.

The spiral cooling channel was also critically evaluated and it was established that this design concept involves lower pressure losses than axial flow designs due to the smaller turning losses. However, a potential disadvantage is that the spiral channel may tend to act as a liquid separator in the two phase region due to centrifugal force effects and this could influence the diborane heat transfer characteristics. For example, in the copper wall designs previously cited (25 cm condenser diameter, 0.63 cm nickel wall, 3 to 6 m/sec inlet velocity) the ratio of centrifugal forces to frictional forces was found to be about 5/1. The significance of the centrifugal effect is not known; however, it appears that axial flow designs should be evaluated in future work so that a choice between these two concepts can be made at a later date.

V, Preliminary Thrust Chamber Design (cont.)

The potential of diborane decomposition within the flow passages of the cooling jacket is a matter of concern because the occurrence of decomposition can lead to the deposition of solids and eventual plugging of downstream flow passages. In addition, shock sensitive "yellow solids" which are potentially hazardous can be formed during diborane decomposition. Diborane decomposition data at relative low temperature are available and these are summarized in Reference 14. Extrapolations of these low temperature data have been made and the results indicate that significant amounts of decomposition can occur during relatively short periods of time at temperatures over 366°K as shown in the following tabulation.

Temperature, °K	Time Required for 1% Decomposition, sec	Time Required for 10% Decomposition, sec
310	12,000	100,000
366	120	1,500
421	1.7	20
478	0.043	0.41

NOMENCLATURE

A	=	Area
$\bar{A}$	=	Average area
d_s	=	Cooling channel depth
f	=	Friction factor
g	=	Gravitational Constant
h	=	Enthalpy
h_{ave}	=	Average heat transfer coefficient
h_g	=	Gas side heat transfer coefficient
h_L	=	Coolant heat transfer coefficient
k	=	Thermal conductivity of nickel
L	=	Land width
ΔL	=	Distance between stations
P	=	Pressure
ΔP_f	=	Frictional Pressure Drop
Q	=	Heat transfer rate
Q_{CJ}	=	Heat transfer rate to cooling jacket
R	=	Reynolds number
R_w	=	Wick and wall thermal resistance
T	=	Temperature
T_{aw}	=	Adiabatic wall temeperature
T_b	=	Coolant bulk temperature
T_{hp}	=	Heat pipe or vapor temperature
T_{out}	=	Coolant outlet temperature
T_w	=	Coolant side wall temperature
T_{wg}	=	Gas-side wall temperature
ΔT	=	Temperature difference

ΔT_{evap} = Temperature drop at evaporative surface

$(\Delta T)_{axial}$ = Temperature drop along heat pipe axis

$(\Delta T)_{lateral}$ = Temperature drop perpendicular to heat pipe axis

ΔT_{radial} = Radial temperature drop

t = thickness

t_{eff} = Effective wall thickness = t wall + $\left(\frac{\rho W}{\rho N_i}\right)$ (t) wick

$\frac{\rho W}{\rho N_i}$ = Wick to solid nickel density ratio

U = Overall heat transfer coefficient

V = Velocity

W = Weight flow or coolant passage width

where:

x = Lateral distance from the evaporator midplane, in.

X = Quality

ρ = Density

$\emptyset$ = Heat flux

Subscripts

liq = refers to liquid

vap = refers to vapor

1 = upstream condition

2 = downstream condition

1D = one-dimensional conduction

REFERENCES

1. D. C. Rousar, Heat Pipe Technology for Advanced Rocket Thrust Chambers, Interim Report on Contract NAS 7-697, Aerojet Liquid Rocket Co., Report 697-I, July 1970

2. J. E. Deverall, J. E. Kemme, L. W. Florschuetz, Sonic Limitations and Startup Problems of Heat Pipes, Los Alamos Sci. Lab., LA-4518, Los Alamos, New Mexico, Nov. 1970.

3. Discussion of Heat Pipe Principles, RCA Corp., Electronic Components and Devices, Lancaster, Penn. (Code 661)

4. Development of Heat Pipe Technology for Advanced Rocket Thrust Chambers, RCA Corporation, ALRC Purchase Order No. L-800771, August 1971, Final Report

5. R. W. Riebling and others, A Survey of the Current Status of Thrust Chamber Technology for Oxygen Difluoride/Diborane Propellants, Paper No. 70-717, AIAA 6th Propulsion Joint Spec. Conf. San Diego, Calif. June 15 - 19, 1970

6. Report 659-F, Flox-Diborane Technology Boundary Reactions, Aerojet-General Corporation, Sacramento, California, September 1969

7. Report R7985, Fourth Interim Report: Chamber Technology for Space Storable Propellants, Rocketdyne, Canoga Park, California, September 1969

8. Davidson, D. L., Altitude Performance Evaluation of OF_2/B_2H_6 Propellant Combination, Report No. AEDC-TR-65-172, Rocket Test Facility, Arnold Engineering Development Center, Air Force Systems Command, Arnold Air Force Station, Tennessee, September 1965.

9. John W. Gregory, Flox/Methane Pump-Fed Engine Technology Review, Paper No. 70-718, AIAA 6th Propulsion Joint Spec. Conf. San Diego, Calif.

10. Advanced Injectors for Space Storable Propellants, Final Report on Contract NAS 8-713, Aerojet-General Corporation Report 713-F, 3 October 1969

11. L. W. Carlson and E. Talmor, Gaseous Film Cooling at Various Degrees of Hot Gas Acceleration and Turbulence Levels, AIChE Preprint 31, Presented at the Tenth National Heat Transfer Conference, Philadelphia, Penn., Aug 11-14, 1968

12. J. D. Gaski, L. C. Fink, T. Ishimoto, Systems Improved Numerical Differencing Analyzer, Users Manual, TRW Systems, Redondo Beach, California; Contract NASA 9-8289, September 1970

13. Mellor's Comprehensive Treatise of Inorganic and Theoretical Chemistry, Volume II, Supplement II, "Alkali Metals" (1962)

14. B. J. Waldmen, Fluorine-Hydrogen Performance Evaluation, Phase II: Space Storable Propellant Performance Demonstration, Rocketdyne Report R-6636-3, NASA CR-725542, April 1969

15. B. J. Waldman, Regeneratively Cooled Rocket Engine For Space Storable Propellants, Monthly Status Report for the Period 1 July 1970, Contract NAS 7-765, Rocketdyne Report PR 9268-2, July 1970

16. P. S. Giarratano, and R. V. Smith, "Comparative Study of Forced Convection Boiling Heat Transfer Correlations for Cryogenic Fluids", Advances in Cryogenic Engineering, Volume II, 492 (1966).

TABLE 1

SUMMARY OF HEAT PIPE DESIGNS AND TEST RESULTS

Heat Pipe	Wick Design Features	Evaporator Wick Thick., cm (in.)	Evaporator Wall Thick., cm (in.)	(4) Z, cm (in.)	Maximum Heat Flux w/cm²	Maximum Heat Flux Btu/in.² sec	T_{wall}, °C Evap Midplane	T_{wall}, °C Under Feeder	°C T_{ID}	°C T_{vapor}	Estimated Dry Zone	Remarks
15(1)(7)	Composite Screen 2 Platelet Feeder, 0.69 in. apart Blended Screen Evap. Joint	0.163 (0.064)	0.236 (0.236)	0.152 (0.06)	72	0.44	926	684	639	639	-	Evap. Wick separated from wall Posttest wick clean Zr strip on side of platelets
14(1)(7)	Sintered Nickel Powder(3) 2 Platelet Feeder, 0.69 in. apart "Tounge and Groove" Evap. Joint	0.178 (0.070)	0.236 (0.093)	0.152 (0.06)	433 652	2.66 4.0	930 1200	836 950	898 991	655 625	0.38 cm wide	Normal behavior to 433 w/cm² Posttest wick clean Zr strip on side of platelets
13(1)(7)	Sintered Nickel Powder(3) 2 Screen Feeders and Joint Same as 14 Sacrificial Evap. on Cyl. Wall	0.178 (0.070)	0.236 (0.093)	0.152 (0.06)	306	1.88	-	712	-	589	-	Insufficient sodium loaded Sacr. Evap. burnout Black deposits less extensive
12(7)	Sintered Nickel Powder(3) 2 Screen Feeders, 0.69 in. apart "Tounge and Groove" Evap. Joint	0.178 (0.070)	0.236 (0.093)	0.152 (0.06)	607	3.72	1165	973	(6)923	577	0.685 cm wide	Black deposits, wick erosion (8)$\phi_{evap} \simeq$ 1000
11	Sintered Nickel Powder(3) 3 Screen Feeders, 0.345 in. apart "Tounge and Groove" Evap. Joint	0.178 (0.070)	0.236 (0.093)	0.140 (0.055)	478	2.93	1115/1110	932	913	652	0.635 cm wide	Black deposits, wick erosion $\phi_{evap} \simeq$ 1600
10	Sintered Nickel Powder(3) 2 Screen Feeders, 0.69 in. apart "Tounge and Groove" Evap. Joint	0.178 (0.070)	0.236 (0.093)	0.122 (0.048)	486	2.97	1202	874	876	636	1.0 cm wide	Black deposits, wick erosion $\phi_{evap} \simeq$ 1100 to 1500
9	Sintered Nickel Powder(3) 2 Screen Feeders, 0.69 in. apart Plate-type Evap. Joint	0.178 (0.070)	0.152 (0.060)	0.152 (0.06)	234	1.43	Approx. 1450	-	725	600	1.8 cm wide	Inadequate Feeder Operation No black deposits
8	Sintered Nickel Powder(3) 2 Cylindrical Screen Feeders Feeders Bottomed Out on Evap. Wall	0.178 (0.070)	0.089 (0.035)	NA	228	1.4	(5)772	-	623	535	2.3 cm dia	Sodium leakage problem Severe wick erosion Some black deposits
7(2)(7)	Sintered Nickel Powder(3) One Cylindrical Screen Feeder Feeder Bottomed Out	0.178 (0.070)	0.234 (0.092)	0.152 (0.06)	797	4.9	1069	-	1051	608	-	Normal Wall Temperature No Deposits Feeders in Unheated Zone
5(2)	Sintered Nickel Powder(3) One Cylindrical Screen Feeder Feeder Bottomed Out	0.104 (0.041)	0.234 (0.092)	0.152 (0.06)	644	3.95	1132	-	990	709	0.76 cm dia	Black deposits at center of evap. Feeders in Unheated Zone.

(1) Sodium loaded by distillation.
(2) Heat pipes 5 and 7 tested on previous program and included for comparison.
(3) Nickel powder characterized by following information: Manufacturer - Sherrit Gordon Mines, Ltd, Fort Saskatchewan, Alberta, Canada
Designation - N161P1
Grade - E150 x 270
Density - 22% of Ni when sintered
Sintering Condition - Wet H_2 environment 1100°C temperature
(4) Z = Distance between thermocouple centerline and wick/wall interface.
(5) Measurement made at midplane of outer evaporator area.
(6) Corrected to account for temperature drop at evaporator surface.
(7) Denotes Argon gas loaded heat pipe
(8) ϕ_{evap} = Estimated Heat Flux at Evaporative Surface, watt/cm²

TABLE 2

TABULATED HEAT PIPE TEST DATA

HEAT PIPE 10 TEST DATA

Run	Q watts	Q/A watt/cm^2	T_1 °C	T_2 °C	Vapor T_4 °C
25	820	126	806	755	698
26	683	105	847	815	749
27	1421	219	919	777	659
28	1647	253	971	835	703
29	2190	337	1049	850	681
31	979	151	777	675	615
32	668	103	848	817	752
33	2389	368	989	788	617
34	2290	352	1043	810	635
35	2915	449	1163	853	646
38	1940	299	921	743	588
39	2500	386	1022	805	615
40	2890	445	1133	855	640
41	3101	478	1192	877	642
42	3152	486	1202	874	636

HEAT PIPE 11 TEST DATA

Run	Q watts	Q/A watt/cm^2	T_1 °C	T_3 °C	T_2 °C	Vapor T_4 °C
23	474	73	504	525	497	472
24	590	91	772	811	765	720
25	615	95	792	820	790	742
26	542	83.5	790	810	785	742
27	553	85	774	803	773	741
28	1432	220	809	861	768	650
37	1139	175	697	801	642	561
38	1682	259	777	861	716	604
39	2265	349	820	962	788	625
40	2855	440	1005	1068	868	642
41	3003	467	1092	1099	917	647
42	2432	374	987	1034	836	634
43	3024	465	1105	1110	926	652
44	3106	478	1110	1115	932	652

Table 2 (cont.)

HEAT PIPE 11 TEST DATA (cont.)

	Run	Q watts	Q/A watt/cm^2	T_1 °C	T_3 °C	T_2 °C	Vapor T_4 °C
(1)	46	2210	341	905	1042	765	615
(1)	47	2197	338	935	1082	763	595
(1)	48	2474	381	952	1092	796	616
(1)	49	2584	398	964	1095	808	620
(2)	52	2175	335	886	1082	750	667
(2)	53	2355	363	898	1107	761	618
	54	2353	363	1031	1045	840	624
	55	2892	446	1114	1094	916	651
	56	3016	465	1147	1107	950	667
	57	2318	357	1002	1025	856	638

(1) Heater Rotated 90°
(2) Heater Rotated 180°

HEAT PIPE 12 TEST DATA

	(1) Run No.	Total Power watts	Q/A W/cm^2	T_1 °C	T_2 °C	T_3 °C	T_4 °C	T_5 °C	Vapor T_6 °C	°C Δ Temp	Gas Press. kN/m^2
	* 3 BC	276	44	550	546	NR	517	NR	546	-	NA
	* 6 BC	424	65	678	677	NR	618	NR	647	-	NA
	*10 BC	910	140	850	865	NR	800	NR	812	-	NA
	*19 BC	1048	159	890	890	NR	820	NR	837	-	NA
	*30 BC	1162	179	910	892	NR	834	NR	843	-	NA
	*33 AC	825	127	842	854	NR	757	NR	797	-	NA
	*34 AC	924	142	866	876	NE	796	NR	808	-	NA
(2)	37 W	1185	183	820	768	780	660	788	657	10	8.5
	38 W	1958	302	954	836	860	668	902	661	12	8.5
	39 W	2386	360	971	820	851	625	902	607	25	4.0
	40 W	2470	381	971	820	852	609	897	583	40	2.7
	43 W	2480	382	1104	887	933	677	1000	653	15	8.0
	44 W	2532	406	1128	888	942	657	1028	625	22	5.3
	45 W	3146	485	1130	885	938	623	1010	577	50	2.7

(1) Letter In Run No. Denotes Coolant: W - water
(2) Heat Pipe Vertical, Test No. 37-65

* Processing Data, Heat Pipe Horizontal: BC - Before Closure
AC - After Closure

Table 2 (cont.)

HEAT PIPE 12 TEST DATA (cont.)

(1) Run No.	Total Power watts	Q/A W/cm^2	T_1 °C	T_2 °C	T_3 °C	T_4 °C	T_5 °C	T_6 °C	°C ΔTemp	Gas Press. kN/m^2
48 Ar	2205	340	960	830	865	670	887	657	13	8.9
51 He	1279	197	813	779	785	660	798	654	8	8.5
52 M	2628	405	1005	867	898	650	917	620	29	5.3
53 M	3183	490	1061	896	937	630	955	576	80	2.7
54 M	3378	520	1127	917	975	643	1002	594	48	2.7
55 M	3458	533	1142	930	1032	641	1043	577	75	2.7
56 M	3578	551	1137	932	997	643	1016	580	75	2.7
57 M	3830	590	1154	970	1042	658	1040	588	70	2.7
58 M	3936	607	1165	973	1049	687	1048	577	80	2.7
60 M	3372	520	1149	982	1047	697	1032	642	23	8.0
61 M	3019	465	1081	935	986	698	983	643	21	8.0
62 M	2797	431	1041	910	950	693	948	643	20	8.0
63 M	2797	431	1033	901	940	682	934	620	27	6.6
64 M	3214	495	1102	945	1000	693	989	620	29	6.6
65 M	3471	535	1156	986	1050	704	1043	623	32	6.6

(1) Letter in Run No. Denotes Coolant: Ar - Argon, He - Helium, M - N_2/H_2O Mixture

HEAT PIPE 13 TEST DATA

Q_{EB}	Q_{tot}	Q/A $watt/cm^2$	T_1 °C	T_5 °C	T_3 °C	T_2 °C	Vapor T_4 °C
-	150	23	576	583	595	586	401
216	366	56	629	625	649	645	589
868	1018	157	681	675	720	712	589
1850	2000	306	NR	725	795	791	587

Table 2 (cont.)

HEAT PIPE 14 TEST DATA

Data Pt.	(1) Q_{EB} watts	(1) Q_{total} watts	Q/A watts/cm^2	Vapor T_4 °C	T_1 °C	T_2 °C	Argon Press., mm Hg	kN/m^2
1a	531	695	107	600	656	656	20	2.7
2a	815	979	151	605	691	687	23	3.1
3a	1200	1364	210	615	742	730	23	3.1
4a	1660	1824	281	609	785	745	23	3.1
2	735	899	139	657	754	739	48	6.4
3	1170	1334	206	652	781	758	48	6.4
4	1710	1874	289	640	826	775	48	6.4
5	2290	2454	378	650	887	815	48	6.4
6	2640	2804	433	655	930	836	48	6.4
7	2900	3059	470	640	970	835	48	6.4
8	3200	3359	518	642	1061	852	48	6.4
9	3360	3519	542	640	1099	865	48	6.4
10	2630	2789	428	632	968	815	49	6.5
11	2690	2849	440	608	943	799	21	2.8
12	2980	3139	484	620	1000	824	21	2.8
13	3220	3379	520	622	1055	835	21	2.8
14	3440	3599	555	630	1103	860	21	2.8
15	3550	3709	571	615	1136	885	21	2.8
16	3640	3799	585	615	1128	872	15	2.0
17	3800	3959	610	617	1152	890	15	2.0
18	4000	4159	641	620	1184	925	15	2.0
19	4080	4239	652	625	1200	950	15	2.0
21	1320	1446	223	610	759	717	50	6.7
22	2100	2226	348	617	861	774	50	6.7
23	2370	2496	384	656	974	812	50	6.7
24	2730	2856	440	610	1035	798	50	6.7

(1) Q_{EB} = Electron Bombardment Heat Input

$Q = Q_{EB} + Q_{Rad}$

Q_{Rad} = Thermal Radiation Heat Input

TABLE 3

SPECTROGRAPHIC ANALYSIS RESULTS

(Technique used does not detect oxygen or oxides)

Sample	Major Constituents	0.1 - 1.0 wt %	0.01 - 0.1 wt %	0.001 - 0.01 wt %	0.0001 - 0.001 wt %
Heat Pipe No. 5 Black Deposit	Ni	Mn, Cu, Na	Al, Sn, Ti	Pb, Mn	-
Heat Pipe No. 6 Black Deposit	Ni	Cu, Na	B, Ti, Fe, Si	Pb, Mn, Mg	
Heat Pipe No. 10 Black Deposit	Ni	Cu, Na	B, Ti, Mn	Si, Mn, Al	
Heat Pipe No. 11 Black Deposit (See Note Below)	Ni	-	Ti, Si	Al, Cu, Fe, Mg, Pt	Pb
Typical Portion of Heat Pipe Cylindrical Walls	Ni	Mn	Mg, Fe	Si, Ti, Cu	Pb, Al
Typical Portion of End Cap Material	Ni	Mn	Fe	Si, Ti, Cu	
120 Mesh Screen and 60 Mesh Screen	Ni	Mn	Fe	Pb, Mg, Si, Ti, Cu	Al

TABLE 4

POSSIBLE FAILURE MODES

Failure Mode	Heat Pipe No.	Maximum Heat Flux watt/cm^2	Wick Type
Wick Degradation or Contamination (Erosion, Deposits, Apparent Dry Zone)	5	646	Sintered Powder
	6	262	Sintered Powder - Channel Composite
	8	229	Sintered Powder
	10	486	Sintered Powder
	11	478	Sintered Powder
	12	607	Sintered Powder
	13*	-	Sintered Powder
Mechanical Failure (Capillary Structure Separated from Evaporator)	1	146	Multi-layer 120 mesh
	2	519	Felt Metal
	3	371	Composite Screens
	4	199	Screen Covered Channels
	6*	-	Sintered Powder - Channel Composite
	15	80	Composite Screen
Wicking Limit	5*	-	Sintered Powder
	7	805	Sintered Powder
	14	652	Sintered Powder
Limit Related to Heat Pipe Temperature (Boiling Limit, Evaporation Limit)	2*	-	Felt Metal
	3*	-	Composite Screen
	4*	-	Screen Covered Channels
	7*	-	Sintered Powder
Inadequate Feeder Joint	9	233	Sintered Powder
Insufficient Sodium Quantity	13	308	Sintered Powder

*Denotes least probable limiting mechanism for heat pipes with more than one listed

TABLE 5

THERMOCOUPLE - ORIFICE ALIGNMENTS

P_c Fitting Position	"A" Scribe Position	Position of 30° Thermocouples
A	1	Under Orifice A6
A	2	Halfway between A6 and A7
B	1	Under Orifice A12
B	2	Halfway between A12 and A1
C	1	Under Orifice A11
C	2	Halfway between A11 and A12

Chamber Circumferential Position	Thermocouple Numbers (See Notes Below)
30°	21, 31, 41
90°	12, 22, 32, 42
180°	13, 23, 33
270°	24, 34
300°	25, 35
330°	46

NOTE: Thermocouple numbers marked on thrust chamber wall. First Digit in thermocouple number indicates axial position from adapter-chamber flange interface as follows:

First Digit:	1	2	3	4
Axial Position:	1.5"	3.0"	4.5"	6" (throat)

TABLE 6 - CIRCUMFERENTIAL FUEL DISTRIBUTION

Nominal W_i/W_{total} = 5%

QUADRANT	HOLE	INITIAL W_i/W_{total}, %	FINAL W_i/W_{total}, %
I	* 1	3.5	4.9
	2	5.5	5.25
	3	5.9	5.65
	4	5.6	5.45
	5	5.1	5.0
	Total	25.6	26.3
II	6	5.1	4.9
	7	5.2	5.3
	8	5.6	5.1
	9	5.4	5.15
	* 10	3.90	4.65
	Total	25.2	25.1
III	* 11	3.7	4.65
	12	5.2	4.8
	13	5.1	5.25
	14	5.20	4.95
	15	5.20	5.1
	Total	24.4	24.8
IV	16	4.7	4.65
	17	5.1	4.9
	18	5.6	5.0
	19	5.6	4.65
	* 20	3.8	4.7
	Total	24.8	24.2

* Adjacent to inlet

Test Conditions:

N_2 Flow Rate = 0.115 lb/sec = .052 kg/s
Inlet Pressure = 4.3 psig = 29.6 kN/m^2
Inlet Temperature = 43°F = 280°K

TABLE 7

FLOX/H_2 INJECTOR PROPELLANT DISTRIBUTION

Row	Orifice	$W_f/W_{f\ ave}$	$W_o/W_{o\ ave}$	MR/MR_{ave}	Nominal MR 15% FFC, MR_{ave} = 5.85
A	1	0.955	0.995	1.043	6.1
	2	1.0	1.028	1.028	6.0
	3	0.955	1.015	1.062	6.2
	4	0.985	0.995	1.01	5.9
	5	1.01	0.962	0.951	5.55
	6	1.045	0.985	0.97	5.7
	7	1.01	1.0	0.95	5.55
	8	1.005	1.0	0.99	5.8
	9	0.985	0.944	0.96	5.6
	10	0.99	1.015	1.06	6.2
	11	0.99	1.02	1.02	5.95
	12	0.98	1.03	1.08	6.3
B	1	0.985	1.05	1.07	6.25
	2	1.0	0.995	0.99	5.8
	3	1.0	0.97	0.97	5.7
	4	0.99	0.97	0.98	5.75
	5	1.0	1.0	1.0	5.85
	6	1.005	1.028	0.98	5.75
	7	1.0	1.005	1.0	5.85
	8	0.97	1.028	1.06	6.2
C	1	1.025	1.0	0.97	5.7
	2	1.02	0.995	0.97	5.7
	3	1.025	1.0	0.97	5.7
	4	1.02	0.984	0.96	5.6
D	1	1.025	1.025	1.0	5.85

Circuit	Fluid	Inlet Pressure kN/m^2 (psi)	Total Flow Rate, kg/sec (lb/sec)	Inlet Temp. (^oF)	^oK
Fuel	GN_2	29.6 (4.3)	0.052 (0.115)	(43)	280
Oxidizer	Water	226 (32.6)	0.69 (1.53)	(66)	292

(Chamber Pressure = Atmospheric pressure)

TABLE 8

CALCULATED HEAT PIPE VAPOR TEMPERATURES

Gas Side Boundary Condition	Fluid Temperature °C (°F)	Average Vapor Temperature °C (°F)
15% H_2 Film Cooling, Nominal Q	600/650 (1112/1200)	531/626 (988/1158)
15% H_2 Film Cooling, Q 30% Below Nominal	600/650 (1112/1200)	552/631 (1023/1167)
15% H_2 Film Cooling, Q 30% Above Nominal	600/650 (1112/1200)	(1)/620 ((1)/1147)
25% H_2 Film Cooling Nominal Q	600/650 (1112/1200)	573/638 (1064/1178)
25% H_2 Film Cooling Q 30% Below Nominal	600/650 (1112/1200)	578/640 (1070/1183)
25% H_2 Film Cooling Q 30% Above Nominal	600/650 (1112/1200)	568/636 (1053/1175)

NOTES: Q = Net heat transfer rate from combustion gases

(1) Not an allowable condition due to evaporation limitation

TABLE 9

THRUST CHAMBER HEAT PIPE DESIGN PARAMETERS

15% Barrier Cooling

Fluid Temperature = 650°C

Cell Profile - Axial Length = 1.0 in/cell

	#1	#2	#3	#4	#5	#6	#7	#8	Units
Power	-12.5 -13.2	4.84 5.1	15.40 16.2	22.5 23.8	28.2 29.8	31.26 33.0	32.1 33.9	29.2 30.8	BTU/sec kw
Power Density	-204	82	270	409	532	613	689	458	watts/cm^2
Evaporator									
Wall ΔT	-	20.3	66.9	101.3	132	151.6	145.9	113.9	°C
Mesh ΔT	-	20.9	68.9	104.1	135	155.2	149.8	117.7	°C
Inner Surface Temp.	-	691	785	855	917	957	945	882	°C
Vapor Temp.	-	646	636	627	618	612	615	625	°C
Condenser Thermal Resistance				0.660 0.348					°F-sec/BTU °K/kw
Total Power				172					kw
Axial Vapor Loss				4.56 x 10^{-4}					kN/m^2
Average Vapor Temp				625 1160					°C °F
Cond Q/A				84.3					watts/cm^2
Assumed diameter				(11.684) 29.6					(inches) cm
Area (15%)				1888 292					cm^2 in^2
Average Wall Loss				ΔT = RQ = 55.3 = 99.6					°C °F
Average Outer Wall				T_W = 625 - 55.3 = 570 = 1060					°C °F

TABLE 9 (cont.)

THRUST CHAMBER HEAT PIPE DESIGN PARAMETERS

25% Barrier Cooling

Fluid Temperature = 650°C

Cell Profile - Axial Length = 1.0 in/cell

	#1	#2	#3	#4	#5	#6	#7	#8	Units
Power	-23.9	-11.57	-2.34	4.52	10.81	15.0	16.96	18.2	BTU/sec
	-25.2	-12.2	2.47	4.76	11.4	15.8	17.9	19.2	kw
Power Density	-392	-196	-41	82	204	294	311	286	watts/cm^2
Evaporator									
Wall ΔT	-	-	-	20.3	50.5	72.7	77.0	71.1	°C
Mesh ΔT	-	-	-	20.8	51.8	74.4	79.0	73.4	°C
Inner Surface Temp.	-	-	-	692	752	797	806	794	°C
Vapor Temp.	-	-	-	646	640	635	633	635	°C
Condenser Thermal Resistance				.657 .346					°F-sec/BTU
Total Power				62.1					kw
Axial Vapor Loss				9.1x 10^{-4}					kN/m^2
Average Vapor Temp				63.7 1188					°C °F
Cond Q/A				15.45					watts/cm^2
Average Wall Loss				10.1 18					°C °F
Average Outer Wall				T_W = 637-10 = 627 = 1160					°C °F

Table 9
Sheet 2 of 2

TABLE 10

COPPER WALL COOLING JACKET THERMAL DESIGN RESULTS

One Circuit Spiral Channel Cooling Jacket Design
Copper Wall with Nickel Liner
1.27 cm Channel Width, 0.38 cm Land Width

Condenser Diameter, (in) cm	Wall Thickness, cm	V_{in} m/sec	ΔP kN/m^2	Channel Area Ratio	Channel Height, (in) cm
30.4	.216	1.5	6.9	6.3	1.62 - 10.3
30.4		3	6.2	16.6	.81 - 13.4
30.4		4.5	5.8	28.4	.54 - 15.4
30.4		6	5.5	40	.4 - 16.3
30.4	.635	1.5	16.5	3.8	1.62 - 6.2
30.4		3	14.5	10.4	.81 - 8.4
30.4		4.5	13.1	18	.54 - 9.8
25.4	.216	1.5	55	1.9	1.62 - 3.1
25.4		3	34.4	5.8	.81 - 4.7
25.4		4.5	27.6	10.8	.54 - 5.8
25.4		6	24.8	16.8	.4 - 6.8
25.4	.635	3	110	3	.81 - 2.4
25.4		4.5	99.5	5.8	.54 - 3.1
25.4		6	79.3	9.2	.4 - 3.7
22.8	.216	3	117	2.9	.81 - 2.3
22.8		4.5	83	5.65	.54 - 3.1
22.8		6	68.9	9	.4 - 3.7
22.8		7.5	67.5	12.7	.325 - 4.1
22.8	.635	4.5	317	3	.54 - 1.6
22.8		6	268	4.7	.4 - 1.9
22.8		7.5	228	6.75	.325 - 2.2
20.3	.216	6	241	6.6	.4 - 2.7
20.3	.216	7.5	201	6.6	.325 - 2.1
20.3	.216	9	193	8.7	.28 - 2.8

TABLE 11

COPPER WALL COOLING JACKET THERMAL DESIGN RESULTS

		1 Circuit Design W = 1.27 cm L = 0.635 cm			3 Circuit Design W = .635 cm L = .318 cm		
Condenser Diameter, cm	V_{in} m/sec	Channel Height, cm	P kN/m^2	Wt. kg	Channel Height, cm	P kN/m^2	Wt. kg
30.4	1.5	1.62 - 2.03	114	22.4	1.08 - 5.5	13.8	
30.4	3	.81 - 3.25	75	24.8	.54 - 7.0	12.4	42.3
30.4	4.5	.54 - 3.93	69	26.3	.36 - 7.6	12.4	
30.4	6	.4 - 4.4	65.4	28	.27 - 8.1	13.1	48
30.4	7.5	.32 - 4.9	64.7	30.2	(wt. excessive)		
25.4	1.5	(ΔP excessive)			1.08 - 2.5	42.7	
25.4	3				.54 - 3.5	33	20.9
25.4	4.5				.36 - 4.0	31.7	
25.4	6	.4 - 2.3	193	16	.27 - 4.5	33	24.1
25.4	7.5	.32 - 2.5	186	16.6	(wt. excessive)		
25.4	9	.27 - 2.7	180	17			
22.8	1.5	(ΔP excessive)					
22.8	3				.54 - 1.3	165	10.4
22.8	4.5				.36 - 2.0	124	
22.8	6				.27 - 1.86	114	11.4
22.8	7.5				.216 - 2.07	110	

NOTE: W = Channel Width

L = Land Width

Condenser Wall Thickness = 0.10 inches = .254 cm

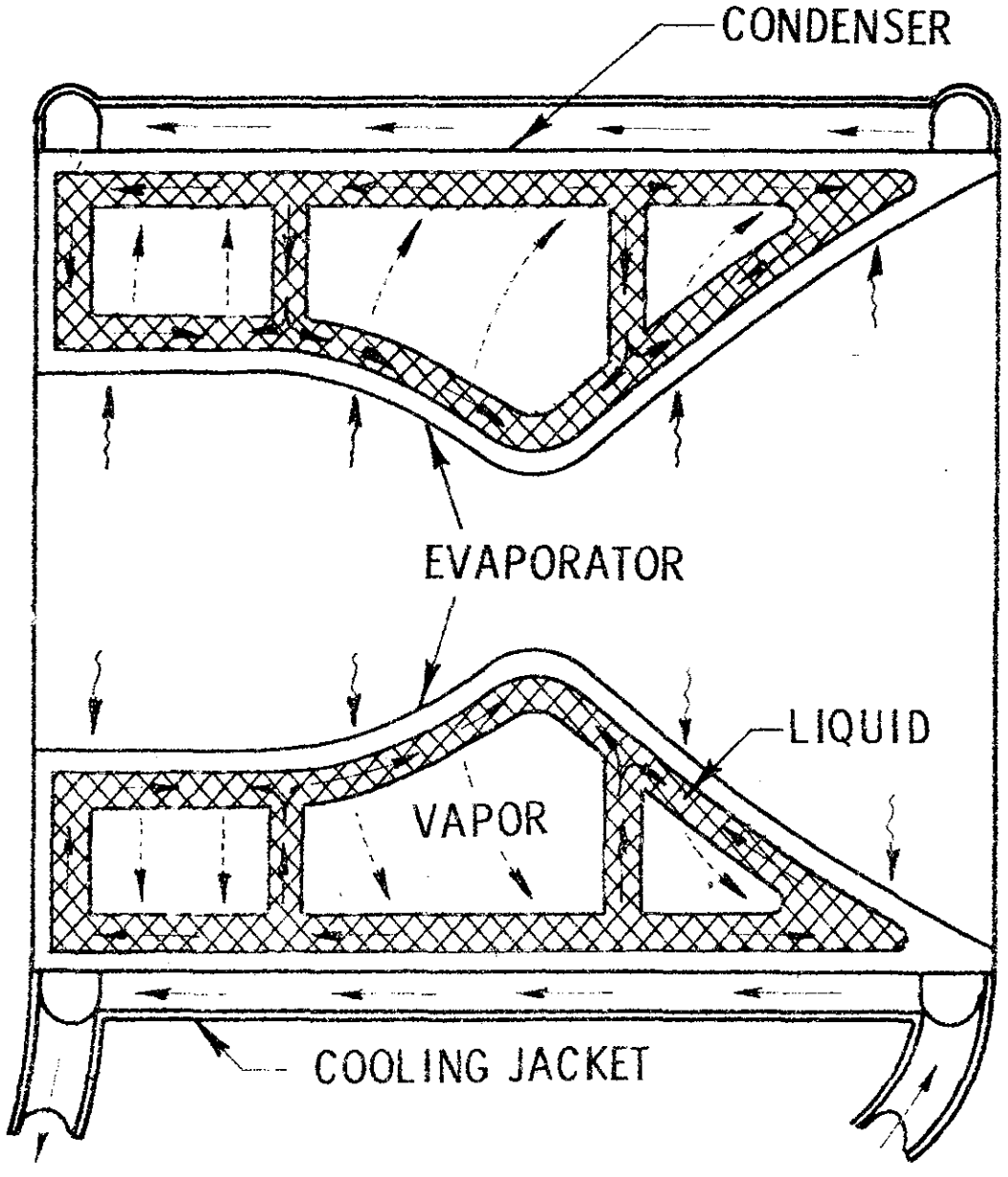

Regeneratively Cooled Heat Pipe Thrust Chamber Concept

Figure 1

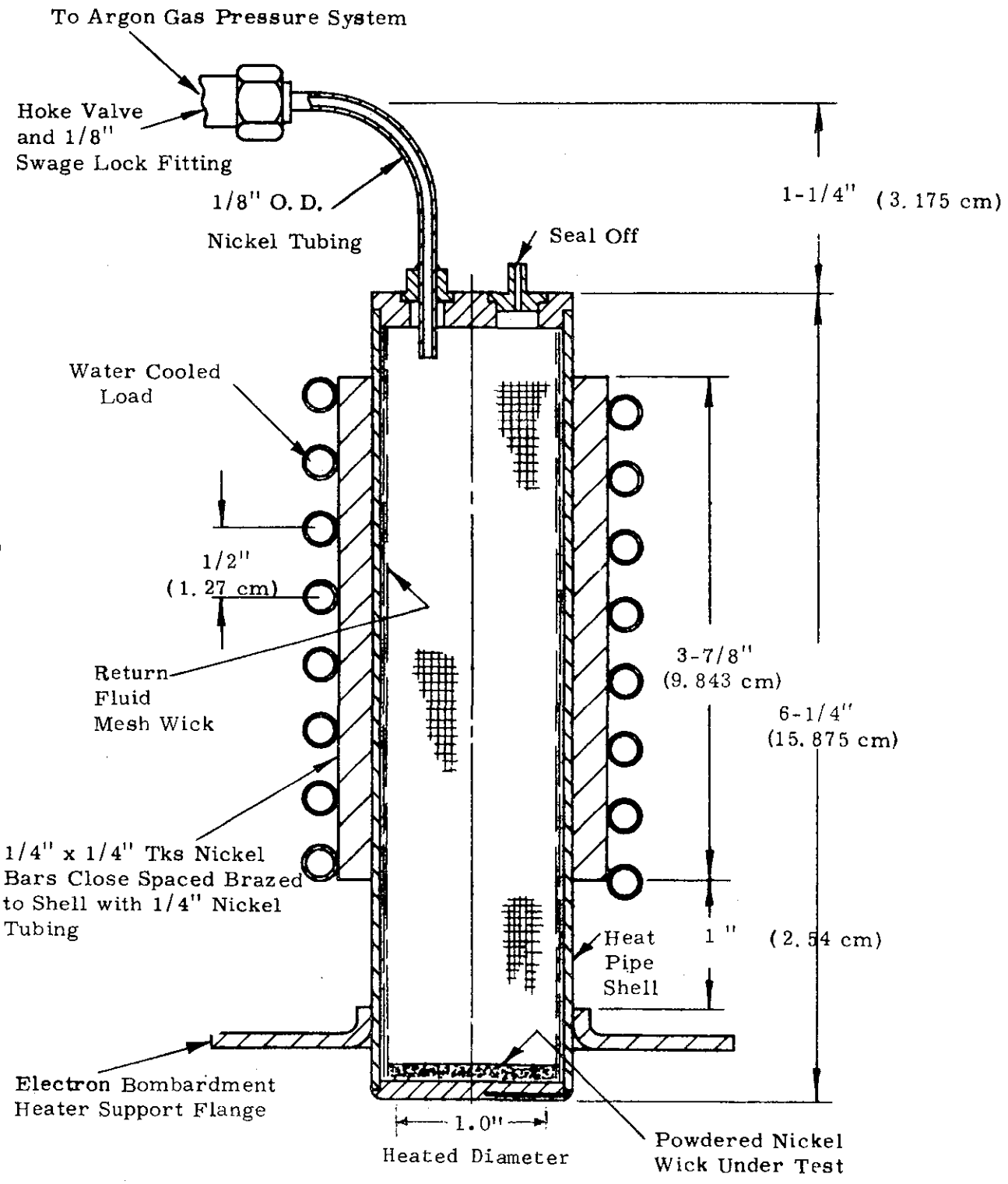

Heat Pipe 7 Design

Figure 2

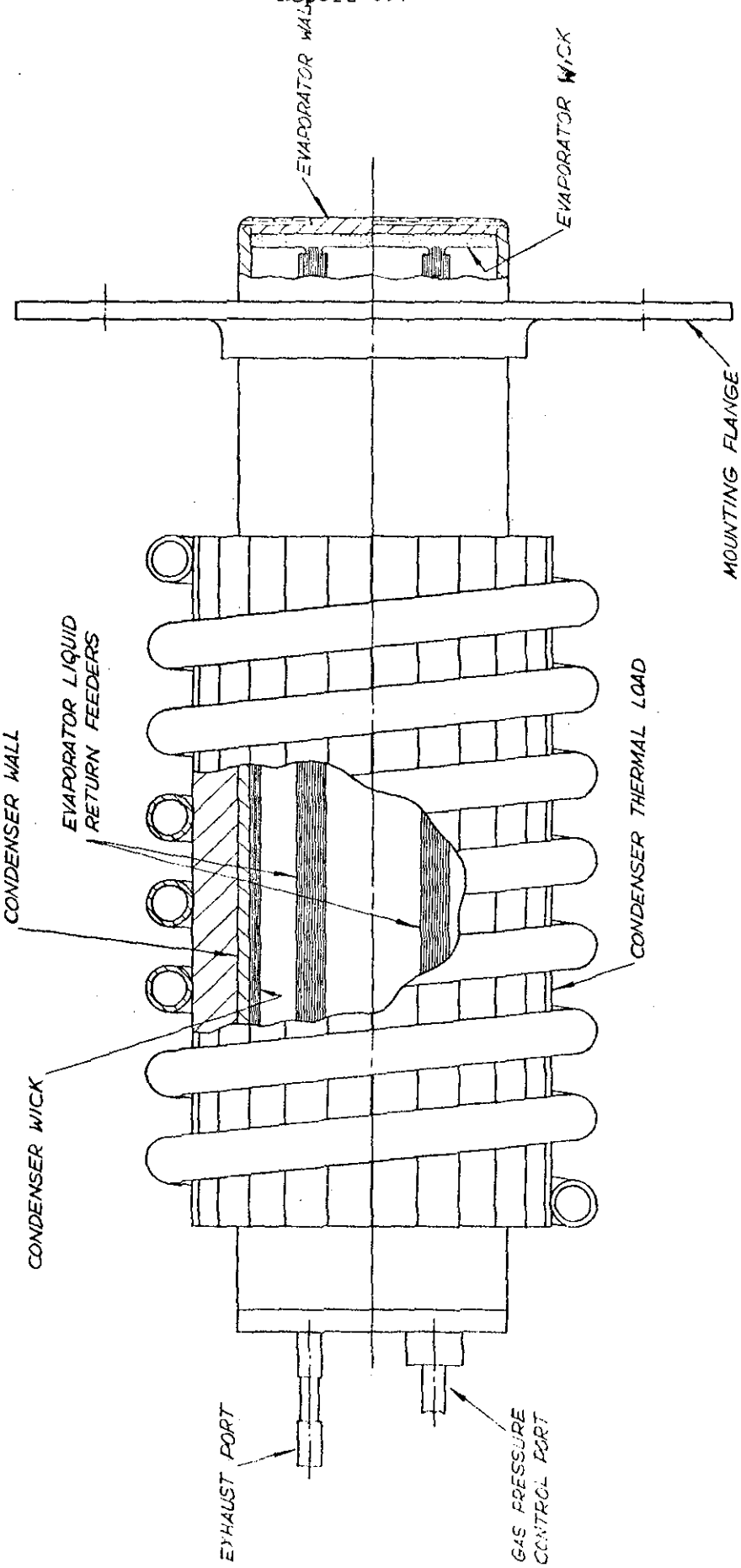
EVAPORATOR WICK
MOUNTING FLANGE
EVAPORATOR LIQUID RETURN FEEDERS
CONDENSER WALL
CONDENSER THERMAL LOAD
CONDENSER WICK
EXHAUST PORT
GAS PRESSURE CONTROL PORT

Figure 3

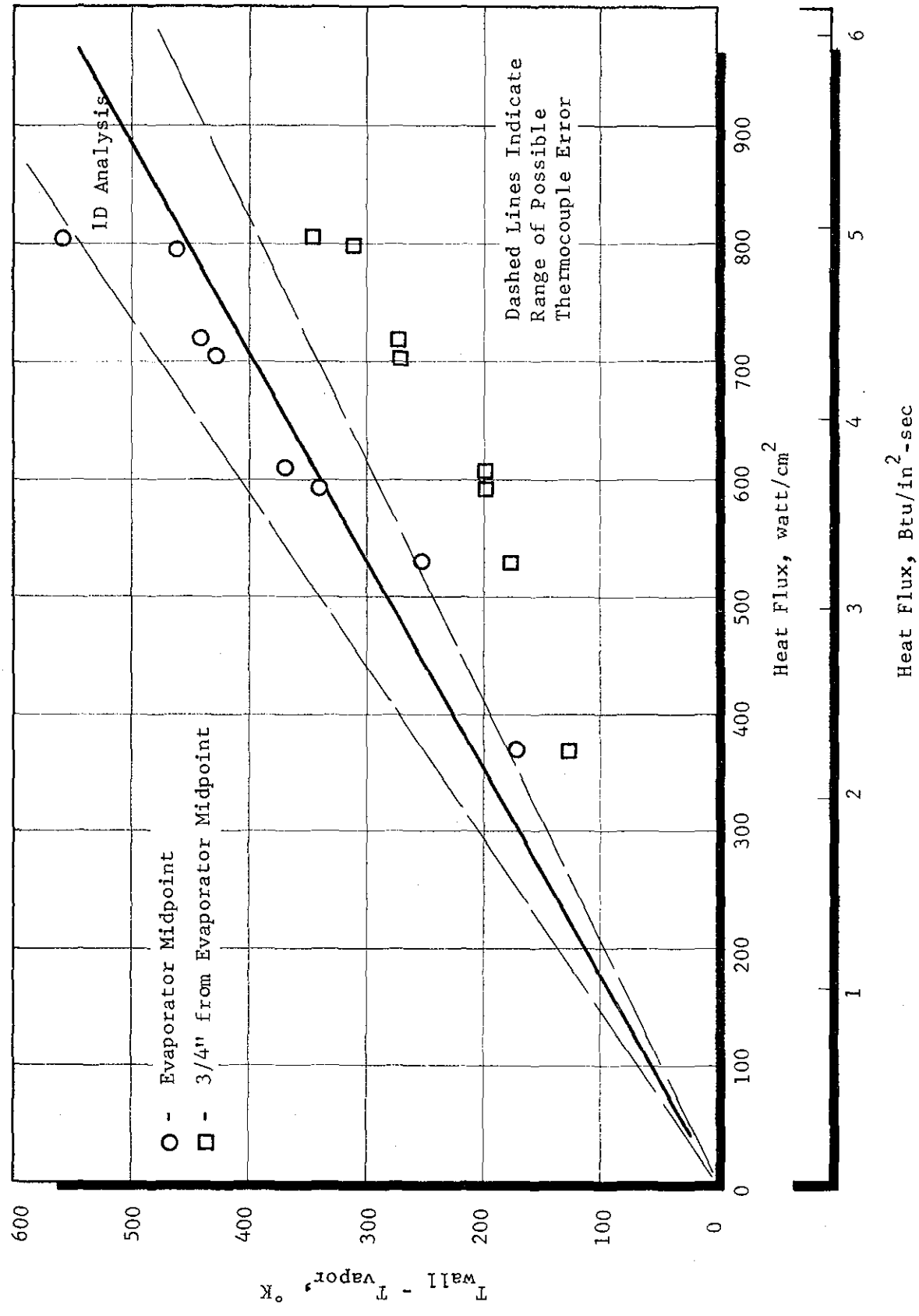
1D Analysis
Dashed Lines Indicate
Range of Possible
Thermocouple Error
○ - Evaporator Midpoint
□ - 3/4" from Evaporator Midpoint
$T_{wall} - T_{vapor}$, °K
0
100
200
300
400
500
600
Heat Flux, watt/cm^2
0
100
200
300
400
500
600
700
800
900
Heat Flux, Btu/in^2-sec
1
2
3
4
5
6
Heat Pipe 7 Test Data

Figure 4

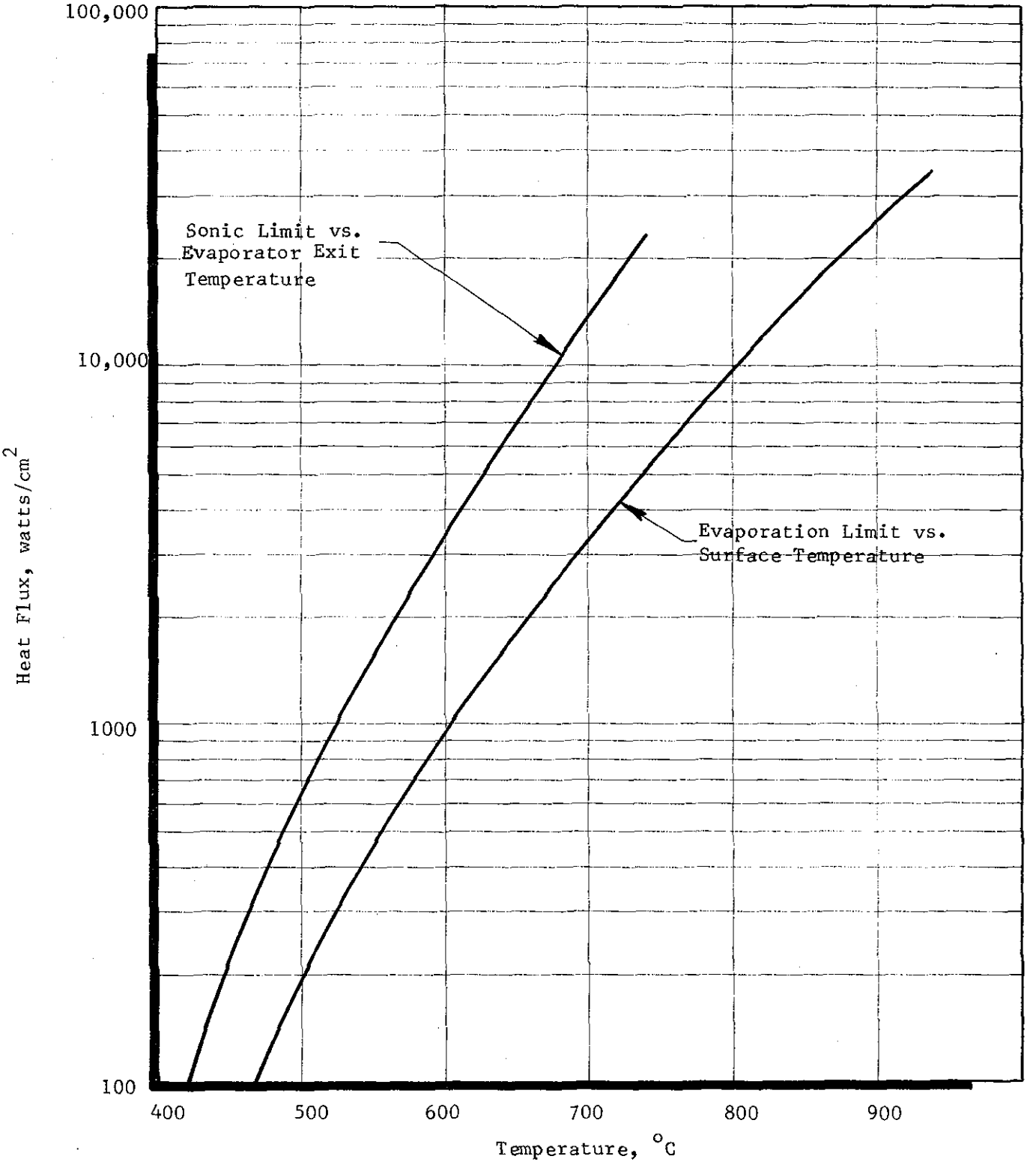

Evaporation and Sonic Limit for Sodium

Figure 5

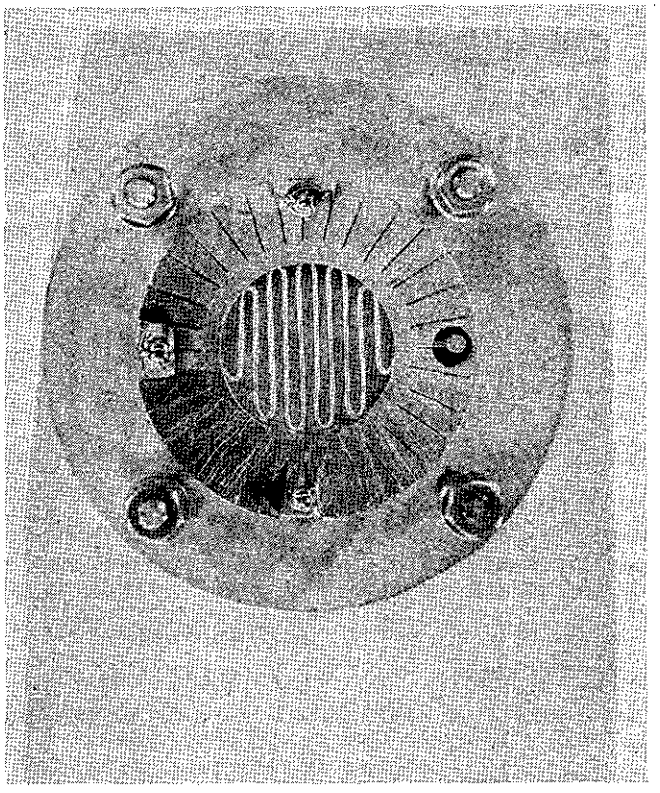

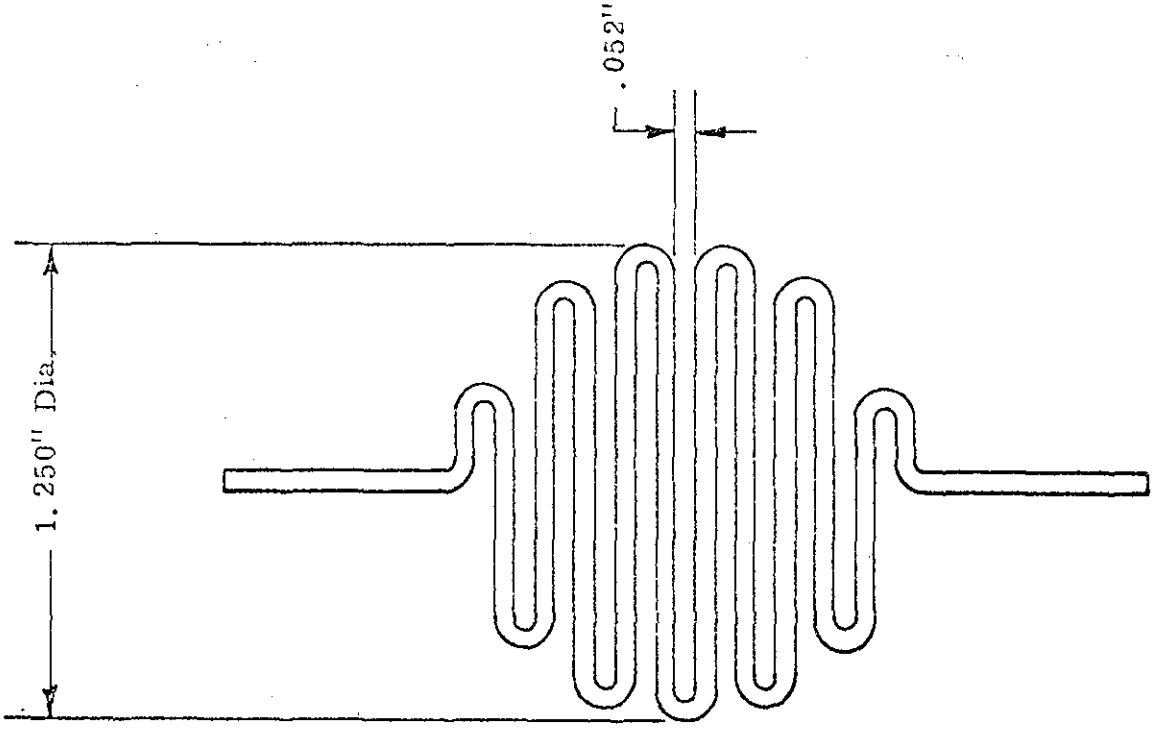

Figure 6 - Modified Electron Bombardment Heater Filament and Heater Assembly

Figure 6

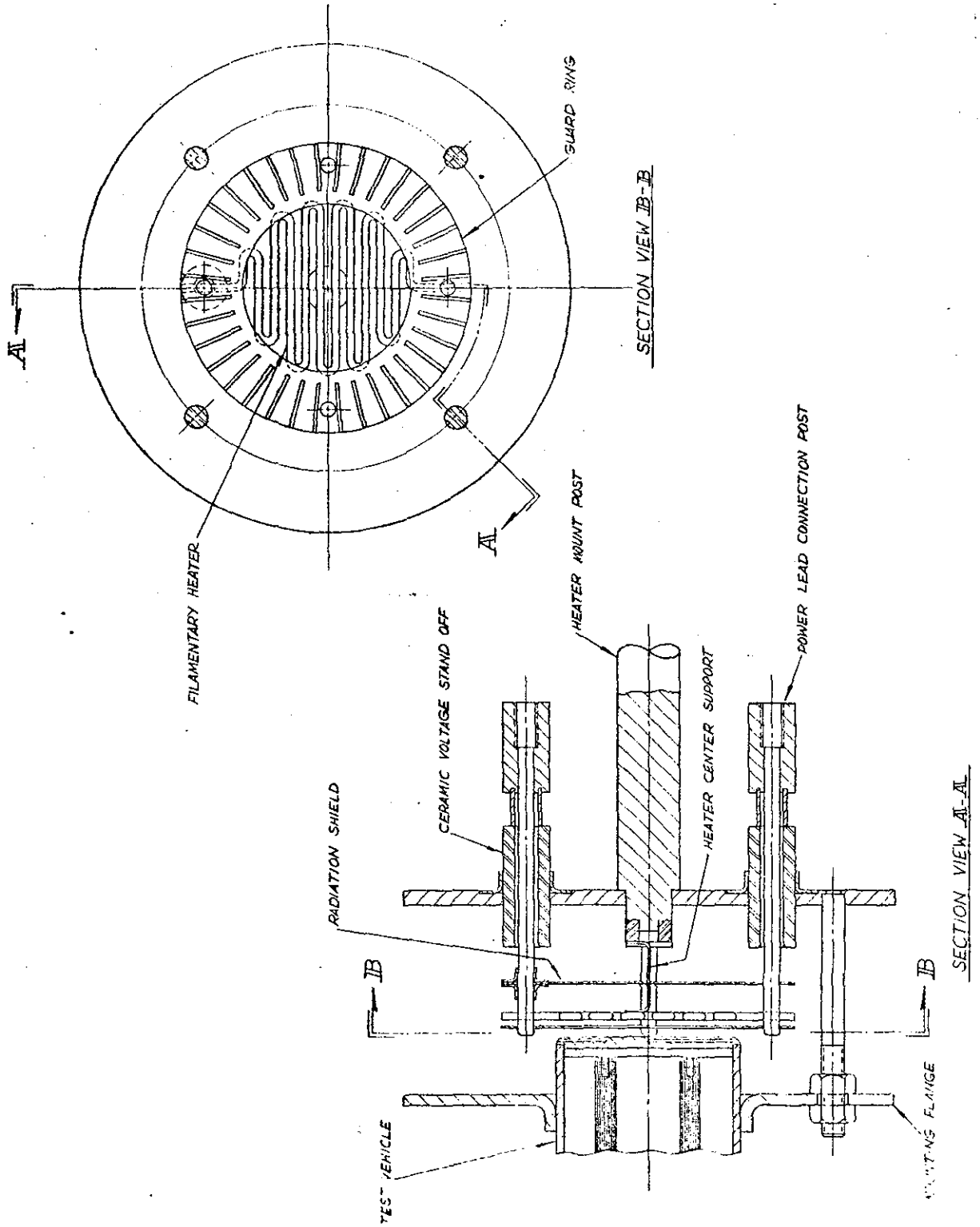

Figure 7

Electron Bombardment Heater Installed on Heat Pipe 12

Filament Geometry - Twelve Cells, .261cm spacing, 0.137 cm diameter thoriated tungsten 38.42cm length

Filament Characteristics - for thoriated wire with 20% W_2C at 2025°K
Current = 52 Amperes
Voltage = 13.5 Volts

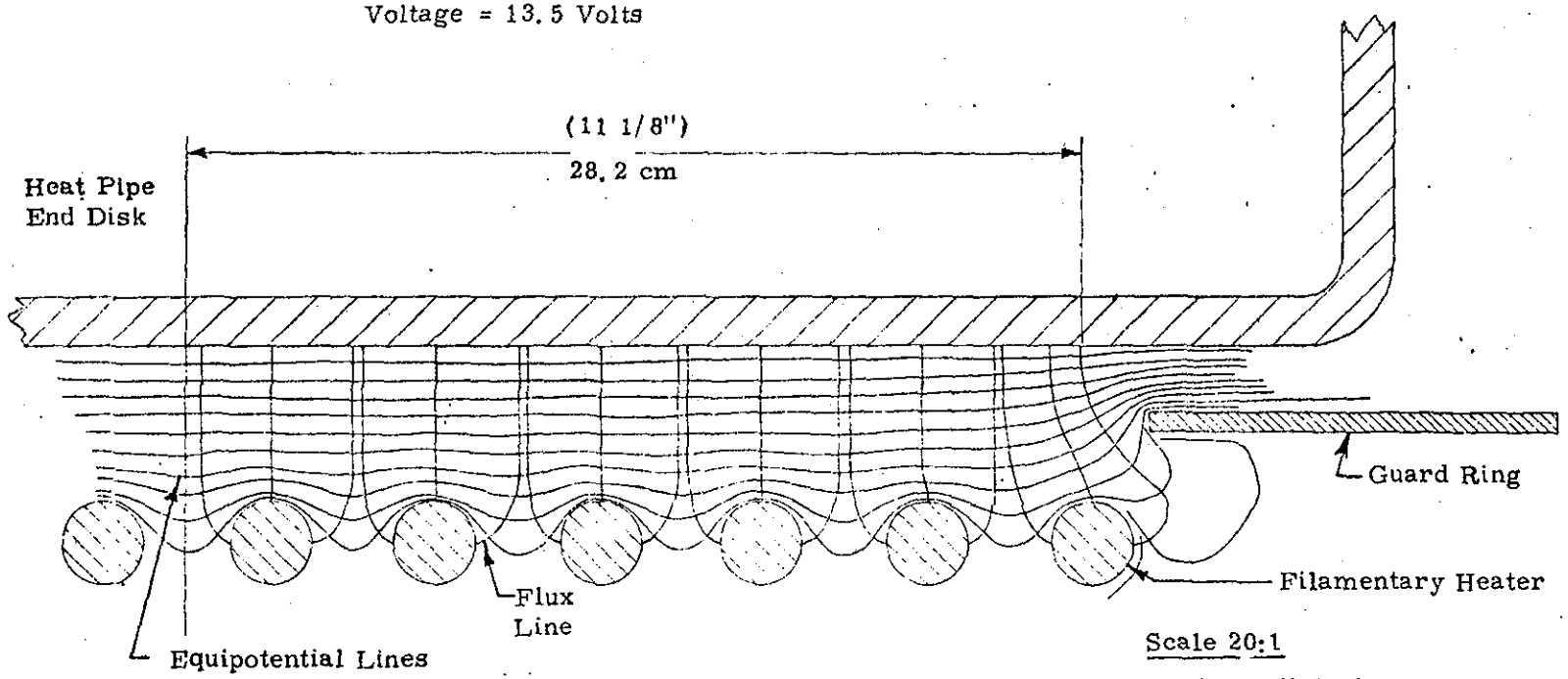

Figure 8

Electrostatic Field Plot of Electrode Configuration

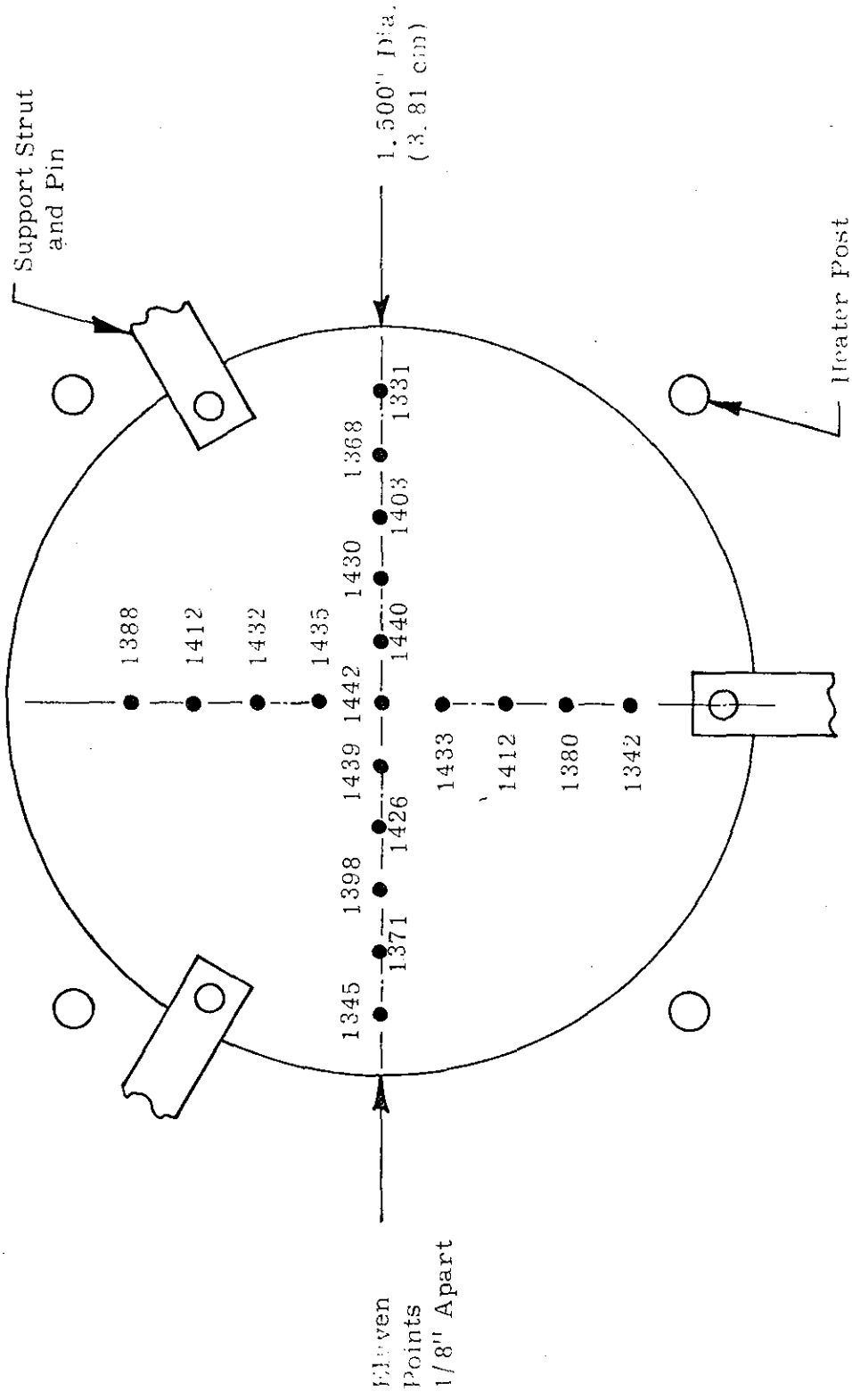

Temperature Profile for Steady-State Heated Disk

Figure 9

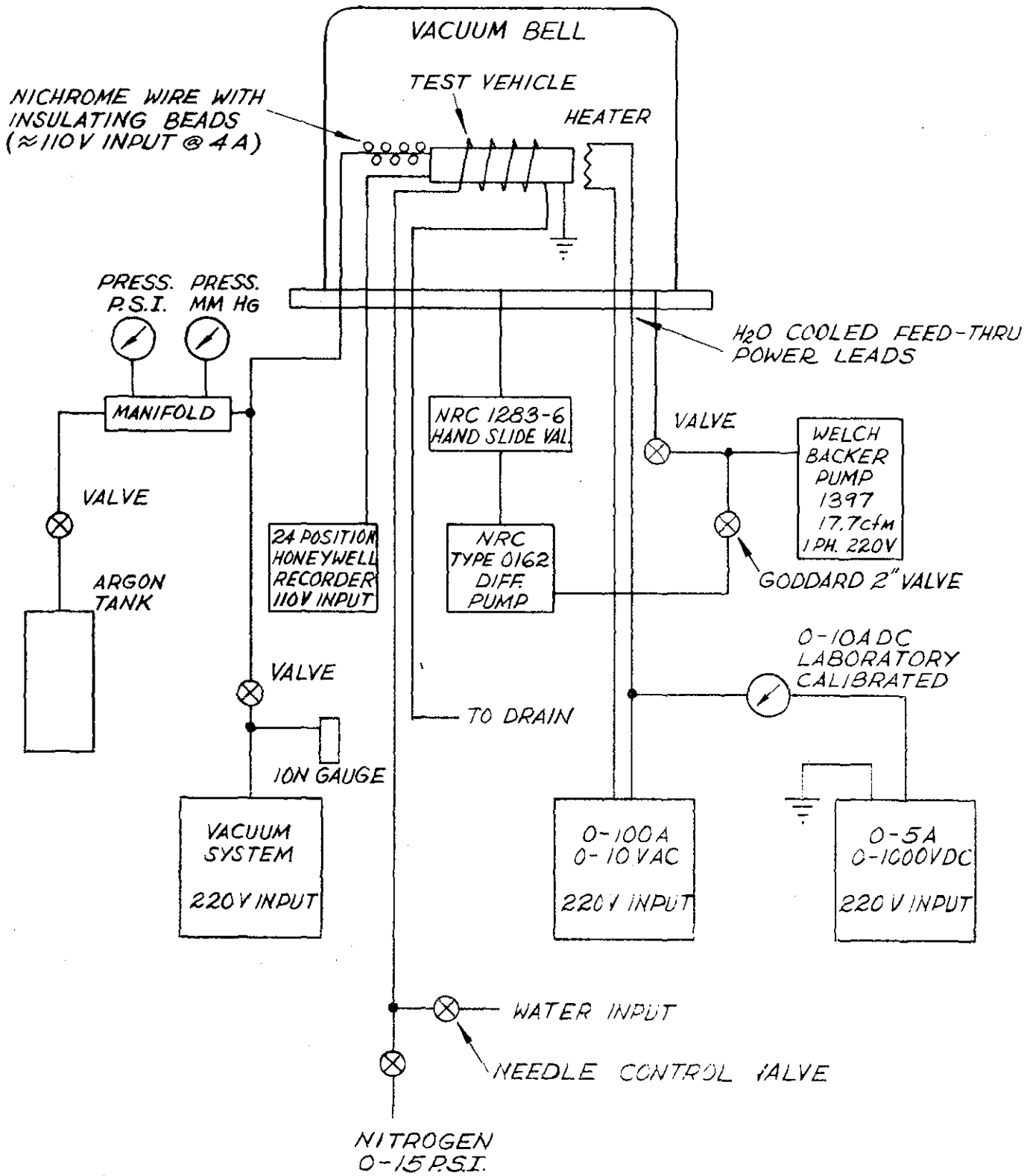

Test Apparatus Schematic

Figure 10

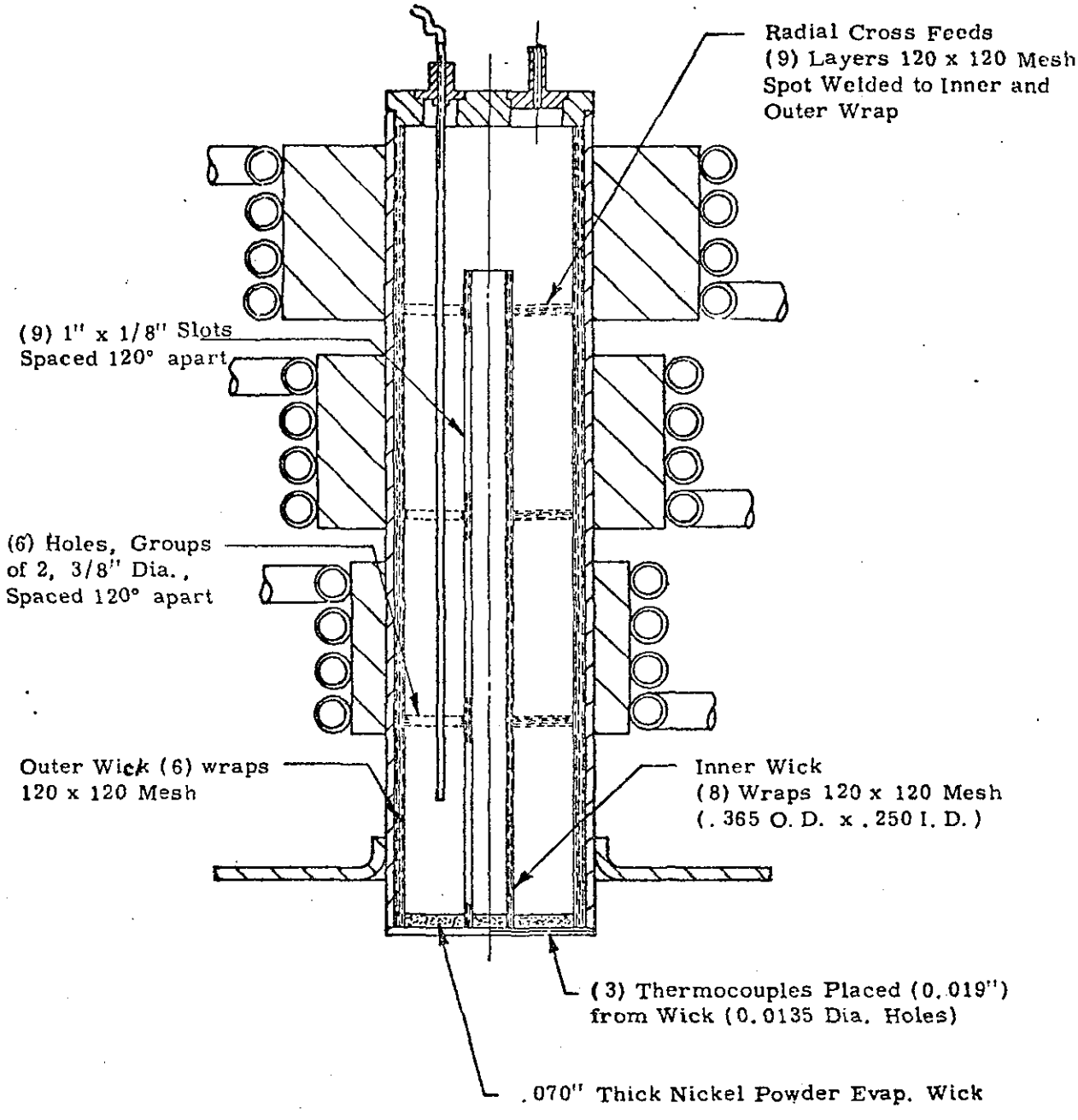

Heat Pipe 8 Design

Figure 11

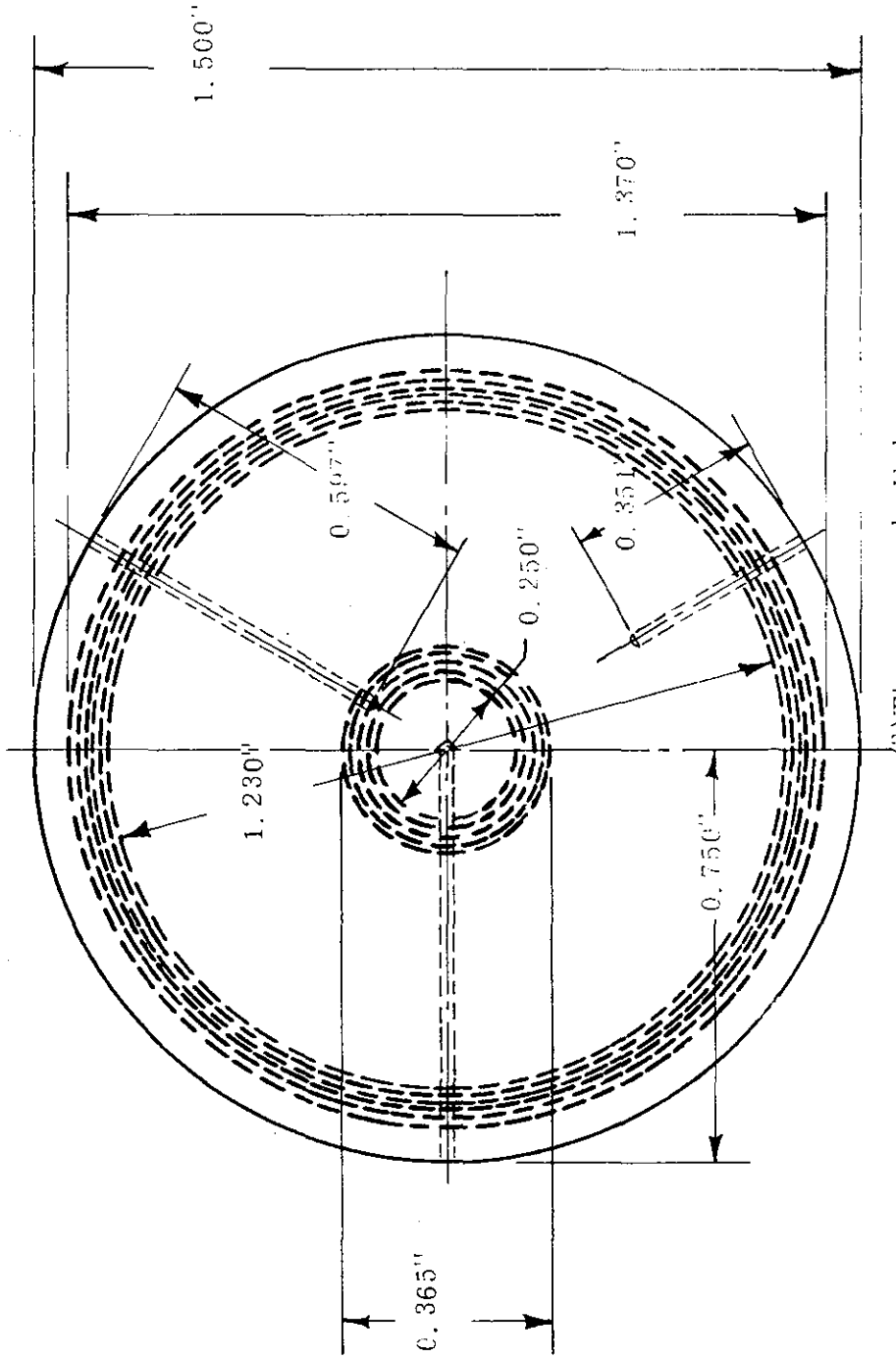

Evaporator Wall Thermocouple Locations, Heat Pipe 8

Figure 12

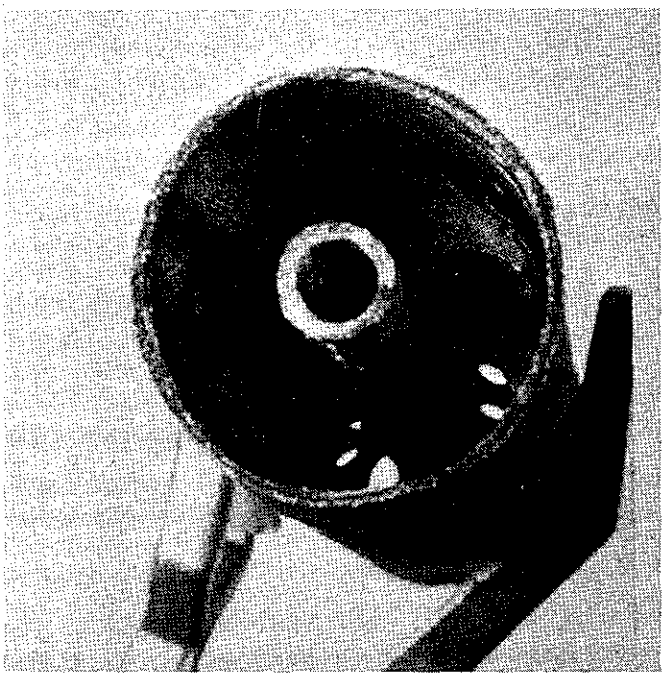

Figure 13 - View of Heat Pipe 8 Condenser and Return Wick Structure

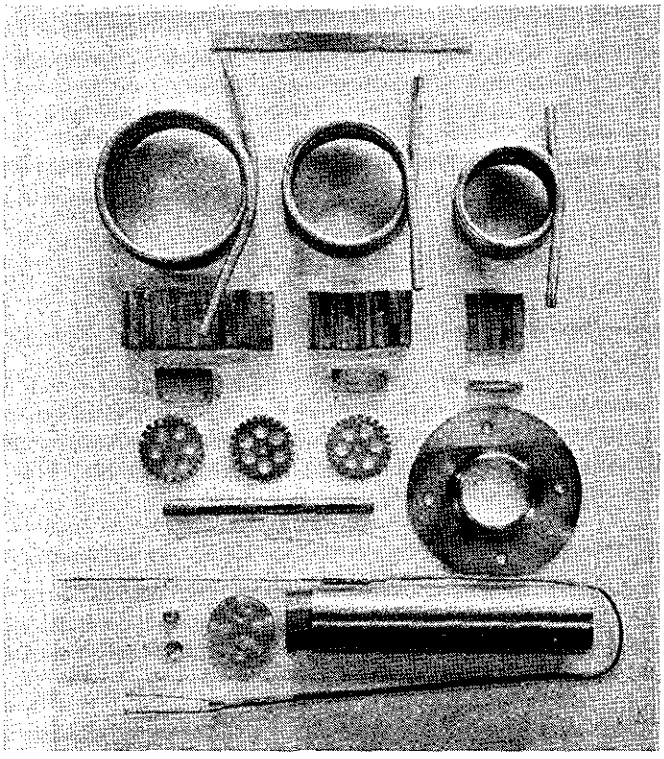

Figure 14 - Heat Pipe 8 Components

Figure 13 and Figure 14

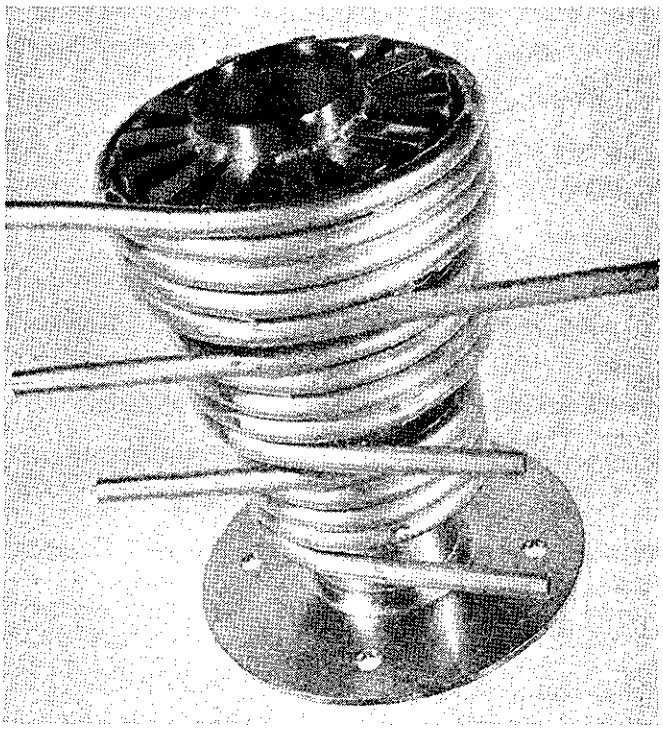

Figure 15 - Heat Pipe 8 After Assembly

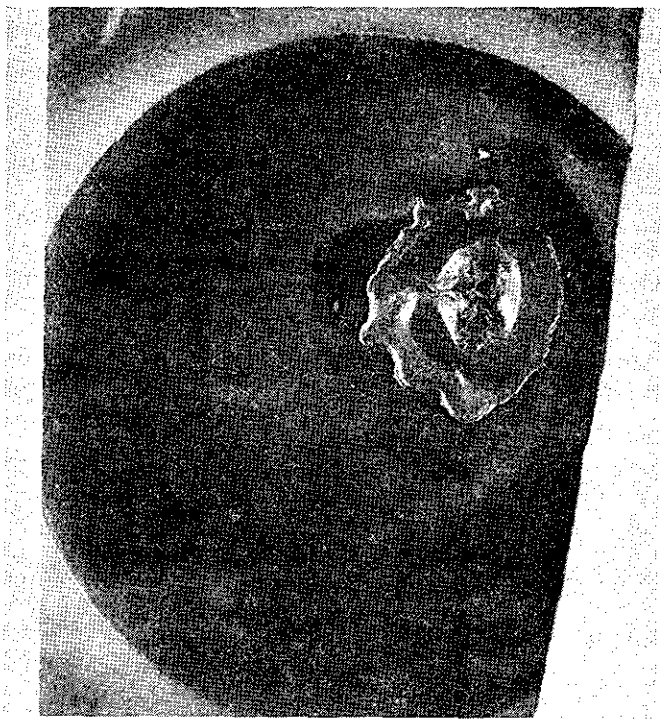

Figure 16 - Heat Pipe 8 Evaporator Wall Burnout

Figure 15 and Figure 16

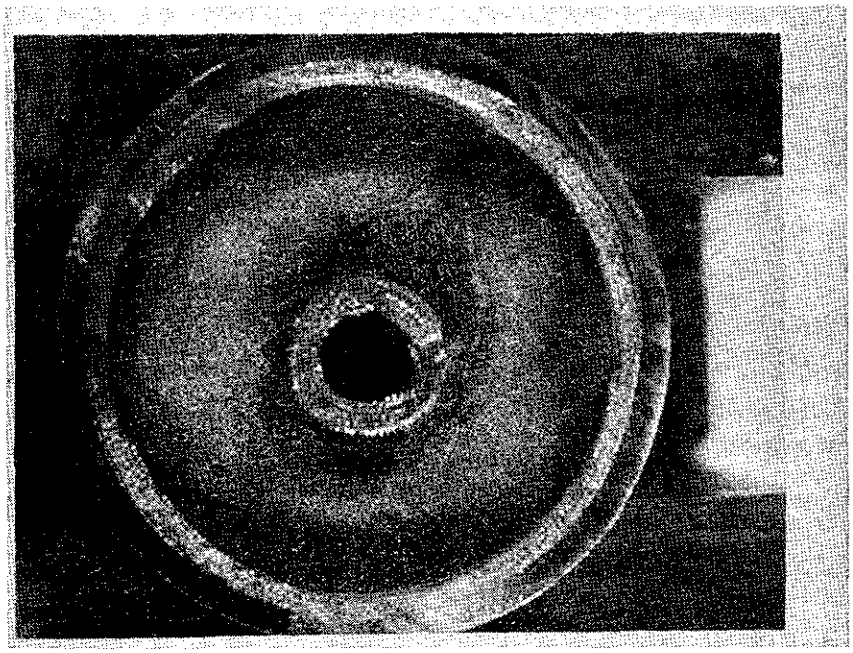

Figure 17 - Heat Pipe 8 Evaporator (Post Test)

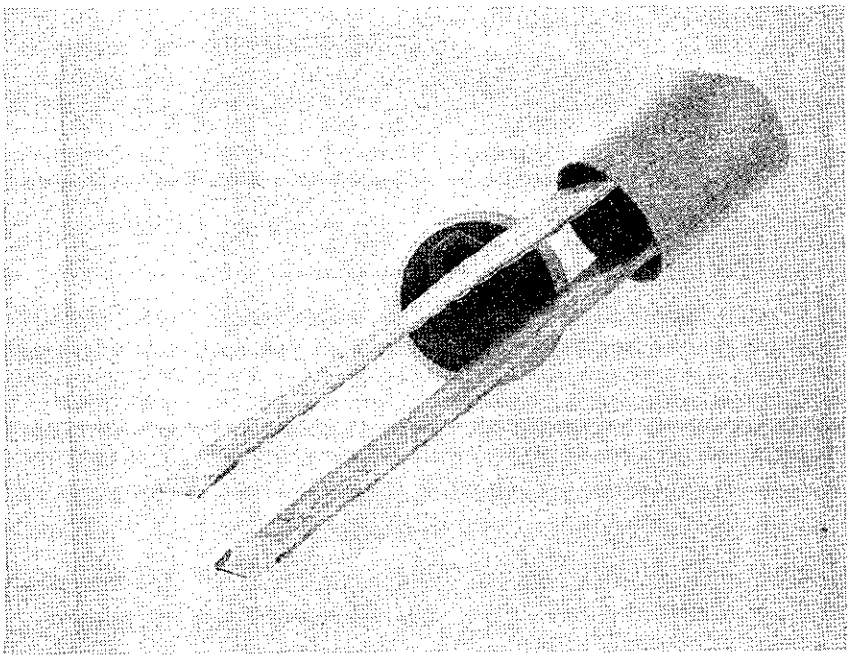

Figure 18 - Heat Pipe 9A Feeders and Condenser Wick

Figure 17 and Figure 18

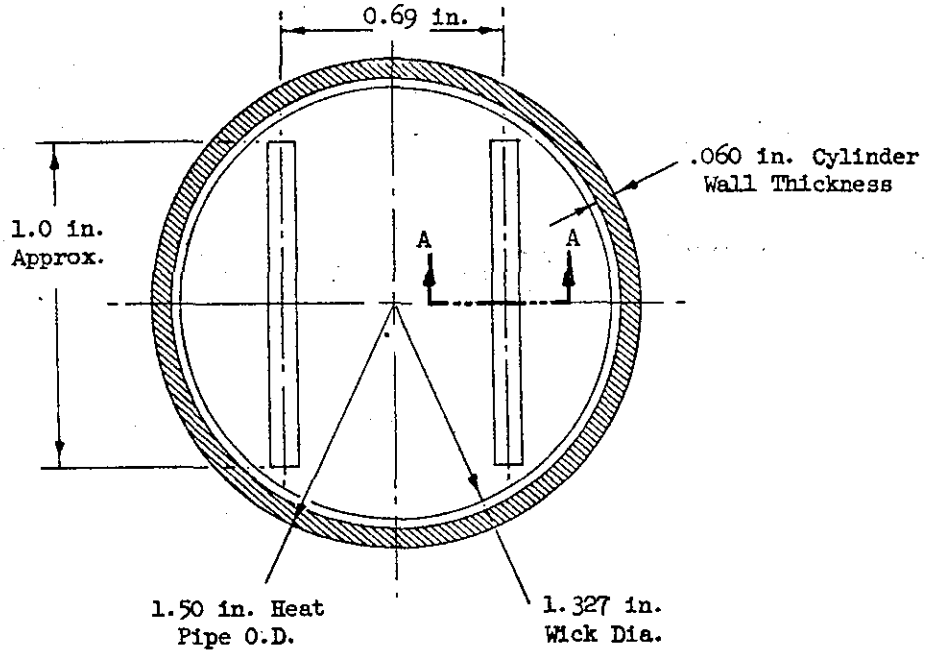

Evaporator Wick Viewed From The Condenser End of The Heat Pipe.

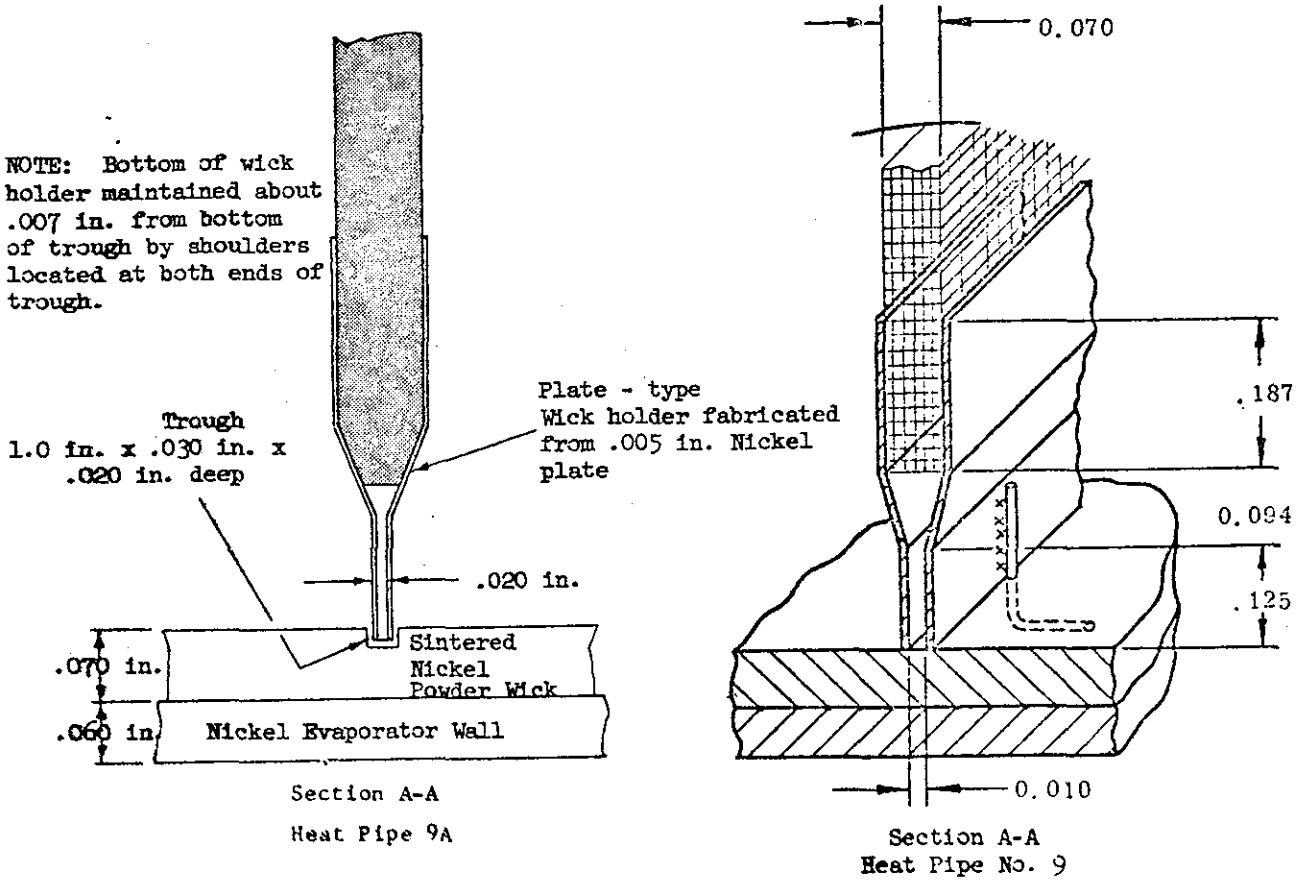

Heat Pipe 9 and 9A Evaporator/Feeder Joint Detail

Figure 19

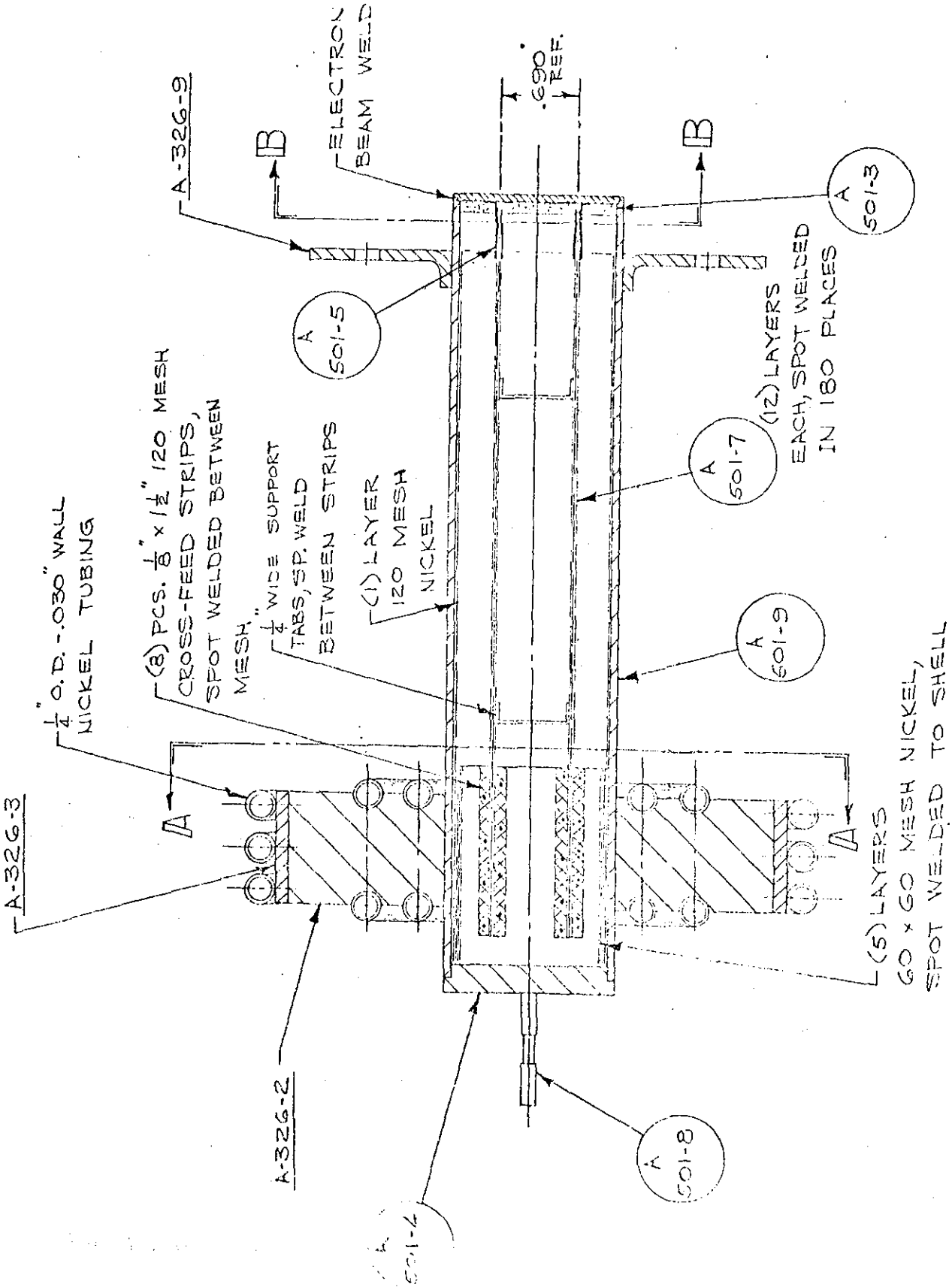

Cross-Section of Heat Pipe 9

Figure 20

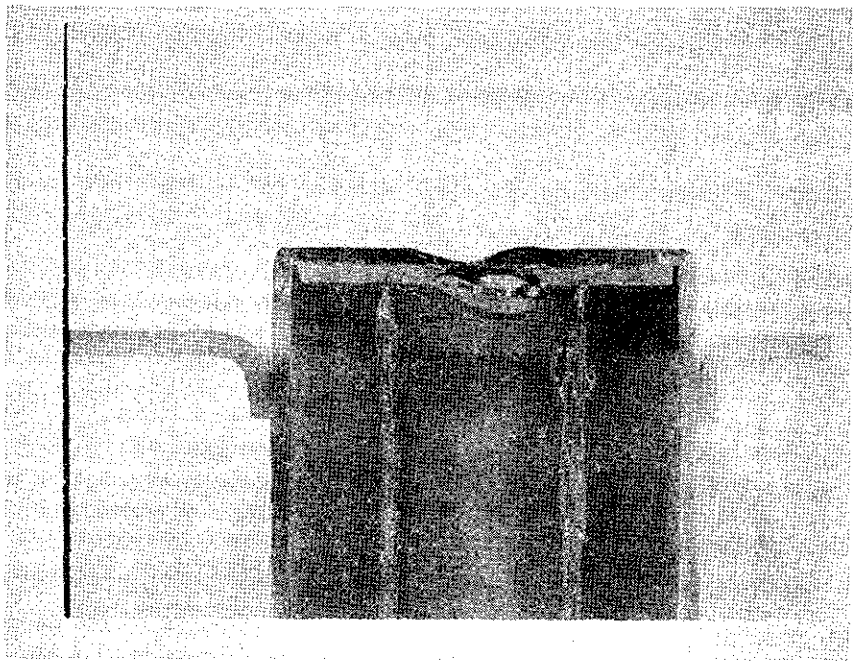

Figure 21 - Cross Section of Burnout Area, Heat Pipe 9A

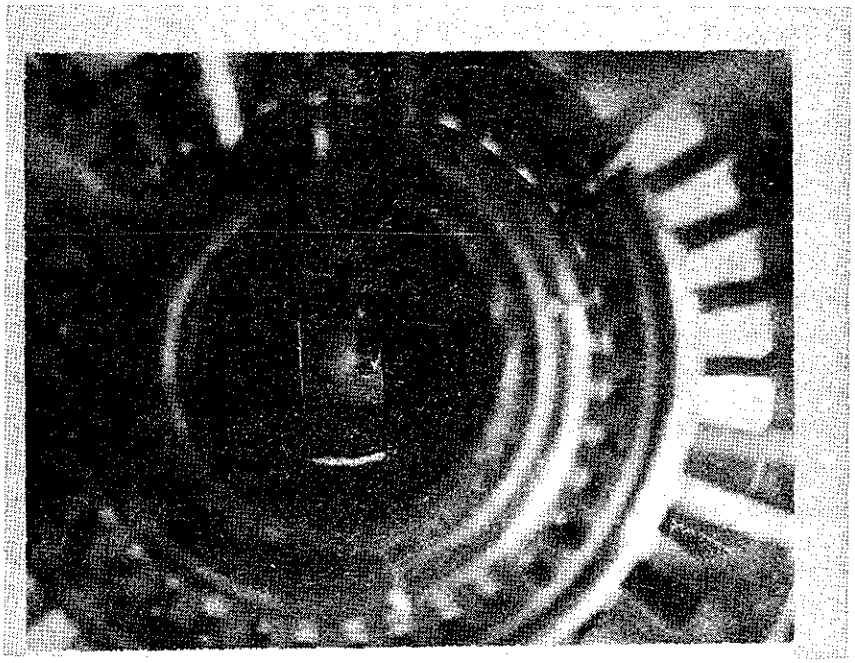

Figure 22 - View of Evaporator Wick "Blister" from Aft End of Heat Pipe 9A

Figure 21 and Figure 22

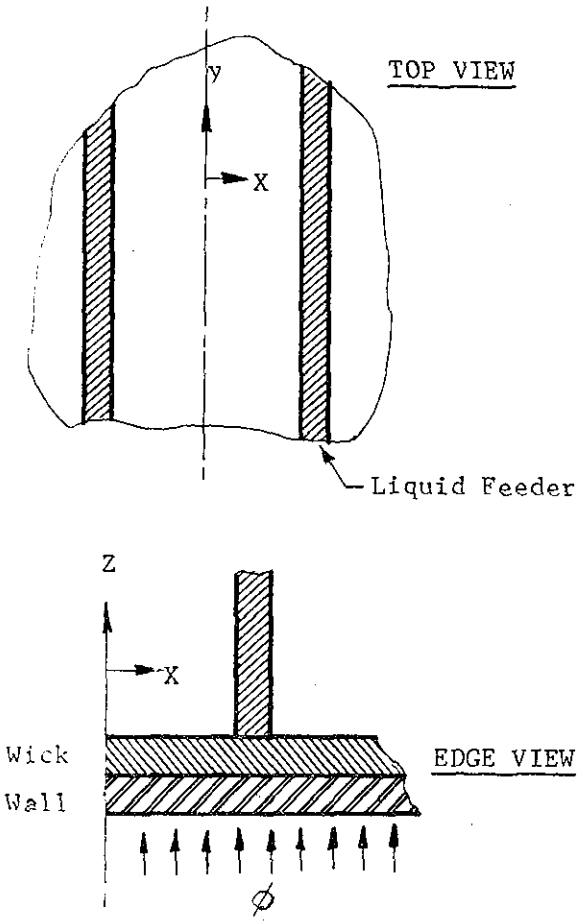

Figure 23

FORMULATION

- Apply conduction equation at a distance x from midplane.
- Neglect temperature gradient in y and Z directions

$$Q = k\,A\,\frac{dT}{dx} = \emptyset\,xy$$

$$A = yt$$

$$\emptyset X = kt\,\frac{dT}{dx}$$

$$\Delta T = T_o - T_x = \frac{\emptyset X^2}{2kt}$$

Q = Heat Transfer Rate
A = Heat Transfer Area
k = Thermal Conductivity
t = Conduction Thickness
T_o = Temperature at X = 0
T_x = Temperature at Point X

One Dimensional Lateral Conduction Model

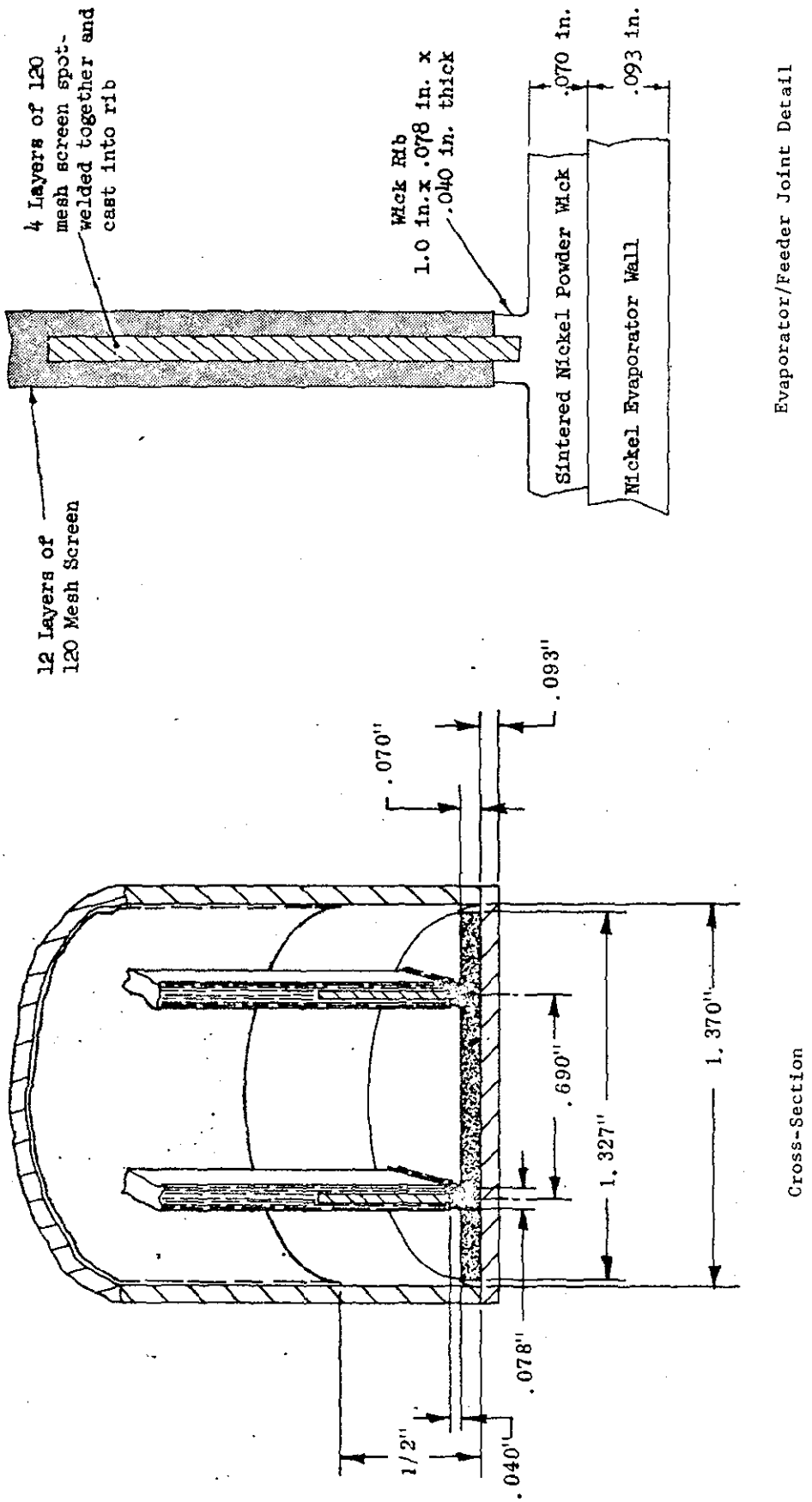

Figure 24

Heat Pipe 10 Evaporator Design

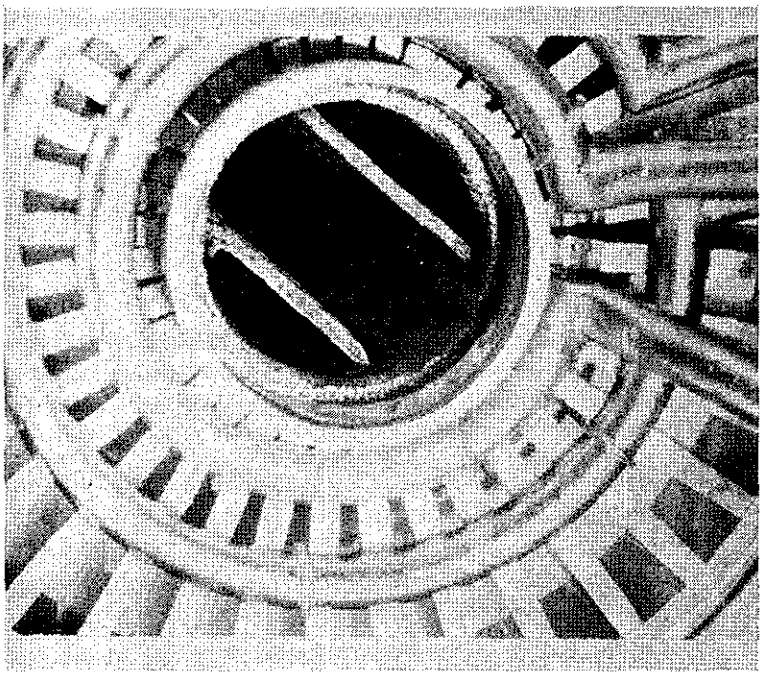

Figure 26. View of Heat Pipe 10 Condenser/Feeder Joint

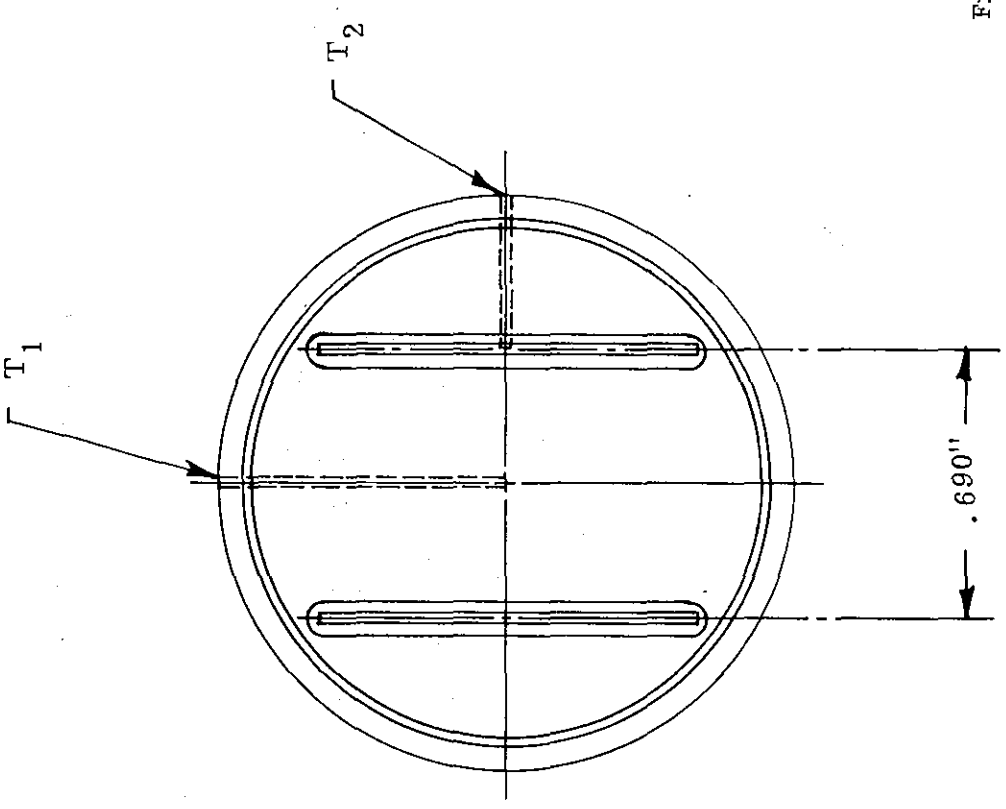

Figure 25. Heat Pipe 10 Evaporator Instrumentation

Figure 25 and Figure 26

All Components

Evaporator Wick and Mold

Figure 27 - Heat Pipe 10 Components

Figure 27

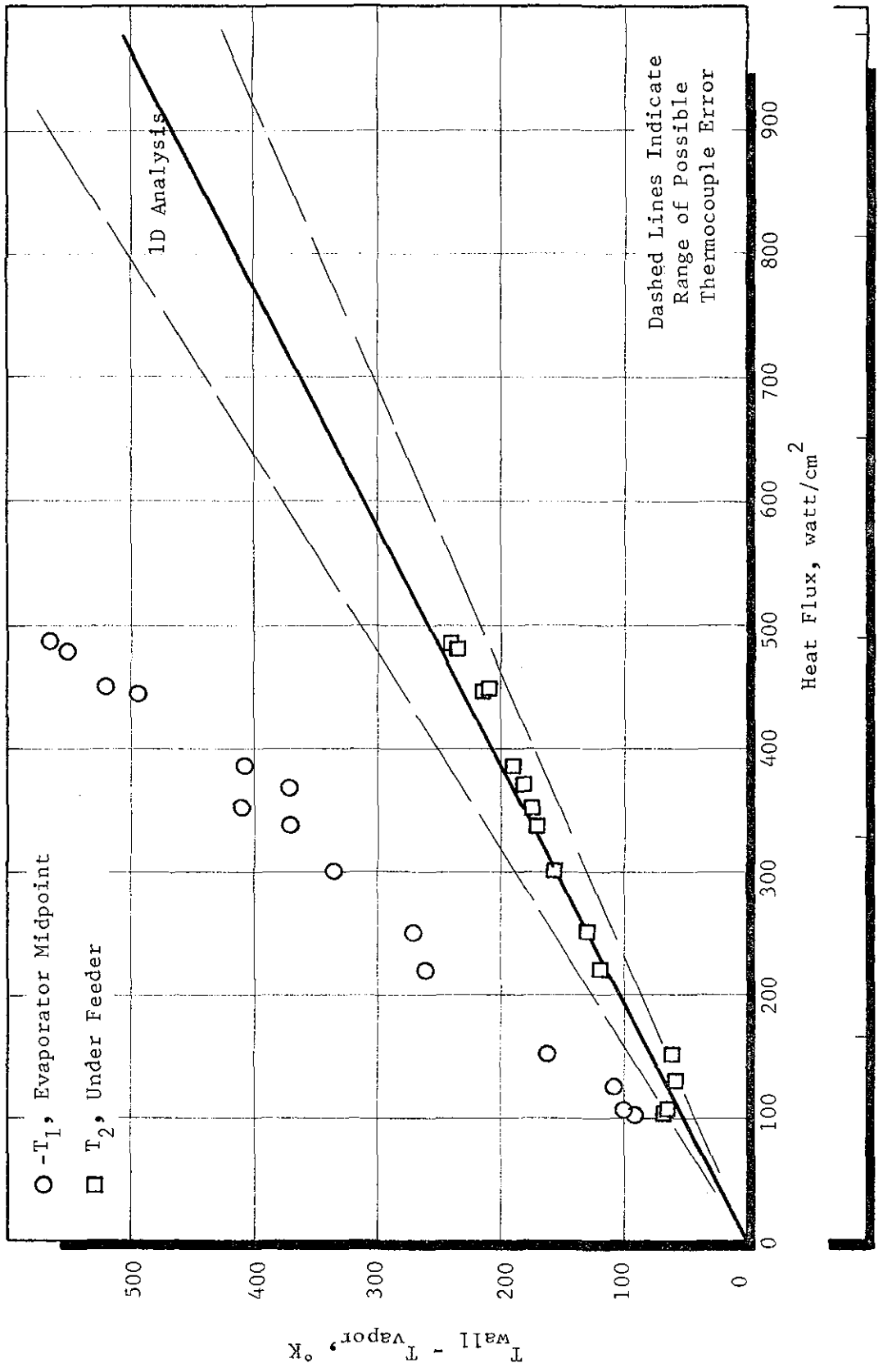

Heat Pipe 10 Test Results

Figure 28

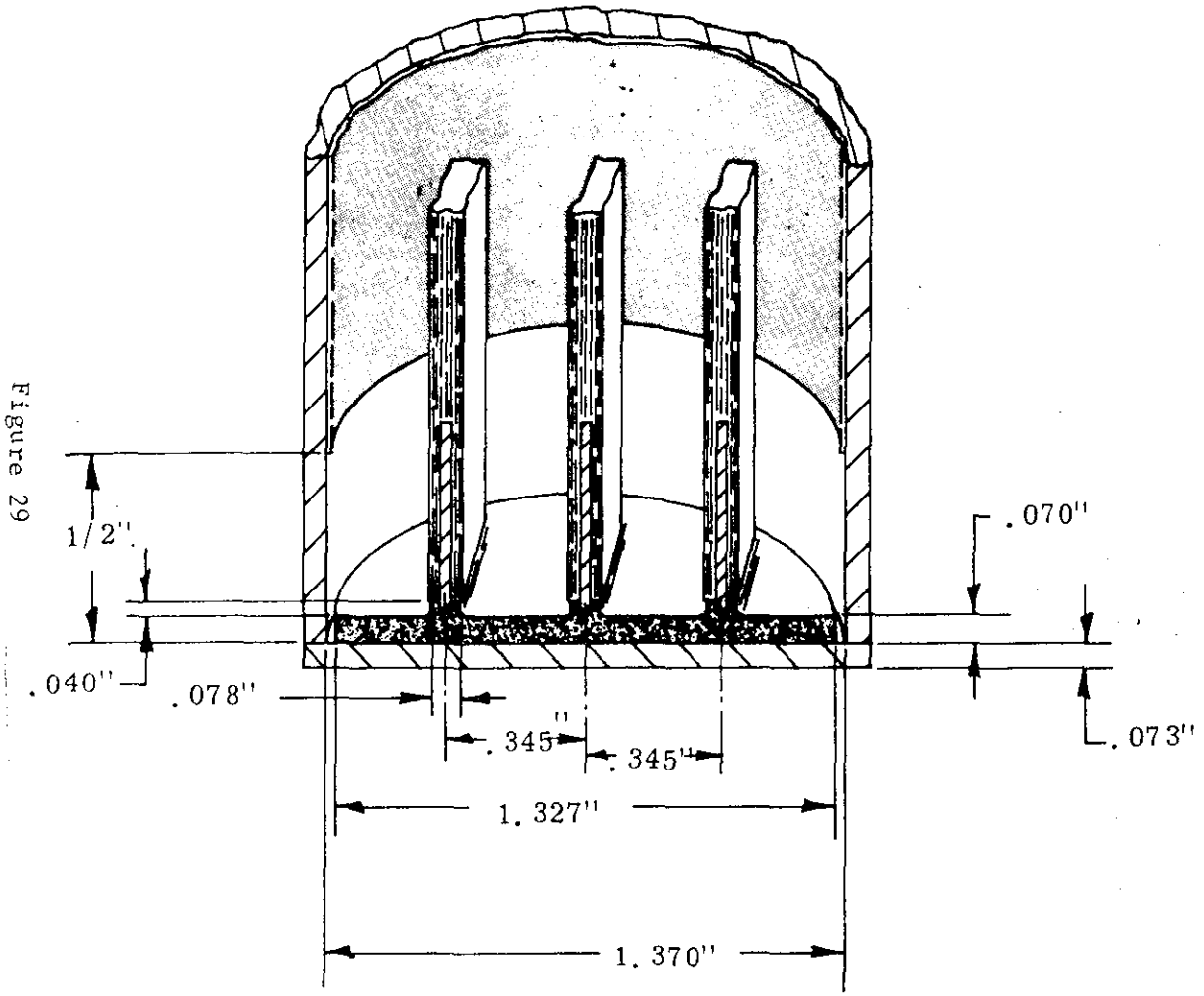

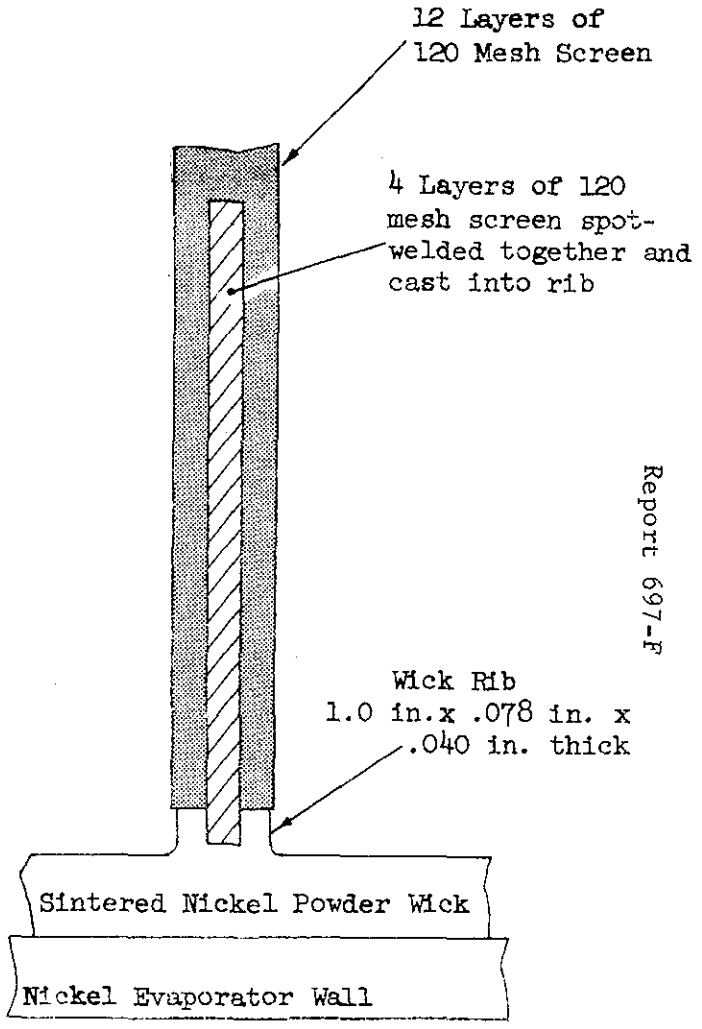

Feeder Wick Joint Detail

Figure 29

Heat Pipe 11 Evaporator Design

Report 697-F

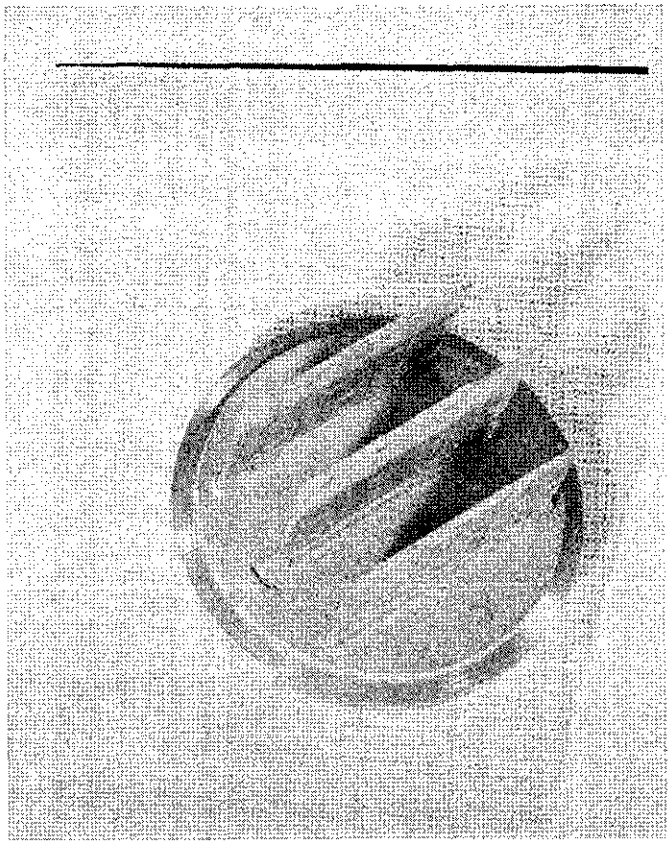

Figure 30 - Heat Pipe 11 Evaporator Before Testing

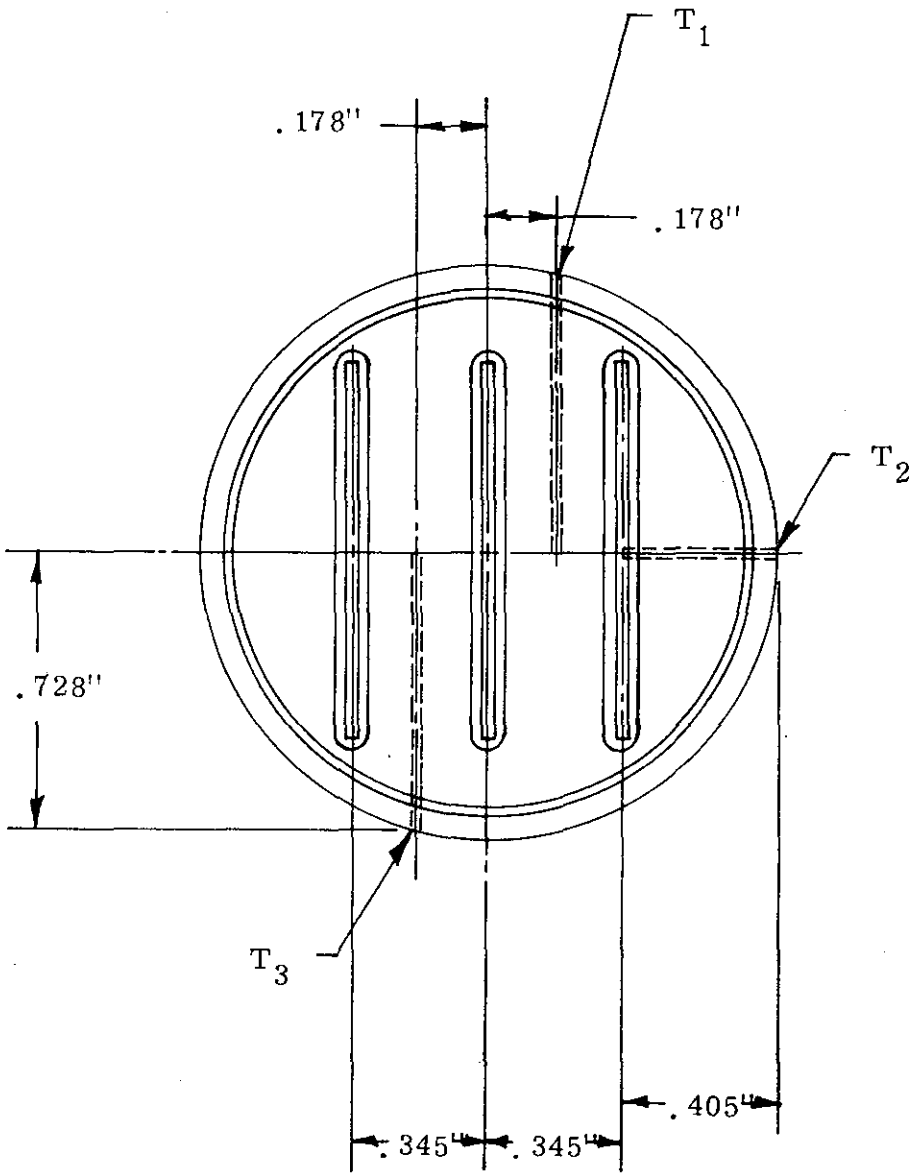

Figure 31 - Heat Pipe 11 Evaporator Instrumentation

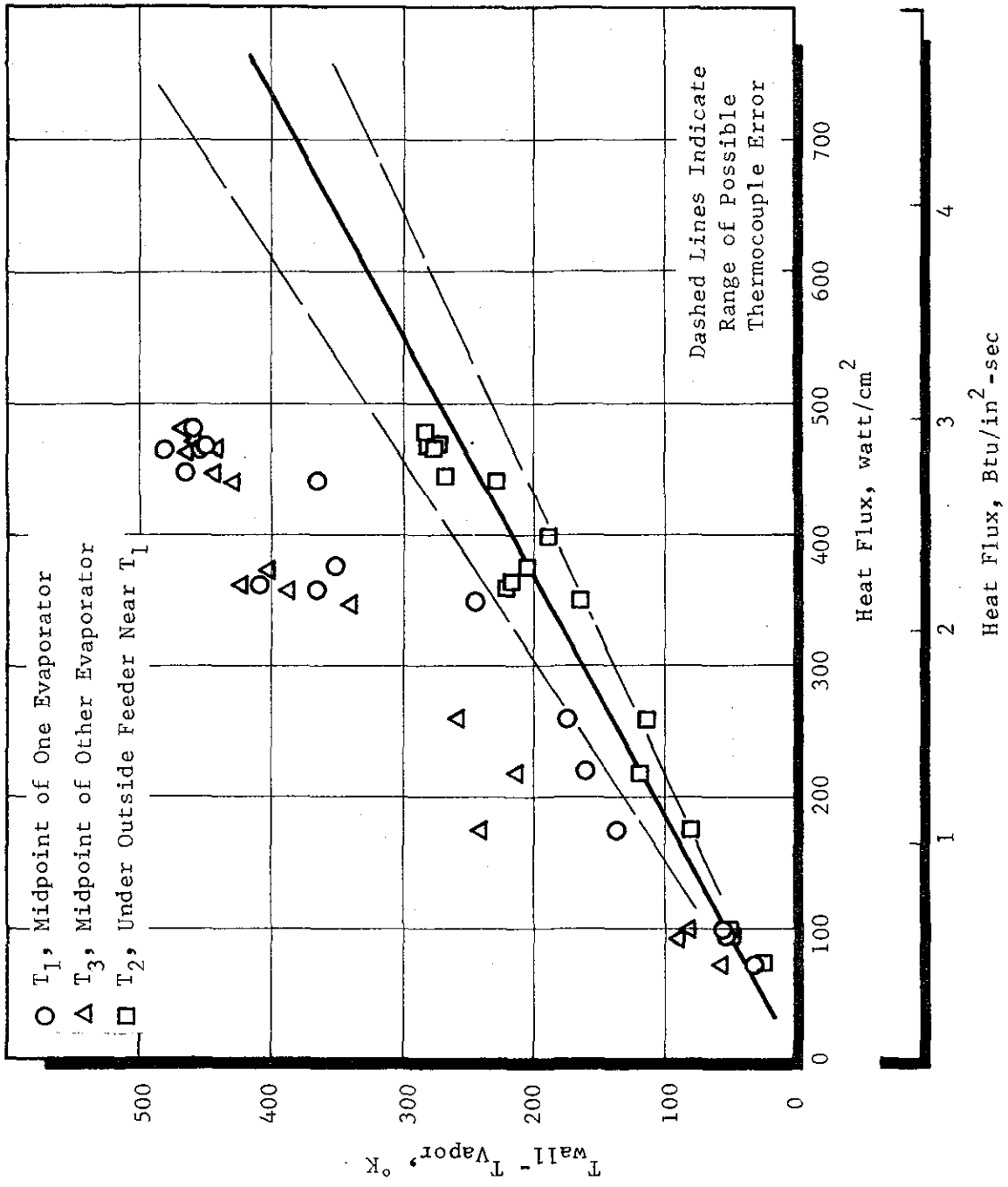

Heat Pipe 11 Test Results

Figure 32

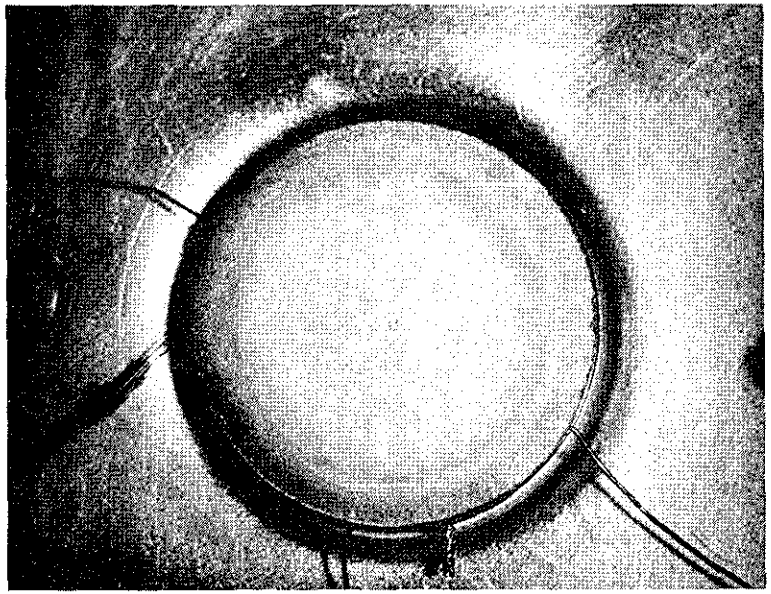

Heated Side of Evaporator Wall

Wick Evaporative Surface

Figure 33 - Heat Pipe 11 Evaporator After Testing

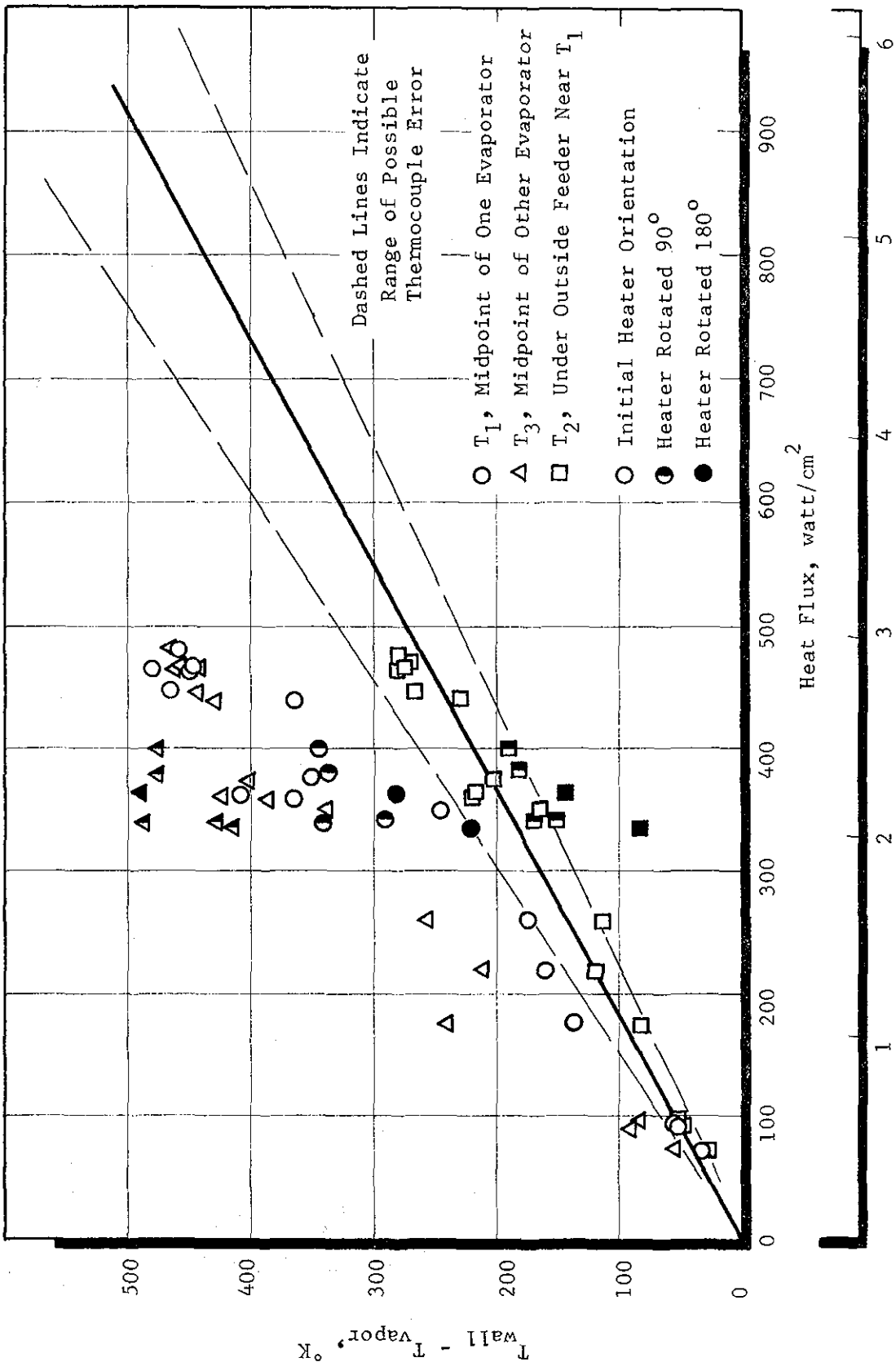

Effect of Heater Rotation on Heat Pipe 11 Evaporator Wall Temperature

Figure 34

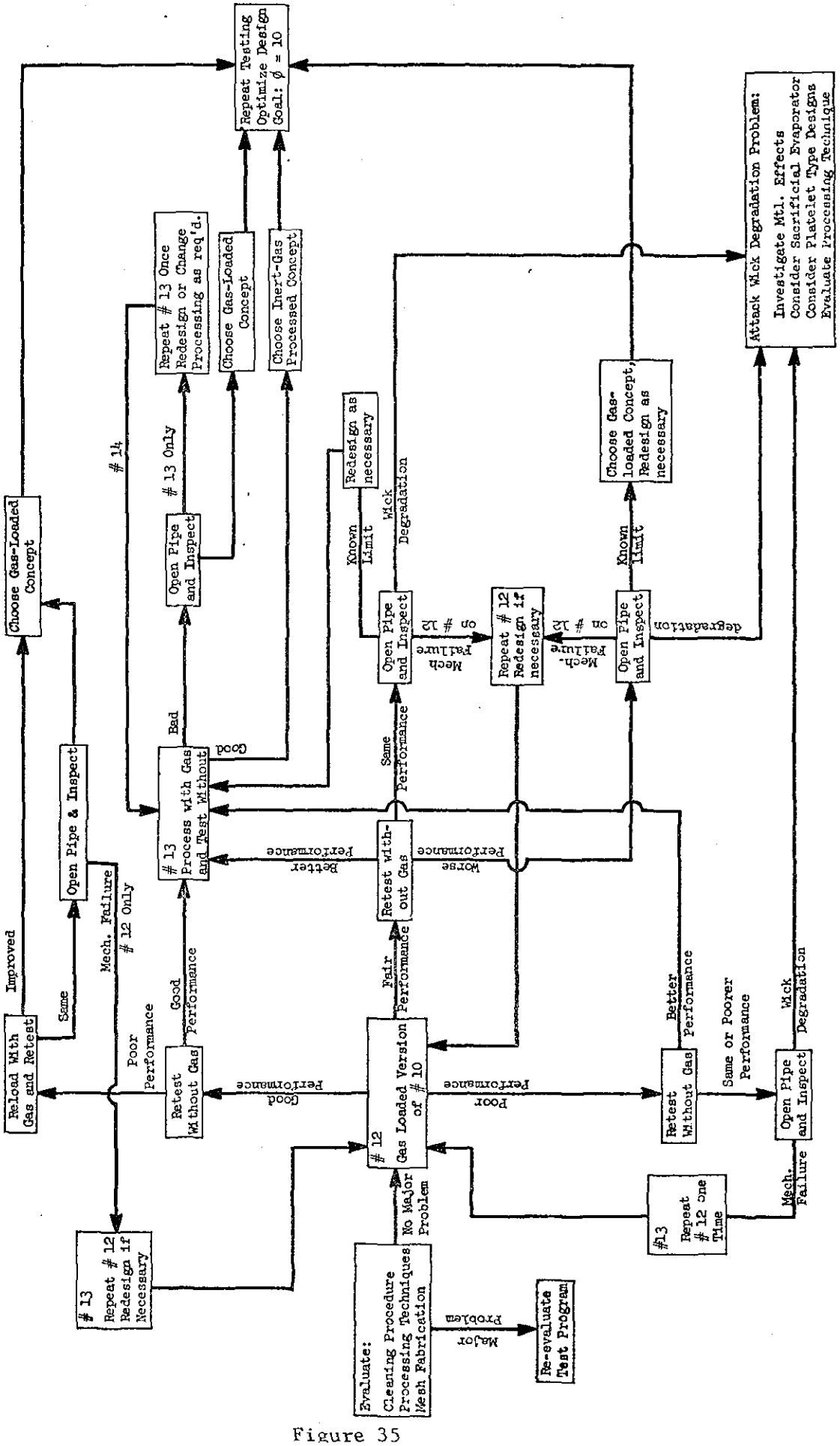

Test Logic Diagram

Figure 35

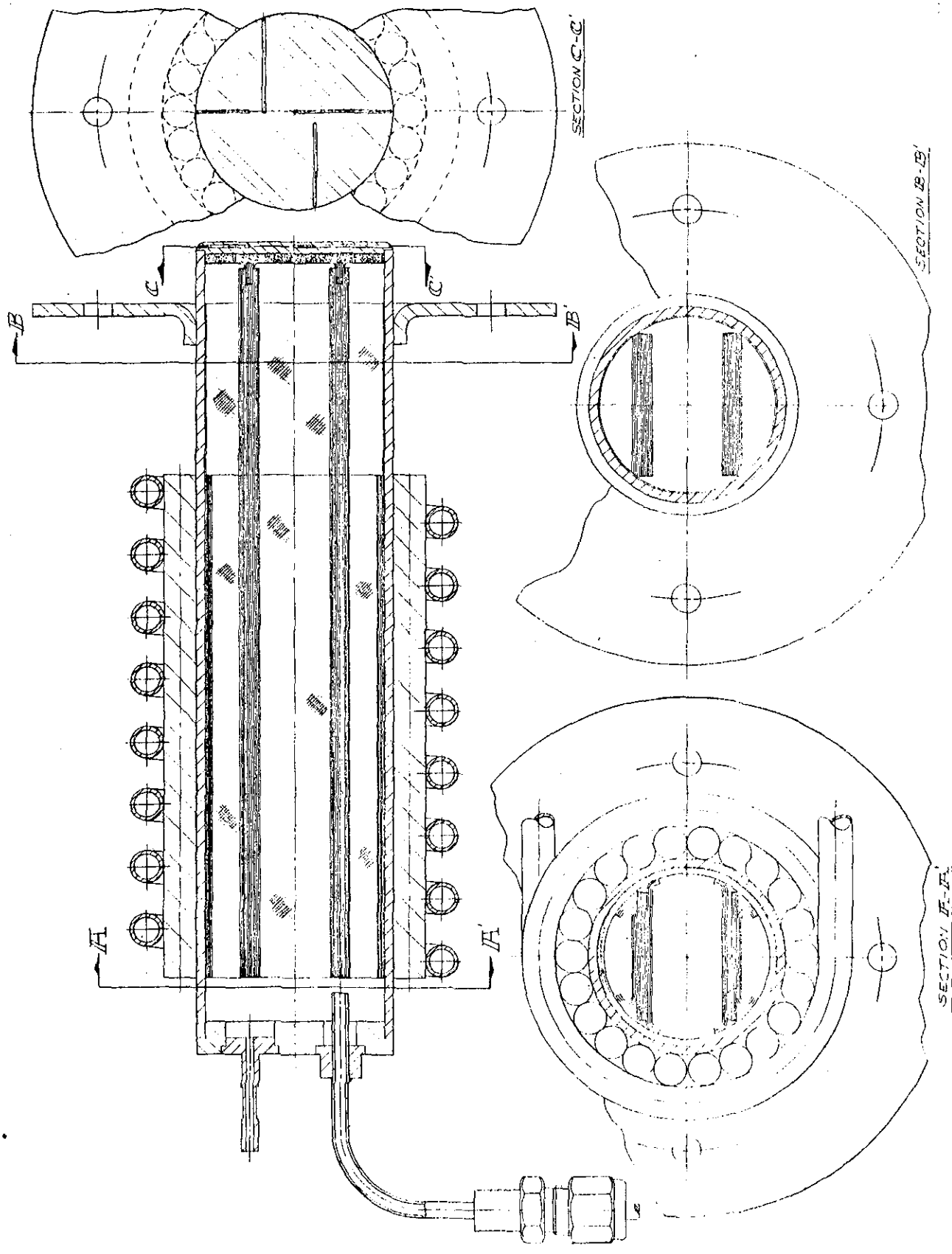

Heat Pipe 12 Design

Figure 36

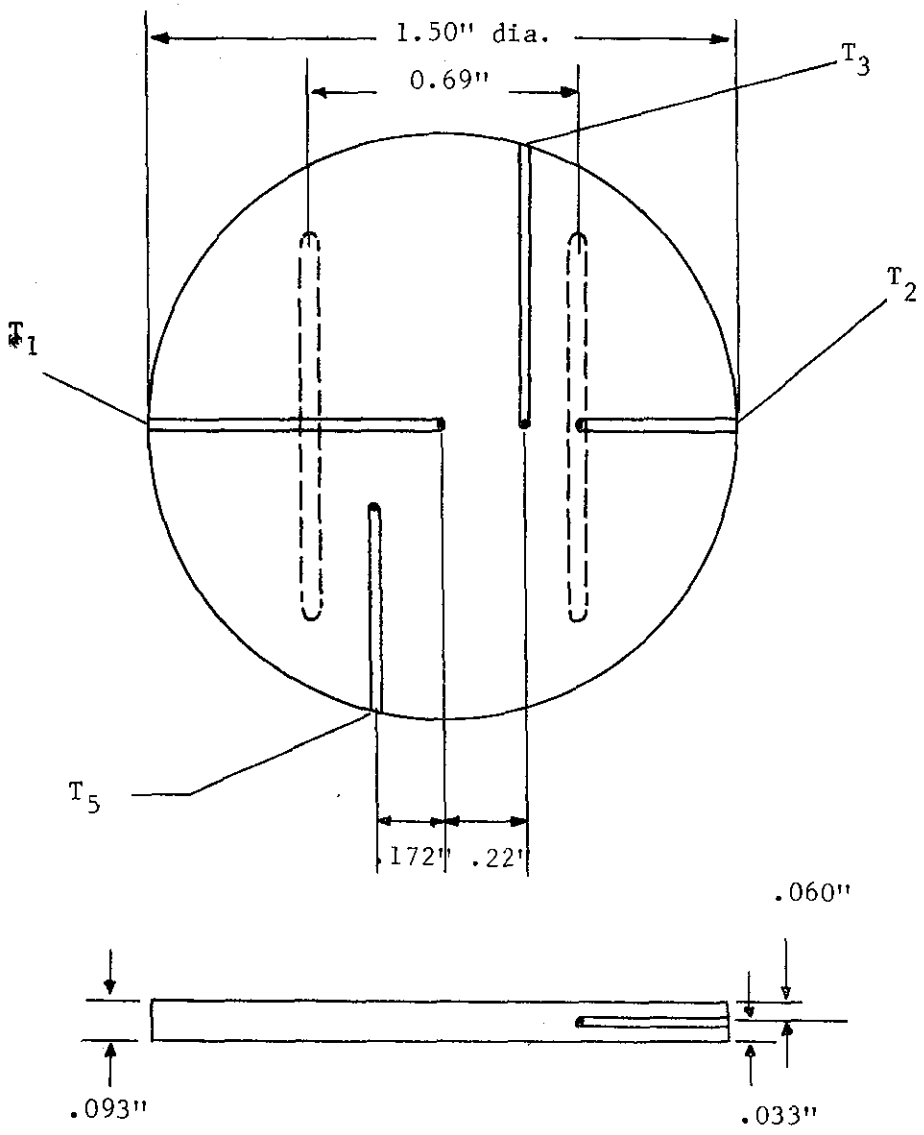

Thermocouple Locations, Heat Pipe No. 12

Figure 37

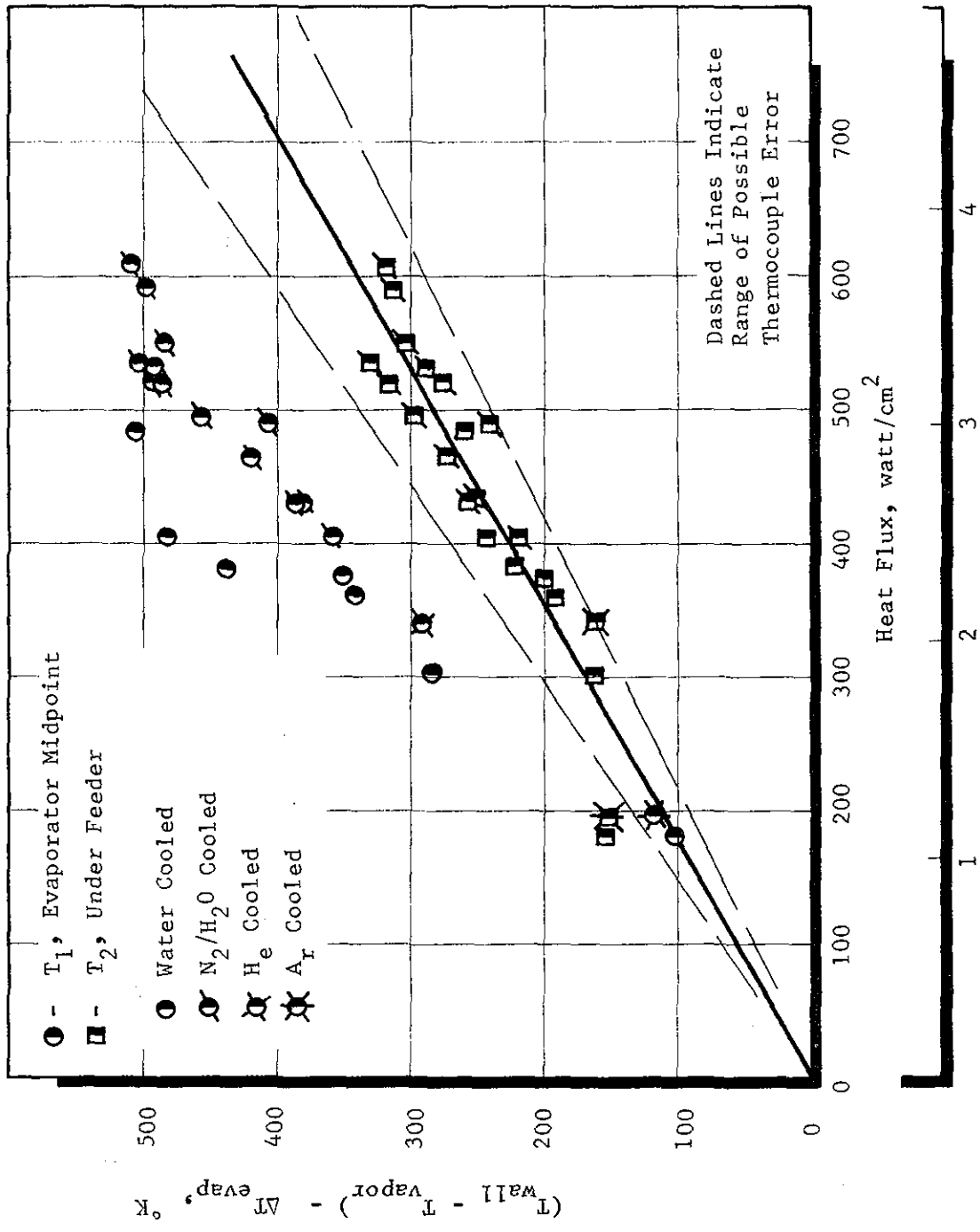

Heat Pipe 12 Test Results

Figure 38

Curve	Temp (°C) °K	Press. (Torr) kN/m^2
1	(1200) 1473	(6800) 906
2	(1100) 1373	(3797) 506
3	(1000) 1273	(1998) 266
4	(900) 1173	(852) 113
5	(800) 1073	(332) 44
6	(700) 973	(106) 14
7	(600) 873	(25) 3.3

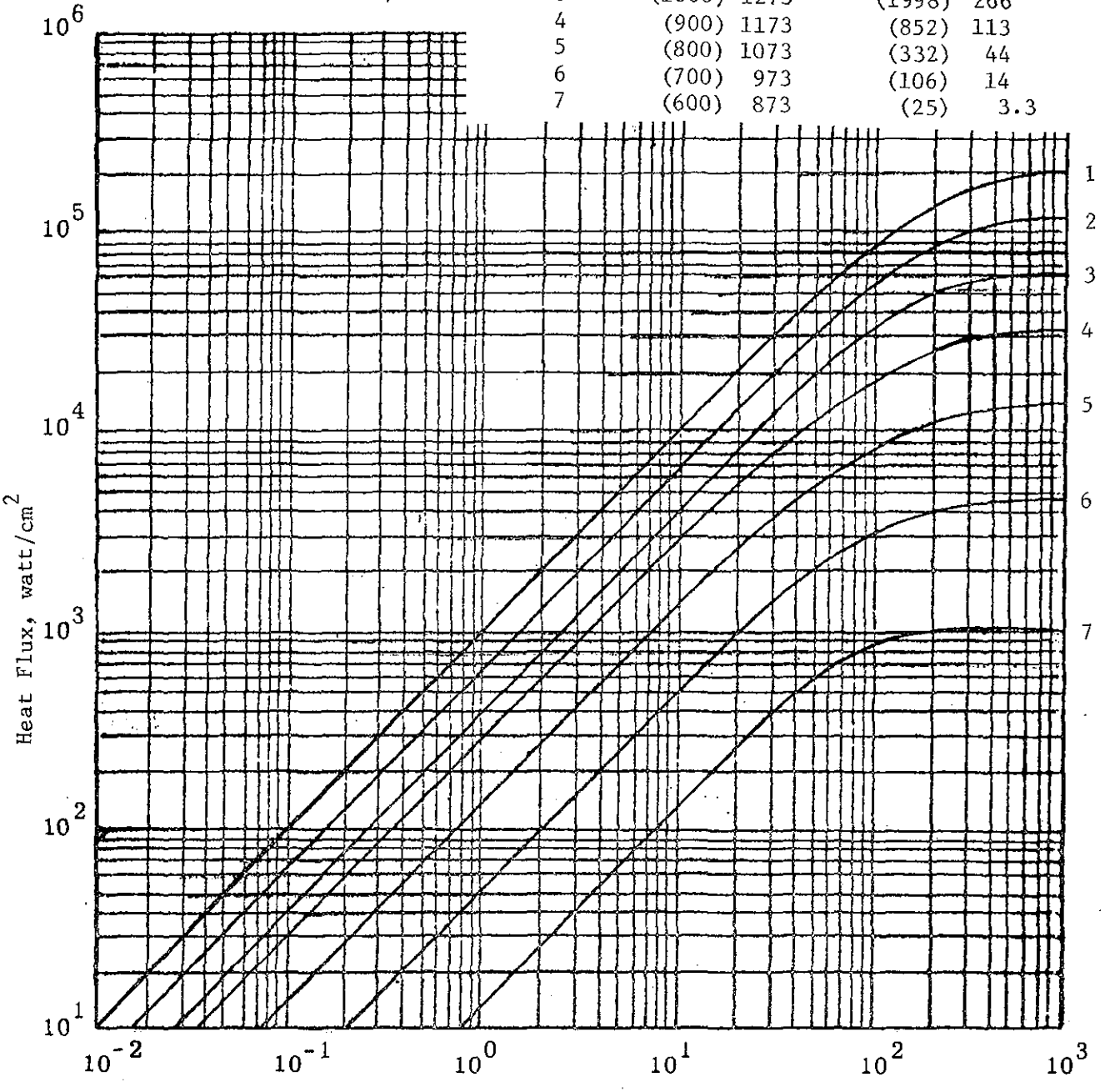

Estimated Evaporative Temperature Drop for Sodium

Figure 39

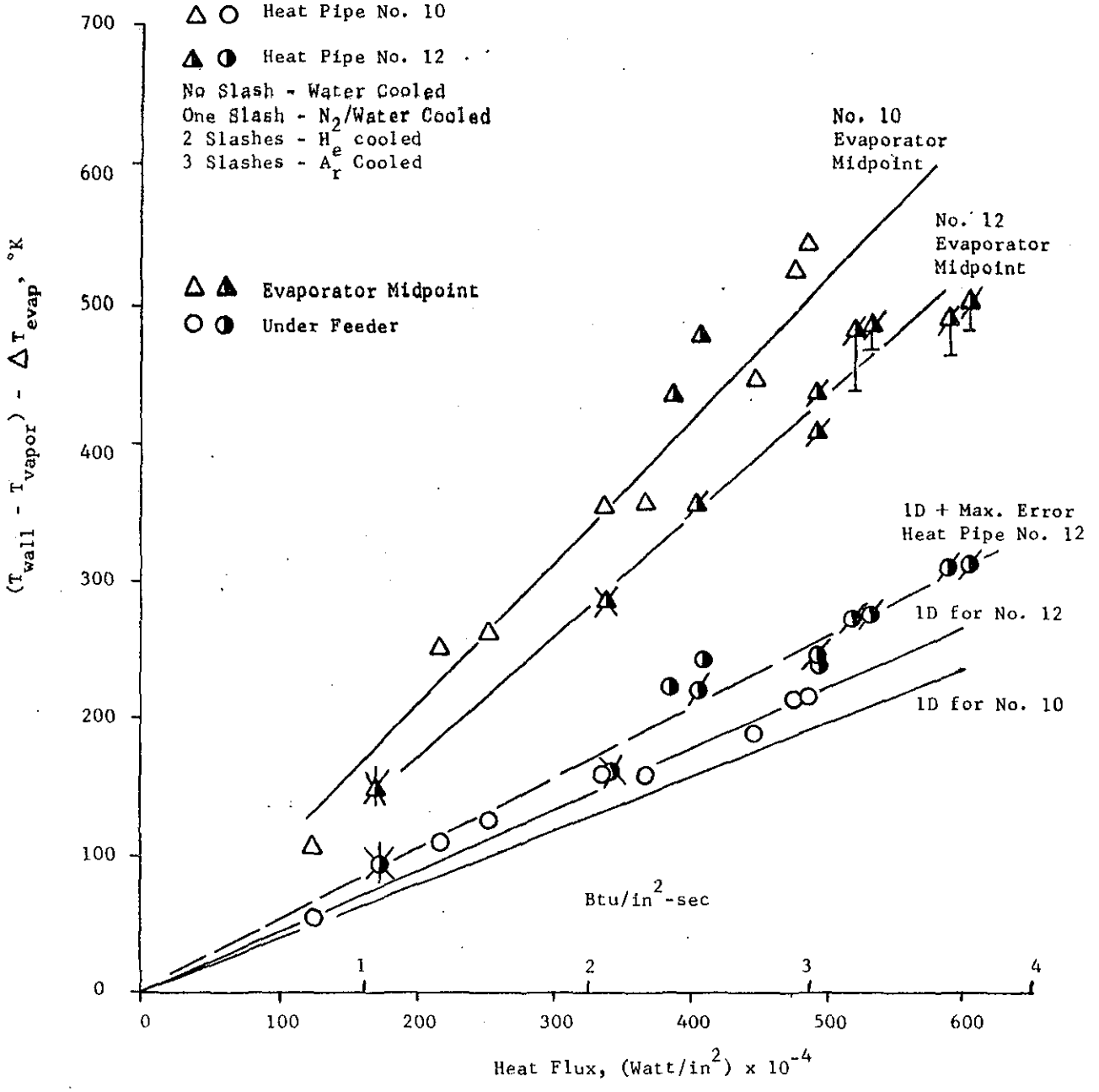

Comparison of Heat Pipe No. 12 and Heat Pipe No. 10 Test Data

Figure 40

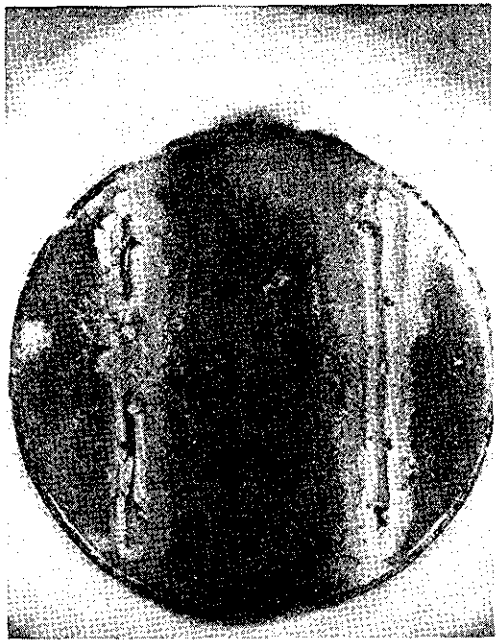

EVAPORATOR
(Liquid Return Feeders Removed)

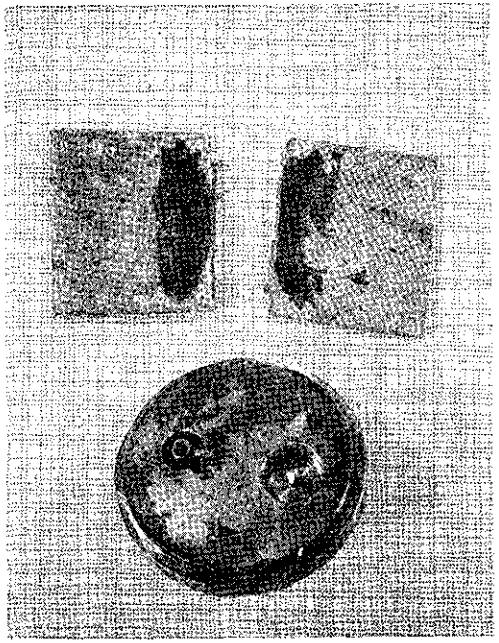

CONDENSER END CAP AND LOWER
PORTION OF LIQUID RETURN FEEDERS
(Interior Side of Feeders Shown, Blackened
Edges Were Adjacent to Evaporator Wick)

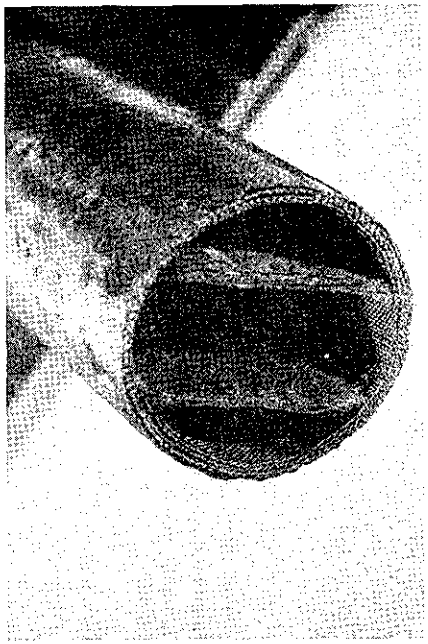

Condenser and Return Wicks

Figure 41. Posttest Photographs of Heat Pipe 12 Components

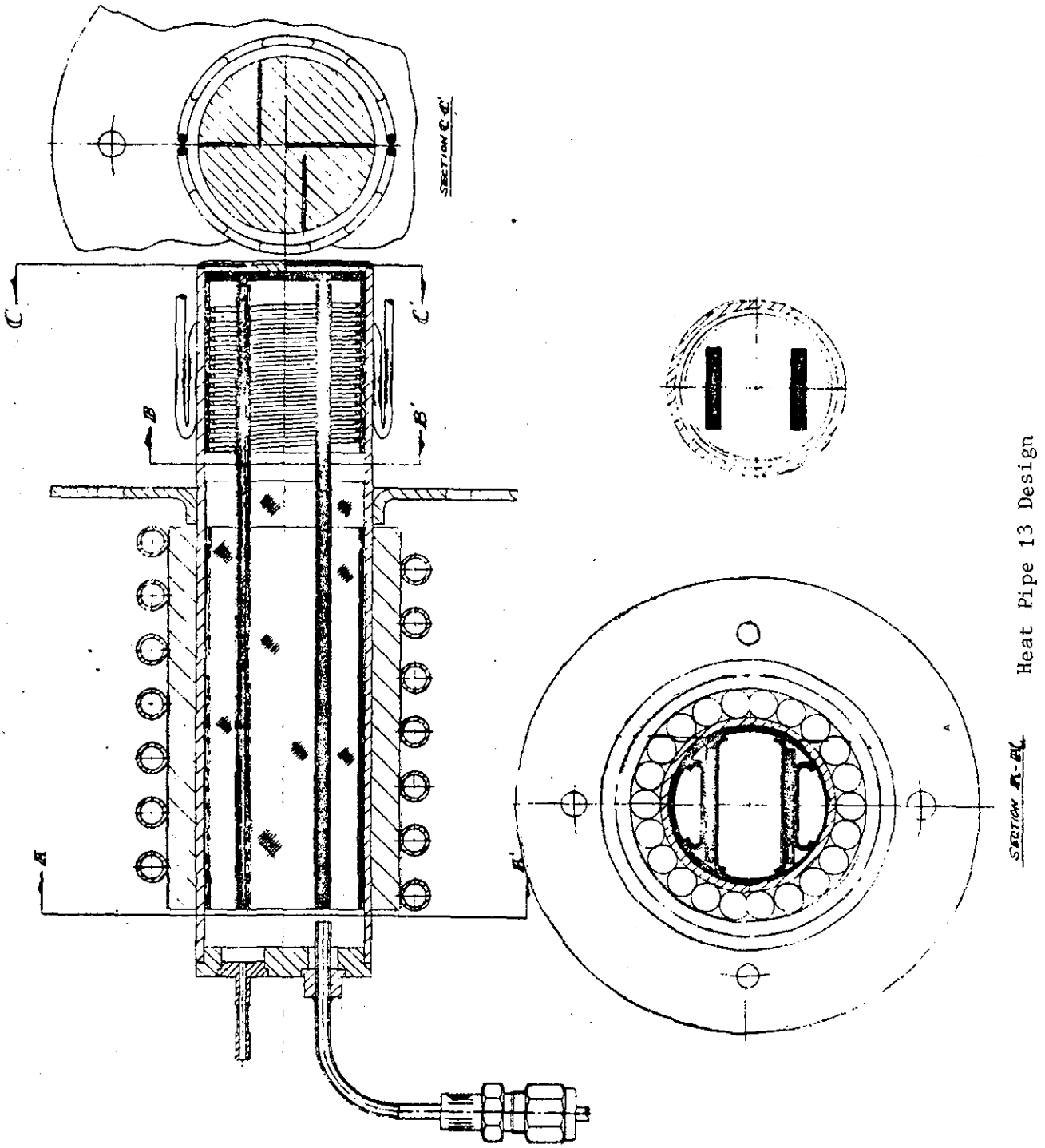

Heat Pipe 13 Design

Figure 42

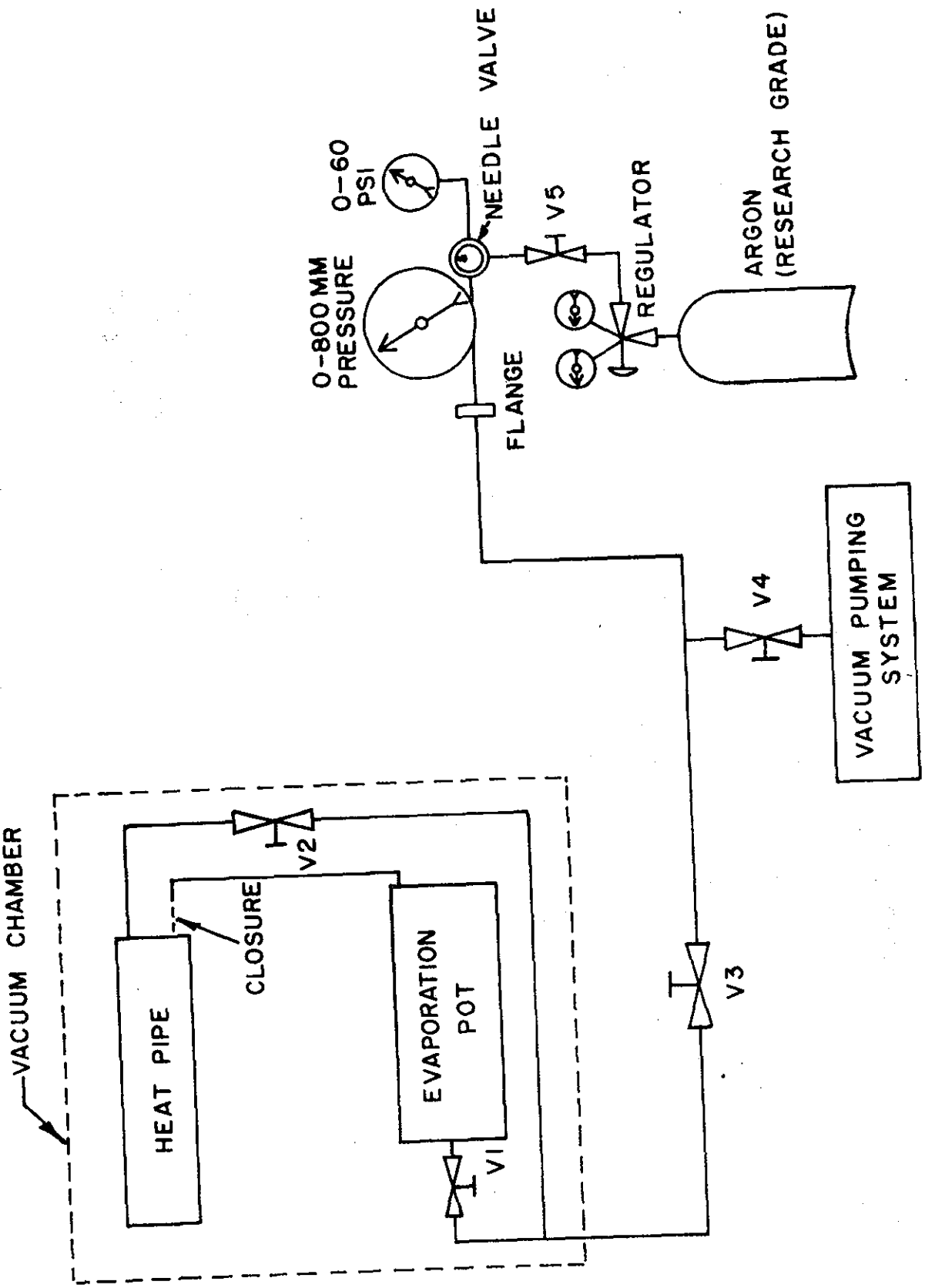

RCA Vacuum Distillation and Gas Dosing System

Figure 43

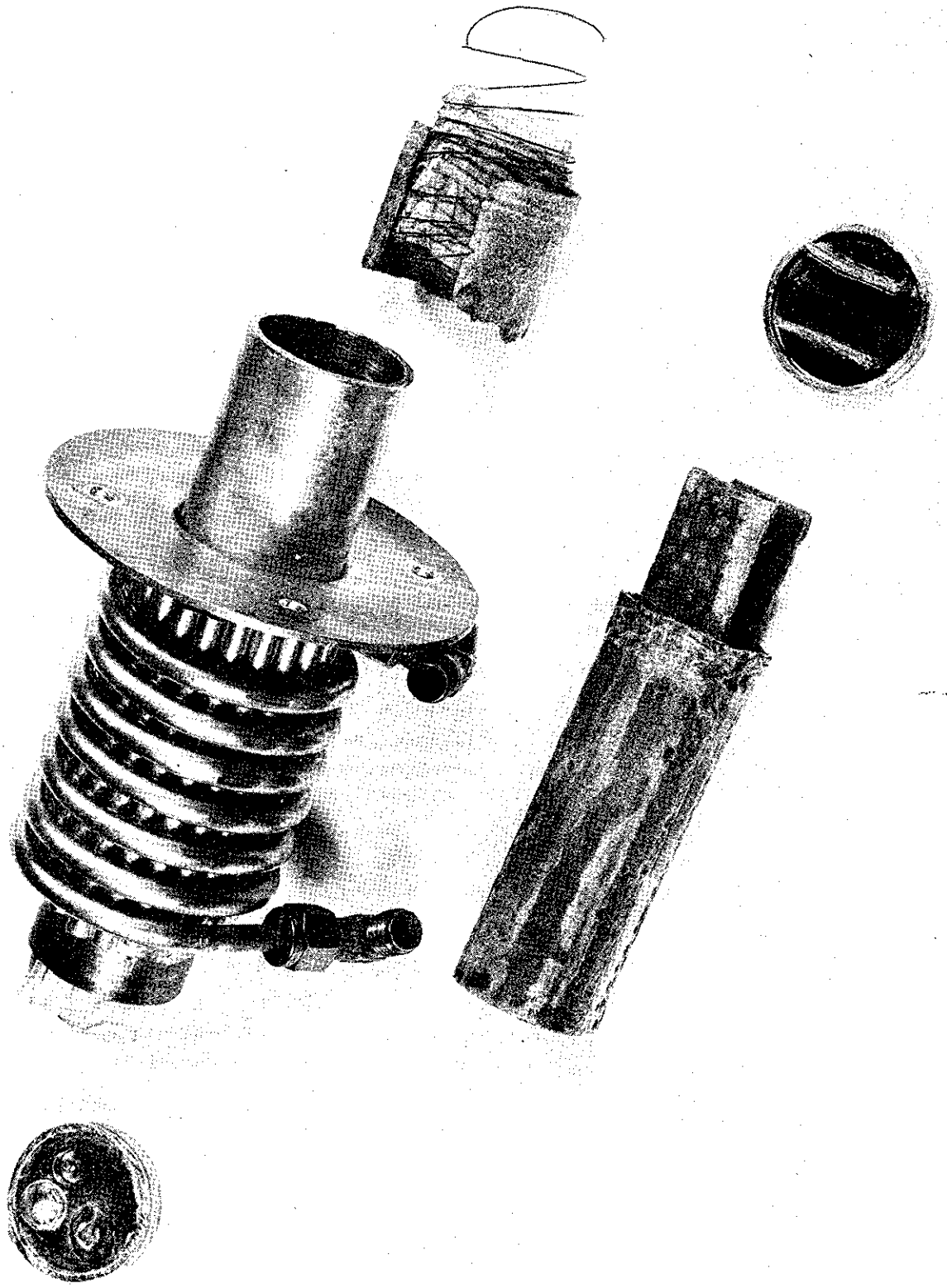

Heat Pipe 13 Components

Figure 44

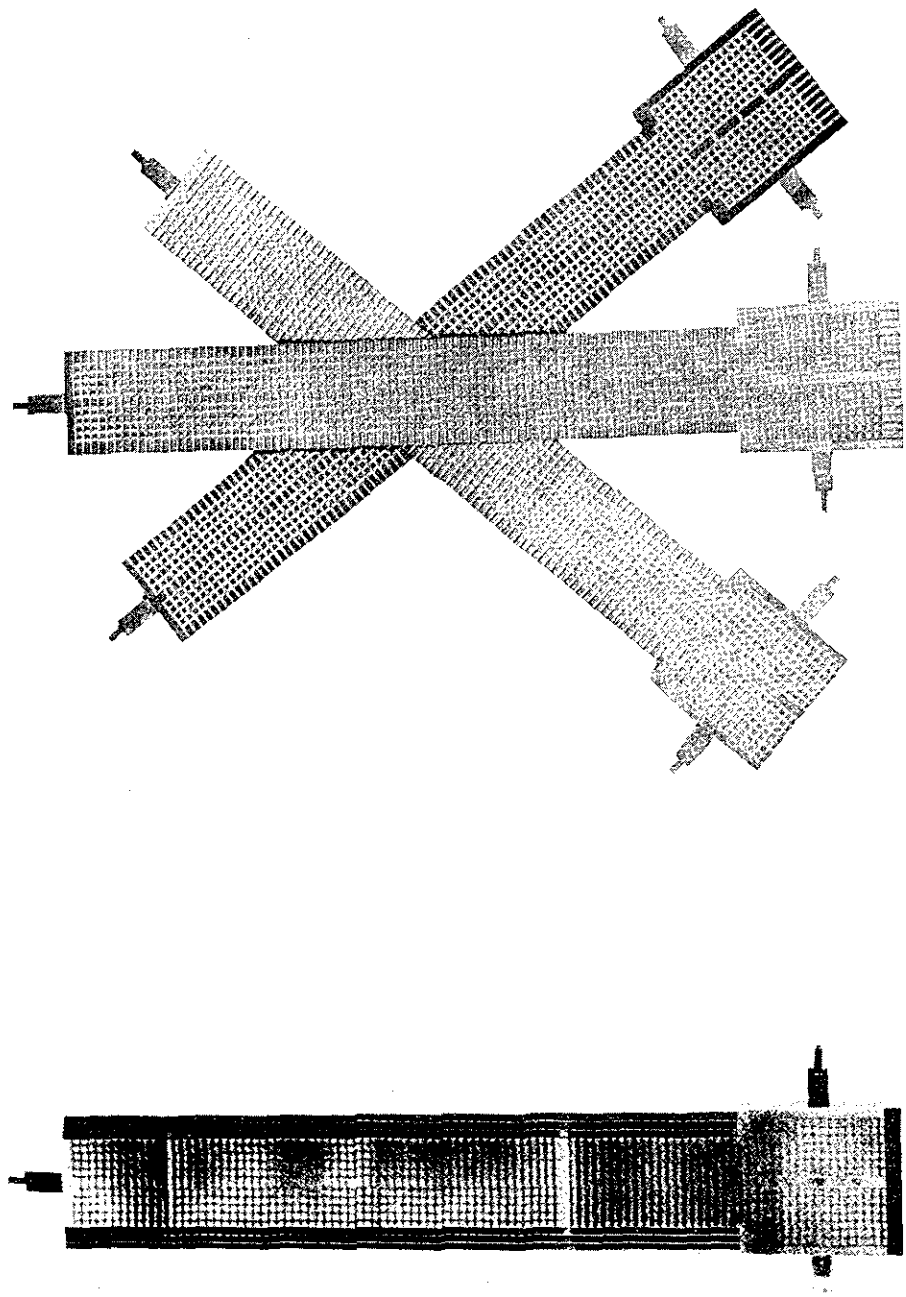

Typical Platelet Feeder and Unbonded Platelets

Figure 45

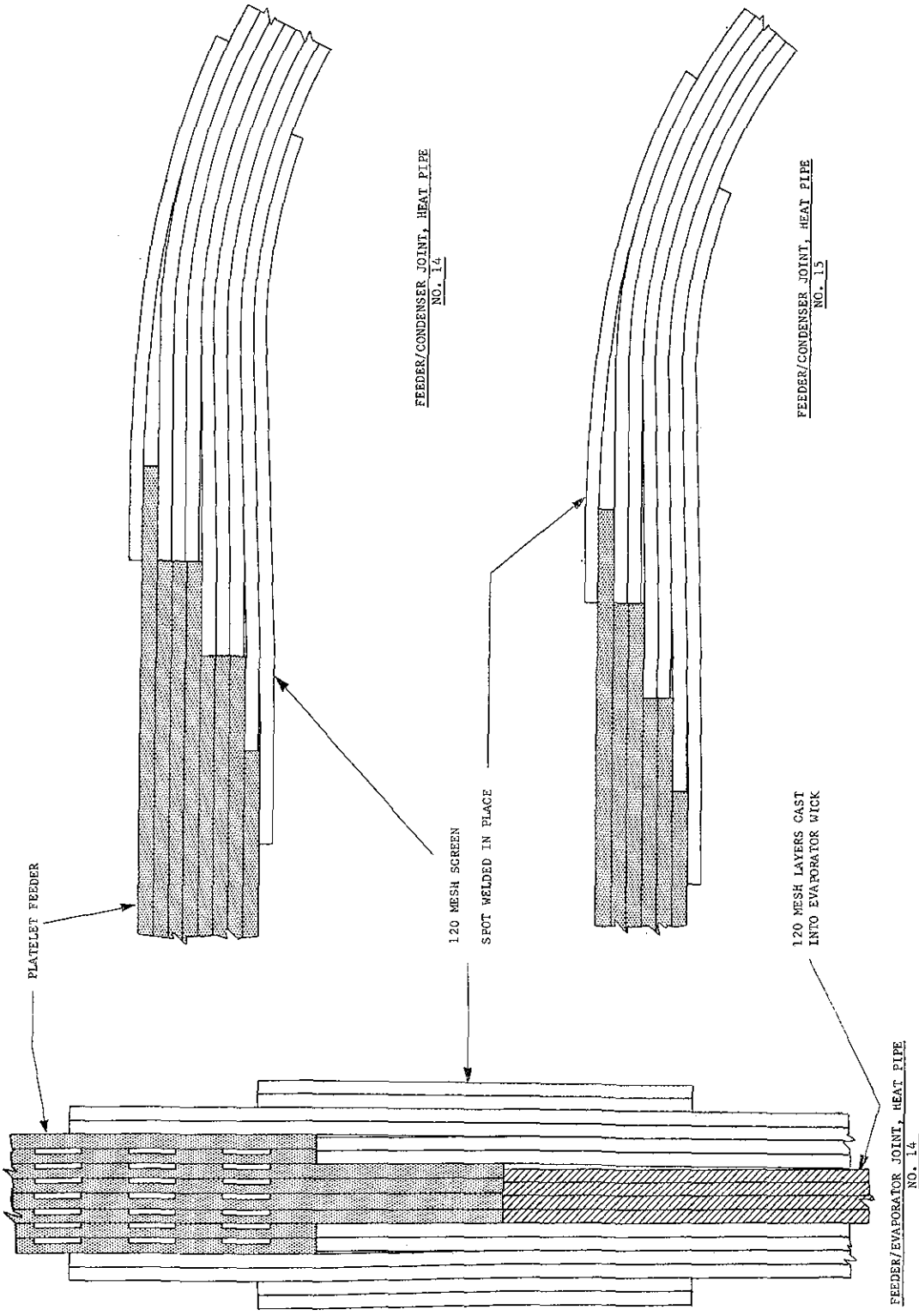

Figure 46 - Platelet Feeder Joint Designs

Figure 46

Condenser/Feeder Joint

Evaporator/Feeder Joint

Figure 47 Heat Pipe 14

Heat Pipe 14 Mounted on Test System

Figure 47

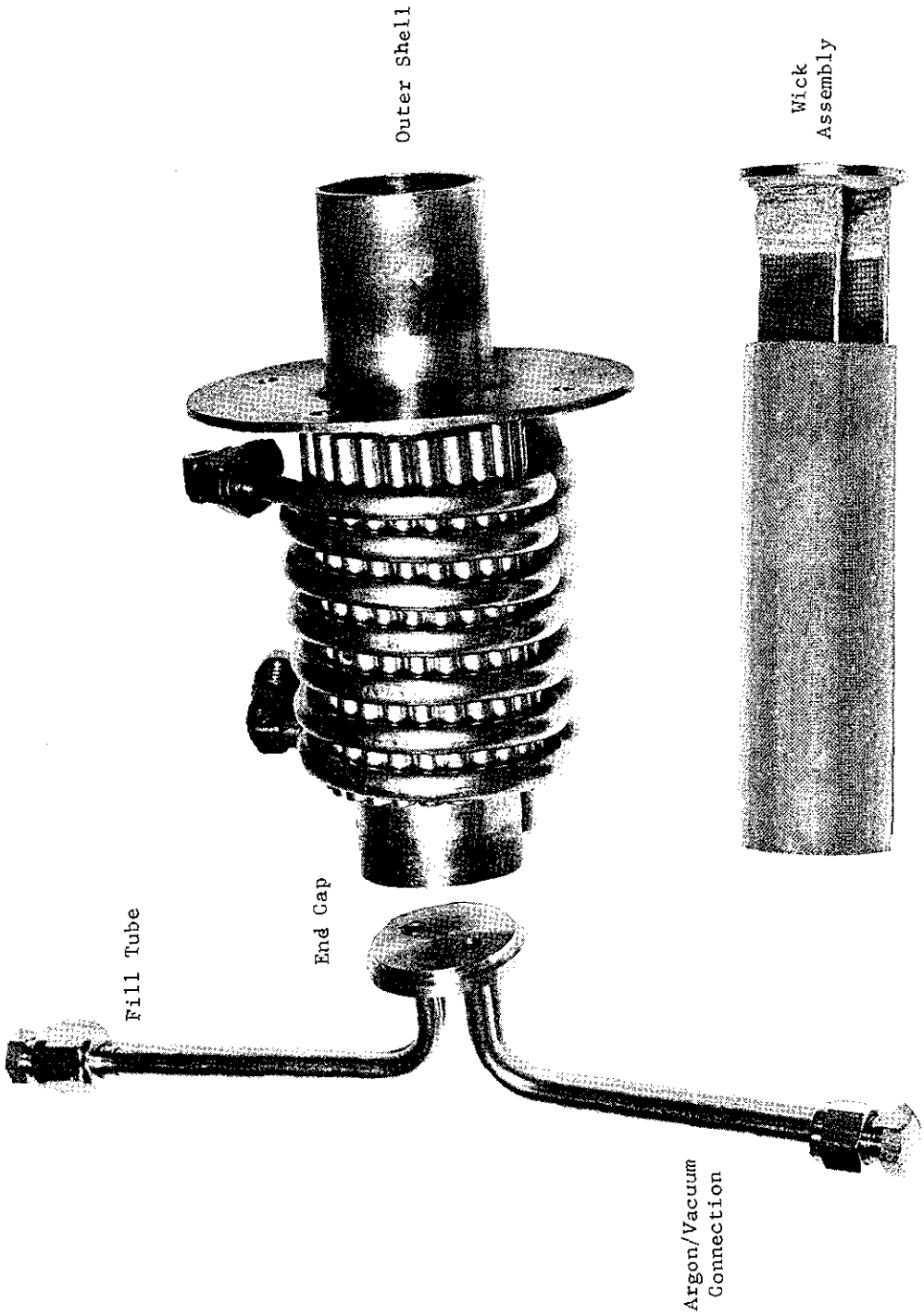

Figure 11. Heat Pipe No. 14 Components Before Final Welding

Heat Pipe No. 14 Components Before Final Welding

Figure 48

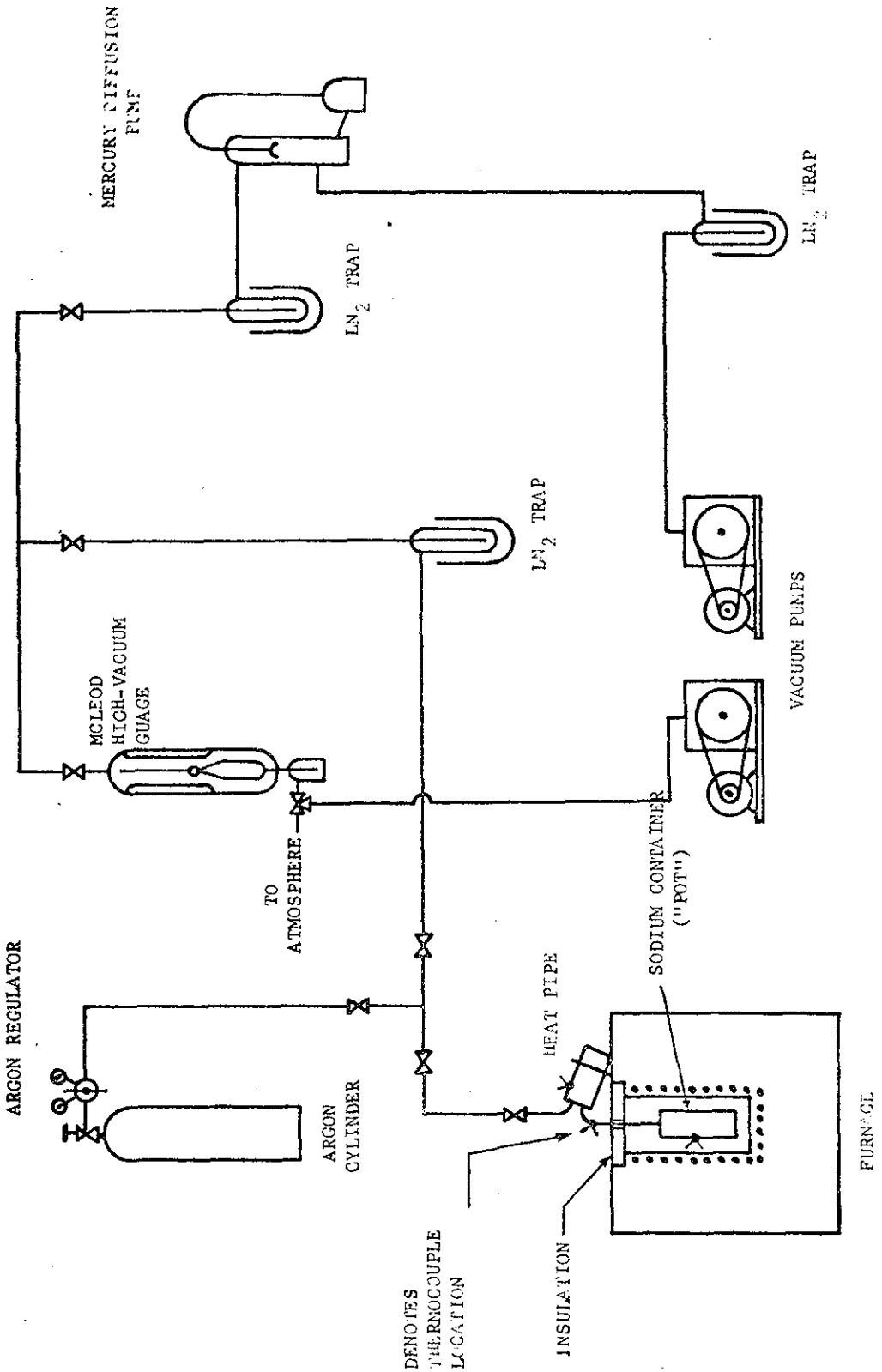

Aerojet Heat Pipe Loading System

Figure 49

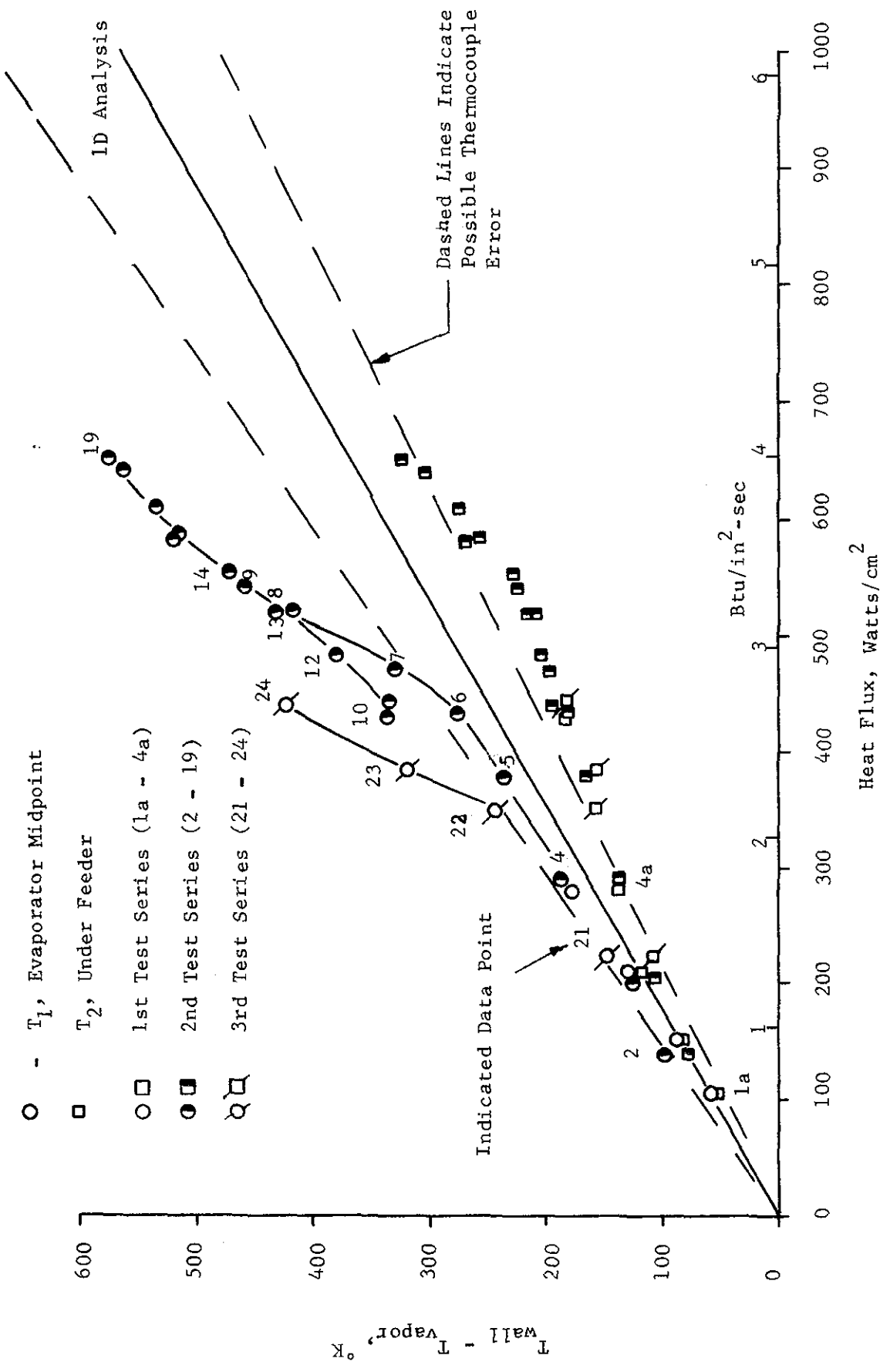
○ - T1, Evaporator Midpoint
□ T2, Under Feeder
1st Test Series (1a - 4a)
2nd Test Series (2 - 19)
3rd Test Series (21 - 24)
1D Analysis
Dashed Lines Indicate Possible Thermocouple Error
Indicated Data Point
Twall - Tvapor, °K
Heat Flux, Watts/cm2
Btu/in2-sec
Heat Pipe No. 14 Test Results

Figure 50

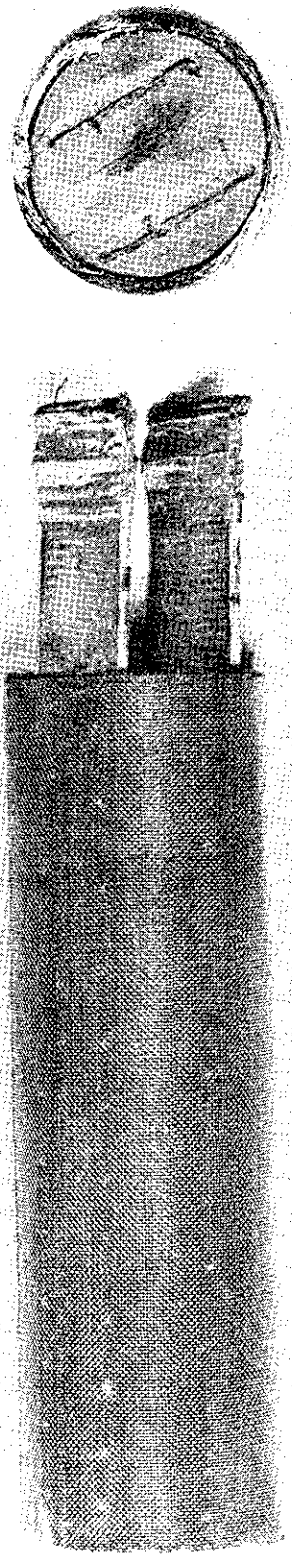

Heat Pipe 14 Components After Testing

Figure 51

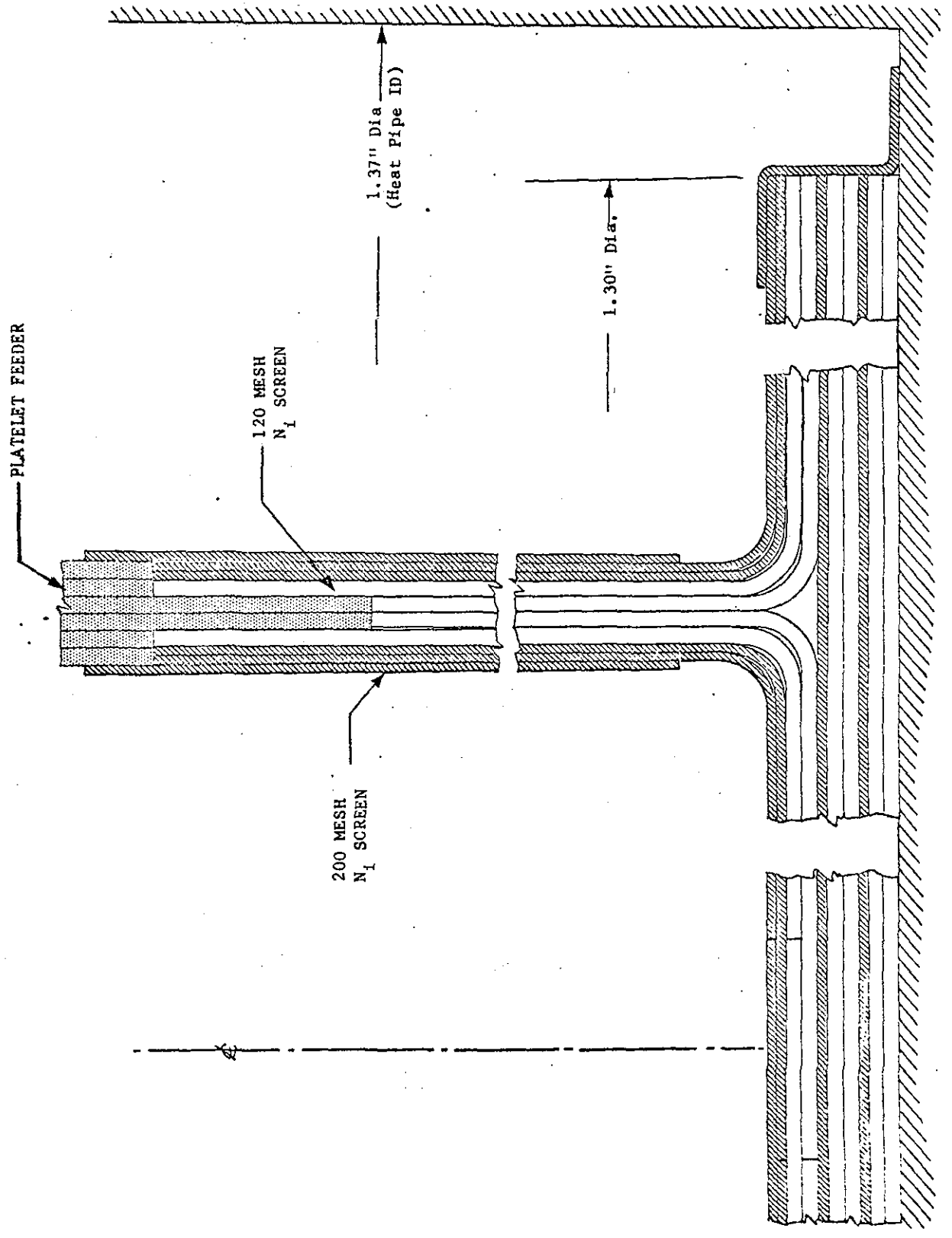

Heat Pipe No. 15 Evaporator Design

Figure 52

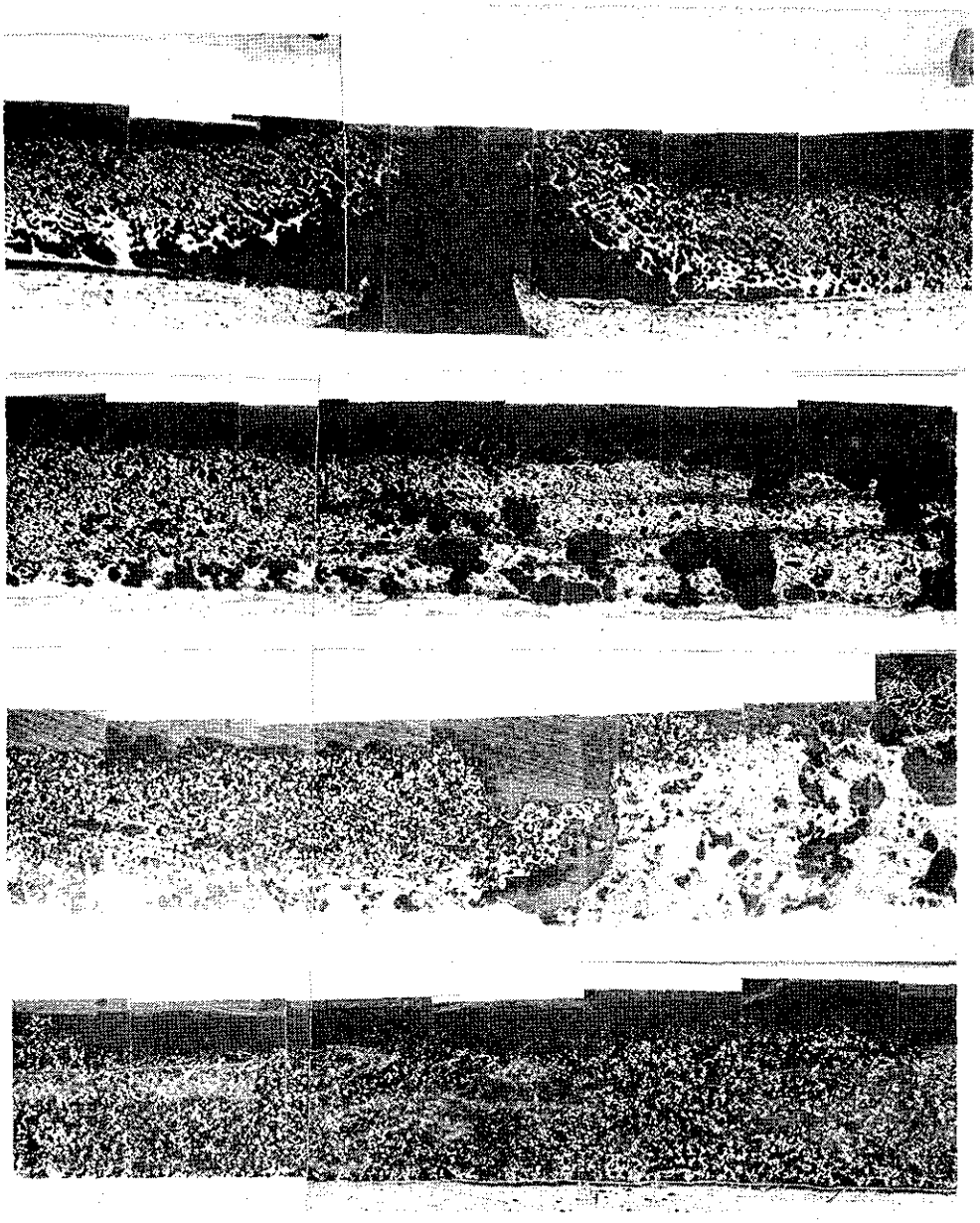

Heat Pipe No. 7

Heat Pipe No. 10

Heat Pipe No. 11

Heat Pipe No. 12

Cross-sections of Center Evaporator Areas for Heat Pipes 7, 10, 11 and 12

Figure 53

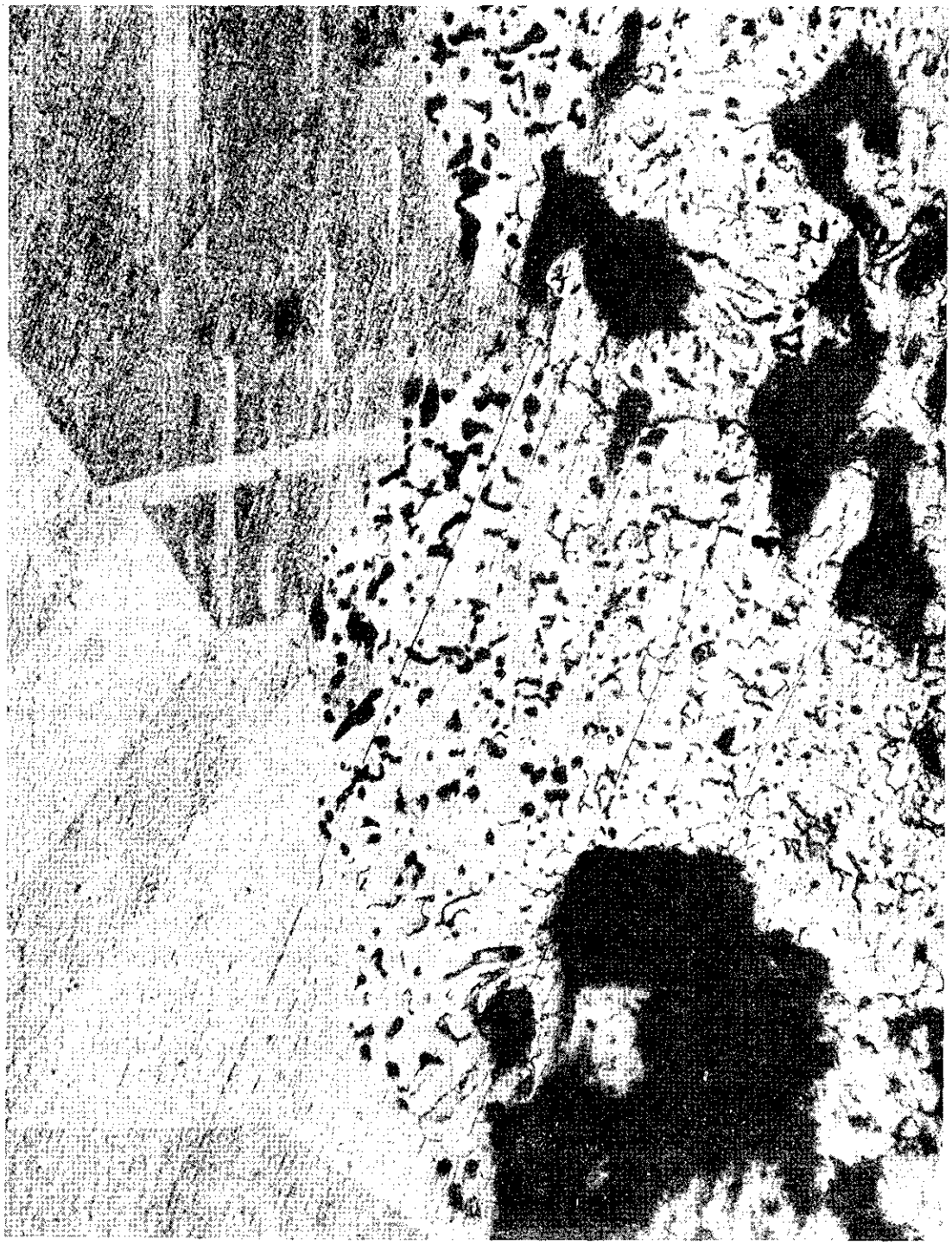

Photograph Showing Evaporator Erosion in Device No. 11
(Magnification 276X)

Figure 54

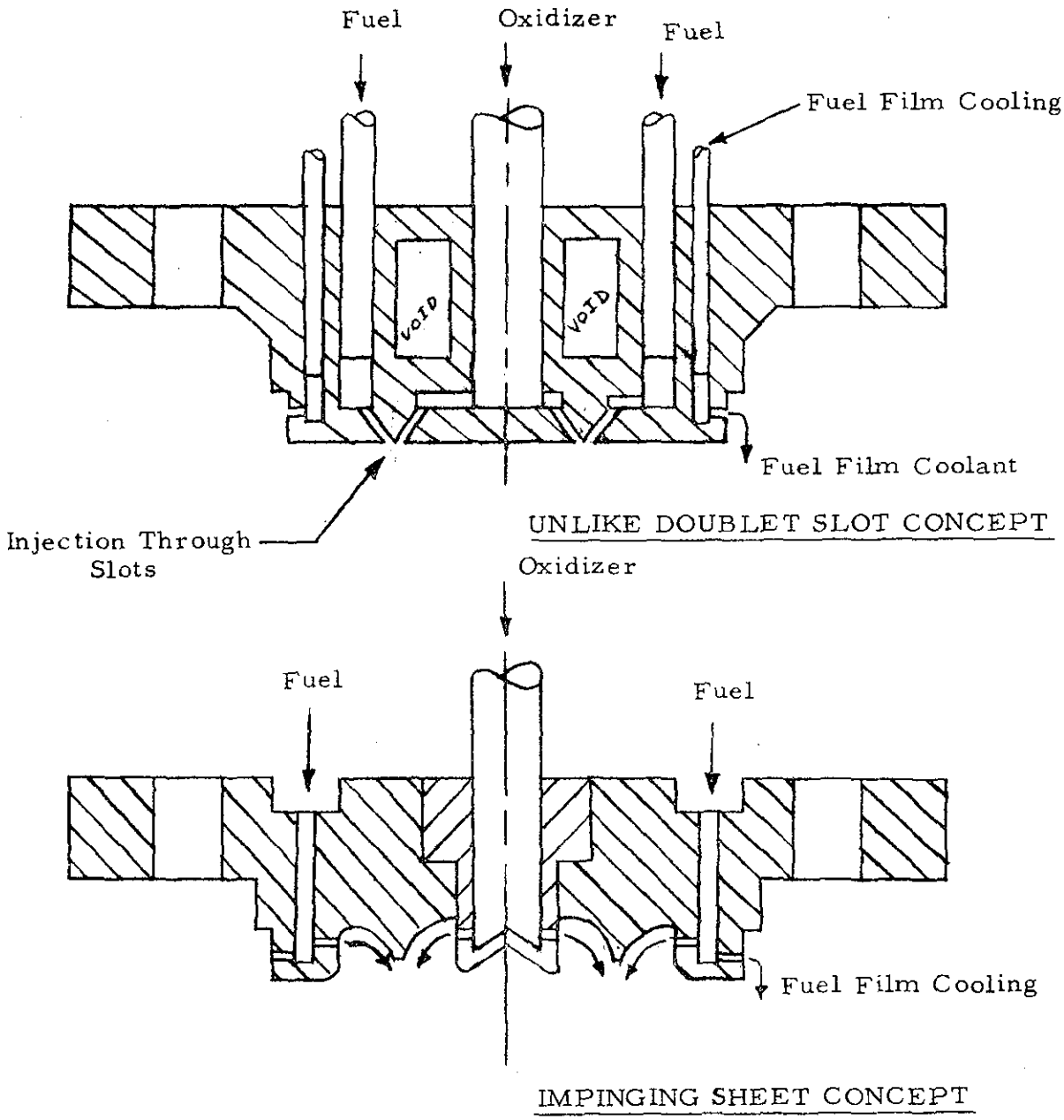

Impinging Sheet and Unlike Doublet Slot Injector Concepts

Figure 55

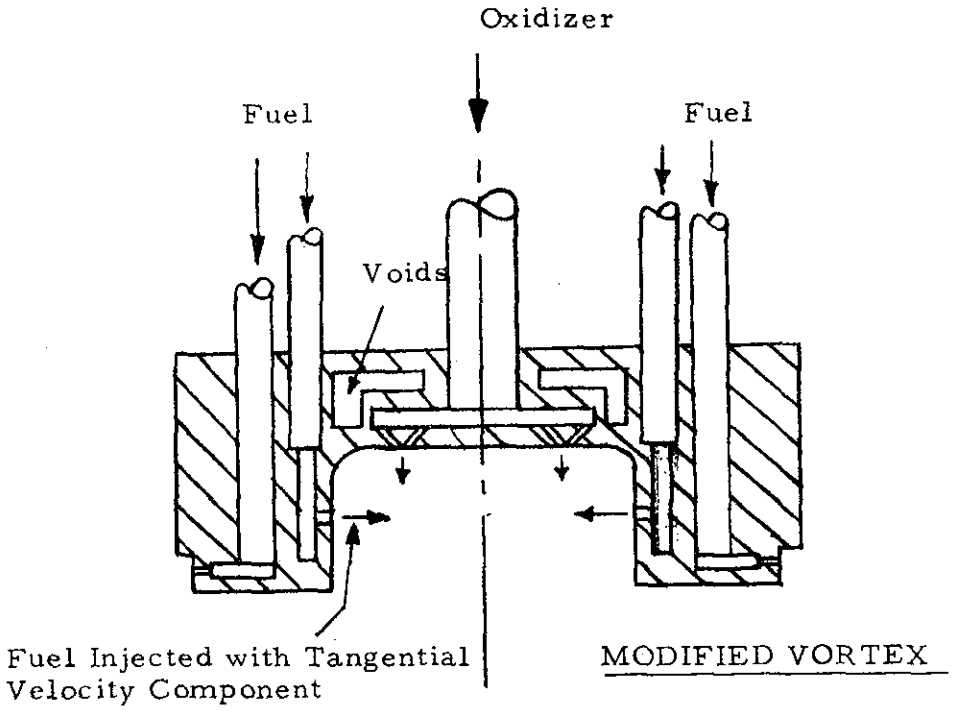

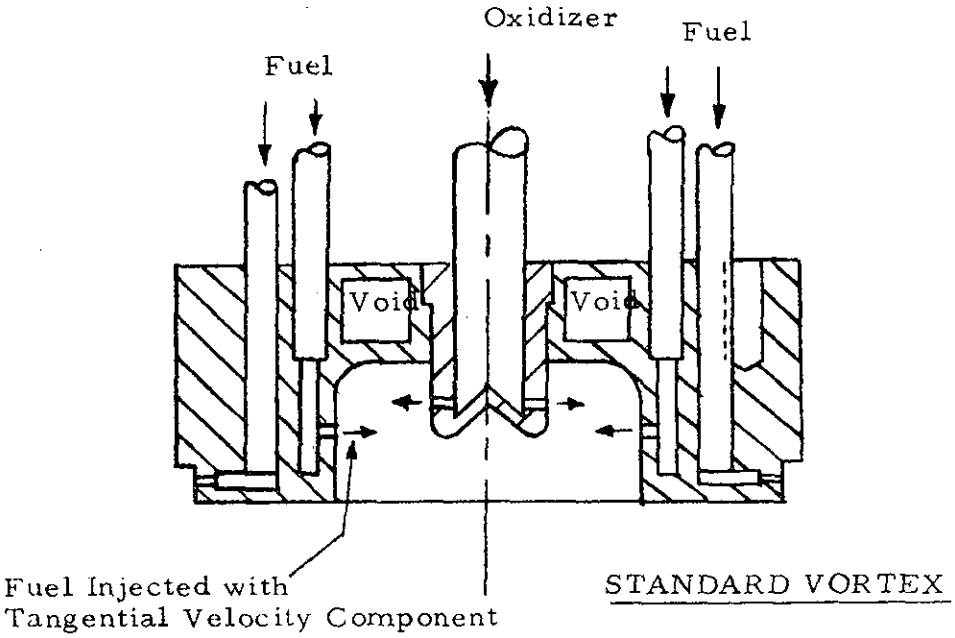

Vortex Injector Concepts

Figure 56

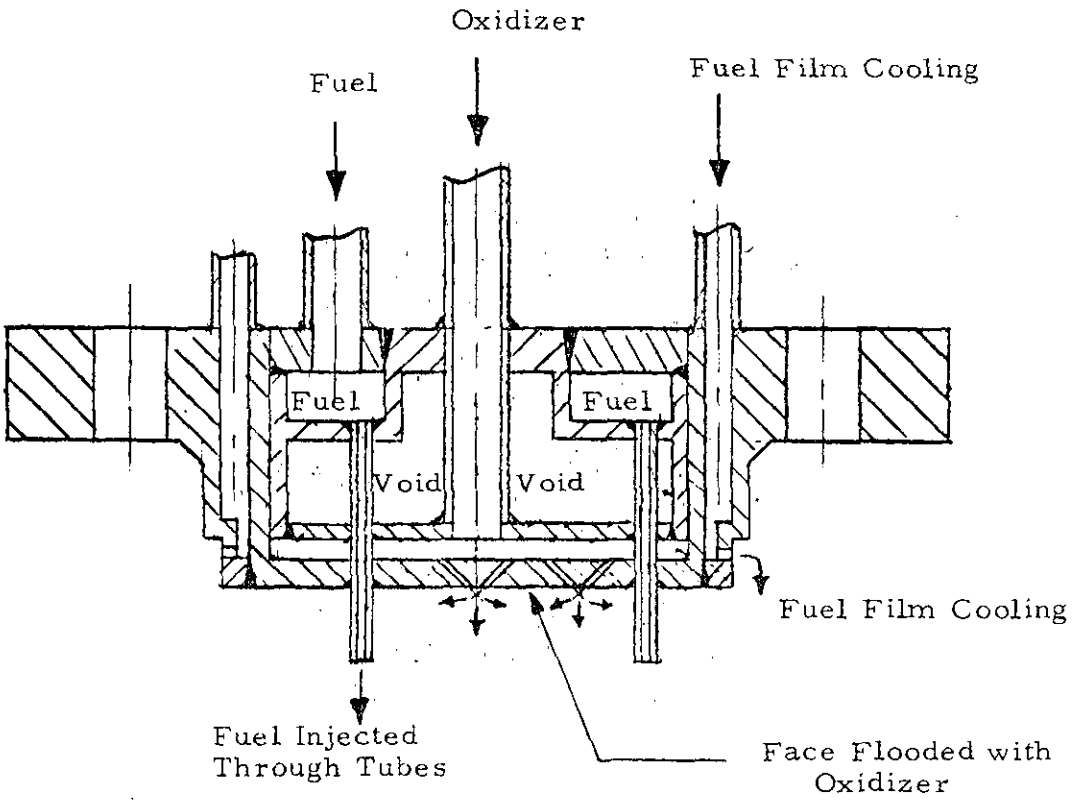

Showerhead - Tube Injector Concept

Figure 57

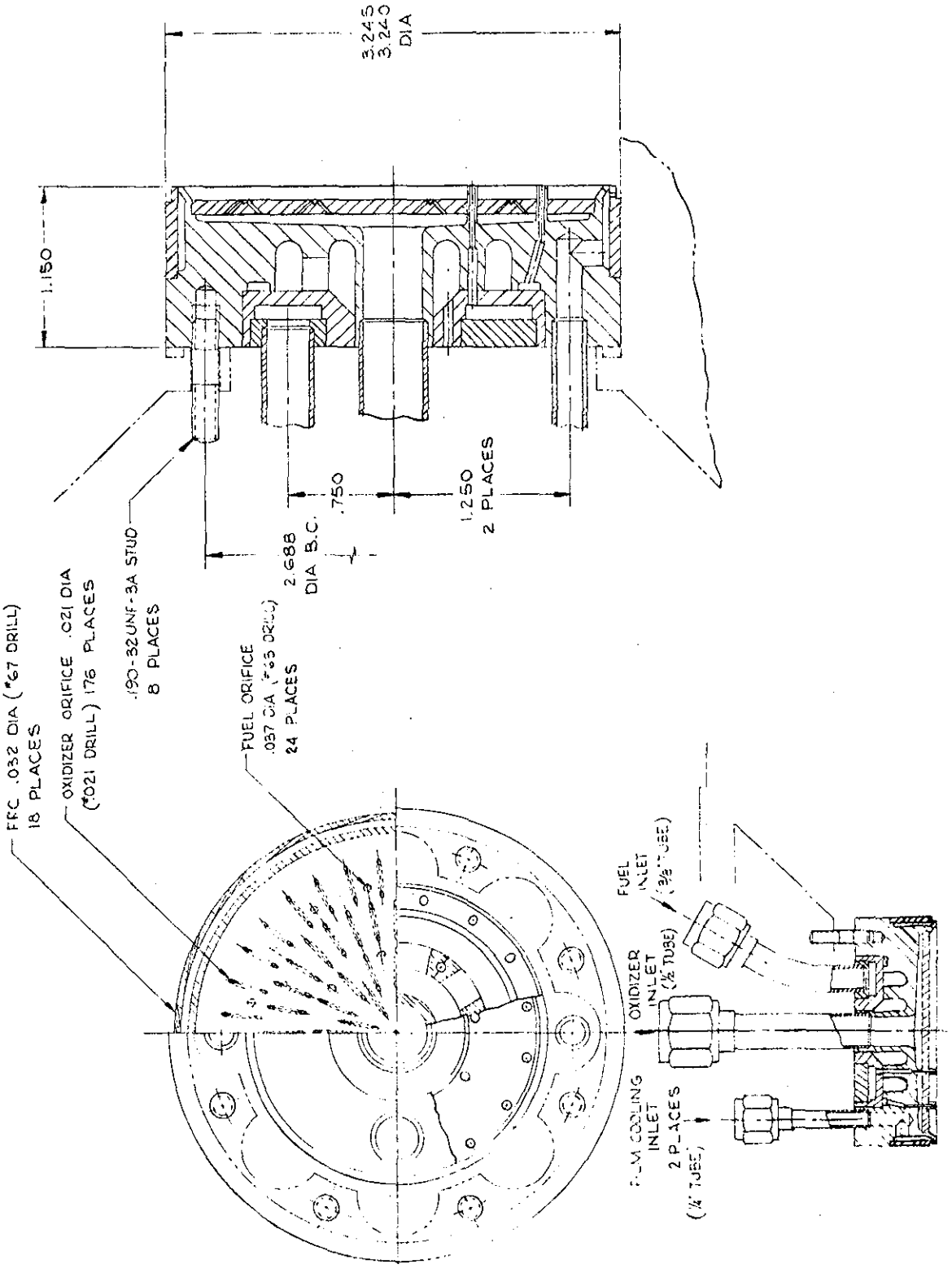

Showerhead - Tube Injector Concept for OF_2/B_2H_6

Figure 58

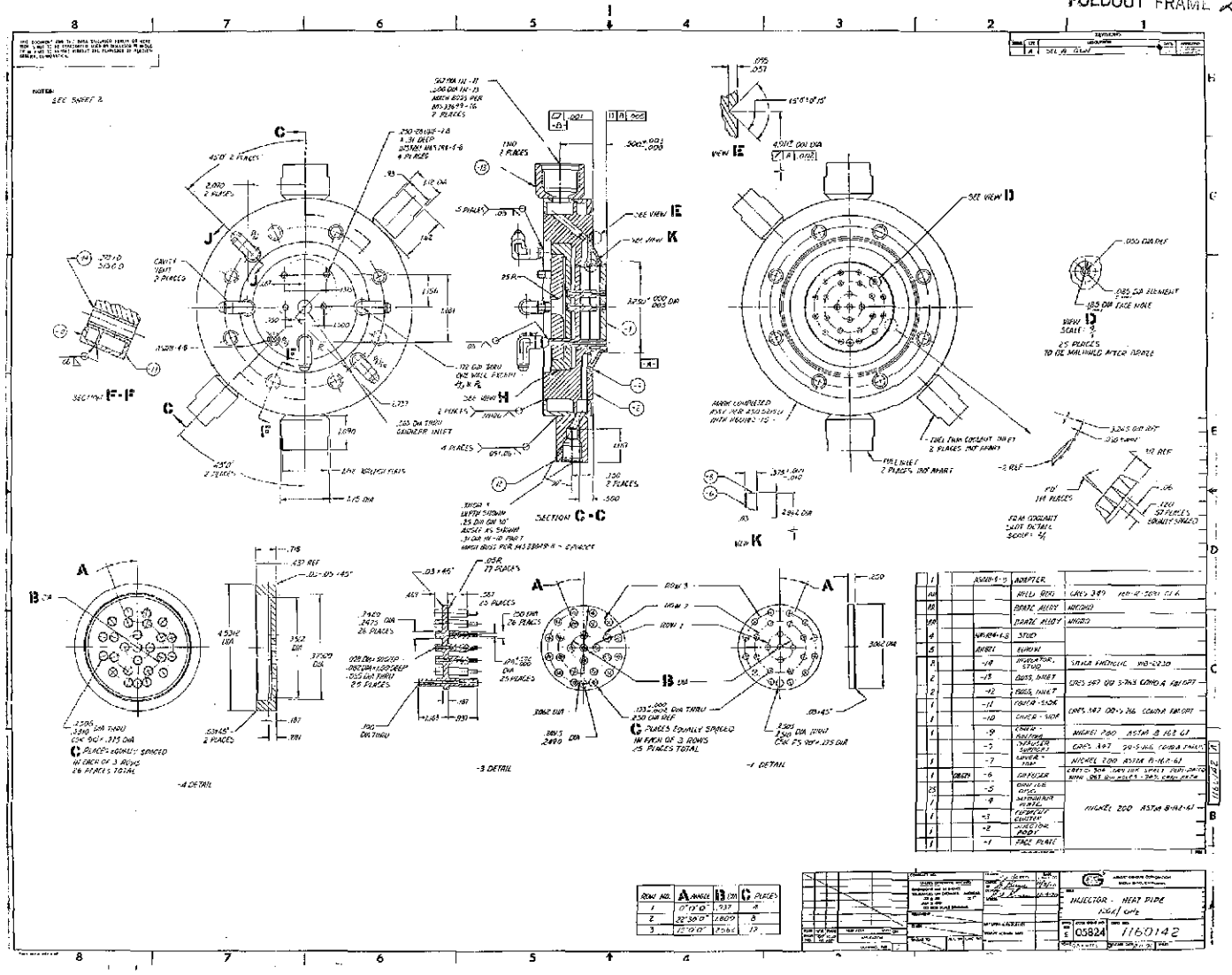

FLOX/H_2 Injector Design

Figure 59, Sheet 1 of 2

FOLDOUT FRAME 1

FOLDOUT FRAME 2
Report 697-F

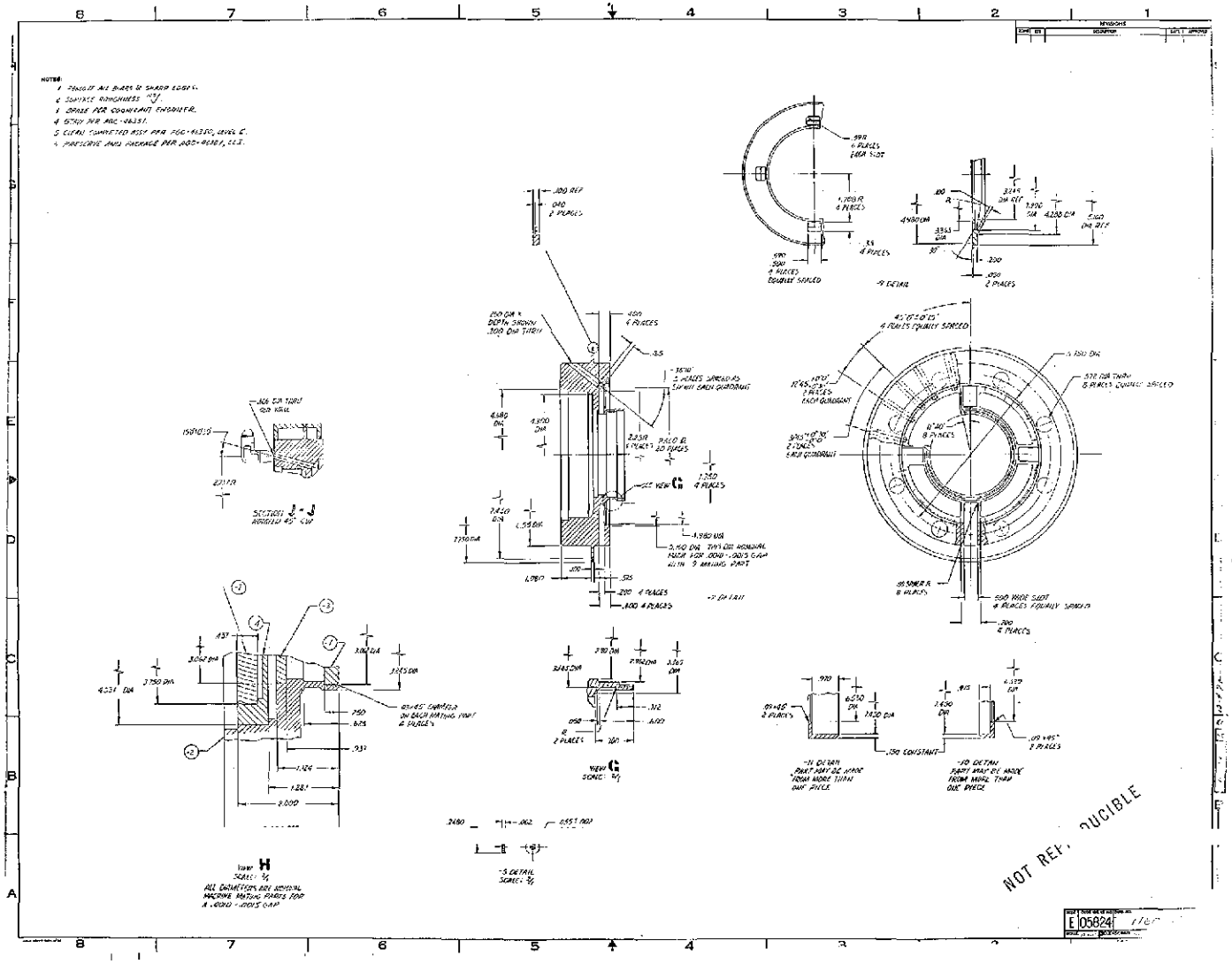

FLOX/H_2 Injector Design

Figure 59, Sheet 2 of 2

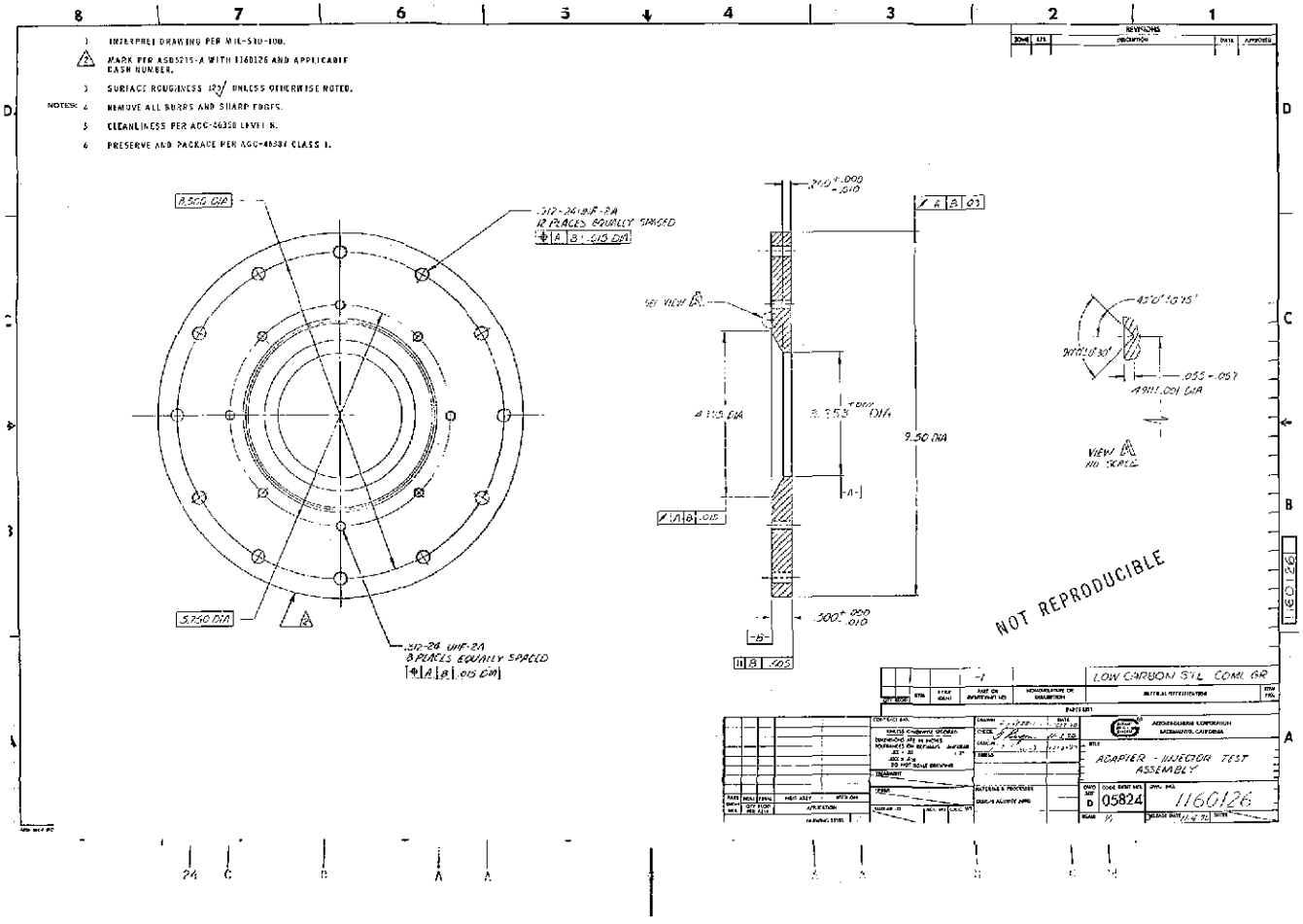

Injector-Chamber Adapter

Figure 60

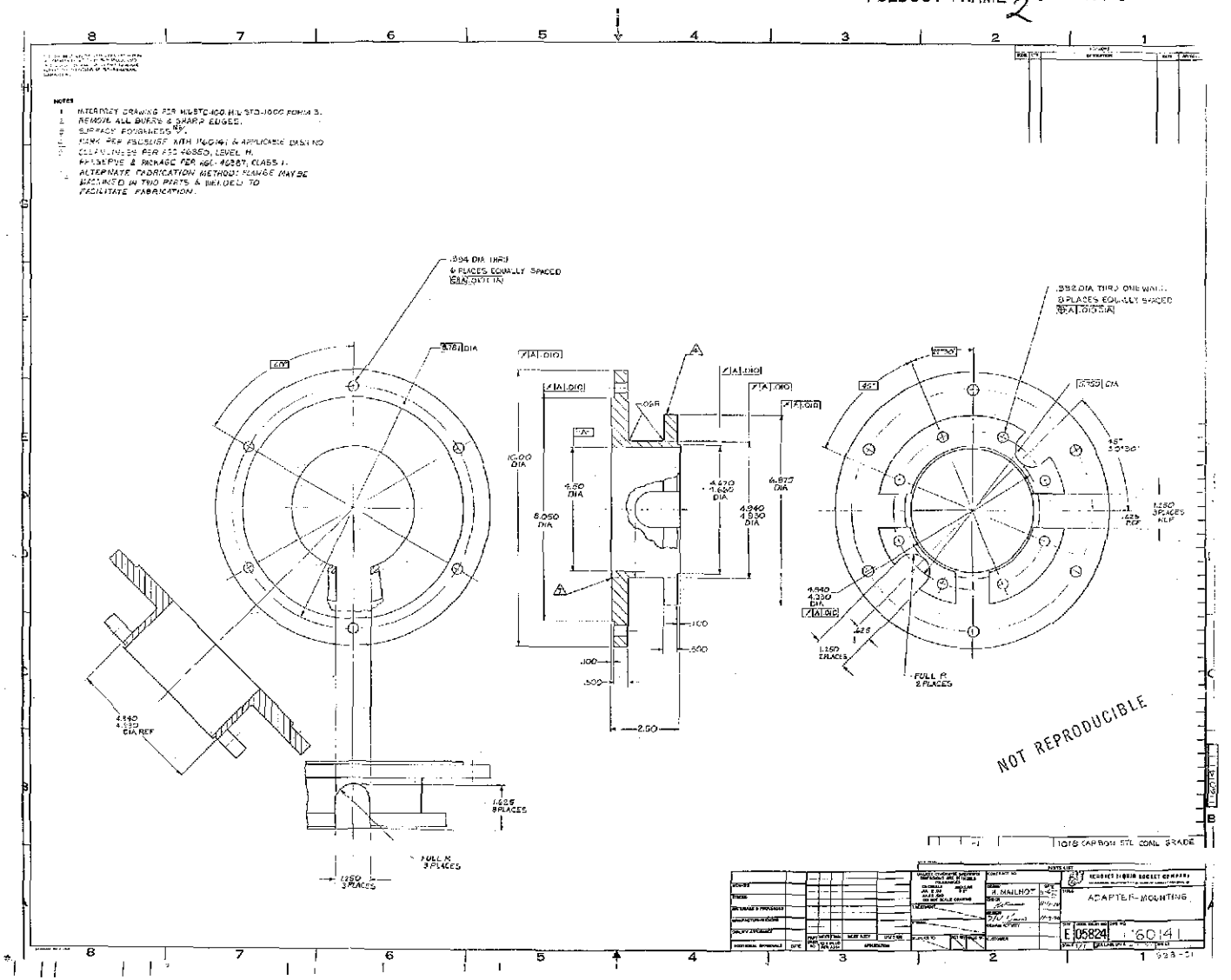

Injector - Thrust Mount Adapter

Figure 61

FOLDOUT FRAME 1

FOLDOUT FRAME 2

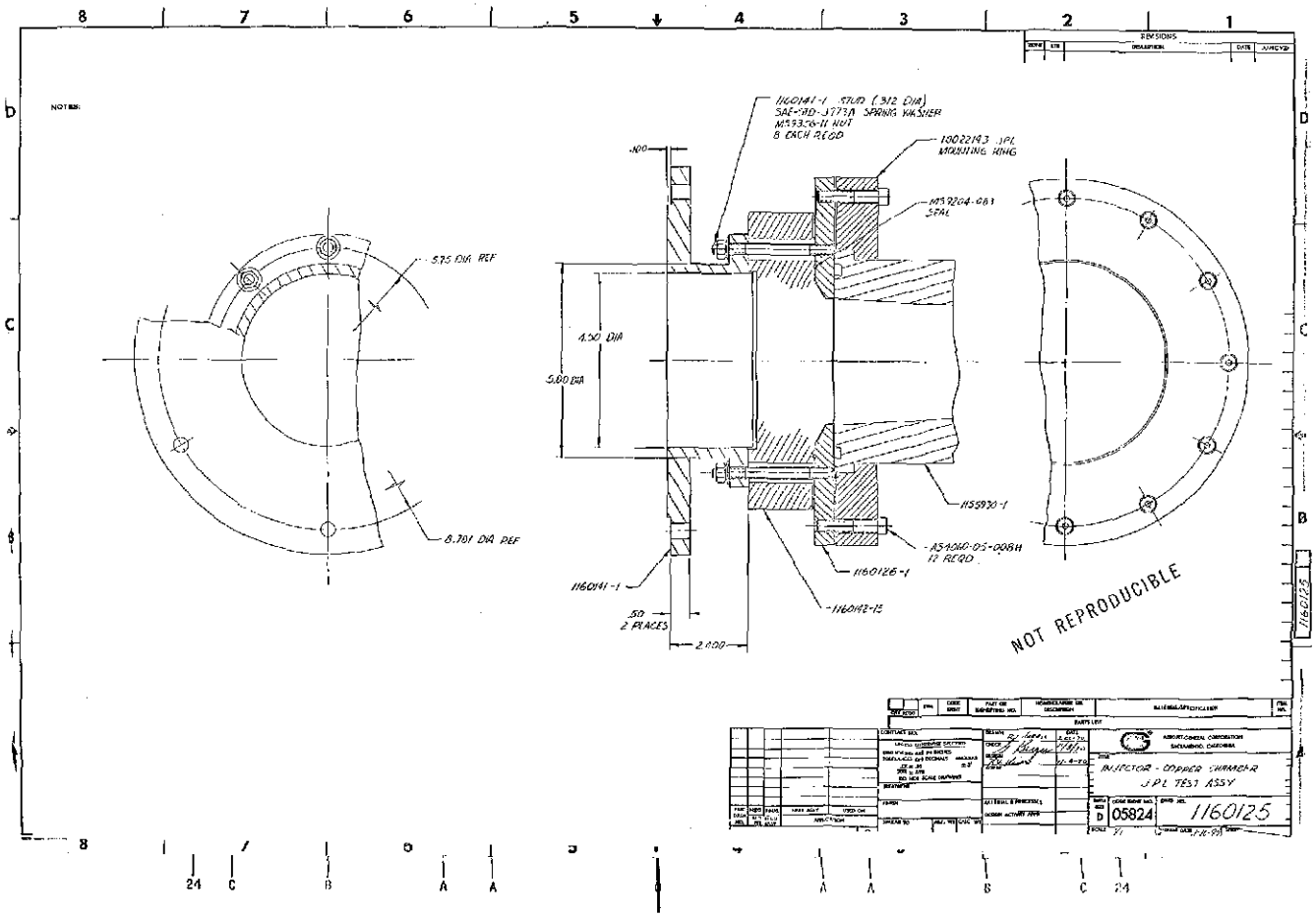

Injector - Copper Chamber Assembly

Figure 62

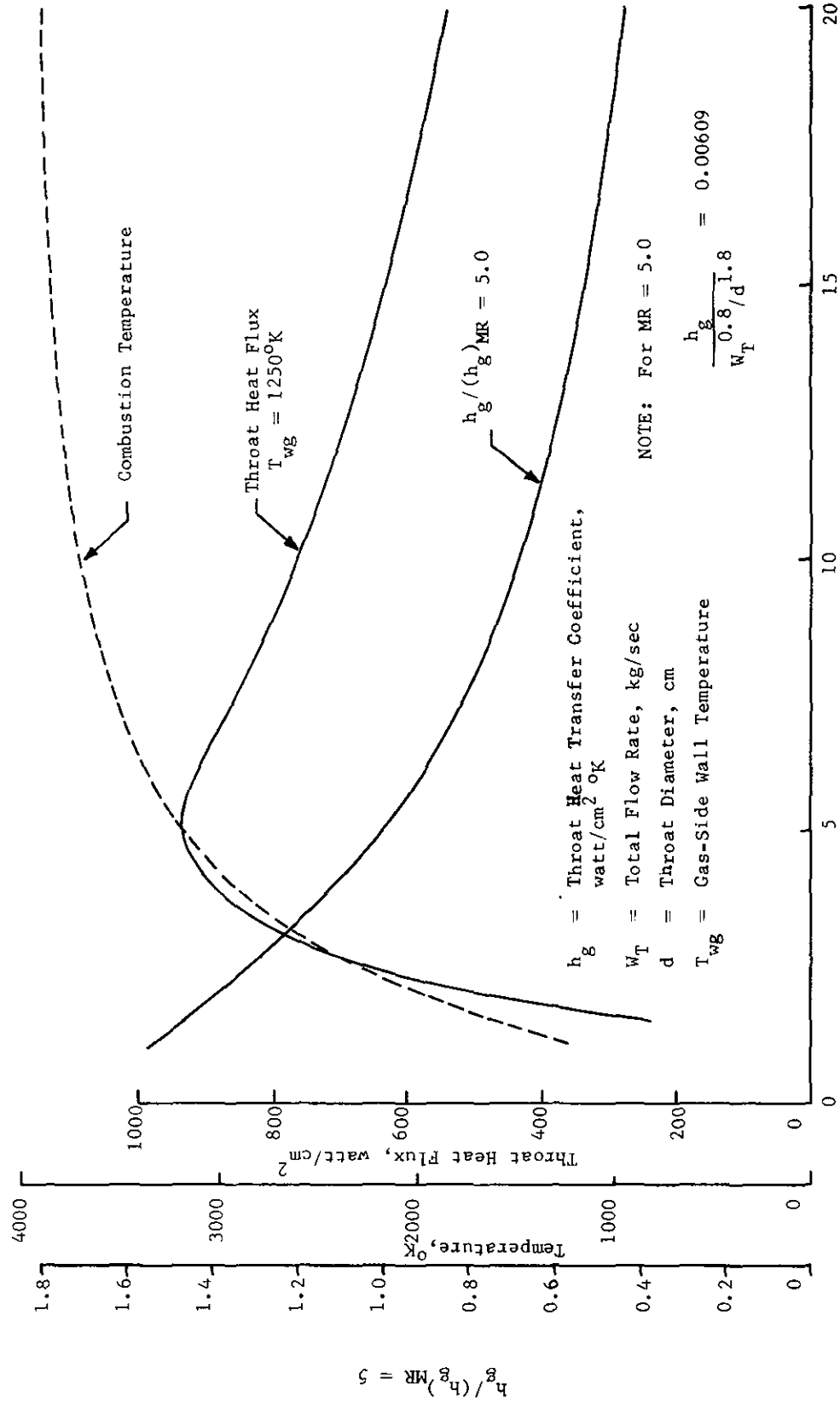

Estimated Throat Heat Flux for FLOX/H_2 Propellants

Figure 63

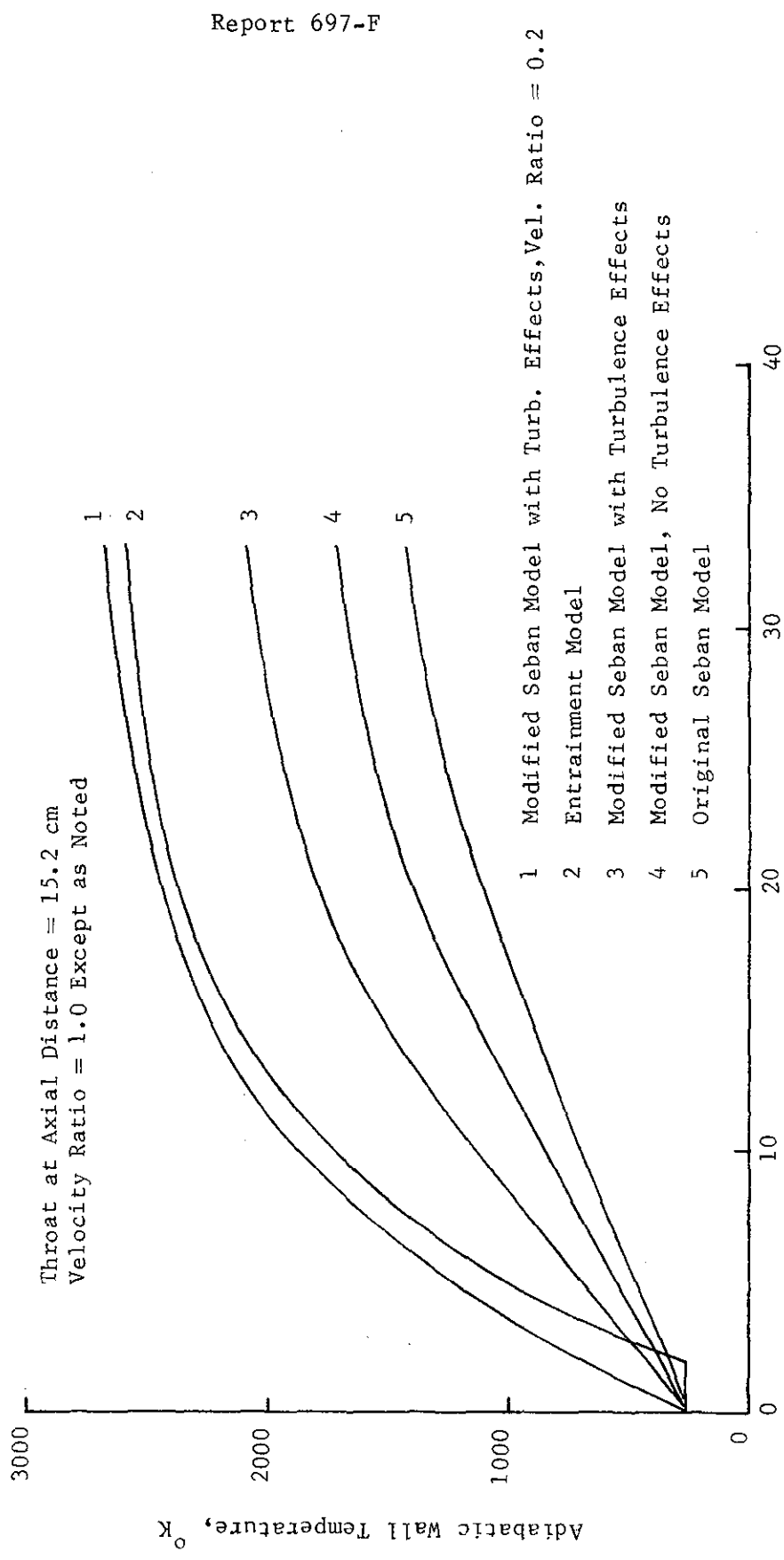

Figure 64

Comparison of Predictions From Film Cooling Models

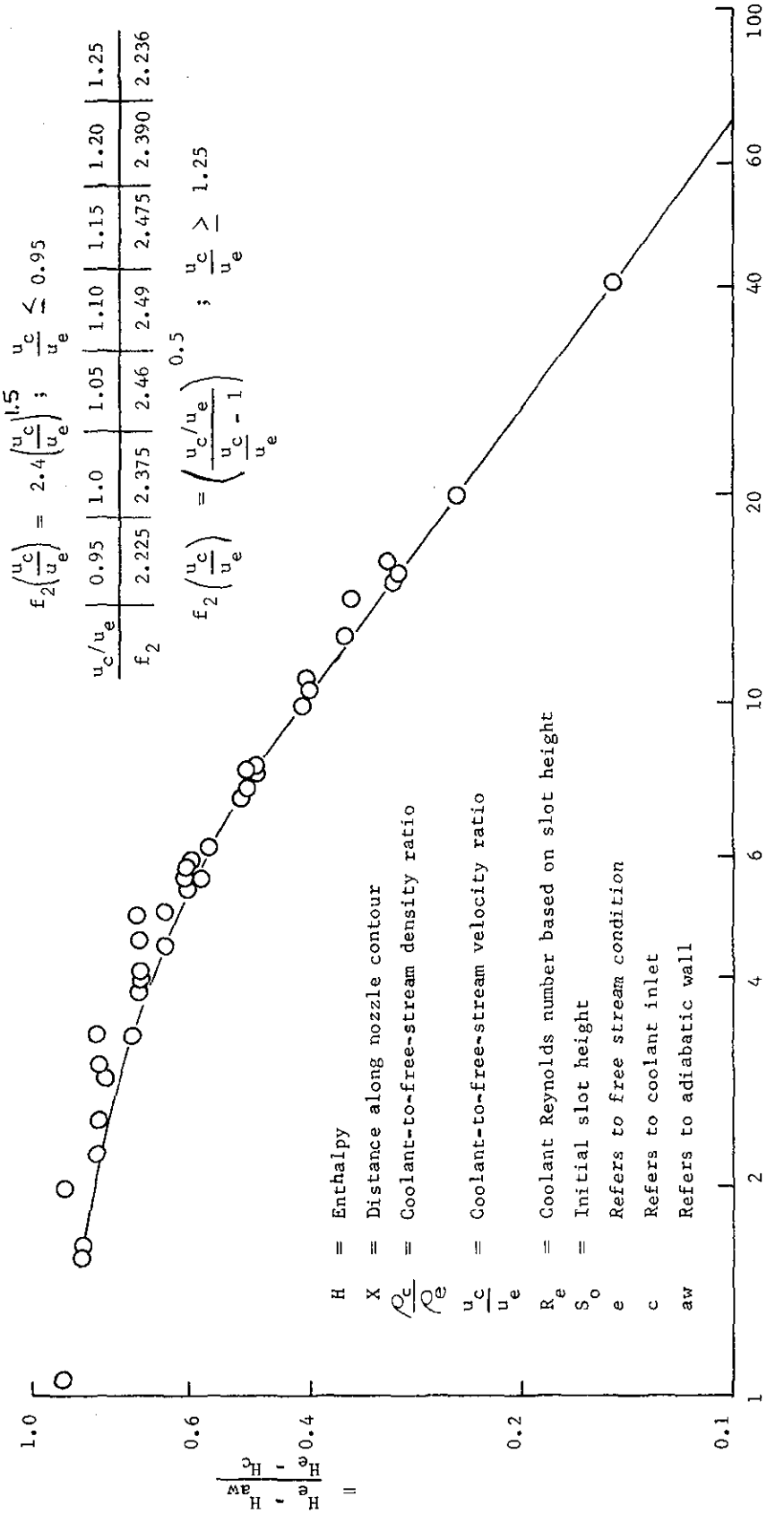

u_c/u_e	0.95	1.0	1.05	1.10	1.15	1.20	1.25
f_2	2.225	2.375	2.46	2.49	2.475	2.390	2.236

Modified Seban Effectiveness Correlation (Turbulence Effects Included)

Figure 65

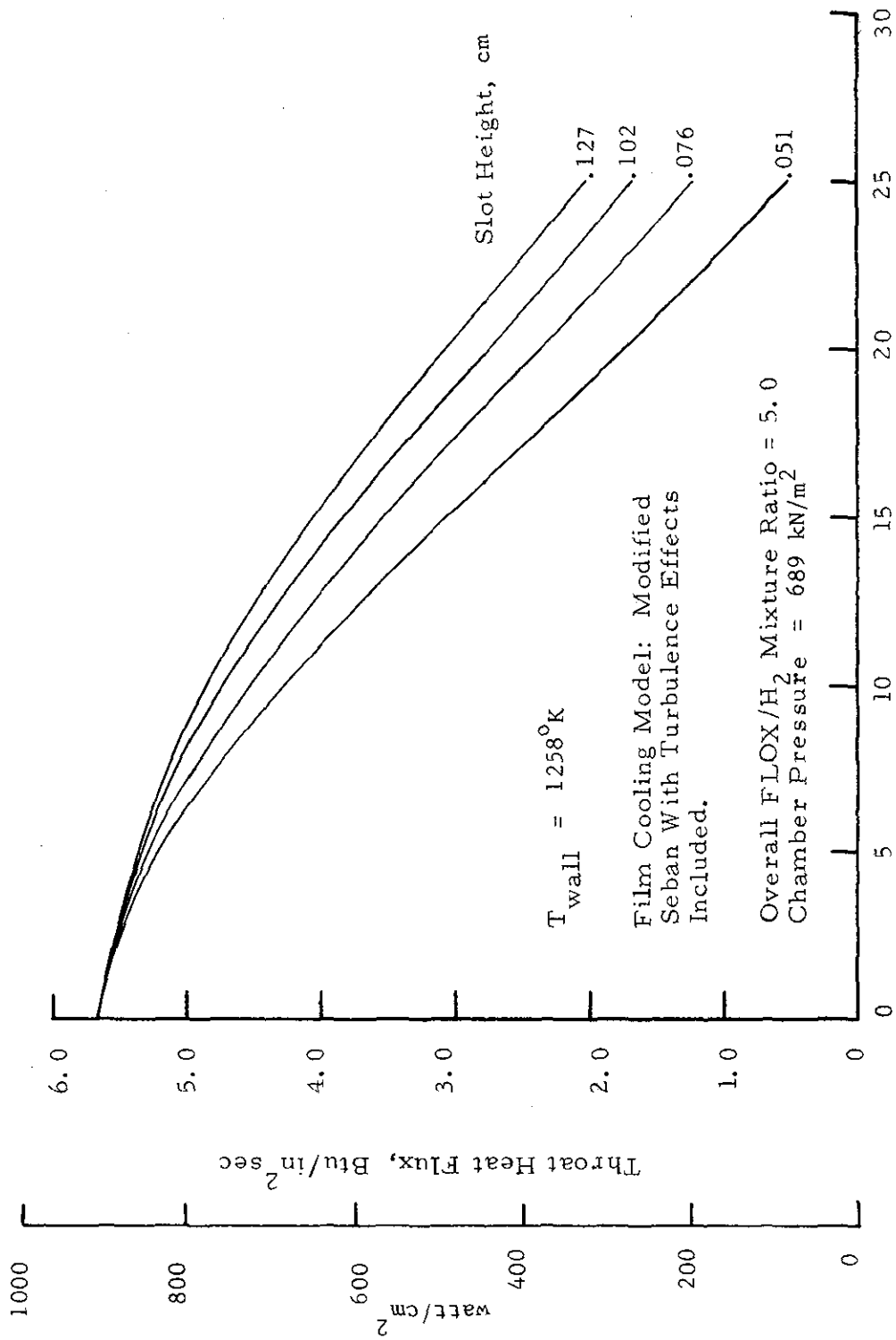

Heat Flux Predictions For the Nozzle Throat

Figure 66

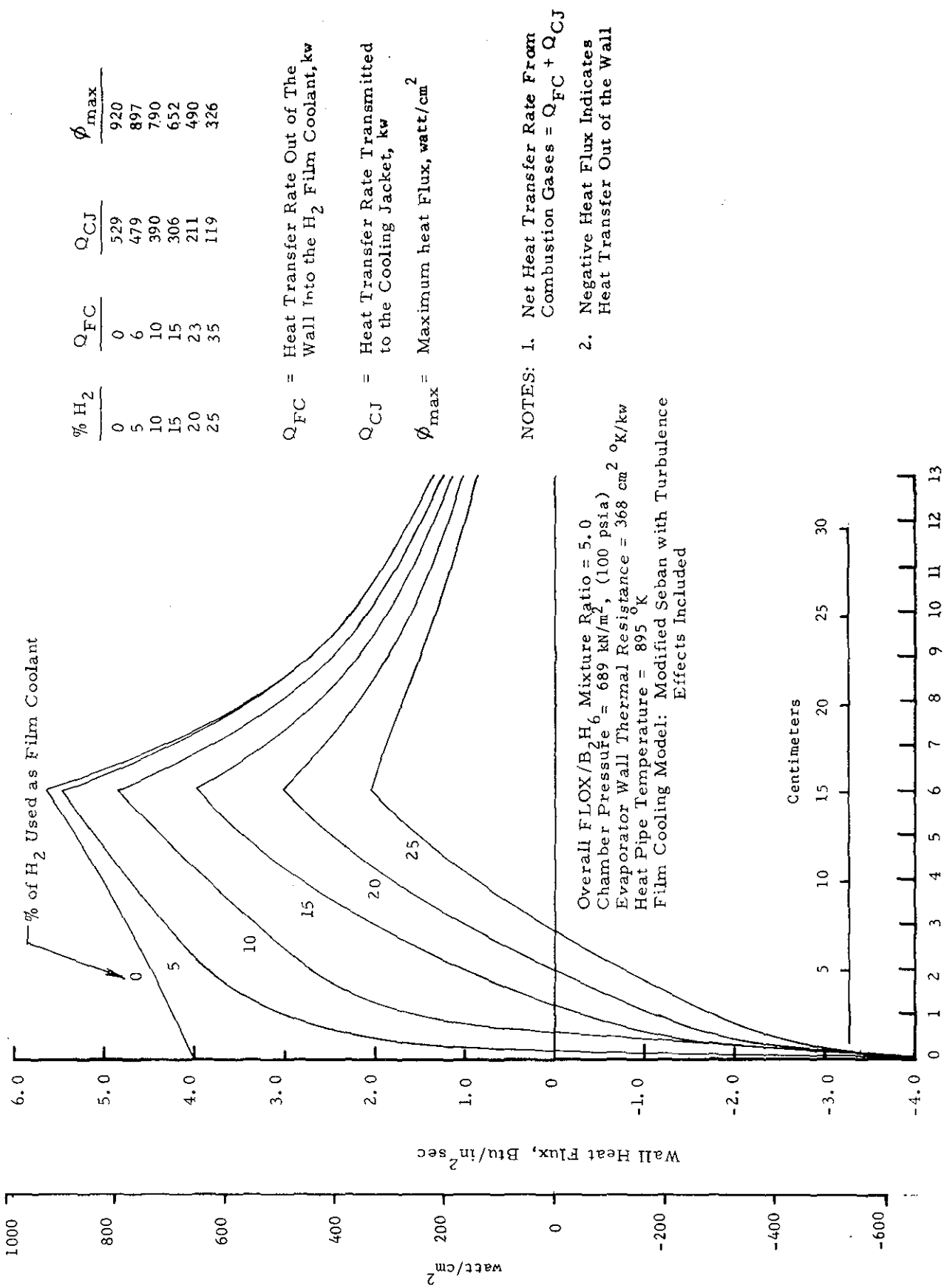

% H_2	Q_{FC}	Q_{CJ}	ϕ_{max}
0	0	529	920
5	6	479	897
10	10	390	790
15	15	306	652
20	23	211	490
25	35	119	326

Q_{FC} = Heat Transfer Rate Out of The Wall Into the H_2 Film Coolant, kw

Q_{CJ} = Heat Transfer Rate Transmitted to the Cooling Jacket, kw

ϕ_{max} = Maximum heat Flux, watt/cm^2

NOTES: 1. Net Heat Transfer Rate From Combustion Gases = $Q_{FC} + Q_{CJ}$

2. Negative Heat Flux Indicates Heat Transfer Out of the Wall

Axial Heat Flux Distribution

Figure 67

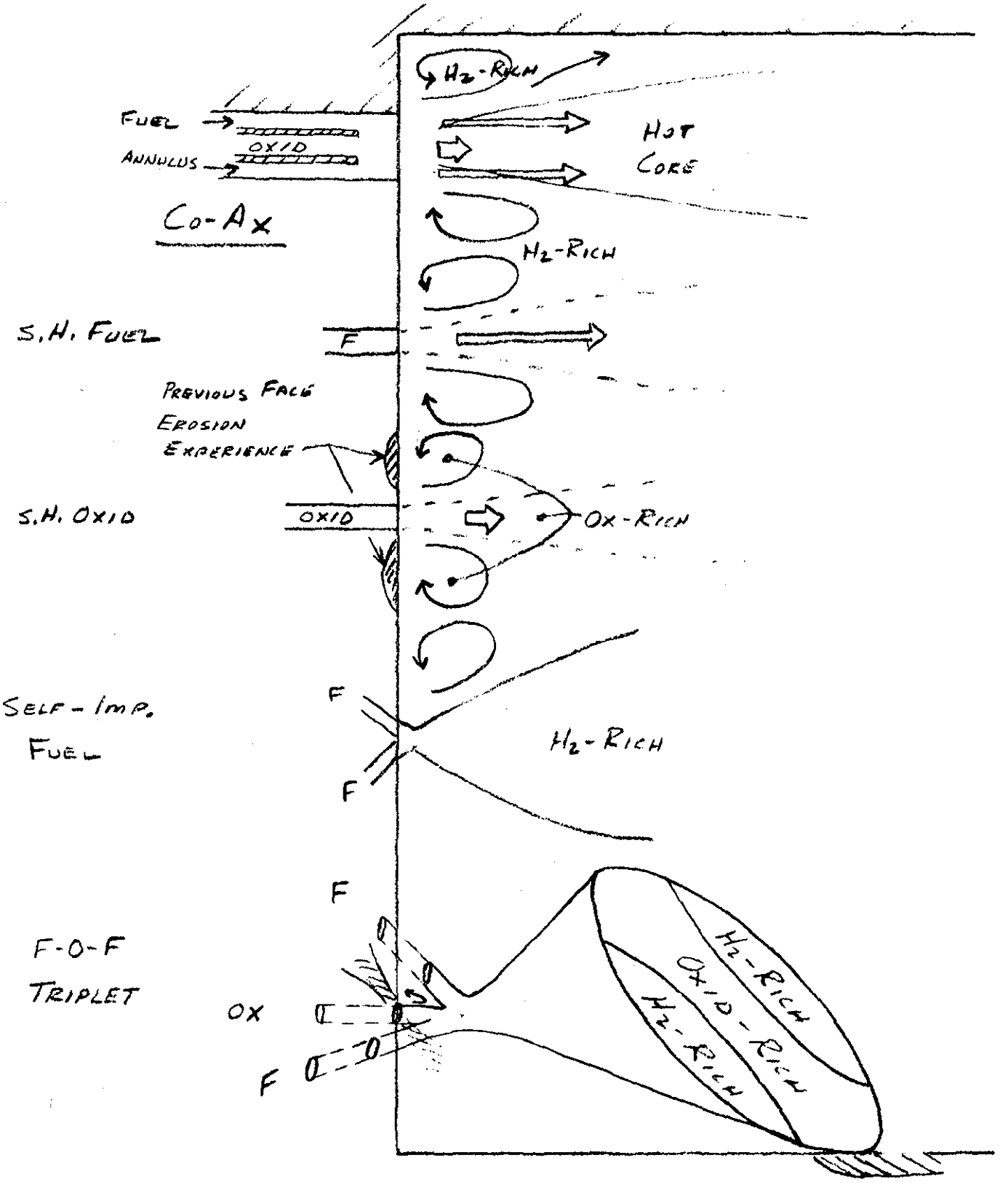

Injection Element/Face Compatibility Characteristics

Figure 68

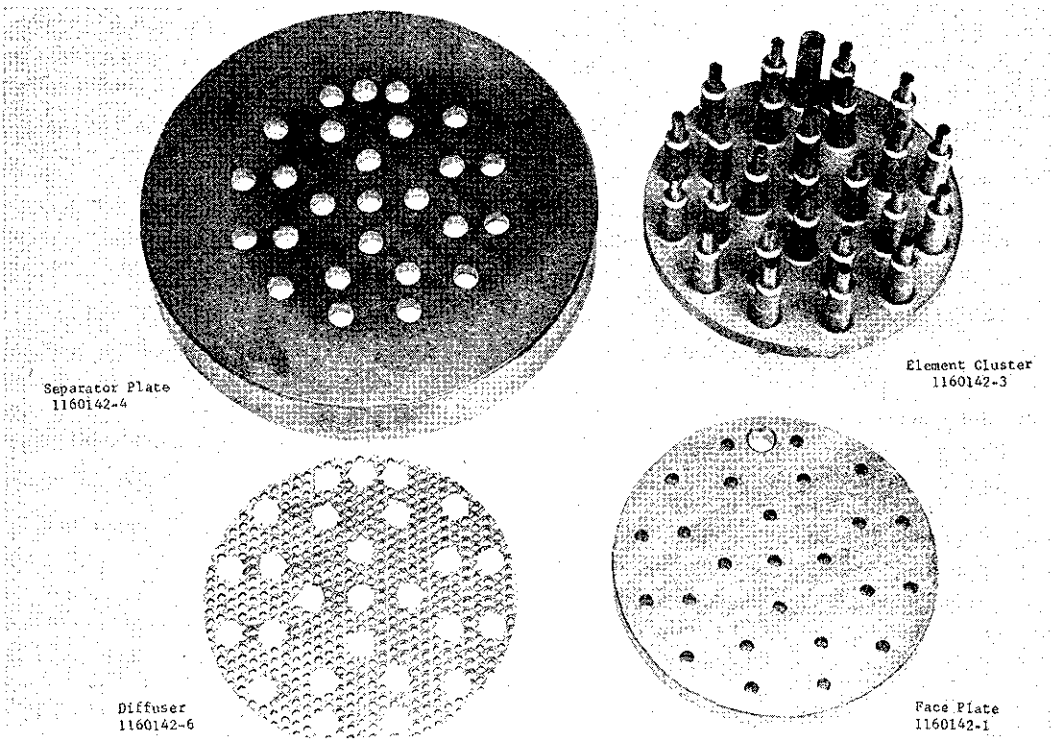

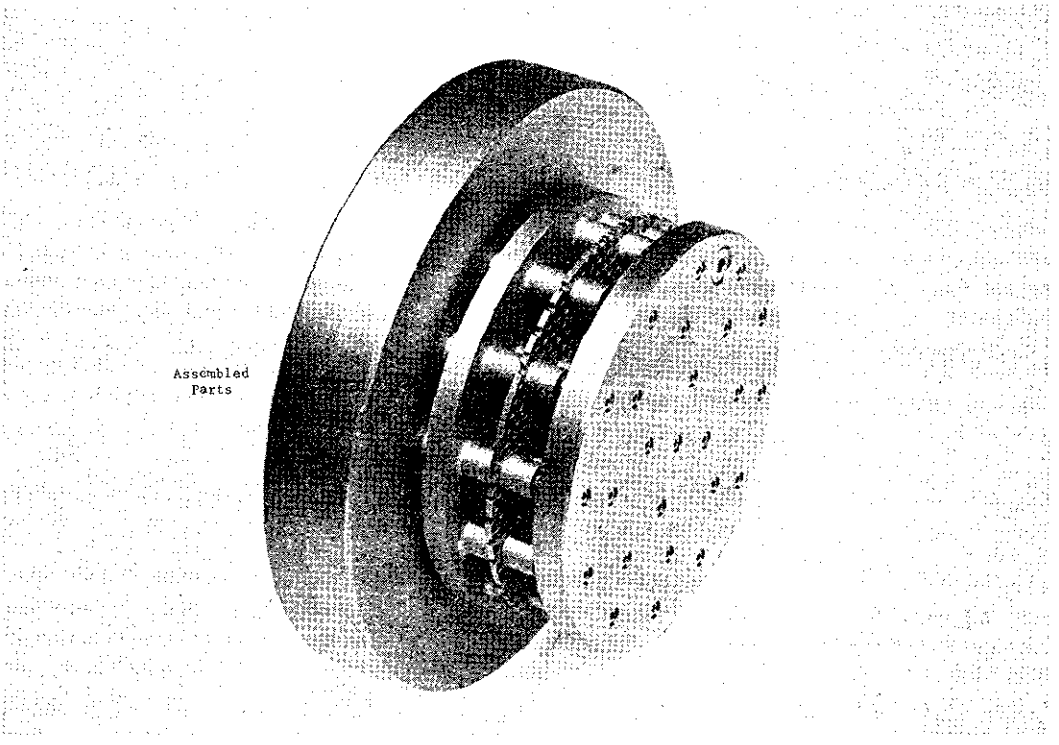

Injector Element Cluster Assembly

Figure 69

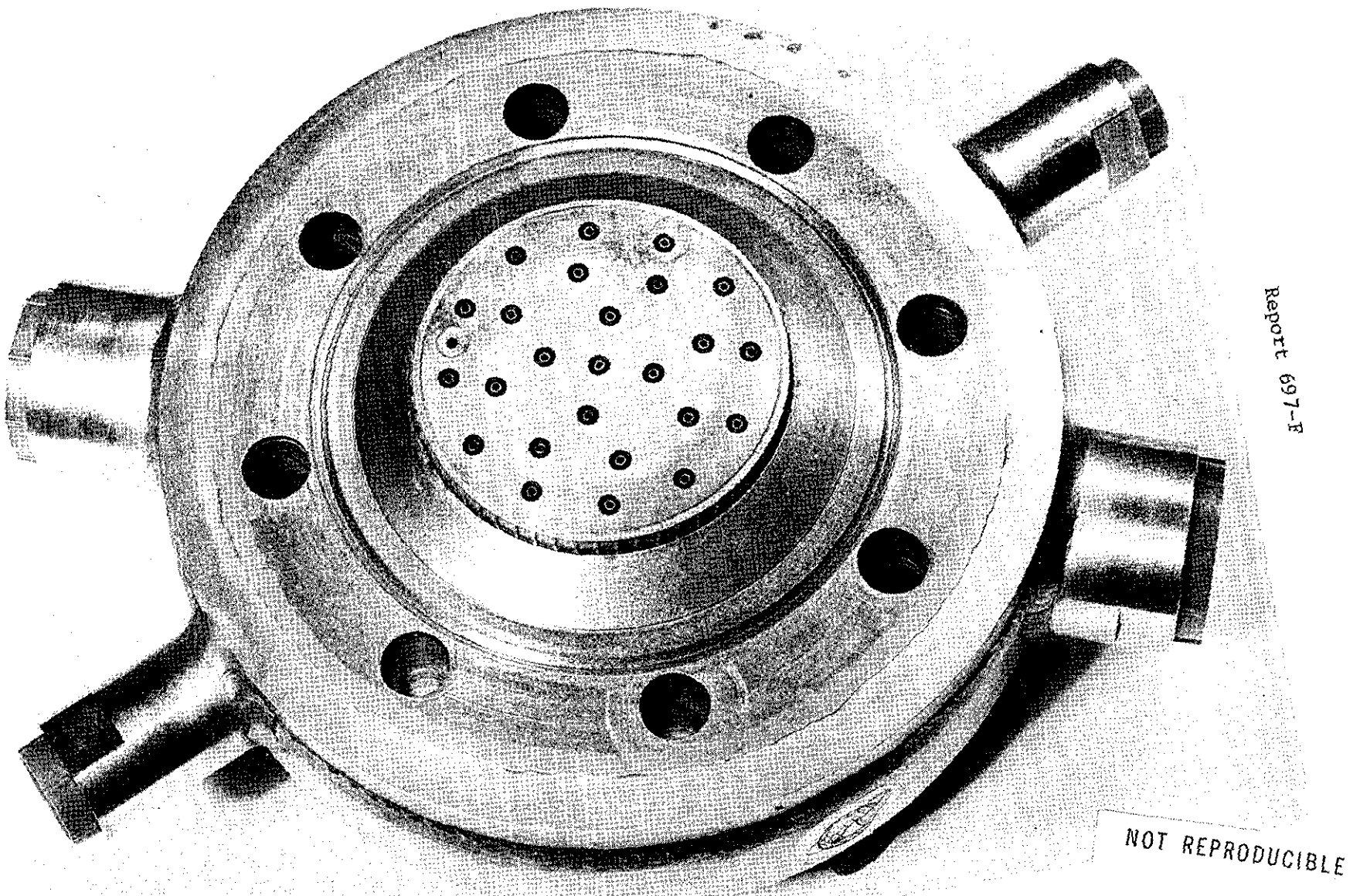

Figure 70 Completed FLOX/H_2 Injector

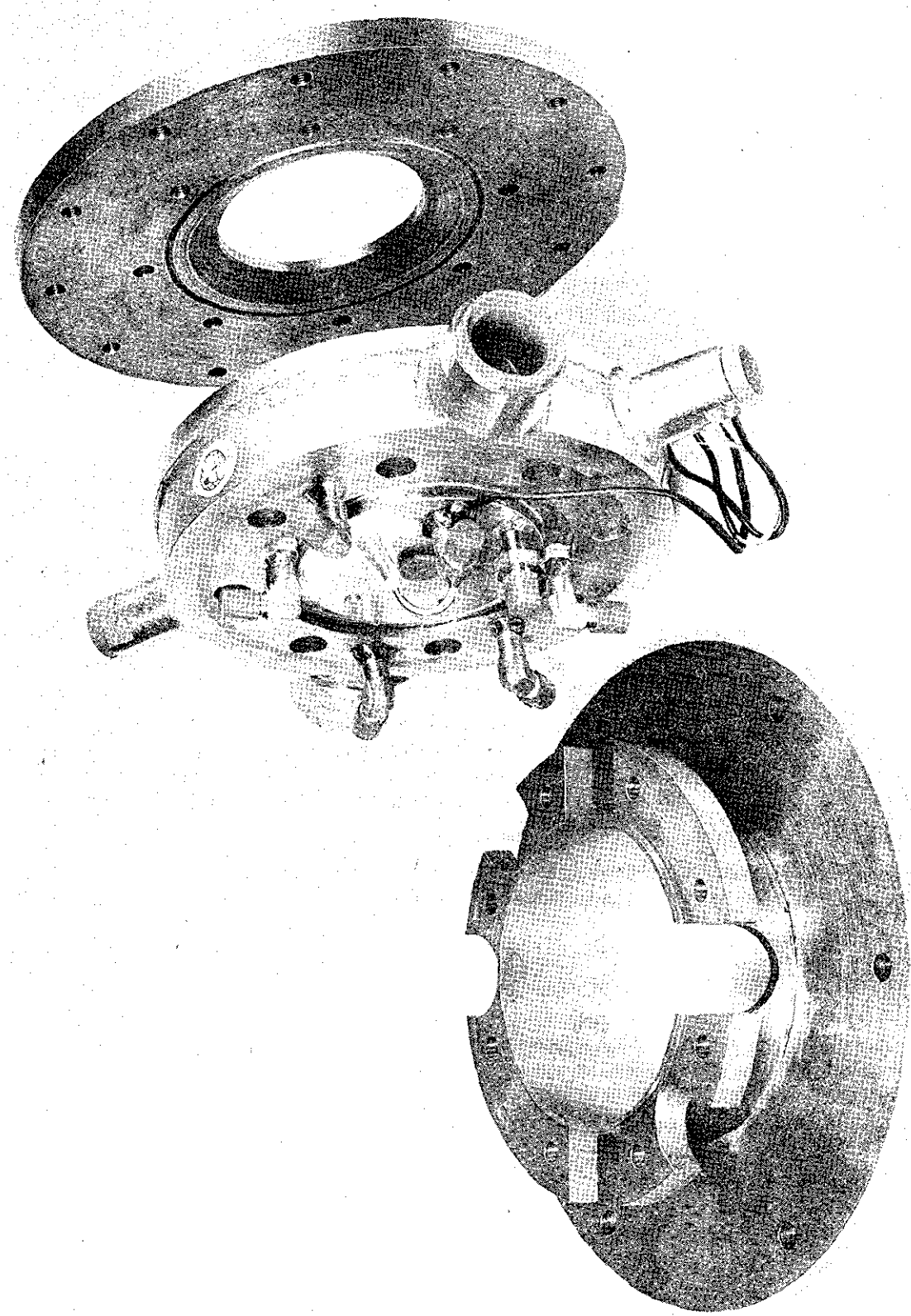

FLOX/H_2 Injector and Adapters

Figure 71

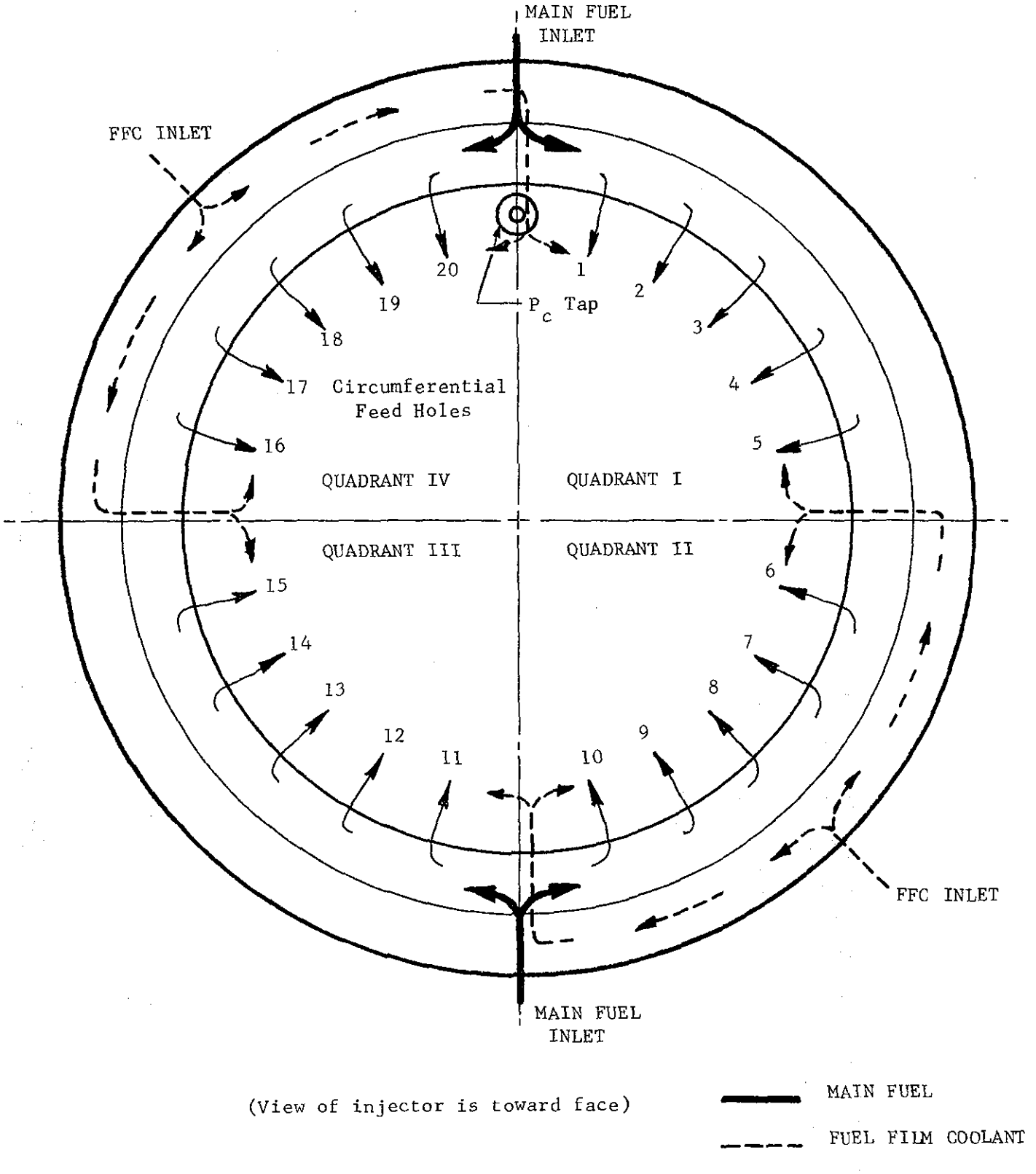

Schematic Diagram of Fuel Distribution Circuits

Figure 72

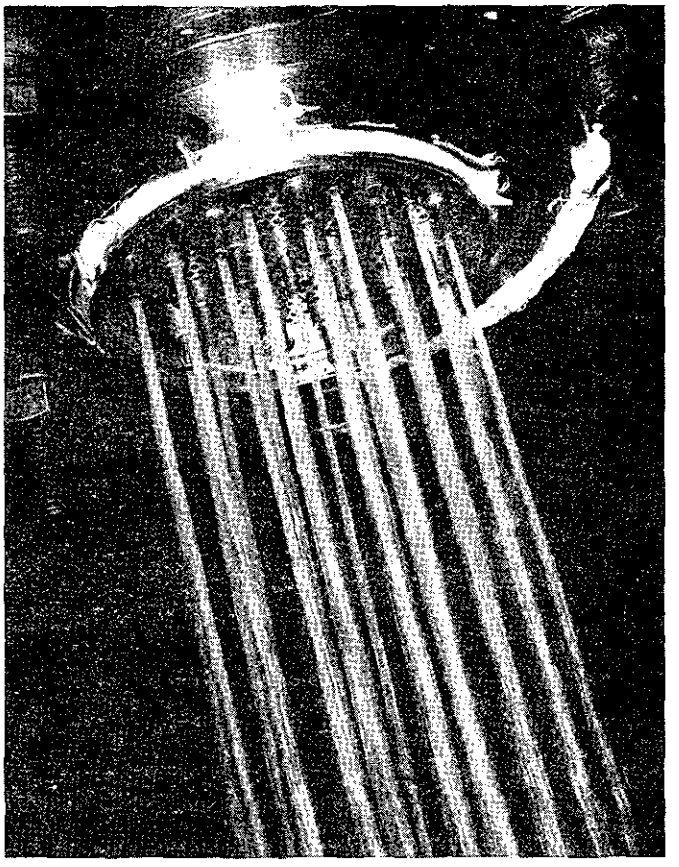

OXIDIZER CIRCUIT COLD FLOW SETUP
Fluid: Water

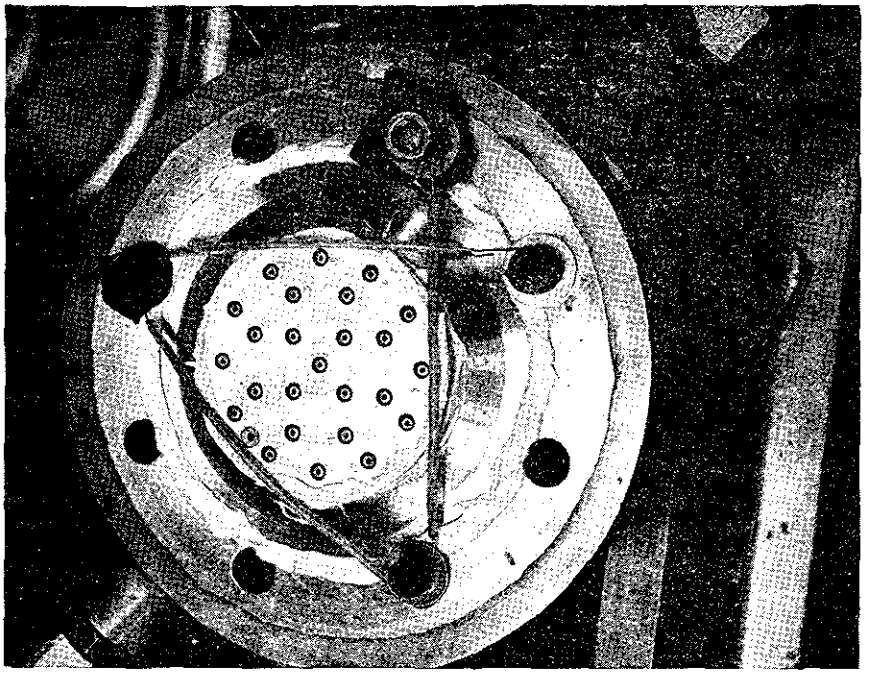

FUEL CIRCUIT COLD FLOW SETUP
(Dummy Face Plate)
Fluid: Gas N_2

Test Setup for Injector Cold Flow Tests

Figure 73

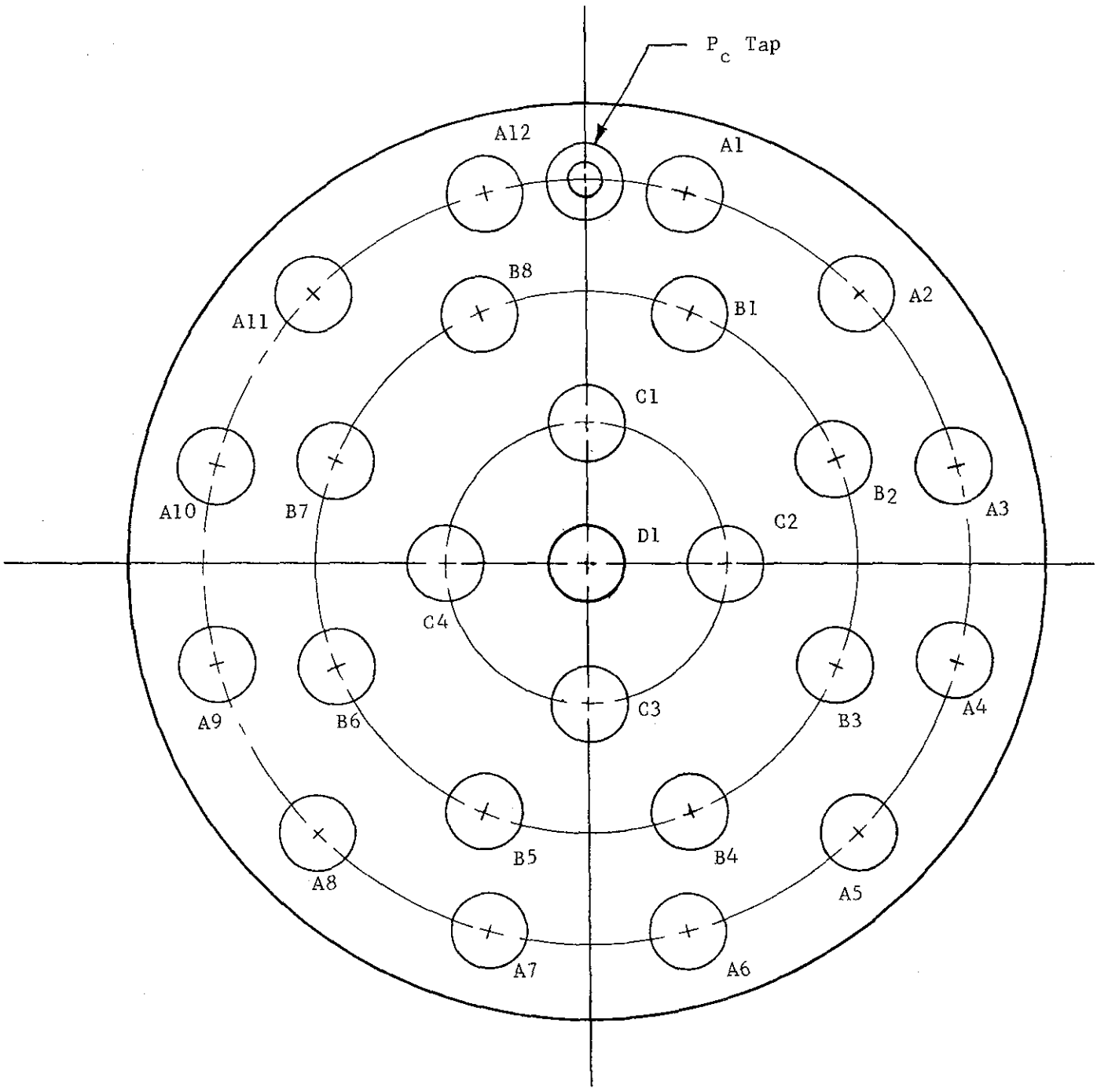

Orifice Nomenclature, FLOX/H_2 Injector

Figure 74

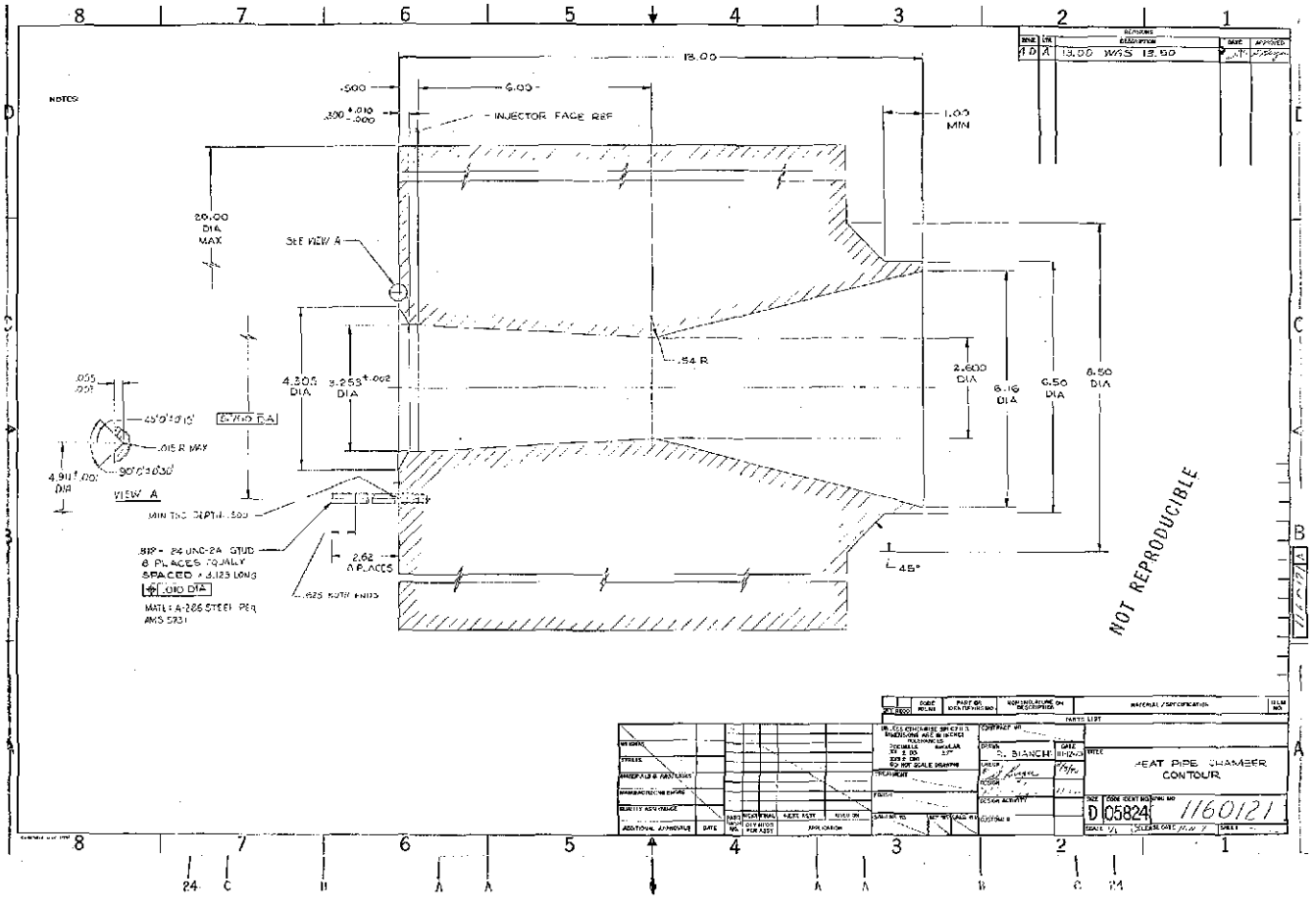

Heat Pipe Thrust Chamber Interface Drawing

Figure 75

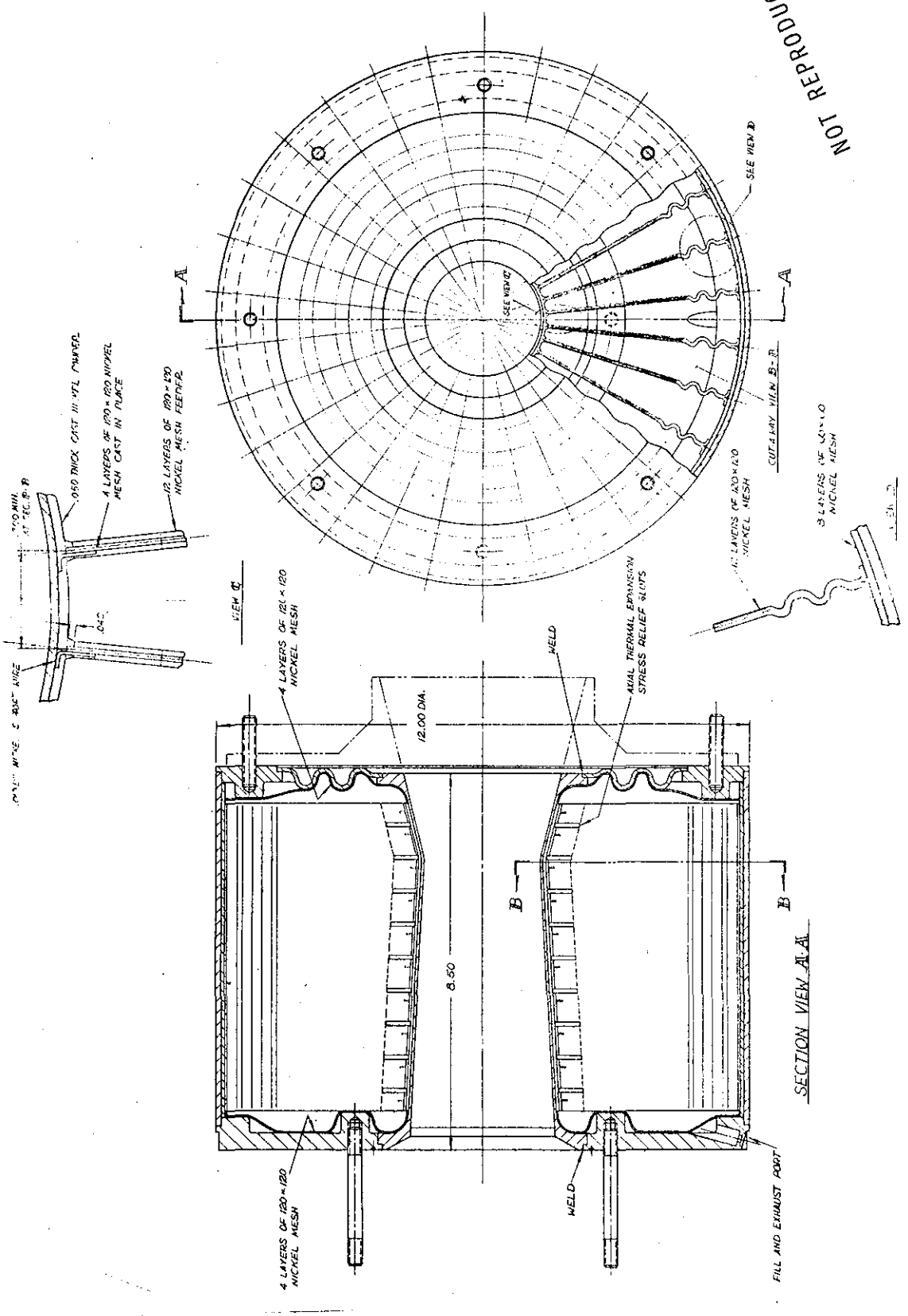

Heat Pipe Thrust Chamber Design Concept

Figure 76

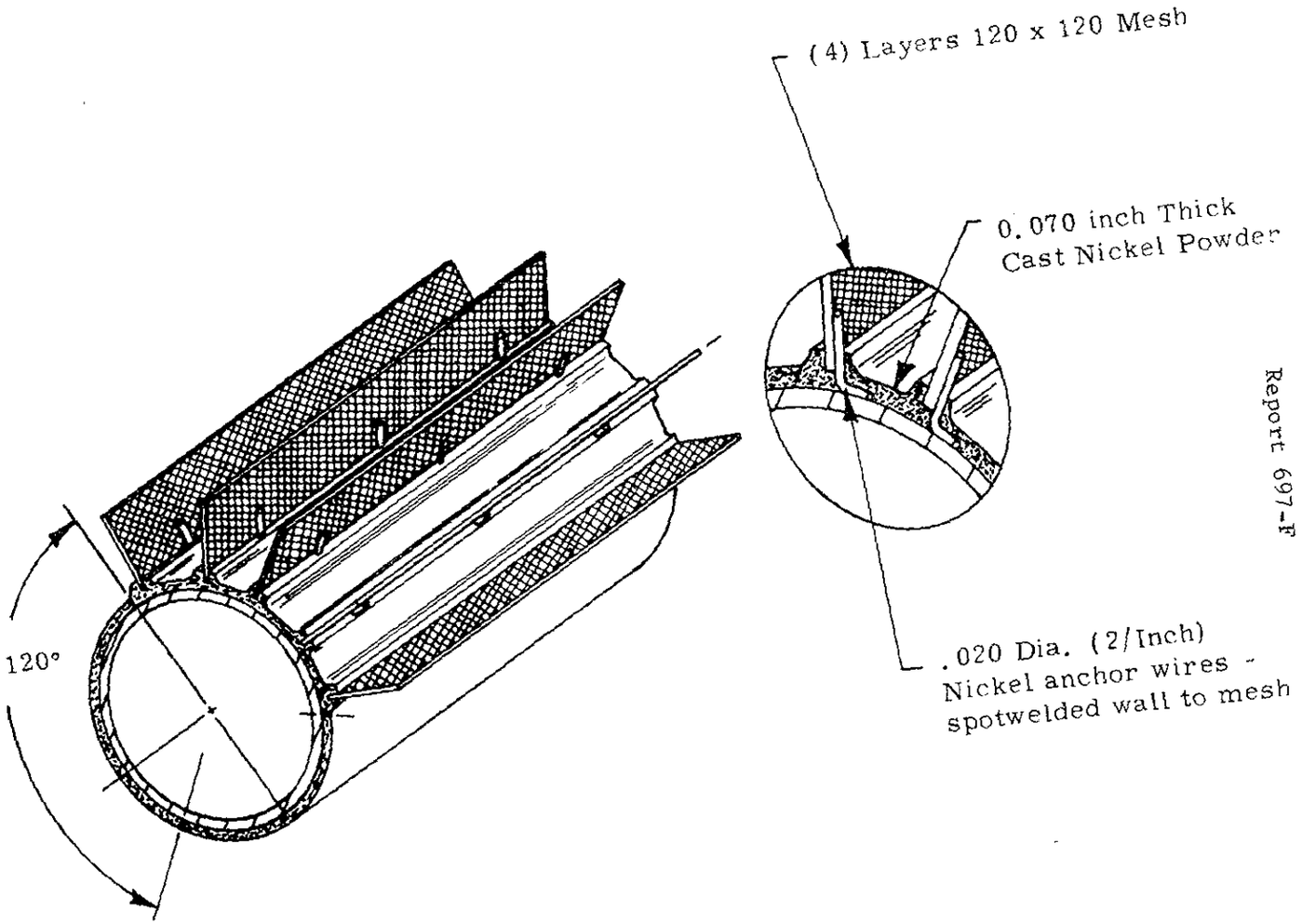

Fabrication Experiment for Sintered Nickel Powder Wicks

Figure 77

Report 697-F

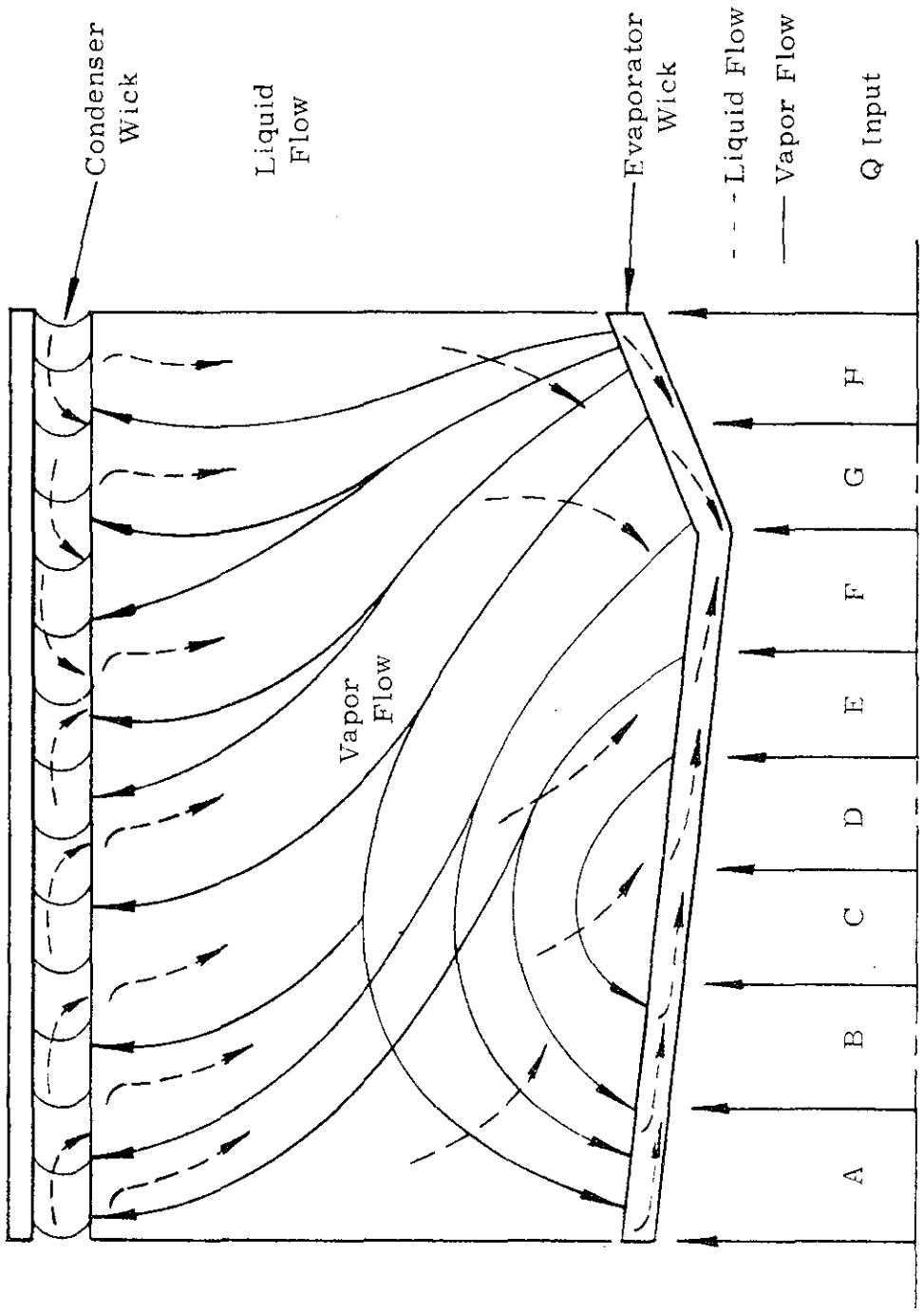

Heat Pipe/Thrust Chamber Thermal Analysis
Segmentation and Fluid/Vapor Flow for Axial Feeders

Figure 78

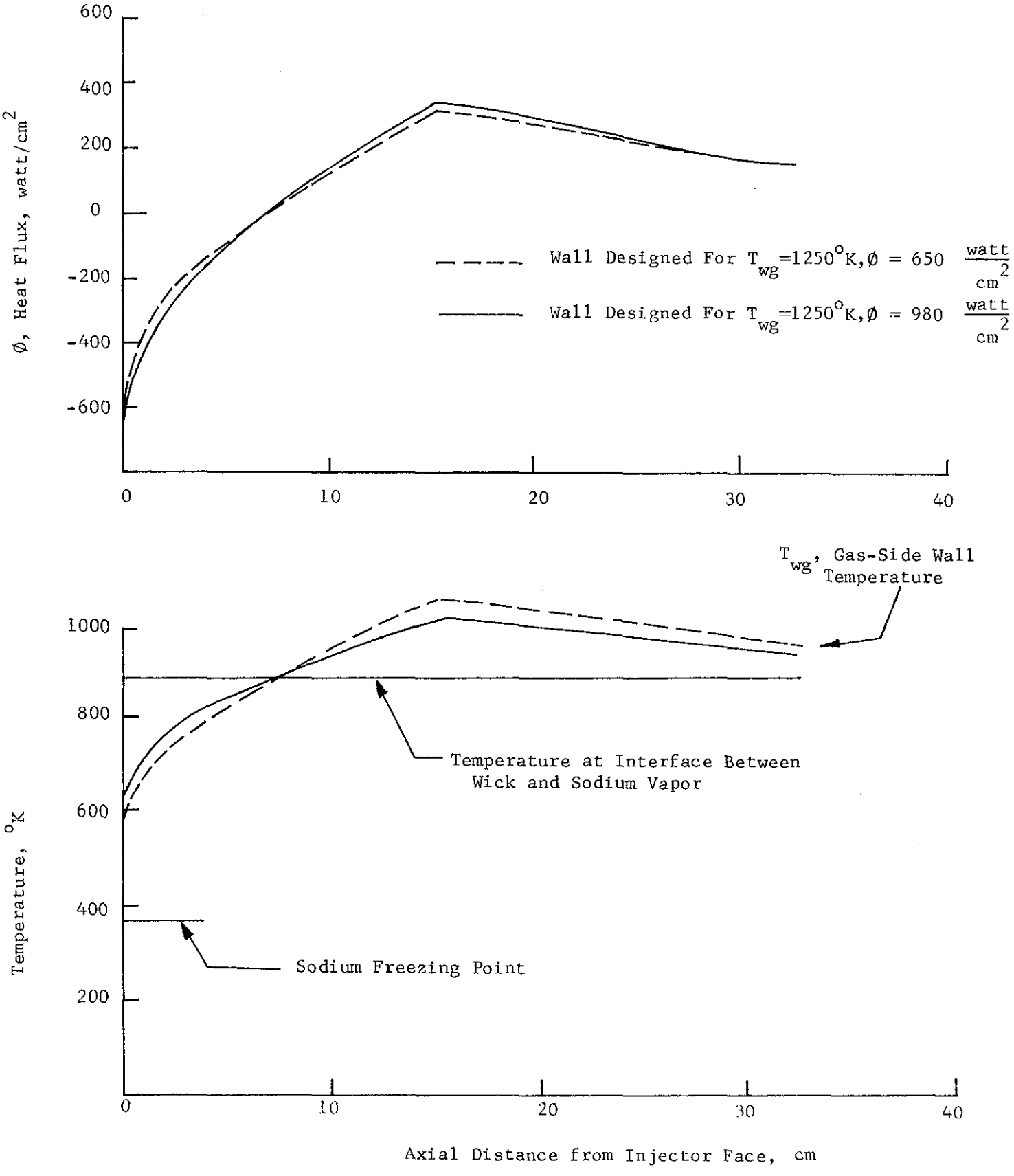

Wall Temperature and Heat Flux Distribution

Figure 79

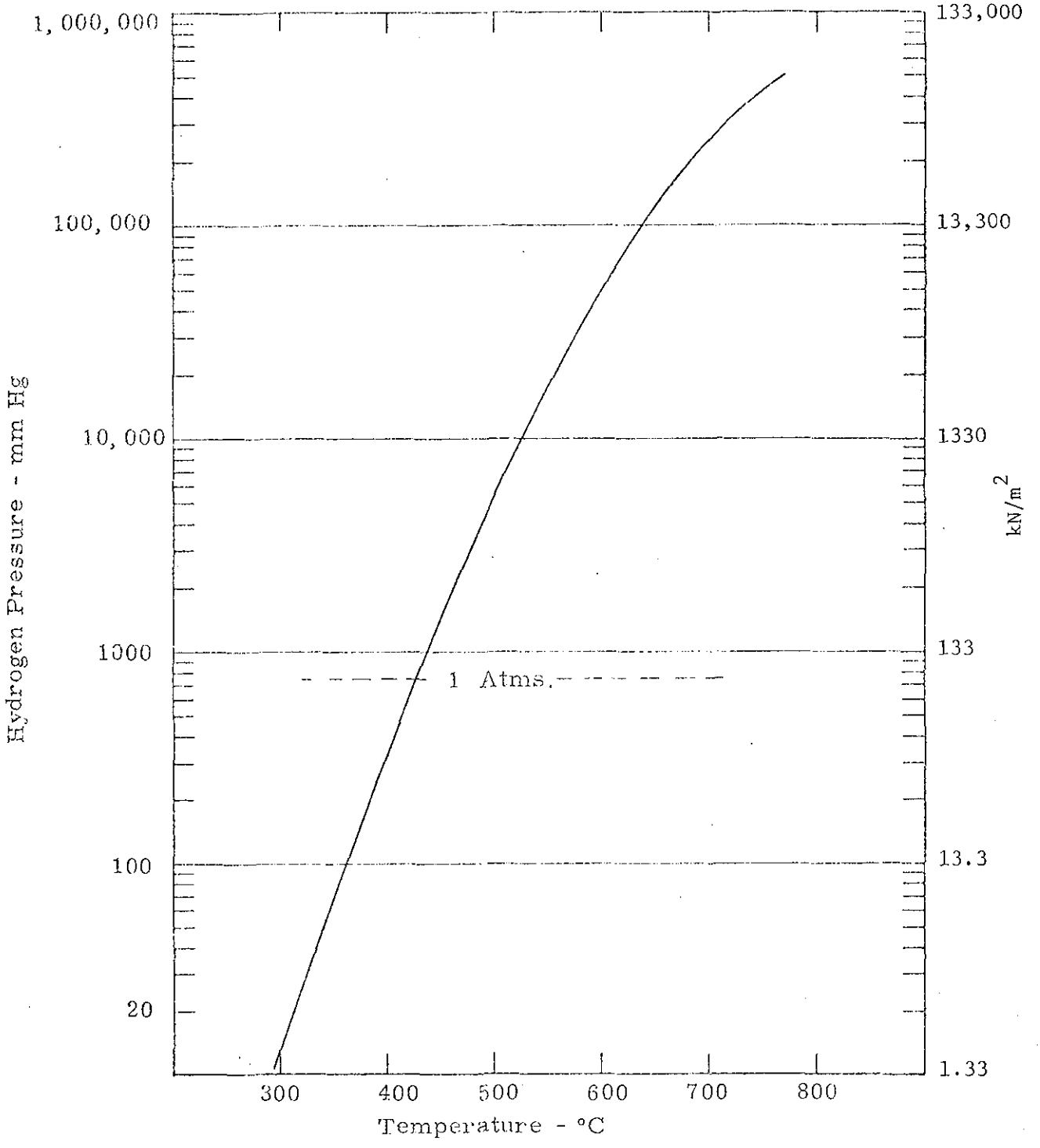

$(2NaH \rightleftharpoons 2Na + H_2 \uparrow)$
$(s) \quad (l) \quad (g)$

Sodium Hydride Dissociation

Figure 80

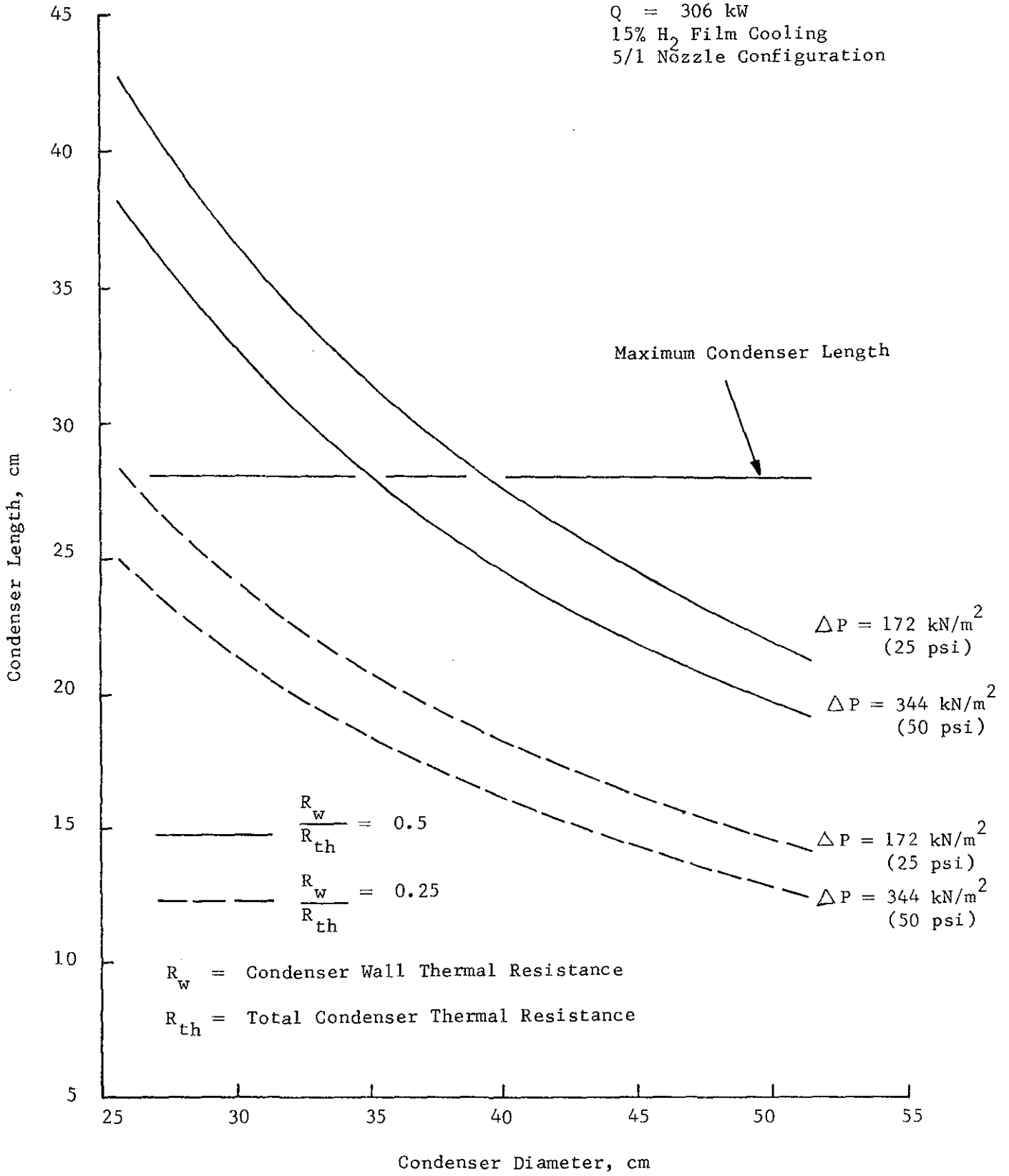

Initial Thermal Design Results for the Cooling Jacket

Figure 81

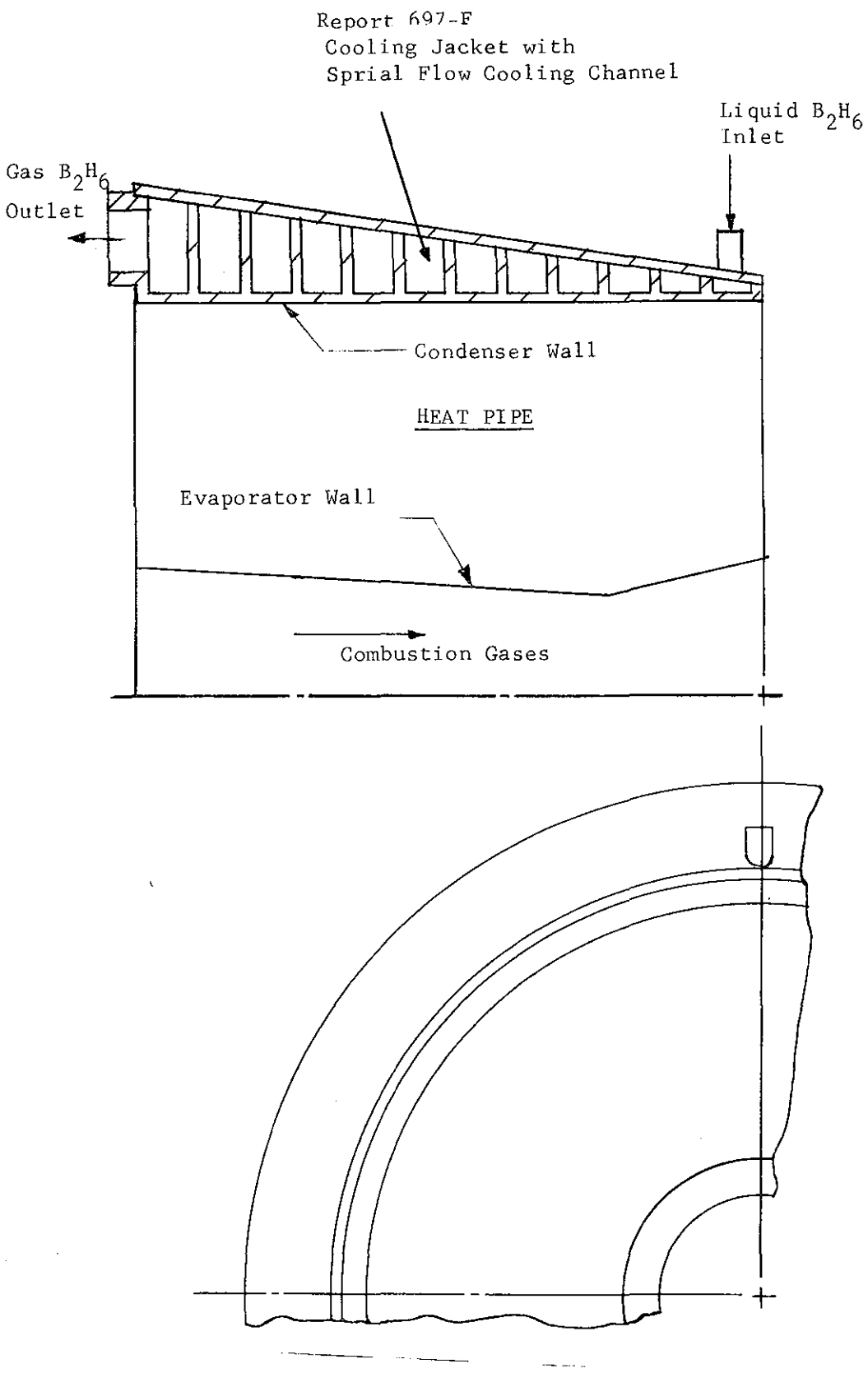

Cooling Jacket Design Concept

Figure 82

Appendix A

COMPUTER PROGRAM FOR COOLING JACKET THERMAL DESIGN

The computer program utilized to perform thermal design calculations for the condenser cooling jacket is listed on the following pages. The program was written specifically for the case of diborane cooling and considers liquid, 2 phase, or gaseous flow. The program was written in Fortran V language for the Univac 1108 computer.

The analysis utilizes a one-dimensional control volume approach, dividing the coolant passage into sections and solving the continuity, momentum and energy equations for each section.

Continuity:

$$\rho \; V \; A = \dot{W} \text{ at any station}$$

Momentum:

$$P_2 - P_1 = -\Delta P_f + \frac{W^2}{\bar{A}} \left[\frac{1}{\rho_1 \; A_1} - \frac{1}{\rho_2 \; A_2} \right]$$

Energy:

$$h_2 - h_1 = Q/\dot{W} + \frac{\dot{W}^2}{2gJ} \left[\frac{1}{(\rho_1 \; A_1)^2} - \frac{1}{(\rho_2 \; A_2)^2} \right]$$

The pressure drop is calculated using the mean area of the section. Single phase pressure drop is calculated using the Carcy equation:

$$\Delta P_f = \frac{144 \; f \; \Delta L}{2 \; g \rho D_{eq}} \left(\frac{W}{\bar{A}} \right)^2$$

where f, the moody friction factor, is given by:

$$f = 0.3164/R^{1/2} \quad \text{for } R < 2.6 \times 10^5, \text{ and}$$

$$f = 0.014 \quad \text{for } R > 2.6 \times 10^5$$

In the two phase region the following approximate relations were used:

$$\Delta P_f = \Delta P_{f_{liq}} \left[\frac{1}{.85} \; 1.6 \; \frac{\Delta P_{f_{vap}}}{\Delta P_{f_{liq}}} - 1 \quad X + 1 \right] ; \quad 0 < X \leq 0.85$$

$$\Delta P_f = \Delta P_{f_{liq}} \left[(5.0 - 4.0X) \; \frac{\Delta P_{f_{vap}}}{\Delta P_{f_{liq}}} \right] ; \quad .85 < X < 1.0$$

Where X is the vapor quality. These equations were derived by observing the general characteristics of two phase flow pressure drop data.

The heat transfer to the fluid is calculated utilizing an overall heat transfer coefficient and the thermal network shown in Figure A1.

$$Q = UA \left(T_{\text{heat pipe}} - T_{\text{coolant}} \right)$$

The hot sodium side film coefficient is assumed to be very large, thus U becomes:

$$U = \left[1/h_{ave} + R_w \right]^{-1}$$

The parameter h_{ave} is an equivalent film coefficient which includes the effect of heat transfer from the land adjacent to the flow passage. The effect of heat transfer from the land is approximated by assuming the land behaves as a fin which has a constant base temperature, is cooled on the sides via constant h_L value, and is insulated on the end. The fin effect is then incorporated into the analysis as an effective heat transfer coefficient as shown in Figure A1.

In the subcooled liquid region of the cooling jacket, forced convection heat transfer is initially assumed. The validity of this assumption is then evaluated by comparing the wall temperature to the local saturation temperature (T_{sat}). If $T_w > T_{sat}$, the forced convection assumption is discarded and nucleate boiling is assumed to occur. The nucleate boiling mechanism is approximated by setting $T_w = T_{sat} + 50^{\circ}R$ and a nucleate boiling heat flux is calculated. This heat flux is compared to the peak nucleate boiling or "burnout" heat flux (φ_{BO}) and if it is greater than φ_{BO} the nucleate boiling assumption is also discarded and a film boiling mechanism is assumed. The equation of Giarratano and Smith is used to estimate the film boiling h_L. Whenever film boiling is found to occur, it is assumed that film boiling exists throughout the rest of the liquid and 2-phase region.

```
C    HEAT PIPE COOLING JACKET DESIGN PROGRAM
C   PROGRAM NAME HPCOOL
C*****************************************************************
C    INPUT PARAMETERS
C      PIN            INLET PRESSURE - PSIA
C      TIN            INLET TEMPERATURE - DEG R
C      QIN            INLET QUALITY - DEFAULT VALUE QIN=0.
C      WC             FLOW RATE - LBM/SEC
C      LENGTH         CHANNEL LENGTH - INCHES
C      DELX           INCREMENT LENGTH - INCHES
C      THP            HEAT PIPE TEMPERATURE - DEG R
C      IPRINT         PRINT FLAG - STATIONS/OUTPUT LINE
C      ITURN          FLAG = 1 FOR AXIAL FLOW. INCREMENT LENGTH MUST EQUAL
C                     THRUSTER LENGTH AS A 180 DEGREE TURN IS INSERTED AT
C                     THE END OF EACH SECTION. DEFAULT FOR HELICAL GEOMETRY.
C      MAT            MATERIAL FLAG
C                         MAT=1 - HASTALLOY X
C                         MAT=2 - STAINLESS STEEL 304
C                         MAT=3 - COPPER
C      NP             NUMBER OF GEOMETRY STATIONS
C         XWS         CHANNEL WIDTH - INCHES
C         XTS         CHANNEL HIGHT - INCHES
C         LANDW       LAND WIDTH - INCHES
C         DCURVE      DIAMETER OF CURVATURE - INCHES
C         RWALL       WALL RESISTANCE -  IN2-SEC-R/BTU
C         XPOS        GEOMETRY STATIONS - INCHES
C*****************************************************************
      DIMENSION XWS(25),XTS(25),DCURVE(25),RWALL(25),XPOS(25),
     1LANDW(25),XAXC(25),XDEQ(25),DRC(100), RC2(100),RCG(100)
      REAL LENGTH,LANDW
      NAMELIST/INPUT/PIN,TIN,QIN,WC,LENGTH,DELX,THP,IPRINT,MAT,NP,
     1 XWS,XTS,LANDW,DCURVE,RWALL,XPOS
     1,ITURN
C
C     READ AND LIST INPUT PARAMETERS
C
 999  Q=0.
      ITURN =1
      IPRINT=1
      READ(5,INPUT)
      WRITE(6,INPUT)
C
C     START CALCULATIONS
C
      DO 1 I=1,NP
      XAXC(I)=XWS(I)*XTS(I)
 1    XDEQ(I)=2.*XAXC(I)/(XWS(I)+XTS(I))
      ICOUNT=IPRINT-1
      JCOUNT=10
      XL=0.
      Q=QIN
      QQUAL=0.
      CALL PROP(PIN,TIN,Q,EC,RC,VC,CC,CPC,VEC,2)
      PC=PIN
      TC=TIN
      TW=900.
      WRITE(6,1001)
      WRITE(6,1111) WC,PIN,TIN
```

```
      WRITE(6,1003)
C
C     CALCULATE CHANNEL GEOMETRY
C
 100  CALL PROP(PC,TC,W,EC,RC,VC,CC,CPC,VEC,1)
      CALL SINTP(XPOS,XAXC,NP,XL,AXC,J)
      CALL SINTP(XPOS,XDEQ,NP,XL,DEQ,J)
      CALL SINTP(XPOS,RWALL,NP,XL,RW,J)
      CALL SINTP(XPOS,XWS,NP,XL,WS,J)
      CALL SINTP(XPOS,LANDW,NP,XL,XWL,J)
      CALL SINTP(XPOS,DCURVE,NP,XL,DCUR,J)
      CALL SINTP(XPOS,XTS,NP,XL,TS,J)
      XLN=XL+DELX
      CALL SINTP(XPOS,XAXC,NP,XLN,AXCN,J)
      ABAR = (AXC+AXCN)/2.
C
C     CALCULATE WALL TEMPERATURE
C
      CALL HLDIB(PC,EC,DEQ,WC,AXC,HL,TW)
      CM=COND(TW,MAT)
      FIN=((2.*HL)/(XWL *CM))**0.5*TS
      HLEFF=(2.*HL*CM/XWL )**0.5*TANH(FIN)
      HLOAR= (XWL/(XWL + WS))*HLEFF +( WS/(XWL + WS))*HL
      U= 1./(1./HLOAR+RW)
      TW=THP- U*RW*(THP-TC)
      CALL HLWCOB(TW,THP,RW,HL,QFLUX,INB)
      IF(INB.EQ.2) GO TO 110
      CM=COND(TW,MAT)
      FIN=((2.*HL)/(XWL *CM))**0.5*TS
      HLEFF=(2.*HL*CM/XWL )**0.5*TANH(FIN)
      HLOAR= (XWL/(XWL + WS))*HLEFF +( WS/(XWL + WS))*HL
      U= 1./(1./HLOAR+RW)
      TW=THP- U*RW*(THP-TC)
C
C     CALCULATE HEAT FLUX
C
      QFLUX=U*(THP-TC)
 110  QC=QFLUX*(WS+XWL)*DELX
      QQUM = QQUM + QC
C
C     CALCULATE FRICTIONAL PRESSURE DROP
C
      CALL DPFTPD(DELX,WC,EC,PC  ,DPF,RE,DEQ,ABAR,XMACH)
      IF(ITURN)111,112,111
 111  DPF=DPF*(RE*(DEQ/DCUR)**2)**0.05
 112  PCO=PC-DPF
      ICOUNT=ICOUNT+1
      VEL =144.*WC /(AXC*RC)
      IF(JCOUNT.GT.47) GO TO 43
 34   IF(ABS(ICOUNT-IPRINT).EQ.0) GO TO 35
 36   IF(XMACH .GT.1.0) GO TO 37
      IF(XL.GE.LENGTH) GO TO 600
C
C     SOLVE CONSERVATION EQUATIONS ACROSS SECTION
C
      I=1
      ECO=EC
      CALL PROP(PCO,TCO,W,PCO,RCO(I),XVC,XCC,XCP,XVS,1)
C     ITERATE ON COLD SIDE DENSITY
```

```
 500  PC2=PC-DPF+ (WC*WC/ABAR)*(1./(RC*AXC)-1./(RCG(I)*AXCN)) *4.47
      EC2= EC + QC/WC + (1./64.4)*(WC*WC)*(1./((RC*AXC)**2.) -
     1 1./((RCG(I)*AXCN)**2.))*26.2
      CALL PROP(PC2,TC2,Q,EC2,RC2(I),XVC,XCC,XCP,XVS,1)
      DRC(I)=RC2(I)-RCG(I)
      DELR=ABS(DRC(I))
      RBAR=ABS((RC2(I)+RCG(I))/2.)
C     CHECK DELTA RHO FOR CONVERGENCE
      IF(I.GT.98 )GO TO 503
      IF((DELR/RBAR  ).LT..0001) GO TO 502
C     INCREMENT COLD SIDE DENSITY
C
      IF(ILVEN(I).EQ.1) GO TO 501
      CM=(RCG(I)-RCG(I-1))/(DRC(I)-DRC(I-1))
      RCG(I+1)=RCG(I)-CM*DRC(I)
      I=I+1
      GO TO 500
 501  RCG(I+1)=0.999*RCG(I)
      I=I+1
      GO TO 500
 502  PC=PC2
      RC=RC2(I)
      EC=EC2
      TC=TC2
      XL=XL+DELX
C
C     CALCULATE TURNING LOSS WHEN APPLICABLE
C
      IF(ITURN)100,550,100
 550  RELR=(XWL+WS)/(2.*DEQ)
      IF(RELR.GT.1.5) GO TO 551
      EQL=(52.-28.*RELR)*DEQ*1.5
      GO TO 552
 551  RESL=1.55*RELR
      RESS=0.606*RELR+7.1
      REST=2.22*RELR+6.67
      EQL=(REST+RESL+RESS/2.)*DEQ
 552  CALL DPFTPD(EQL,WC,EC,PC,DPT,XRE,DEQ,ABAR,XM)
      PC=PC-DPT
      GO TO 100
 503  WRITE(6,9999) DELR
 9999 FORMAT(1H0,20X,'ITERATIVE SOLUTION TO BALANCE EQUATIONS DOES NOT C
     1ONVERGE. DELTA DENSITY =',F7.4)
      GO TO 999
C
C     PROGRAM OUTPUT SECTION
C
 45   WRITE(6,1002)
      WRITE(6,1003)
      JCOUNT=1
      GO TO 54
 55   WRITE(6,1004)XL,PC,TC,V,VEL,HL,RE,TS,WS,AXC,QQUM,QFLUX
     1 ,LW
      JCOUNT=JCOUNT+1
      ICOUNT=0
      GO TO 56
 57   WRITE(6,1005) XL, XM/CH
      GO TO 999
 600  WRITE(6,1001)
```

```
      WRITE(6,1006)
      DP=PIN-PC
      DT=ABS(TC-TIN)
      WRITE(6,1007)THP,PIN,PC,DP,TIN,TC,DT,QQUM
      WRITE(6,1008)
      WRITE(6,1009)(XPOS(IJ),XTS(IJ),XWS(IJ),LANDW(IJ),DCURVE(IJ),
     1RWALL(IJ),IJ=1,NP)
      GO TO 999
 1001 FORMAT(1H1,45X,'AEROJET LIQUID ROCKET COMPANY'//34X, 'HEAT PIPE TE
     ACHNOLOGY FOR ADVANCED ROCKET THRUST CHAMBERS'// 46X,'COOLING JACKE
     0T DESIGN PROGRAM')
 1002 FORMAT(1H1)
 1003 FORMAT(2X,'POSITION  PRESSURE  TEMPERATURE  QUALITY  VELOCITY
     1FILM      REYNOLDS    PASSAGE      FLOW AREA    HEAT         HEAT
     A WALL'/
     2       2X,'                                                    COE
     3FFICIENT   NUMBER  HEIGHT--WIDTH              ADDITION      FLUX
     0 TEMP'/
     4       2X,' INCHES     PSIA       DEG R                FT/SEC (BTU/
     5IN2-SEC-R)              INCHES     SQ INCHES   BTU/SEC   (BTU/IN2-S
     6EC)   DEG R'//)
 1004 FORMAT( 4X,F5.1,F10.1,F11.1,F11.3,F10.1,2E12.4,2F7.2,F9.3,F11.1,F1
     i2.2,F6.0)
 1005 FORMAT(1H ,10X,'STATION ',F6.2,' INCHES  -  MACH NUMBER =',F6.0)
 1006 FORMAT(1H ///51X,'DESIGN SUMMARY SHEET')
 1007 FORMAT(1H /// 46X,'HEAT PIPE TEMPERATURE =',F6.1,' DEG R'//
     1 30X,'PRESSURE:   INLET =',F6.1,' PSIA,  OUTLET =',F6.1,' PSIA,  D
     2ELTA P =',F6.1,' PSIA'//
     3 30X,'TEMPERATURE:   INLET =',F6.1,' R,  OUTLET =',F6.1,' R,  DELT
     4A T =',F6.1,' R'//
     5 44X,'TOTAL HEAT TRANSFER RATE =',F6.1,' BTU/SEC'//)
 1008 FORMAT(1H   //57X,'GEOMETRY TABLE'//30X,'POSISION     PASSAGE
     1LAND WIDTH   HEAT PIPE  THERMAL WALL'/
     2                                  30X,'           HEIGHT--WIDTH
     3              DIAMETER  RESISTANCE'/
     4                                  30X,' INCHES       INCHES
     5  INCHES       INCHES  (IN2-SEC-R/BTU)'//)
 1009 FORMAT(1H ,30X,F7.1,F9.2,F7.2,F10.2,2F12.1)
 1111 FORMAT(1H ////45X,'MASS FLOW RATE =',F6.3,' LBM/SEC'//30X,'INLET P
     1RESSURE =',F6.1,' PSIA     INLET TEMPERATURE =',F6.1,' R'////)
      END

      SUBROUTINE HLDIB(P,H,D,W,AXC,HL,TW)
C
C     FILM COEFFICIENT OF DIBORANE AS LIQUID, TWO-PHASE, OR GAS
C
      DATA/PCRIT/581./
      CALL PROP(P,T,G,H,RHO,VIS,CON,CP,VS,1)
C   BULK PROPERTY HL FOR GAS
      RE=W*D/(AXC*VIS)
      PR=CP*VIS/CON
      IF(Q.LT.1.0) GO TO 1
      HL=0.026*RE**0.8*PR**0.33*(CON/D)
      RETURN
C   BULK PROPERTY HL FOR LIQUID AND TWO-PHASE BASED ON VAPOR PROPS
 1    TS=TSAT06(P)
      IF(INB.EQ.3) GO TO  4
      HL=0.023*RE**0.8*PR**0.40*(CON /D)
      RETURN
```

```
C     RE-ENTER SUBROUTINE WITH CALCULATED WALL TEMPWRATURE
      ENTRY HLWCOB(TW,THP,RW,HL,QFLUX,INB)
      IF(P.GT.PCRIT.OR.Q.GE.1.0) GO TO 2
      IF(INB.EQ.3) GO TO 4
      IF(TW.LE.TS.AND.Q.LE.0.) GO TO 3
      IF(Q.GT.0.) GO TO 4
      TWNB=TS+50.
      QNB=(THP-TWNB)/RW
      V=W/(AXC*RHO*1728.)
      QBO=0.8+0.00058*V*(TS-T)
      IF((V*(TS-T)).GT.3000.) QBO=1.4+0.00012*V*(TS-T)
      IF(QNB.GE.QBO) GO TO 4
      TW=TWNB
      QFLUX=QNB
      HL=0.0
      INB=2
      RETURN
C     SUPERCRITICAL OR GAS
 2    XQ=1.
      CALL PROP(P,TW,XQ,HW,RHOW,VISW,CONW,CPW,VSW,2)
      HL=HL*(VIS/VISW)**0.14 *0.82
      INB=1
      RETURN
C     FORCED CONVECTION LIQUID
 3    RE=W*D/(AXC*VIS)
      PR=CP*VIS/CON
      HL=0.023*RE**0.8*PR**0.4*(CON/D)
      INB=1
      RETURN
C     FILM BOILING
 4    XQ=1.
      CALL PROP(P,TS,XQ,HX,RHOV,VIS,CON,CP,VS,2)
      RE=W*D/(AXC*VIS)*(RHOV/RHO)
      PR=CP*VIS/CON
      CALL PROP(P,TW,XQ,HW,RHOW,VISW,CONW,CPW,VSW,2)
      IF(Q.LT.0.004) Q=0.004
      FX=2.71828**(-.185-.252*ALOG(Q)-.00767*(ALOG(Q))**2.)
      HL=0.026*RE**0.8*PR**0.33*(CON /D)*FX*(VIS/VISW)**0.14
      INB=3
      RETURN
      END

      SUBROUTINE DPFTPD(DELTL,W,H,P   ,DPF,RE,D,A,XMACH)
C
C     FRICTIONAL PRESSURE DROP
C
      CALL PROP(P,T,Q,H,RHO,VIS,CON,CP,VS,1)
      IF(Q.LT.1.0.AND.Q.GT.0.0) GO TO 10
      RE=W*D/(A*VIS)
      F=0.014
      IF(RE.LT.2.6E+5)  F=0.3164/RE**0.25
      DPF =144.*F*DELTL*(W/A)**2./(2.*32.2*RHO*D)
      XMACH=144.*W/(RHO*A*VS)
      RETURN
 10   XQ=0.0
      CALL PROP(P,T,XQ,XH,RHOL,VIS,CON,CP,VSL,2)
      RE=W*D/(A*VIS)
      F=0.014
      IF(RE.LT.2.6E+5)  F=0.3164/RE**0.25
```

```
      DPFL=144.*F*DELTL*(W/A)**2./(2.*32.2*RHOL*D)
      XQ=1.0
      CALL PROP(P,T,XQ,XH,RHOV,VIS,CON,CP,VSV,2)
      RE=W*D/(A*VIS)
      F=0.014
      IF(RE.LT.2.0E+5)  F=0.3164/RE**0.25
      DPFV=144.*F*DELTL*(W/A)**2./(2.*32.2*RHOV*D)
      DPF=DPFL*(((1.6*(DPFV/DPFL)-1.)/0.85)*Q+1.)
      IF(Q.GT.0.85) DPF=DPFL*((-4.*Q+5.)*(DPFV/DPFL))
      ALPHA = (RHOL-RHO)/(RHOL-RHOV)
      C =SQRT(1./( (ALPHA*RHOV+(1-ALPHA)*RHOL) * (ALPHA/(RHOV*VSV**2.)
     A   +(1-ALPHA)/(RHOL*VSL**2.))))
      XMACH=144.*W/(RHO*A*C)
      RETURN
      END

      SUBROUTINE PROP(P,T,Q,H,RHO,VIS,CON,CP,VS,K)
C
C     PROPERTY INTERFACE SUBROUTINE
C
      CALL PB2H6(P,T,Q,H,RHO,VIS,CON,CP,K)
      VS=1000.
      RETURN
      END

      SUBROUTINE PB2H6(P,T,Q,H,RHO,VIS,CON,CP,K)
C     ******************************************************************
C
C
C     PROPERTIES OF DIBORANE (B2H6)
C        P      PRESSURE - PSIA - INDEPENDANT VARIABLE
C        T      TEMPERATURE - DEG R - INDEPENDANT VARIABLE (IF K=2)
C        Q      QUALITY - INDEPENDANT VARIABLE (IF K=2)
C        H      ENTHALPY - BTU/LBM - INDEPENDANT VARIABLE (IF K=1)
C        RHO    DENSITY - LBM/FT3
C        VIS    VISCOSITY - LBM/IN-SEC
C        CON    CONDUCTIVITY - BTU/IN-SEC-R
C        CP     SPECIFIC HEAT - BTU/LBM-R
C        K      INDEPENDANT VARIABLE FLAG
C
C
C     ******************************************************************
      DIMENSION XT(41),CPVAP(41),CONVAP(41),XP(52),XHLIQ(52),PSAT(29),
     1XTSAT(29),HX(15),TX(15)
      COMMON/SATL/PTAB(12)/TARRAY/XXT(15,12)/ZARRAY/XZ(15,12)
C     CALCULATED PYHSICAL PROPERTIES OF DIBORANE (B2H6) IDEAL GAS
C     TEMPERATURES-R FOR CALC. PROPERTIES FOR  CP AND COND.
      DATA/XT/180.,200.,250.,300.,350.,400.,450.,500.,550.,600.,650.,
     1        700.,750.,800.,850.,900.,950.,1000.,1050.,1100.,1150.,
     2        1200.,1250.,1300.,1350.,1400.,1450.,1500.,1550.,1600.,
     3        1650.,1700.,1750.,1800.,1850.,1900.,1950.,2000.,2050.,
     4        2100.,2150./
C     CALC. HEAT CAPACITY (BTU/LBM)  FOR  (B2H6)
      DATA/CPVAP/.297,.305,.319,.337,.356,.381,.412,.448,.490,.532,.570,
     1          .606,.645,.680,.715,.745,.780,.810,.840,.870,.900,.926,
     2          .954,.977,1.001,1.024,1.048,1.065,1.076,1.105,1.120,
     3          1.137,1.154,1.170,1.183,1.200,1.211,1.225,1.2375,1.250,
     4          1.260/
C     CALC. THERMAL CONDUCTIVITY (BTU/IN-SEC-R) FOR (B2H6)
```

```
      DATA/CONVAP/.0000625,.0000655,.0000740,.0000865,.000105,.000135,
     1            .0001660,.0002450,.0002950,.0003450,.000395,.000450,
     2            .0005600,.0005700,.0006320,.0006900,.000750,.000810,
     3            .0008700,.0009300,.0010000,.0010600,.001130,.001195,
     4            .0012500,.0013200,.0013900,.0014500,.001500,.001560,
     5            .0016200,.0016900,.0017400,.0018000,.001850,.001910,
     6            .0019800,.0020200,.0020900,.0021400,.002200/
C     VAPOR PRESSURE OF DIBORANE (B2H6) (PSIA)
      DATA/XP/60.,70.,80.,90.,100.,110.,120.,130.,140.,150.,160.,170.,
     1       180.,190.,200.,210.,220.,230.,240.,250.,260.,270.,280.,
     2       290.,300.,310.,320.,330.,340.,350.,360.,370.,380.,390.,
     3       400.,410.,420.,430.,440.,450.,460.,470.,480.,490.,500.,
     4       510.,520.,530.,540.,550.,560.,565./
C     LIQUID ENTHALPY (BTU/LBM)
      DATA/XHLIQ/-85.85,-81.0,-77.0,-73.2,-69.0,-65.5,-61.5,-58.0,-54.0,
     1           -50.60,-47.2,-43.5,-40.9,-37.5,-34.8,-31.9,-29.0,-26.5,
     2           -24.00,-20.0,-19.2,-17.4,-15.5,-13.5,-12.0,-10.5,-09.0,
     3            -8.00,-06.5,-05.2,-4.0,-2.5,-1.0,0.8,2.6,4.5,6.0,8.5,
     4            10.50,13.5,16.0,19.3,23.0,26.0,30.5,35.0,39.0,44.5,
     5            50.00,57.5,61.5,65.5/
C     PRESSURE ARRAY FOR TSAT
      DATA/PSAT/    .345,.680,1.170,1.93,2.90,4.40,6.30,9.00,12.5,17.1,
     1              22.5,29.5,37.5,47.5,59.,74.5,90.8,110.,132.,157.,
     2              184.,218.,251.,290.,333.,385.,440.,508.,580./
C     SATURATION TEMPERTURE
      DATA/XTSAT/    240.,250.,260.,270.,280.,290.,300.,310.,320.,330.,
     1               340.,350.,360.,370.,380.,390.,400.,410.,420.,430.,
     2               440.,450.,460.,470.,480.,490.,500.,510.,520./
C     ENTHALPY VS TEMPERATURE FOR THE GAS ****************************
C     TEMPERATURE ARRAY FOR GAS ENTHALPY CURVE
      DATA/TX/      300.,500.,600.,700.,800.,900.,1000.,1100.,1200.,
     1              1300.,1400.,1500.,1700.,1900.,2100./
C     GAS ENTHALPY ARRAY
      DATA/HX/0.,49.2,98.2,155.2,219.2,290.2,368.2,452.2,542.2,
     1        637.2,737.2,842.2,1066.2,1302.2,1550.2/
      CALL SINTP(PSAT,XTSAT,29,P,TSAT,J)
      HVAP = 1.0621014E+2 +9.6792434E-2*P -2.3361827E-4*P*P
     1   +8.313233E-6*P*P*P
      IF(K.EQ.2) GO TO 2
      CALL SINTP(XP,XHLIQ,52,P,HLIQ,J)
      Q=(H-HLIQ)/(HVAP-HLIQ)
      IF(Q.GT.1.0) Q=1.0
      IF(Q.LT.0.0) Q=0.0
 1    IF(Q.LT.1.0.AND.Q.GT.0.0) GO TO 6
      IF(Q.LT.1.0) GO TO 5
      DH=H-HVAP
      CALL SINTP(TX,HX,15,TSAT,HB,J)
      HA=HB+DH
      CALL SINTP(HX,TX,15,HA,T,J)
      CALL DINTP(XXT,PTAB,XZ,15,12,T,P,Z)
      RHO=144.*P/(Z*55.8*T)
      CALL SINTP(XT,CPVAP,41,T,CP,J)
      VIS =(-3.1102421E-4 +9.9464888E-4*T -2.6373923E-7*T*T                GAS
     1    +4.0967973E-11*T*T*T)*1.E-6
      CALL SINTP(XT,CONVAP,41,T,CON,J)
      CON=CON*.001
      RETURN
 5    T=TSAT + (H-HLIQ)/.66
      RHO = 3.6116509E+1 -7.3016070E-3*T -6.1401123E-5*T*T                 LIQUID
```

```
     1      -7.2533658E-9*T*T*T
            VIS=(0.0142/(2.71828**(0.00895*T))    )*1.0E-2
            CON = 9.2495476E-7 + 1.0006088E-8*T -3.211365E-11*T*T                LIQUID
     1      +1.8465016E-14*T*T*T
            IF(T.GT.400.) CON=-5.E-9*T+3.E-6
            CP     = -4.4572575 + 8.7777717E-2*T  -5.8864402E-4*T *T             LIQUID
     1 +1.9271491E-6*T *T *T    -3.090025E-9*T **4. +1.9558699E-12*T **5.
            IF(T.GT.480.) CP=1.
            RETURN
     6      T=TSAT
            CALL DINTP(XXT,PTAB,XZ,15,12,T,P,Z)
            RHOV=P*144./(Z*55.8*T)
            RHOL= 3.6116509E+1 -7.3016070E-3*T -6.1401123E-5*T*T                 LIQUID
     1      -7.2533658E-9*T*T*T
            RHO = 1./(Q/RHOV+(1.-Q)/RHOL)
            CALL SINTP(XT,CPVAP,41,T,CP,J)
            CALL SINTP(XT,CONVAP,41,T,CON,J)
            CON=CON*.001
            VIS =(-3.1102421E-4 +9.9464888E-4*T -2.6373923E-7*T*T                GAS
     1     +4.0967973E-11*T*T*T)*1.E-6
            RETURN
     2      IF(Q.GT.0.0.AND.Q.LT.1.0) GO TO 4
            IF(Q.LT.1.0) GO TO 3
            CALL SINTP(TX,HX,15,T,HT,J)
            CALL SINTP(TX,HX,15,TSAT,HSATC,J)
            H=HVAP+(HT-HSATC)
            GO TO 1
          3 CALL SINTP(PSAT,XTSAT, 29,P,TSAT,J)
            CALL SINTP(XP,XHLIQ,52,P,HLIQ,J)
            CPBAR=.66
            H=HLIQ+CPBAR*(T-TSAT)
            GO TO 1
          4 CALL SINTP(XP,XHLIQ,52,P,HLIQ,J)
            HVAP = 1.0621014E+2 +9.6792434E-2*P -2.3361827E-4*P*P
           1   +8.313233E-8*P*P*P
            H=Q*HVAP + (1.-Q)*HLIQ
            GO TO 1
            END

            BLOCK DATA
     C      VAPOR DENSITY OF DIBORANE (B2H6)
            COMMON/SATL/PTAB(12)
            COMMON/TARRAY/TT50(15),TT100(15),TT150(15),TT200(15),TT250(15),
           1              TT300(15),TT350(15),TT400(15),TT450(15),TT500(15),
           2              TT550(15),TT571(15)
            COMMON/ZARRAY/XZ50(15),XZ100(15),XZ150(15),XZ200(15),XZ250(15),
           1              XZ300(15),XZ350(15),XZ400(15),XZ450(15),XZ500(15),
           2              XZ550(15),XZ571(15)
     C      PTAB(12)       =PRESSURE TABULATION ARRAY
     C      TT(15)         =TEMPERATURE ARRAY
     C      XZ(15)         =COMPRESIBIBILTY FACTOR,=P/RHO* RT
            DATA/PTAB/ 50.,100.,150.,200.,250.,300.,350.,400.,450.,500.,
           1          550.,571./
            DATA/TT50/     378.0,  400.0,  425.0,  450.0,  460.0,
           1               490.0,  520.0,  565.0,  600.0,  645.0,
           2               680.0,  710.0,  735.0,  900.0, 1500.0/
            DATA/TT100/    404.0,  425.0,  450.0,  460.0,  470.0,
           1               490.0,  520.0,  565.0,  600.0,  645.0,
           2               680.0,  710.0,  735.0,  900.0, 1500.0/
```

```
 DATA/TT150/    425.5,  440.0,  450.0,  460.0,  470.0,
1               490.0,  520.0,  565.0,  600.0,  645.0,
2               680.0,  710.0,  735.0,  900.0, 1500.0/
 DATA/TT200/    444.5,  450.0,  457.5,  470.0,  490.0,
1               520.0,  540.0,  565.0,  600.0,  645.0,
2               680.0,  710.0,  735.0,  900.0, 1500.0/
 DATA/TT250/    460.0,  470.0,  490.0,  505.0,  520.0,
1               540.0,  565.0,  600.0,  630.0,  645.0,
2               680.0,  710.0,  735.0,  900.0, 1500.0/
 DATA/TT300/    472.5,  480.0,  490.0,  505.0,  520.0,
1               540.0,  560.0,  580.0,  600.0,  645.0,
2               680.0,  710.0,  735.0,  900.0, 1500.0/
 DATA/TT350/    482.9,  490.0,  505.0,  520.0,  540.0,
1               560.0,  580.0,  600.0,  620.0,  645.0,
2               680.0,  710.0,  735.0,  900.0, 1500.0/
 DATA/TT400/    492.7,  500.0,  510.0,  520.0,  540.0,
1               560.0,  580.0,  600.0,  620.0,  645.0,
2               680.0,  710.0,  735.0,  900.0, 1500.0/
 DATA/TT450/    501.5,  510.0,  520.0,  530.0,  540.0,
1               550.0,  560.0,  600.0,  620.0,  645.0,
2               680.0,  710.0,  735.0,  900.0, 1500.0/
 DATA/TT500/    508.8,  515.0,  520.0,  530.0,  540.0,
1               560.0,  580.0,  600.0,  620.0,  645.0,
2               680.0,  710.0,  735.0,  900.0, 1500.0/
 DATA/TT550/    515.5,  520.0,  530.0,  540.0,  550.0,
1               560.0,  580.0,  600.0,  620.0,  645.0,
2               680.0,  710.0,  735.0,  900.0, 1500.0/
 DATA/TT571/    522.5,  525.0,  530.0,  540.0,  550.0,
1               560.0,  580.0,  600.0,  620.0,  645.0,
2               680.0,  710.0,  735.0,  900.0, 1500.0/
 DATA/XZ50/    .8810, .9125, .9350, .9500, .9550,
1              .9650, .9700, .9750, .9800, .9890,
2              .9920, .9940, .9975,1.0000,1.0000/
 DATA/XZ100/   .8350, .8700, .9000, .9100, .9140,
1              .9250, .9400, .9550, .9625, .9700,
2              .9770, .9825, .9870,1.0000,1.0000/
 DATA/XZ150/   .7690, .8200, .8350, .8500, .8625,
1              .8825, .9060, .9260, .9375, .9550,
2              .9675, .9825, .9860,1.0000,1.0000/
 DATA/XZ200/   .7475, .7625, .7630, .8060, .8625,
1              .8700, .8850, .9000, .9200, .9390,
2              .9550, .9650, .9250,1.0000,1.0000/
 DATA/XZ250/   .7100, .7400, .7850, .8100, .8300,
1              .8550, .8760, .8975, .9150, .9250,
2              .9440, .9600, .9725,1.0000,1.0000/
 DATA/XZ300/   .6675, .6980, .7300, .7650, .7900,
1              .8200, .8410, .8650, .8770, .9050,
2              .9260, .9470, .9620,1.0000,1.0000/
 DATA/XZ350/   .6300, .6650, .7110, .7440, .7820,
1              .8130, .8350, .8520, .8650, .8825,
2              .9060, .9270, .9450,1.0000,1.0000/
 DATA/XZ400/   .5875, .6250, .6680, .6990, .7450,
1              .7800, .8090, .8290, .8470, .8780,
2              .8975, .9230, .9450,1.0000,1.0000/
 DATA/XZ450/   .5420, .5930, .6400, .6760, .7040,
1              .7450, .7800, .8050, .8250, .8500,
2              .8650, .9150, .9390,1.0000,1.0000/
 DATA/XZ500/   .4925, .5400, .5700, .6200, .6550,
1              .7090, .7490, .7800, .8000, .8290,
```

```
     2               .8675, .9000, .9260,1.0000,1.0000/
      DATA/XZ550/    .4375, .4820, .5499, .6000, .6400,
     1               .6670, .7150, .7500, .7770, .8090,
     2               .8530, .9910, .9250,1.0000,1.0000,
      DATA/XZ571/    .3000, .4000, .4620, .5410, .5960,
     1               .6400, .7000, .7550, .7700, .8000,
     2               .8475, .9880, .9230,1.0000,1.0000/
      END

      FUNCTION TSATDB(P)
C
C     SATURATION TEMPERATURE AND PRESSURE OF DIBORANE
C
      DIMENSION PSAT(29),XTSAT(29)
C     PRESSURE ARRAY FOR TSAT
      DATA/PSAT/    .345,.680,1.170,1.93,2.90,4.40,6.30,9.00,12.5,17.1,
     1              22.5,29.5,37.5,47.5,59.,74.5,90.8,110.,132.,157.,
     2              184.,218.,251.,290.,333.,385.,440.,508.,580./
C     SATURATION TEMPERTURE
      DATA/XTSAT/    240.,250.,260.,270.,280.,290.,300.,310.,320.,330.,
     1               340.,350.,360.,370.,380.,390.,400.,410.,420.,430.,
     2               440.,450.,460.,470.,480.,490.,500.,510.,520./
      CALL SINTP(PSAT,XTSAT,29,P,TSAT,J)
      TSATDB=TSAT
      RETURN
      ENTRY PSATDB(T)
      CALL SINTP(XTSAT,PSAT,29,T,PSA ,J)
      TSATDB=PSA
      RETURN
      END

      FUNCTION COND(T,MAT)
C
C     THERMAL CONDUCTIVITY OF SELECTED MATERIALS
C
C     THERMAL CONDUCTIVITIES  -  BTU/IN-SEC-DEG R
C     K=1    HASTALLOY X,     530 - T - 2160 DEG R
C     K=2    STAINLESS 304,     300 - T - 1500 DEG R
C     K=3    COPPER,      160 - T - 2260 DEG R
C     K=4    NICKEL,       535.-T-2260. DEG R
      DIMENSION TM(9),CM(9),TM2(6),CM2(6),TM3(13),CM3(13)
     1,TM4(13),CM4(13)
      DATA TM/530.,660.,960.,1060.,1460.,1560.,1760.,1960.,2160./
      DATA CM/.000150,.000147,.000189,.000193,.000263,.000277,.000306,
     1          .000335,.000364/
      DATA/TM2/300.,500.,750.,1000.,1250.,1500./
      DATA/CM2/1.51,1.78,2.13,2.46,2.78,3.13/
      DATA/TM3/160.,360.,460.,535.,660.,860.,1060.,1260.,1460.,
     1 1660.,1860.,2060.,2260./
      DATA/CM3/7000.,5730.,5545.,5430.,5290.,5115.,4965.,4850.,
     1  4735.,4615.,4512.,4412.,4315./
      DATA/TM4/535.,660.,860.,1060.,1260.,1460.,1660.,1860.,2060.,2260.,
     12460.,2660.,2860./
      DATA/CM4/857.,980.,795.,615.,620.,667.,735.,783.,775.,828.,873.,
     1 913.,951./
      IF(MAT.EQ.2) GO TO 2
      IF(MAT.EQ.3) GO TO 3
      IF(MAT.EQ.4) GO TO 4
      CALL SINTP(TM,CM,9,T,C,I)
```

```
      CONJ=C
      RETURN
    2 CALL SINTP(TM2,CM2,6,T,C ,1)
      CONJ=C/10000.
      RETURN
    3 CALL SINTP(TM3,CM3,13,T,C,1)
      COND=C*1.E-6
      RETURN
    4 CALL SINTP(TM4,CM4,13,T,C,1)
      COND=C*1.E-6
      RETURN
      END

      FUNCTION IEVEN(I)
C     IF I IS EVEN, IEVEN=2, I ODD, IEVEN=1
      C=FLOAT(I)/2.
      K=IFIX(C)
      D=FLOAT(K)
      E=C-D
      IF(E.LT.0.4) GO TO 1
      IEVEN=1
      RETURN
    1 IEVEN=2
      RETURN
      END

      SUBROUTINE SINTP(U,V,N,X,Y,I)
C     PUNCHED IN 026 SYMBOLS
C
C     SINGLE LINEAR INTERPOLATION ROUTINE
C
      DIMENSION U(1),V(1)
      DO 1 I=2,N
      J=I
      IF((X-U(J))/(U(N)-U(1)))   2,2,1
    1 CONTINUE
    2 I=J-1
      Y=V(1) + (V(J)-V(I)) * (X-U(I)) / (U(J) - U(I))
      RETURN
      END

      SUBROUTINE DINTP(U,V,W,NU,NV,X,Y,Z)
C     PUNCHED IN 026 SYMBOLS
C
C       ***** DOUBLE INTERPOLATION SUBROUTINE *****
C
C     U(J,K)  = ARRAY OF ABSCISSA (INDEPENDENT) VALUES
C     V(K)    = ARRAY OF PARAMETER (INDEPENDENT) VALUES
C     W(J,K)  = ARRAY OF ORDINATE (DEPENDENT) VALUES
C     NU      = NUMBER OF ABSCISSA VALUES
C     NV      = NUMBER OF PARAMETER VALUES
C     X       = INPUT ABSCISSA VALUE
C     Y       = INPUT PARAMETER VALUE
C     Z       = ANSWER
C
      DIMENSION U(NU,1),V(1),W(NU,1)
      CALL SINTP(V,V,NV,1,Y,I)
      CALL SINTP(U(1,I),W(1,I),NU,X,ZA,K)
      CALL SINTP(U(1,I+1),W(1,I+1),NU,X,ZB,K)
      Z= ZA +(ZB-ZA) * (Y-V(I))/ (V(I+1)-V(I))
      RETURN
      END
```

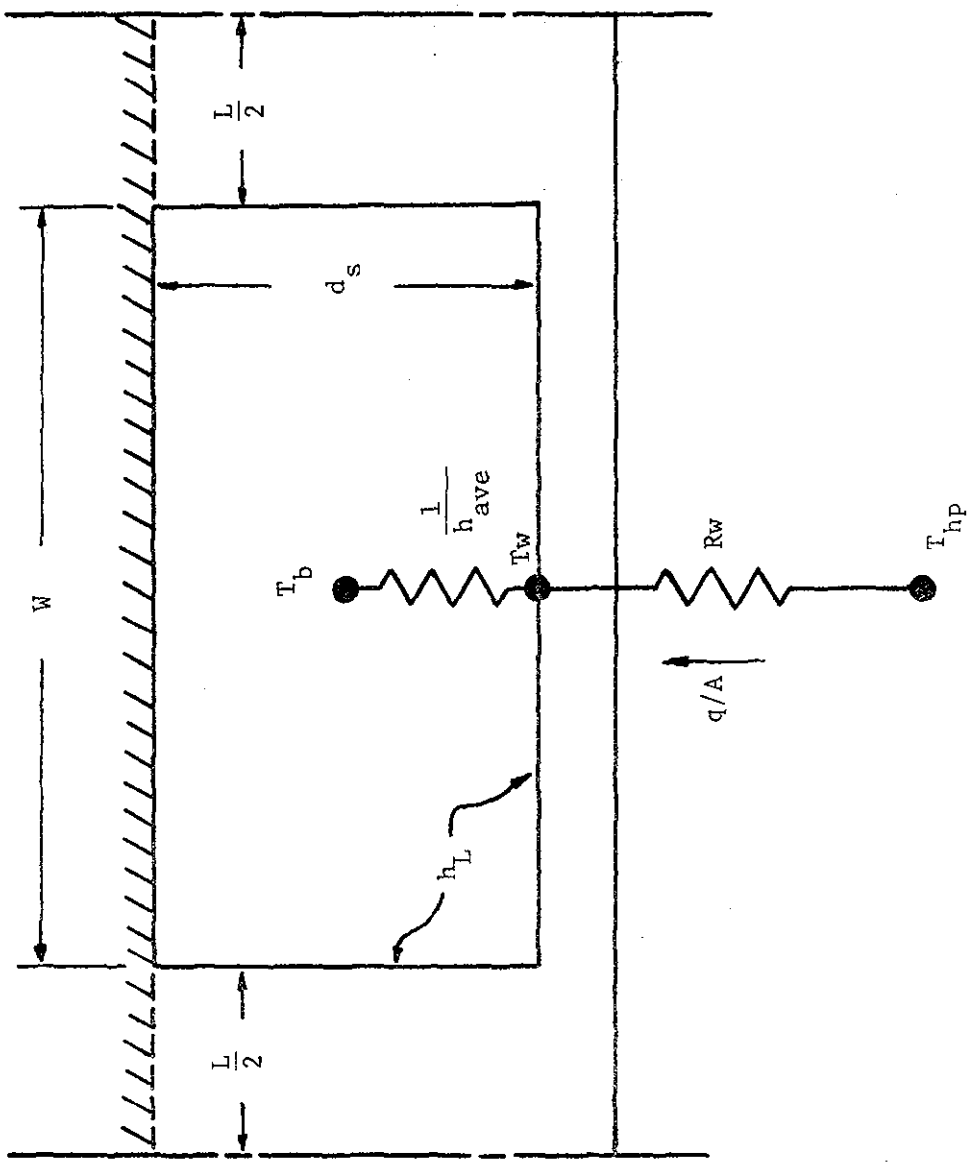

$$h_{ave} = \left(\frac{L}{L+W}\right) h_{fin} + \left(\frac{W}{L+W}\right) h_L$$

$$h_{fin} = \left[\frac{2\, h_L\, k_w}{L}\right]^{1/2} \tanh\left[\left(\frac{2\, h_L}{k\, L}\right)^{1/2} d_s\right]$$

Figure A1 - Coolant Passage Thermal Network

Appendix B

THERMOCOUPLE AND HEAT FLUX ERROR ANALYSIS

The potential errors in surface temperature measurement and in the heat flux values inferred from these measurements were investigated by performing a two dimensional conduction analysis of the thrust chamber wall in the region of the thermocouples installed on the copper thrust chamber delivered to JPL on Contract NAS 8-713. The system analyzed and a portion of the thermal node network utilized is diagrammed in Figure B1. The chromel-alumel thermocouples are stainless-steel sheathed, .051 cm (.020") in diameter, and brazed in place. The junction is formed by fusing the end and griding it flat. This flat end is installed flush with the thrust chamber wall. The thermocouple junction was assumed to be located at the center of the fused end. In the actual installation the junction end is rounded off slightly and a small fillet of braze material forms in the vicinity of the junction when the thermocouple is installed. The effect of this braze fillet is unknown and was not considered in this analysis.

Most of the thermal resistance values were calculated using standard numerical techniques for conduction in cylindrical coordinates. The lone exception was the first thermal resistance radially outward from the thermocouple centerline. This value was calculated utilizing the following equation which is the solution for radial temperature drop in a disk of radius r which is heated on the top, insulated on the bottom, and cooled on the side. Neglecting the axial temperature drop, this becomes:

$$Q = \pi r^2 \varphi = k (2 \pi rt) \frac{dT}{dr}$$

$$\Delta T_{radial} = \frac{\varphi r^2}{4 kt} = \frac{Q}{4 \pi kt}$$

Therefore, the thermal resistance connecting the centerline node to the first node radially outward is defined by the following equation.

$$R_{thermal} = \frac{\Delta T}{Q} = \frac{1}{4 \pi kt}$$

Analysis of the conduction network for a range of assumed surface heat flux values yielded the thermocouple junction temperature as a function of time for each assumed heat flux. These results were then treated as test data and used as input to a data reduction computer program which assumes one-dimensional conduction and calculates surface heat fluc as a function of time given surface temperatures vs time data. Comparison of the heat flux values calculated from the junction temperature to values obtained from the temperature history of a one-dimensional copper wall indicated the error to be expected in heat fluxes calculated from the surface thermocouple data. Input heat fluxes ranging from 326 to 1300 watt/cm^2 were assumed and analyses were performed for junction thicknesses of .0051 and .0254 cm (previous experience has shown that the fused end thickness is in this range). Time increments of .01 to .05 seconds were utilized in the calculations.

Typical results are given in Figures B2 and B3 which show the thermocouple junction and one-dimensional copper wall temperatures histories and the ratio of heat fluxes calculated from them for assumed gas-side heat flux values of 326 and 1300 watt/cm^2. The thermocouple temperature is higher than the actual copper wall temperature because the conductance down the length of the thermocouple is higher than in a copper wall. When this thermocouple temperature is used as input to the data reduction program, erroneously high values of heat flux are obtained. This is indicated by the heat flux ratio which is greater than one. At short time periods (20.5 seconds) the heat flux ratio is large, and

heat flux errors in the range of 40 to 200% are indicated. In addition, the error appears dependent on heat flux, junction thickness, and time.

Quite different behavior is evident after about one second has elapsed as the error becomes relatively independent of heat flux, junction thickness, and time. The error tends to approach a constant of about 20%. This longer time interval case corresponds approximately to athrust chamber firing where the chamber pressure is steady for one second or more. Test durations of 3 to 4 seconds are planned for the FLOX/GH_2 injector checkout tests and it is believed the injector can be characterized sufficiently well by using only the data obtained after 1 second of steady chamber pressure. The experimental error in these heat flux data can be accounted for by simply reducing the indicated heat flux by 20%.

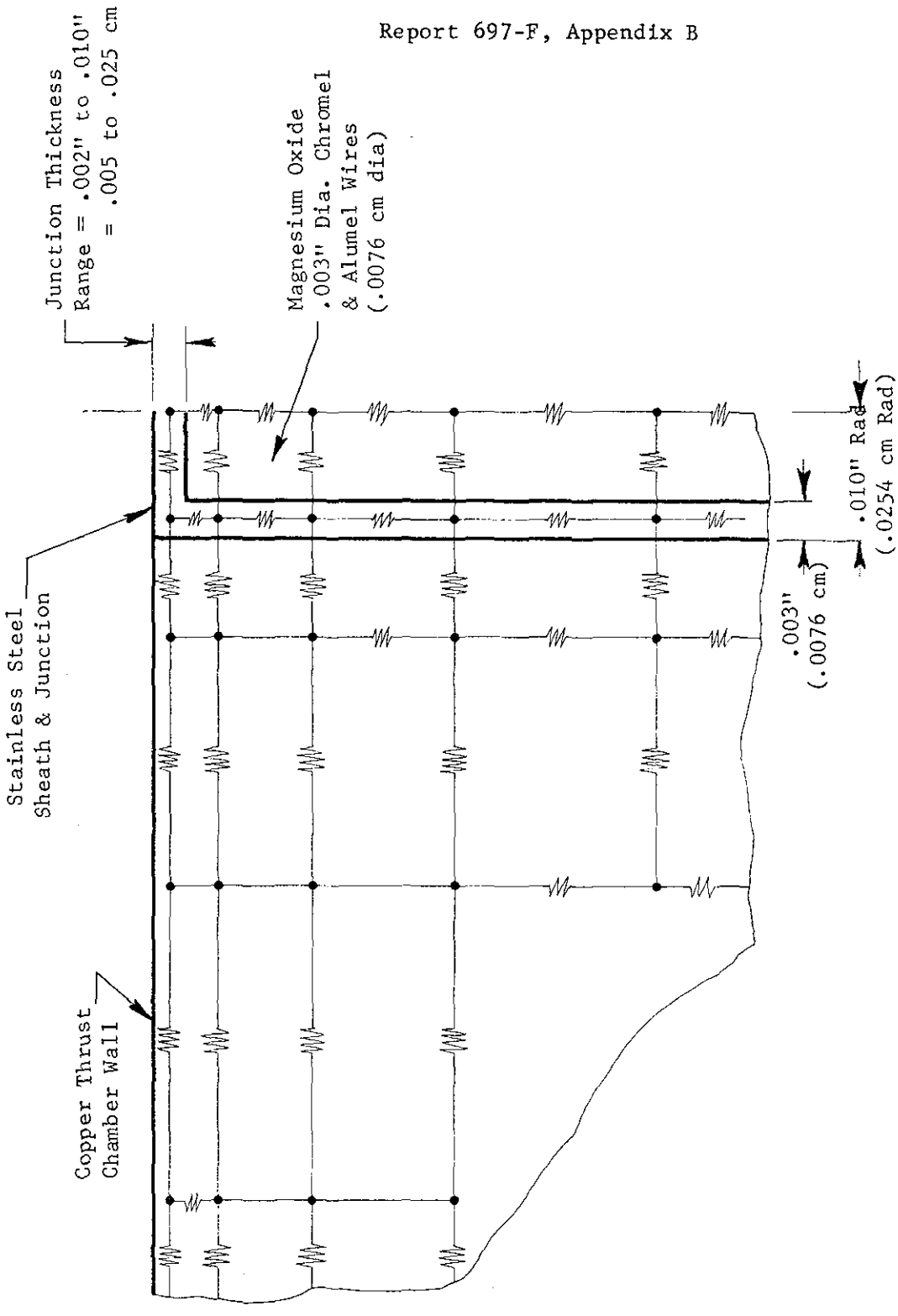

Figure B1 - Portion of Thermal Node Network

Figure B1

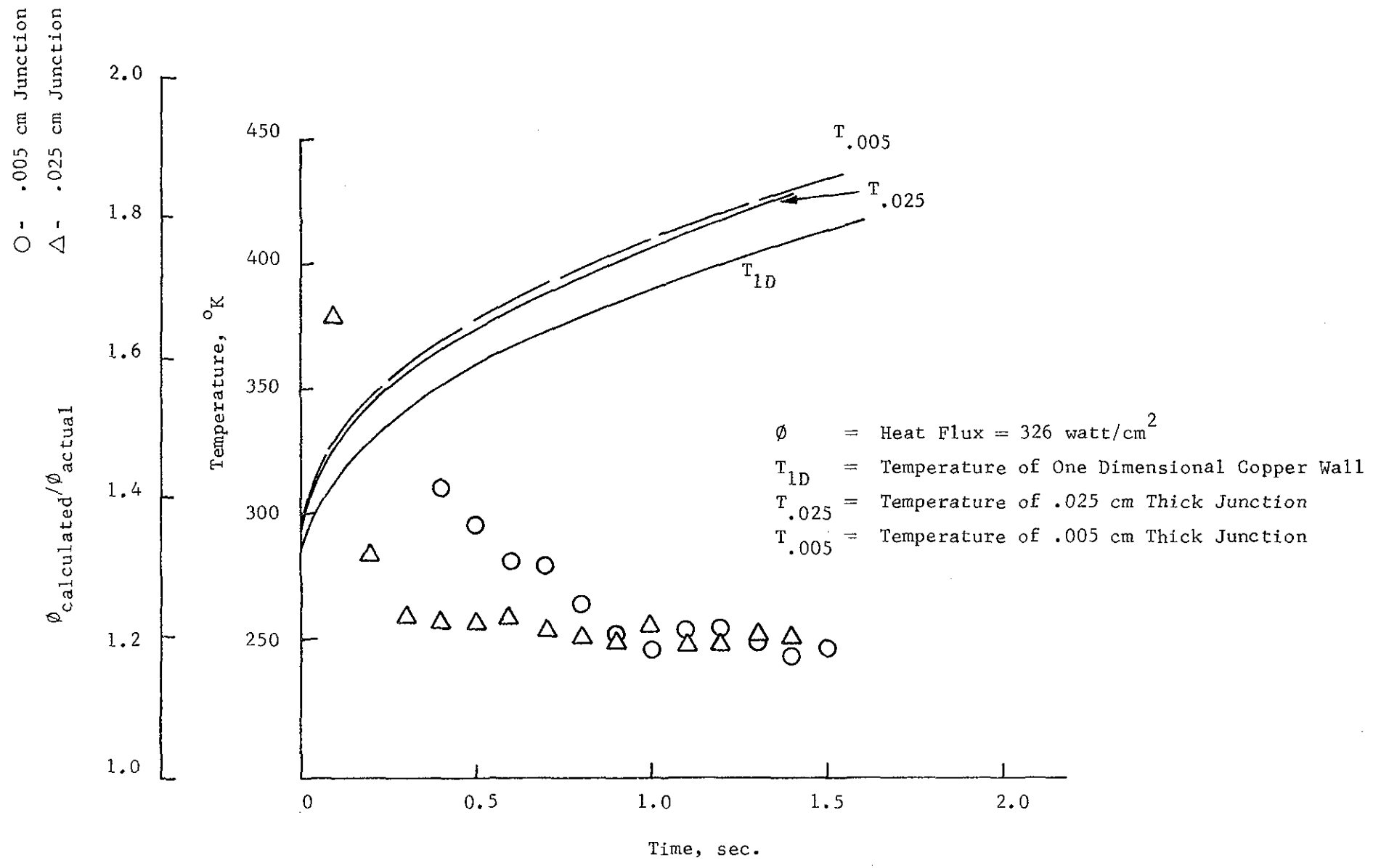

Figure B-2

Figure B2 - Error Analysis for 326 Watt/cm^2 Heat Flux

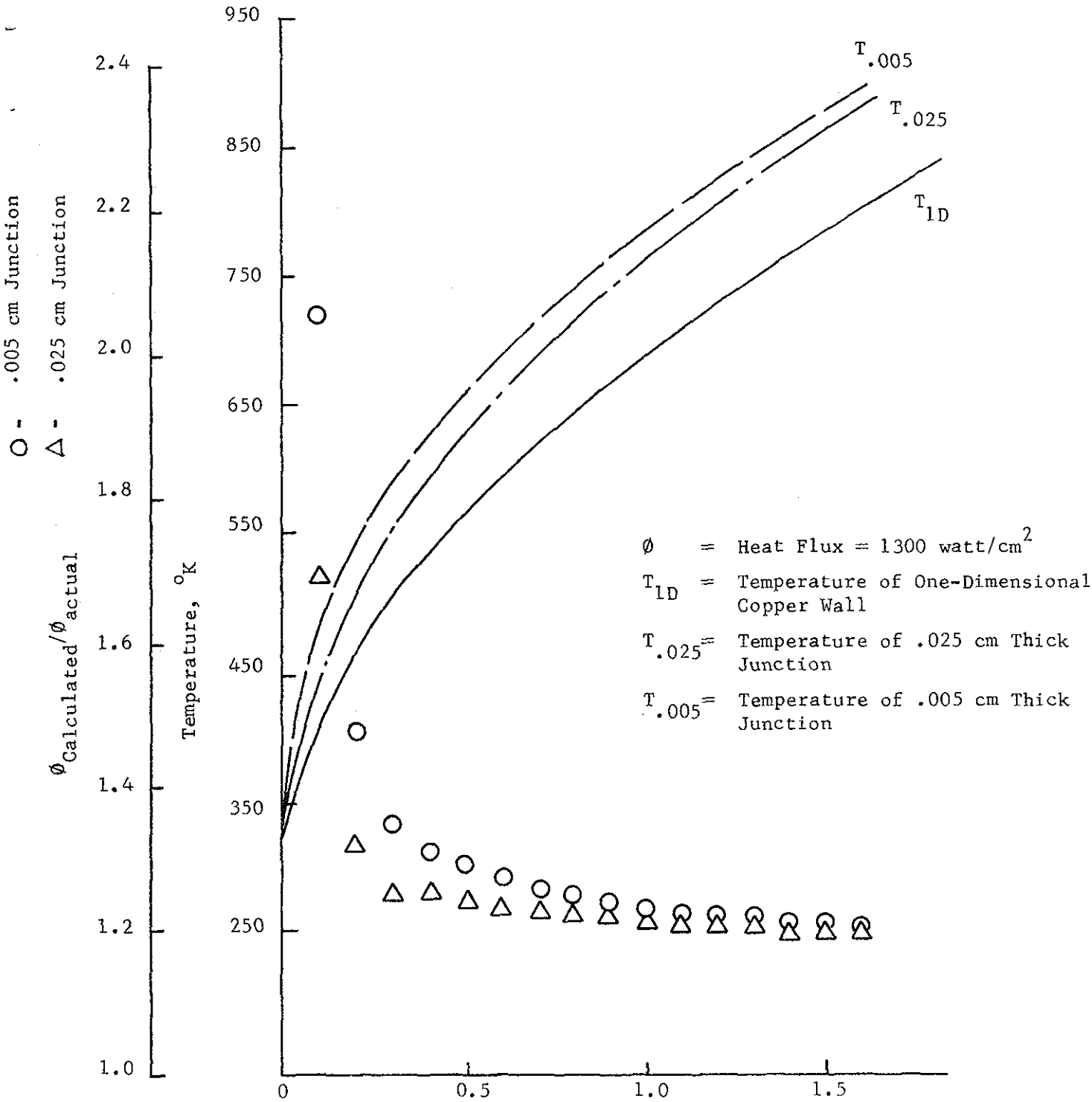

Figure B3 - Error Analysis for 1300 watt/cm^2 Heat Flux

Report 697-F

DISTRIBUTION LIST

Distribution List for Final Report

Contract NAS 7-697

Copies	Recipient	Designee
	NASA Headquarters Washington, D. C. 20546	
1	Contracting Officer	(X)
1	Patent Office	(X)
	NASA Lewis Research Center 21000 Brookpark Rd. Cleveland, Ohio 44135	
1	Office of Technical Information	(X)
1	Contracting Officer	(X)
1	Patent Office	(X)
	NASA Manned Spacecraft Center Houston, Texas 77058	
1	Office of Technical Information	(X)
1	Contracting Officer	(X)
1	Patent Office	(X)
	NASA Marshall Space Flight Center Huntsville, Alabama 35812	
2	Office of Technical Information, MS-IP	(X)
1	Technical Library	(X)
1	Dale Burrows S+E-ASTN-PJ	(X)
1	Technology Utilization Office, MS-T	(X)
	NASA Ames Research Center Moffet Field, Calif. 94035	
1	Patents and Contracts Management	(X)
	Jet Propulsion Laboratory 4800 Oak Grove Dr. Pasadena, Calif. 91103	
2	Technical Manager Robert W. Riebling 125-224	(X)
3	Manager, Liquid Rocket Propulsion Technology Code RPL Office of Advanced Research and Technology NASA Headquarters Washington, D. C. 20546	(X)

DISTRIBUTION LIST (cont.)

Copies	Recipient	Designee
1	Director, Technology Utilization Division Office of Technology Utilization NASA Headquarters Washington, D. C. 20546	(X)
25	NASA Scientific and Technical Information Facility P. O. Box 33 College Park, Maryland 20740	(X)
1	Director, Launch Vehicles and Propulsion, SV Office of Space Science and Applications NASA Headquarters Washington, D. C. 20546	(X)
1	Director, Advanced Manned Missions, MT Office of Manned Space Flight NASA Headquarters Washington, D. C. 20546	(X)
1	Mission Analysis Division NASA Ames Research Center Moffet Field, Calif. 94035	(X)

NASA Field Centers

2	Ames Research Center Moffet Field, California 94035	Hans M. Mark, and Dean Chisel (244-11)
1	Goddard Space Flight Center Greenbelt, Maryland 20771	Merland L. Moseson Code 620
2	Jet Propulsion Laboratory California Institute of Technology 4800 Oak Grove Drive Pasadena, California 91103	Henry Burlage, Jr. Propulsion Div. 38
2	John F. Kennedy Space Center, NASA Cocoa Beach, Florida 32931	Dr. Kurt H. Debus
2	Langley Research Center Langley Station Hampton, Virginia 23365	Ed Cortwright Director

DISTRIBUTION LIST (cont.)

Copies	Recipient	Designee
2	Lewis Research Center 21000 Brookpark Road Cleveland, Ohio 44135	Bruce Lundin Director
2	Marshall Space Flight Center Huntsville, Alabama 35812	Hans G. Paul Code R-P+VED
2	Manned Spacecraft Center Houston, Texas 77058	J. G. Thibodaux, Jr. Chief, Prop. + Power Div. H. Pohl

Government Installations

1	Headquarters, U. S. Air Force Washington 25, D. C. 20546	Col. C. K. Stambaugh AFRST
1	Arnold Engineering Development Center Arnold Air Force Station Tullahoma, Tennessee 37388	Dr. H. K. Doetsch
2	Air Force Rocket Propulsion Laboratory Research and Technology Division Airforce Systems Command Edwards, California 93523	RPRPD/Mr. H. Main
1	Air Force Missile Test Center Holloman Air Force Base,New Mexico 45433	Library
1	Air Force Missile Test Center Patrick Air Force Base, Florida	L. J. Ullian
1	Aeronautical Systems Division Air Force Systems Command Wright-Patterson Air Force Base Dayton, Ohio 45433	D. L. Schmidt Code ASRCNC-2
1	Space and Missile Systems Organization Air Force Unit Post Office Los Angeles 45, California 90045	Col. Clark Technical Data Center

DISTRIBUTION LIST (cont.)

Copies	Recipient	Designee
1	Defense Documentation Center Headquarters Cameron Station, Building 5 5010 Duke Street Alexandria, Virginia 22314 Attn: TISIA	
1	Bureau of Naval Weapons Department of the Navy Washington, D. C. 20546	J. Kay RTMS-41
1	U. S. Naval Ordnance Test Station China Lake California 93557	Code 4562 Chief, Missile Propulsion Division
1	Picatinny Arsenal Dover, New Jersey 07801	I. Forsten, Chief Liquid Propulsion Laboratory
1	U. S. Army Missile Command Redstone Arsenal Alabama 35809	Dr. Walter Wharton
	CPIA	
1	Chemical Propulsion Information Agency Applied Physics Laboratory 8621 Georgia Avenue Silver Spring, Maryland 20910	Tom Reedy
	Industry Contractors	
1	Aerojet-General Corporation P. O. Box 296 Azusa, California 91703	W. L. Rogers
1	Aerojet Liquid Rocket Company P. O. Box 13222 Technical Library, Bldg. 2015,Dept. 2410 Sacramento, California 95813	R. Stiff

DISTRIBUTION LIST (cont.)

Copies	Recipient	Designee
1	Aerojet-General Corporation Space Division 9200 East Flair Dr. El Monte, California 91734	S. Machlawski
1	Aerospace Corporation 2400 East El Segundo Boulevard P. O. Box 95085 Los Angeles, California 90045	John G. Wilder MS-2293
1	AVCO Systems Division Wilmington, Massachusetts	Howard B. Winkler
1	Beech Aircraft Corporation Boulder Division Box 631 Boulder, Colorado	J. H. Rodgers
1	Bell Aerosystems Company P. O. Box 1 Buffalo, New York 14240	W. M. Smith
1	Bellcomm 955 L-Enfant Plaza, S. W. Washington, D. C.	H. S. London
1	Bendix Systems Division Bendix Corporation 3300 Plymouth Road Ann Arbor, Michigan 48105	John M. Brueger
1	Boeing Company P. O. Box 3999 Seattle Washington 98124	J. D. Alexander
1	Boeing Company 1625 K Street, N. W. Washington, D. C. 20006	Library
1	Boeing Company P. O. Box 1680 Huntsville, Alabama 35801	Ted Snow
1	Missile Division Chrysler Corporation P. O. Box 2628 Detroit, Michigan 48231	Mr. John Gates

DISTRIBUTION LIST (cont.)

Copies	Recipient	Designee
1	Wright Aeronautical Division Curtiss-Wright Corporation Wood-ridge, New Jersey 07075	G. Kelley
1	Research Center Fairchild Hiller Corporation Germantown, Maryland	Ralph Hall
1	Republic Aviation Corporation Fairchild Hiller Corporation Farmingdale, Long Island, New York	Library
1	General Dynamics, Convair Division P. O. Box 1128 San Diego, California	Library
1	Missile and Space Systems Center General Electric Company Valley Forge Space Technology Center P. O. Box 8555 Philadelphia, Pa.	F. Mezger F. E. Schultz
1	Grumman Aircraft Engineering Corp. Bethpage, Long Island New York 11714	Joseph Gavin
1	Honeywell, Inc. Aerospace Div. 2600 Ridgeway Rd Minneapolis, Minn.	Mr. Gordon Harms
1	Hughes Aircraft Co. Aerospace Group Centinela and Teale Streets Culver City, Calif. 90230	E. H. Meier V. P. and Div. Mgr., Research + Dev. Div.
1	Walter Kidde and Company, Inc. Aerospace Operations 567 Main Street Belleville, New Jersey	R. J. Hanville Dir. of Research Engr.
1	Ling-Temco-Vought Corporation P. O. Box 5907 Dallas, Texas 75222	Library

DISTRIBUTION LIST (cont.)

Copies	Recipient	Designee
1	Arthur D. Little, Inc. 20 Acorn Park Cambridge, Massachusetts 02140	Library
1	Lockheed Missiles and Space Co. Attn: Technical Information Center P. O. Box 504 Sunnyvale, California 94088	J. Guill
1	Lockheed Propulsion Company P. O. Box 111 Redlands, California 92374	Library
1	The Marquardt Corporation 16555 Saticoy Street Van Nuys, California 91409	Library
1	Baltimore Division Martin Marietta Corporation Baltimore, Maryland 21203	Mr. John Calathes (3214)
1	Denver Division Martin Marietta Corporation P. O. Box 179 Denver, Colorado 80201	Dr. Morganthaler A. J. Kullas
1	Orlando Division Martin Marietta Corp. Box 5837 Orlando, Florida	J. Ferm
1	McDonnell-Douglas Astronautics Co. 5301 Bolsa Ave. Huntington Beach, Calif. 92647	
1	McDonnel-Douglas Corp. P. O. Box 516 Municipal Airport St. Louis, Missouri 63166	R. A. Herzmark
1	Space + Information Systems Division North American Rockwell 12214 Lakewood Boulevard Downey, California 90241	Library

DISTRIBUTION LIST (cont.)

Copies	Recipient	Designee
1	Rocketdyne (Library 586-306) 6633 Canoga Avenue Canoga Park, Calif. 91304	S. F. Iacobellis
1	Northrup Space Laboratories 3401 West Broadway Hawthorne, California 90250	Dr. William Howard
1	Aeroneutronic Corporation Philco Corporation Ford Road Newport Beach, California 92663	Library
1	Astro-Electronics Division Radio Corporation of America Princeton, New Jersey 08540	Mrs. Y. Brill
1	Rocket Research York Center Redmond, Washington 98052	F. McCullough, Jr.
1	Stanford Research Institute 333 Ravenswood Avenue Menlo Park, California 94025	Dr. Gerald Marksman
1	Sunstrand Aviation 4747 Harrison Ave. Rockford, Illinois 61101	R. W. Reynolds
1	TRW Systems Group TRW Incorporated One Space Park Redondo Beach, Calif. 90278	G. W. Elverum
1	TAPCO Division TRW, Incorporated 23555 Euclid Avenue Cleveland, Ohio 44117	P. T. Angell
1	Thiokol Chemical Corp. Aerospace Services Elkton Division Bristol, Pennsylvania	Library

DISTRIBUTION LIST (cont.)

Copies	Recipient	Designee
1	Research Laboratories United Aircraft Corp. 400 Main St. East Hartford, Conn. 06108	Erle Martin
1	Hamilton Standard Division United Aircraft Corp. Windsor Locks, Conn. 06096	Mr. R. Hatch
1	United Technology Center 587 Methilda Avenue P. O. Box 358 Sunnyvale, California 94088	Dr. David Altman
1	Florida Research and Development Pratt and Whitney Aircraft United Aircraft Corporation P. O. Box 2691 West Palm Beach, Florida 33402	R. J. Coar
1	Vickers, Inc. Box 302 Troy, Michigan	Library